J. van Grieken

CFD based prediction method for the notional permeability of rubble mound breakwaters

TU Delft

Boskalis

CFD based prediction method for the notional permeability of rubble mound breakwaters

By

Jesper van Grieken

in partial fulfilment of the requirements for the degree of

Master of Science
in Civil Engineering

at the Delft University of Technology,
to be defended publicly on Wednesday September 18, 2019 at 2:00 PM.

Thesis committee:	Prof. Dr. Ir. S. G. J. Aarninkhof,	TU Delft, Chair
	Dr. Ir. A. Antonini,	TU Delft
	Dr. Ir. B. Hofland	TU Delft
	Ir. J. Henrotte,	Boskalis
	Ir. J. van den Bos,	Boskalis

Version	Final
Date	10-9-2019

TU Delft Boskalis

Preface

This report marks the final step to obtain the title of Master of Science in Civil Engineering, the degree obtained by successfully fulfilling the master programme of Hydraulic Engineering at the Delft University of Technology. The research was performed in cooperation with Boskalis. Through this preface I would like to thank a number of people for their help and support during the writing of this thesis.

First of all I would like to thank the members of my committee, Stefan Aarninkhof, Alessandro Antonini, Bas Hofland, Johan Henrotte and Jeroen van den Bos, for their valuable input and feedback which helped me a lot finding the right direction for my thesis.

A special thanks to Jeroen van den Bos, Johan Henrotte and Boskalis for giving me the opportunity to perform my thesis research at such a wonderful company. Without the resources provided by Boskalis, I would not have been able to carry out the computational demanding simulations.

I would also like to thank Markus Muttray for making the data from the physical model tests of his PhD work available, (Muttray, 2000), in order to validate the used model.

Finally, I would like to thank my family and friends for their support during both my graduation as well as during the rest of my study. I would like to thank my girlfriend, Babet Stoffers, for her support and her ability to motivate me when I needed it. And last, but not least, a very special thanks to my parents, Marcel and Petra van Grieken, for giving me the opportunity to study and supporting me in every way they can.

Jesper van Grieken
Rotterdam, September 2019

Abstract

Practically all initial designs of the armour layer of traditional rubble mound breakwaters are made using the Van der Meer formulas before the structure is optimized with physical model testing. In these Van der Meer formulas, the cross-sectional build-up of the structure is represented in the so-called notional permeability, P. Van der Meer determined this P-value for three structures based on physical model-tests (Van der Meer, 1988). The found values for P are in the range of 0.1 (non-porous structure) till 0.6 (structure made of armour stones). For structures with a different cross-section, the P-value is not known, and a value has to be assumed, which causes uncertainties in the design of the armour layer and hence more subsequent testing in a physical wave flume is required to find an optimal design. When the notional permeability of a structure with a different cross-section can be predicted, the number of physical model tests required can be reduced.

In this thesis, a general method to predict the notional permeability for various structure cross-sections is developed further. Inspired by the work of (Franken, 2016), a numerical model is used to find a characteristic hydrodynamic value for structures with different cross-sections: the three structures for which Van der Meer determined the P-value, and a fourth structure of which the P-value has to be predicted. The P-value of the fourth structure is predicted by interpolation of the characteristic value of this structure between the characteristic values found for the structures of Van der Meer, see Figure 1 for a schematic representation of the method. The numerical model used to obtain this hydrodynamic value is the RANS-VOF model OpenFoam.

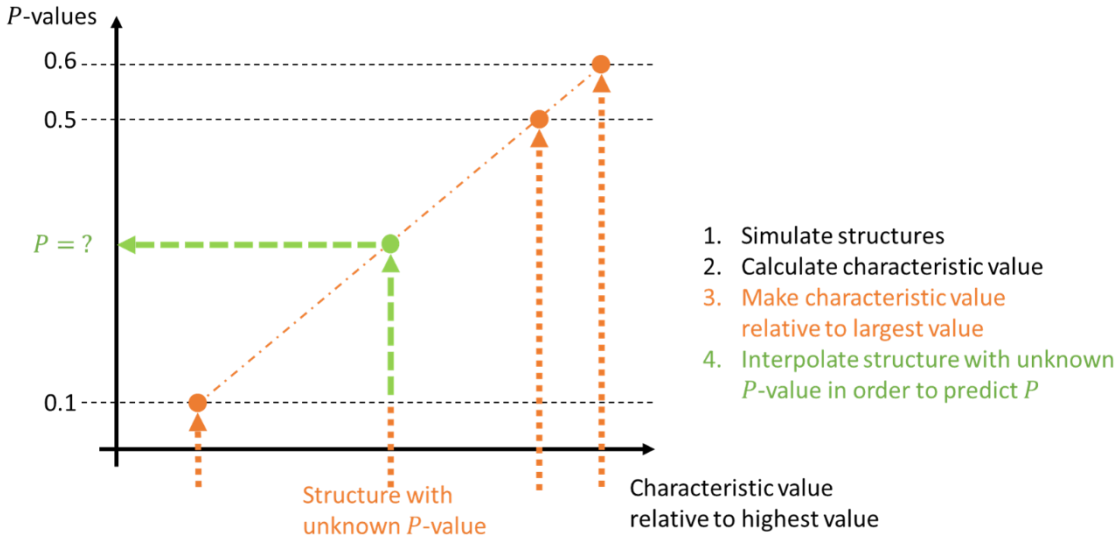

Figure 1 – Concept of the method to predict the notional permeability

The characteristic values that are investigated for the prediction method are based on different stability concepts for rock stability: the velocity stability concept, the shear stress stability concept, the hydraulic head stability concept and the discharge stability concept. From these stability concepts, three different parameters are found which are potentially interesting to use for prediction of the notional permeability. These three parameters are called the hydraulic loading parameters in this thesis. The three hydraulic loading parameters are:

- The wave induced water pressure difference over the armour layer, $\Delta p_{\perp}$
- The discharge through the armour layer perpendicular to the front slope, $Q_{\perp}$
- The flow velocity on top of the armour stones (parallel to the slope), $u_{\parallel}$

See Figure 2 for a schematic representation of the three hydraulic loading parameters.

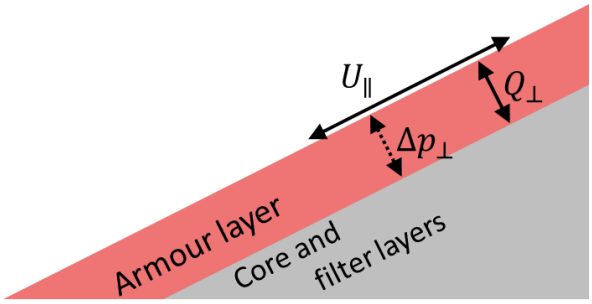

Figure 2 - Schematic representation of the three hydraulic loading parameters

By comparing the results of a numerical model with the results of a physical model test, the model of OpenFoam is validated for the simulation of wave-induced pressures. The results of the water levels and wave induced pressures show a good agreement. Although not measured in the physical model tests, the simulated flow velocities inside of the breakwater seem to be modelled accurate as well in OpenFoam, since the flow velocities inside porous layers are a consequence of the pressure gradient inside these layers and these pressures are modelled correctly. Based on the validation, there are doubts about the accuracy of the simulated flow velocities on top of the armour stones. Therefore, it was decided to not further investigate the flow velocity on top of the armour stones as possible hydraulic loading parameter for the prediction of P.

The hydraulic loading parameter of the wave induced water pressure difference is split into two prediction methods, one for the local pressure difference (looking at a single point in space) and one for the total pressure difference (integrated along the front slope of the structure in space). The prediction method using the discharge as hydraulic loading parameter is also integrated along the front slope of the structure in space. For all three prediction methods, the 2% exceedance value of the hydraulic loading parameter is taken in time.

The prediction methods are validated for a structure cross-section for which a P-value of $0.37 - 0.38$ was found by means of physical model testing, (Kik, 2011) and (Kluwen, 2012).

The prediction method using the total wave induced water pressure over the armour layer ($\Delta p_{\perp,tot,2\%}$) predicts a P-value in line with the P-value found by (Kik, 2011) and (Kluwen, 2012). The predicted P-value is 0.35 with this prediction method, see Figure 3. The prediction method using the local wave induced water pressure over the armour layer ($\Delta p_{\perp,loc,2\%}$), predicts the P-value a bit less well. And the prediction method using the total discharge ($Q_{\perp,tot,2\%}$) predicts the P-value even worse.

A sensitivity assessment of the best prediction method (using the total wave induce water pressure) has been performed by varying the wave conditions, the porosity of the porous layers of the structure and the Forchheimer parameters applied in the numerical simulations. Results show that the prediction is not very sensitive to changes in the wave conditions or changes in the Forchheimer parameters. And although not confirmed by tests, it seems that the prediction method is not very sensitive for changes in the applied porosities of the porous layers of the structure with unknown P-value. Therefore, the method seems to be a robust method and can be practically used in engineering projects. This seems to confirm that the P-value is mainly dependent on the layer build-up and less so on the hydrodynamics.

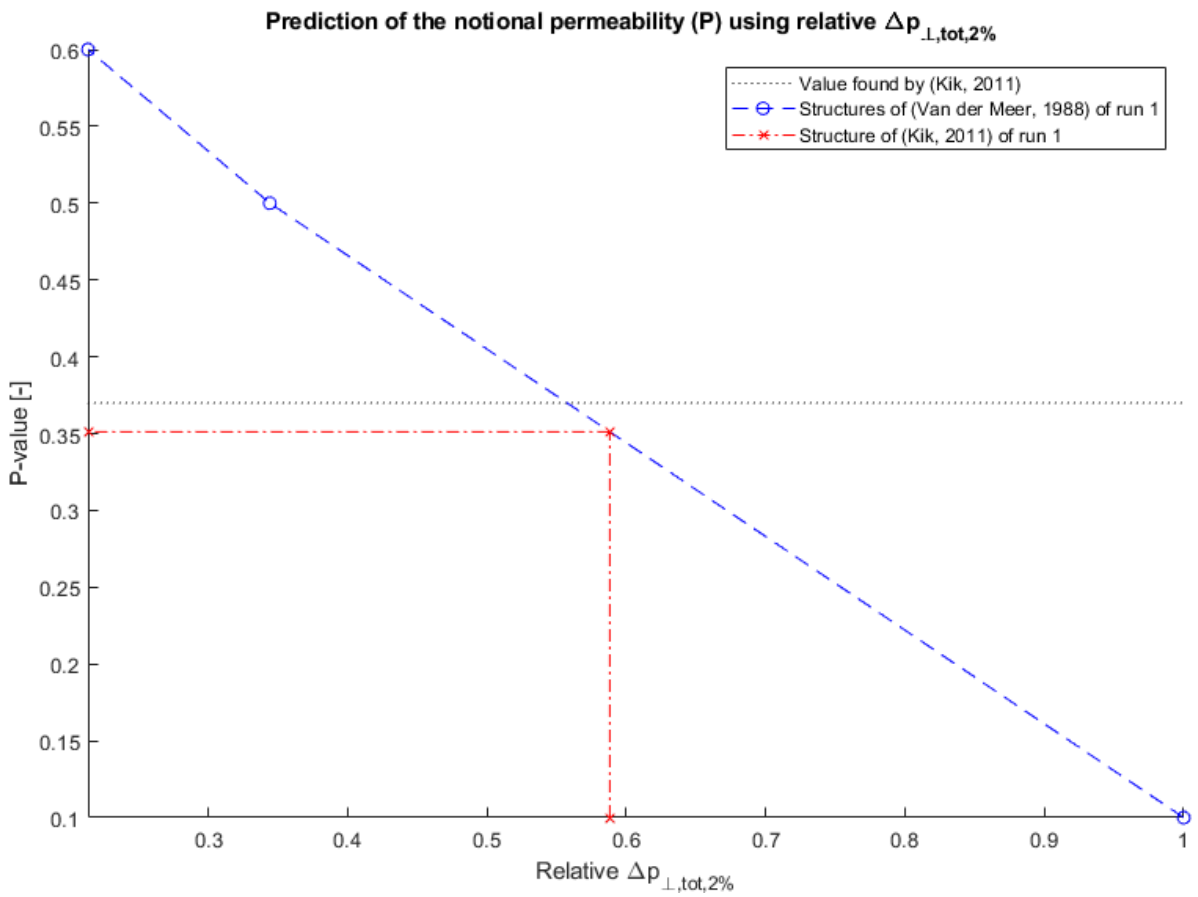

Figure 3 - Prediction of the notional permeability with the total wave induced pressure difference over the armour layer ($\Delta p_{\perp,tot,2\%}$)

With this new prediction method for the notional permeability of a breakwater, it is possible to make a more accurate and objective estimate on the notional permeability for more complex rubble mound structures. A more accurate estimate of the notional permeability will improve the accuracy of the initial design of the armour layer in early stages of a project. A next step to further improve the predictions of the notional permeability and to gain a better understanding of the damage of the armour layer of a rubble mound breakwater, is to determine the correlation between the wave induced water pressure over the armour layer, the discharge through the armour layer and the flow velocity on top of the armour stones and to research how the combination of these three parameters has influence on the armour layer stability.

Contents

List of symbols

c_{pl}	Plunging waves constant Van der Meer	$[-]$
c_s	Surging waves constant Van der Meer	$[-]$
$D_{(n)50}$ or $d_{(n)50}$	Mean (nominal) stone size diameter	$[m]$
D_{15} or d_{15}	15% value of sieve curve	$[m]$
D_{85} or d_{85}	85% value of sieve curve	$[m]$
D_{eq} or d_{eq}	Equivalent stone size diameter	$[m]$
g	Gravitational acceleration	$[m/s^2]$
H_s	Significant wave height	$[-]$
KC	Keulegan-Karpenter number	$[-]$
L	Wave length	$[m]$
M_{50}	Mass of particle for which 50% of the granular material is lighter	$[kg]$
N	Number of waves	$[-]$
n	Porosity	$[-]$
P	Notional permeability	$[-]$
$\Delta p_{\perp,loc,2\%}$	Local wave induced pressure difference over the armour layer, 2% exceedance value in time	$[N/m^2]$
$\Delta p_{\perp,tot,2\%}$	Total wave induced pressure difference over the armour layer, 2% exceedance value in time	$[N/m]$
Q	Dissipation of water into the core	$[m^3/m]$
$Q_{\perp,tot,2\%}$	Discharge through the armour layer perpendicular to the front slope, 2% exceedance value in time	$[m^2/s]$
S	Damage level	$[-]$
s_m	Wave steepness	$[-]$
t	Thickness of a porous layer	$[m]$
T_m	Mean wave period	$[s]$
T_p	Peak wave period	$[s]$
u	Flow velocity	$[m/s]$
$u_{\parallel}$	Flow velocity on top of the armour stones, parallel to the slope	$[m/s]$

α	Slope angle	$[rad]$
α	Laminar flow coefficient	$[-]$
β	Turbulent flow coefficient	$[-]$
γ	Inertia flow coefficient	$[-]$
Δ	Relative mass density	$[-]$
ν	Kinematic viscosity	$[m^2/s]$
ξ	Iribarren number	$[-]$
ξ_{cr}	Critical Iribarren number	$[-]$
ρ	Density	$[kg/m^3]$

1 Introduction

1.1 Problem background

Breakwaters can be found near coasts and harbours all around the world. The main objective of a breakwater is to reduce the incoming wave energy in order to protect the coast or the ships inside the harbour. There are different types of breakwaters, one of the most-applied types is the so-called rubble mound breakwater. The rubble mound breakwater is normally build with a core of quarry run or sand, a filter layer of some larger rocks and an armour layer of even larger rocks. The stability of these large armour rocks is very important for the function of the breakwater since these rocks prevent erosion of the filter layer material and the core material.

In general, for the past decades, the design of the armour layer is made using two engineering design tools: (semi-) empirical formulas and physical model tests. In general, a first preliminary design is made using the (semi-) empirical design formulas which is validated and further optimized using physical model tests.

Several (semi-) empirical formulas have been developed to evaluate the stability of a rock armour layer. In 1953, Hudson developed a formula based on extensive physical model testing. According to (Van den Bos & Verhagen, 2018), the Hudson formula is not often used any more for rock armour layers. In the dataset on which the Hudson formula is based, only a limited range of slope angles, wave conditions and structure types is taken into account. For example, the formula suggest that the permeability of the core has no influence on the stability of the rock armour layer. This is only strictly true within the tested range: the dataset includes only tests with rather permeable structures. From experience it is known that the rock material on a breakwater with a less permeable core is less stable than rock material on a breakwater with a more permeable core.

(Van der Meer, 1988) developed a more generally applicable set of equations for rock armour stability in order to overcome the limitations of the Hudson formula. This method takes more processes into account and is nowadays still widely applied by coastal engineers. The set of the Van der Meer formulas consists of two formulas, formulas (1) and (2). Which formula has to be used depends on the Iribarren number.

$$\frac{H_s}{\Delta D_{n50}} = c_{pl} P^{0.18} \left(\frac{S_d}{\sqrt{N}}\right)^{0.2} \xi_m^{-0.5} \qquad \text{for plunging waves} \quad (\xi < \xi_{cr}) \qquad (1)$$

$$\frac{H_s}{\Delta D_{n50}} = c_s P^{-0.13} \left(\frac{S_d}{\sqrt{N}}\right)^{0.2} \sqrt{\cot \alpha}\, \xi_m^{P} \qquad \text{for surging waves} \quad (\xi > \xi_{cr}) \qquad (2)$$

In the Van der Meer formulas, P is the so-called notional permeability. This notional permeability is an empirical parameter and depends on characteristics of the structure. The value of this parameter has empirically been found to be 0.6 for a homogeneous structure, 0.5 for a structure with a permeable core and 0.1 for a structure with an impermeable core. With the help of model calculations based on the volume of water flowing into the structure, a structure with value of 0.4 is defined by (Van der Meer, 1988). See Figure 4 on the next page for a schematic representation of these structures.

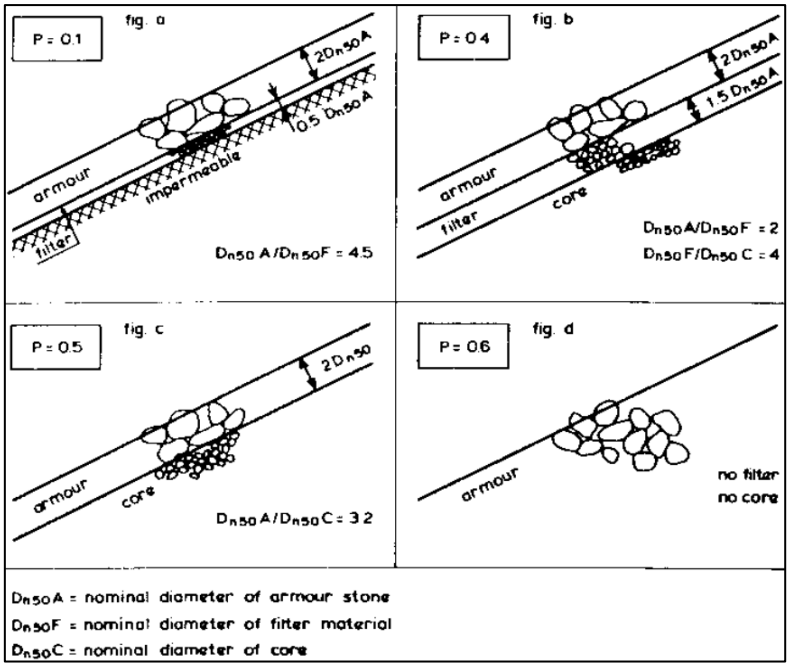

Figure 4 - Permeability coefficient assumptions for various structures (Van der Meer, 1988)

The notional permeability of a breakwater represents the structure cross-section. A structure with thicker permeable layers has a higher notional permeability and vice versa. In case of a structure with a lower notional permeability (a structure with a low permeability of the sub-layer) the incoming waves are reflected on the sub-layer and increase the lift forces on the armour layer, and thus decrease the armour stability.

Since a couple of years, it is also possible to use advanced numerical models to design certain aspects of a breakwater. The advantages and disadvantages of these three design methods for breakwater design are shown in Table 1. For this thesis the Computational Fluid Dynamics model (CFD-model) of OpenFoam is used, because recently a lot of developments are going on for the simulation of rubble mound structures with OpenFoam.

Design method	Advantages	Disadvantages
(Semi-) empirical formulas	- Gives a good and fast first initial approximation of design parameters - Low cost design tool - Widely applied and generally accepted as engineering tool	- Based on physical model tests with a limited range of test cases - Strictly only accurate within this limited range of test cases - Not all physics behind the formulas is understood yet
Physical models	- More accurate compared to (semi-) empirical formulas - More complex structures/geometries can be verified - Widely applied and generally accepted as engineering tool	- Quite expensive (therefore it is tried to limit the number of tests) - Takes quite a lot of time to perform tests and to change structure cross-section - Scale effects can occur
Numerical models (CFD models)	- More flexible than physical model tests - Gives more insight in the occurring phenomena than (semi-) empirical formulas - Structures can be modelled on prototype scale	- Not (yet) possible to design every aspect of a breakwater in a single model - Quite computational demanding - Models are not yet validated for all design aspects and design situations - Not fully recognized as a verification tool yet

Table 1 - Advantages and disadvantages of (semi-) empirical formulas, physical models and numerical models (CFD models).

Despite the cons described in Table 1, numerical models are becoming quite powerful design tools. In the ideal situation, a coastal engineer could use a design tool which is fast, cheap, flexible and completely verified and validated for all design aspects for designing a breakwater. The development of numerical models is not far enough to create such a tool. However, a first step towards this idealized situation would be to have a design process which (Van den Bos, Verhagen, & Kuiper, 2015) describe as the idealized design process, see Figure 5. In this design process, the numerical models are validated by physical model tests or field measurements and the calculation rules and design formulas are (semi-) empirical methods substantiated by the physical and numerical models. In this thesis, the numerical model called OpenFoam is validated using the results of physical model tests and part of a (semi-)empirical design method is investigated using the CFD model OpenFoam.

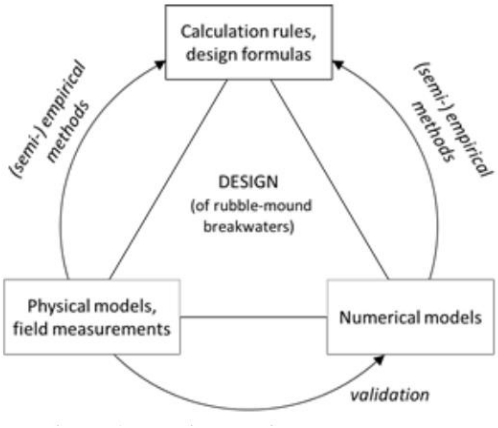

Figure 5 – First step towards the idealized design process, by (Van den Bos et al., 2015)

1.2 Problem analysis

As stated in Table 1, it is not (yet) possible to design every aspect of a breakwater using a single CFD model. For example, it is not yet possible to evaluate the armour layer stability of a rock armour while taking the damage of the armour layer into account in OpenFoam, since it is not yet possible to create a layer with rock elements that will move when the forces on the elements become too high. Therefore, at this moment, also when using a numerical model like OpenFoam, the (semi-)empirical design formulas of Van der Meer are still required for an initial design of an armour layer. However, a numerical model can be used to provide input for the (semi-)empirical design formulas of Van der Meer in order to improve the initial design of an armour layer.

In practice, most of the breakwaters are designed with a structure cross-section which would have a notional permeability value somewhere in between 0.1 and 0.4. Various researches on the topic of notional permeability are already carried out, but there is not a conclusive method to predict the notional permeability. The most important researches on notional permeability are discussed in the literature study, chapter 2.1.

The problem which is researched in this thesis is actually a twofold problem:

PROBLEM DEFENITION I Not all hydraulic processes that influence the stability of (rock) armour layers of statically stable rubble mound breakwaters are understood yet.

PROBLEM DEFENITION II The Van der Meer formulas cannot be used to calculate the armour stability for any given cross-section of a rock armoured breakwater, since the notional permeability, P, is only validated for a few specific cross-sections. There is not a solid, conclusive method which can be used to predict the value for the notional permeability for a structure with a different configuration under loading of irregular waves.

To investigate these problems, there is chosen to use the CFD modelling program called OpenFoam in combination with the wave generation toolbox of Waves2Foam (Jacobsen, Fuhrman, & Fredsøe, 2012). OpenFoam seems very suitable for investigating these problems, since with OpenFoam and Waves2Foam, the pressures and flow velocities inside of a structure under wave loading can be modelled and with the flow velocities, the discharge through the armour layer can be calculated.

1.3 Research objective & research questions

The problems defined can be translated in two research goals, research objective I to create a basis for the long term improvement of the armour stability calculations and research objective II for the short term:

RESEARCH OBJECTIVE I The first goal of the thesis project is to give more insight in the hydraulic processes that influence the armour stability of a rock armoured breakwater.

RESEARCH OBJECTIVE II The second goal of the thesis project is to develop an engineering approach which can be used to predict a value for the notional permeability for rubble mound breakwaters based on the processes relevant for armour stability.

To reach these objectives, the numerical computational fluid dynamics model of OpenFoam is used. The research objectives are translated into the following research questions:

RESEARCH QUESTION I Which hydraulic parameters influence the armour stability of a rock armoured rubble mound breakwater, in which way do these parameters influence the armour stability and how well are these parameters simulated by the numerical model of OpenFoam?

RESEARCH QUESTION II What is an appropriate method, with the help of the numerical model OpenFoam, to predict the notional permeability for rubble mound breakwaters?

By appropriate method, a method which fulfils the following requirements is meant:

- The method should be practically applicable.
- There must be a clear link between the method and the physical processes that influence the armour stability of rock armour layers.

1.4 Structure of this report

This report starts with a literature study where the previous studies on the notional permeability and some general related literature are discussed (chapter 2). After this part, the methodology of the research is explained (chapter 3), before a desk study is performed to find the hydraulic parameters which influence the armour stability (chapter 4), the so-called hydraulic loading parameters. After this desk study, the model of OpenFoam is validated for simulating these hydraulic loading parameters (chapter 5). In the sixth chapter of this report is explained how the characteristic values of the validated hydraulic loading parameters are calculated (chapter 6). After the calculation of these characteristic values, they are used to predict the notional permeability of a structure with unknown P-value (chapter 7). A sensitivity analysis is performed on the outcome of the best of these prediction methods (chapter 8). After these chapters, an engineering approach with the newly developed prediction method is proposed (chapter 9) before the research is discussed (chapter 10) and the conclusions are drawn (chapter 11).

2 Literature study

In this chapter a study of the available literature relevant for this thesis is included. The chapter is divided in two parts, first a part on all previous studies related to the notional permeability and second a part of general related literature.

2.1 Previous studies on notional permeability

2.1.1 Research by Van der Meer (Van der Meer, 1988)

(Van der Meer, 1988) tested three rubble mound breakwater structures with different structure cross-sections: a structure with the armour layer almost directly on an impermeable core (the lower boundary in terms of permeability), a structure with the armour layer directly on a permeable core and a structure made completely of armour material (the upper boundary in terms of permeability). The structures were tested for varying front slopes, varying gradings of the armour layer material, different wave spectra and varying wave conditions, see Table 2 for the test matrix.

Slope angle $\cot(\alpha)$	Grading D_{85}/D_{15}	Spectral shape	Core permeability	Relative mass density	Number of tests	Range $H_s/\Delta D_{n50}$	Range s_m
2	2.25	PM	none	1.63	19	0.8-1.6	0.005-0.016
3	2.25	PM	none	1.63	20	1.2-2.3	0.006-0.024
4	2.25	PM	none	1.63	21	1.2-3.3	0.005-0.059
6	2.25	PM	none	1.63	26	1.2-4.4	0.004-0.063
3	1.25	PM	none	1.62	21	1.4-2.9	0.006-0.038
4	1.25	PM	none	1.62	20	1.2-3.4	0.005-0.059
3	2.25	narrow	none	1.63	19	1.0-2.8	0.004-0.054
3	2.25	wide	none	1.63	20	1.0-2.4	0.004-0.043
3	1.25	PM	permeable	1.62	19	1.6-3.2	0.008-0.060
2	1.25	PM	permeable	1.62	20	1.5-2.8	0.007-0.056
1.5	1.25	PM	permeable	1.62	21	1.5-2.6	0.008-0.050
2	1.25	PM	homogeneous	1.62	16	1.8-3.2	0.008-0.059
2	1.25	PM	permeable	0.95	10	1.7-2.7	0.016-0.037
2	1.25	PM	permeable	2.05	10	1.6-2.5	0.014-0.032
2*	1.25	PM	permeable	1.62	16	1.6-2.5	0.014-0.031
2**	1.25	PM	permeable	1.62	31	1.4-5.9	0.010-0.046

PM = Pierson Moskowitz spectrum
* = test with a foreshore of 1 : 30
** = test with low crested structure and a foreshore of 1 : 30

Table 2 - Test program of tests by (Van der Meer, 1988)

For every test, the profile of the front slope of the structure was measured before the test, after 1000 waves and after 3000 waves. With these measurements, the damage level, S, could be determined. This damage level can be plotted against the dimensionless test-parameter $H_s/\Delta D_{n50}$, to find a relation between S, N and $H_s/\Delta D_{n50}$. Figure 6 shows the results for the structures with a slope of $\cot\alpha = 2$ and damage levels of $S = 3$ and $S = 8$ after 3000 waves.

Van der Meer reasons that for a structure with an impermeable core the flow is more concentrated, which causes larger forces on the rocks during run-down. For a structure with a more permeable core the water dissipates into the core, therefore the forces on the rocks due to the flow are less high.

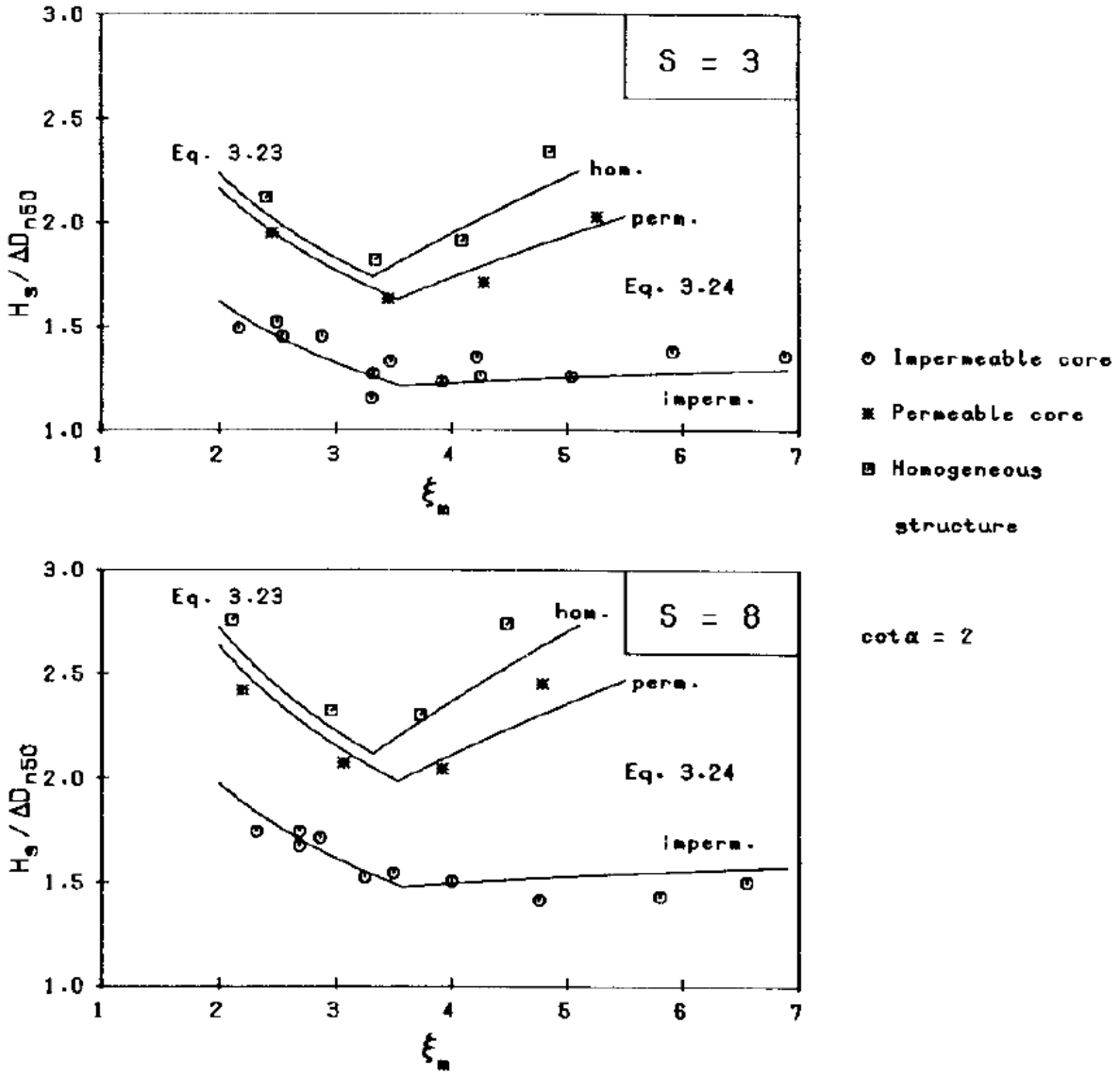

Figure 6 - Influence of permeability on stability numbers for S = 3 and S = 8. (Van der Meer, 1988)

Van der Meer used curve fitting to find a functional relationship for the stability of rubble mound revetments and breakwaters using the following dimensionless variables: $H_s/\Delta D_{n50}$, ξ_m, $\cot\alpha$, $S/\sqrt{N}$ and P. The results of the tests showed a clear difference between plunging and surging waves, therefore a functional relationship was found for plunging waves and one for surging waves. This resulted in the stability formulas of Van der Meer, equations (1) and (2) in the introduction, section 1.1.

Van der Meer proposed a method to calculate the P-value for structures with a different cross-section. In this method it is assumed that the notional permeability of a structure could be linked to the volume of water that dissipates into the core of the breakwater. The HADEER model was used to calculate the flow patterns in the breakwater which were used to calculated dissipation into the core. The results of these calculations is shown in Figure 7.

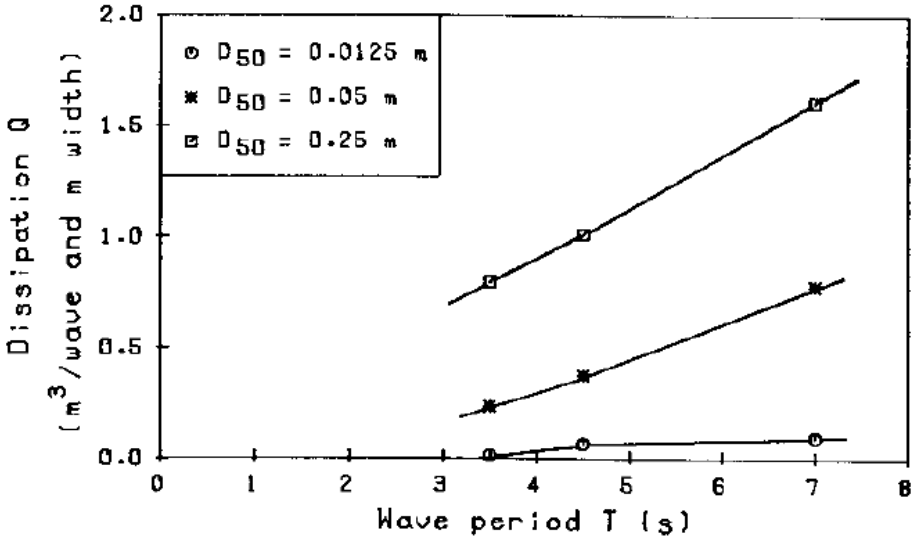

Figure 7 – Dissipation of water into the core, Q, as a function of wave period and core stone diameter. (Van der Meer, 1988)

When the calculated values for dissipated water into the core are plotted as a function of the core stone diameter D_{50}, the dissipation of water into the core can be related to the notional permeability P, see Figure 8.

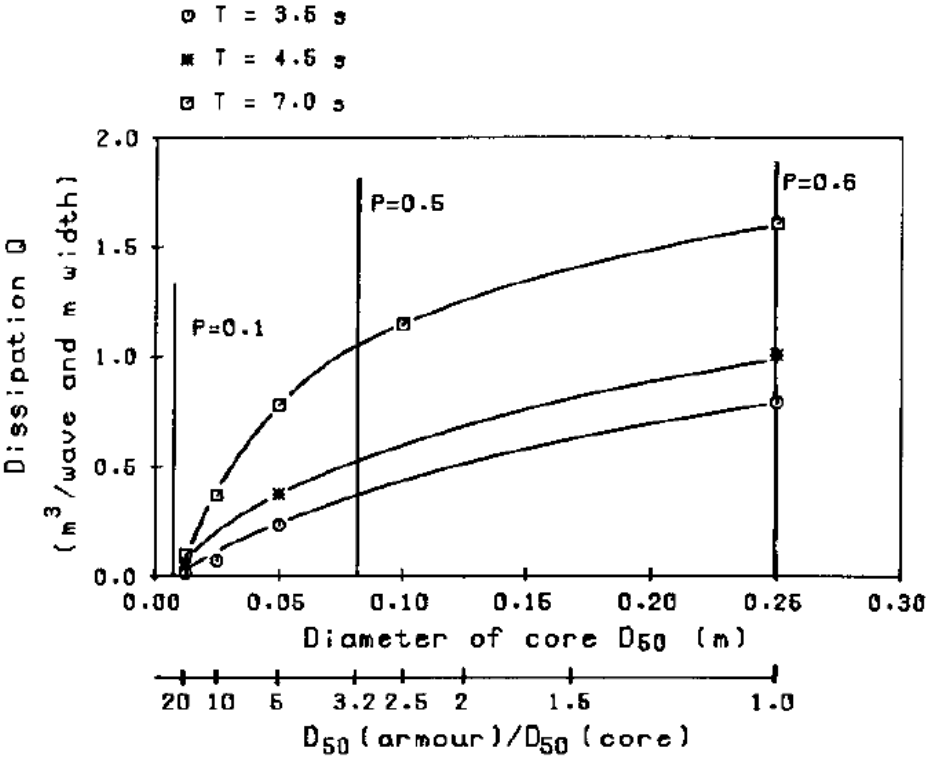

Figure 8 – Dissipation of water into the core, Q, as a function of core stone diameter and wave period. (Van der Meer, 1988)

The last step in the calculation method is to plot the relative dissipation of water into the core versus the permeability of the structure, see Figure 9 for $D_{50} = 0.05\ m$. Van der Meer defined the relative dissipation to be 100% for the structure with fully permeable core (with $P = 0.6$), and to be 0% for the structure with the impermeable core ($P = 0.1$). Using the graph, a permeability coefficient, P, can be calculated for any structure cross-section when the dissipation of water into the core is calculated for this cross-section as well as for the homogeneous structure ($P = 0.6$) and the permeable structure (with $P = 0.5$).

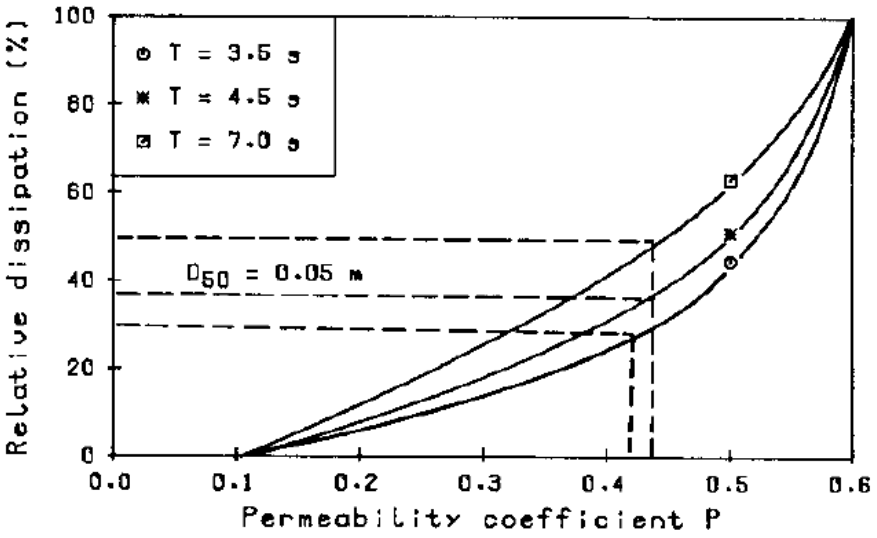

Figure 9 – Relative dissipation into the core as a function of the permeability coefficient P. (Van der Meer, 1988)

2.1.2 Research by Kik (Kik, 2011)

Kik performed physical model tests in order to find the notional permeability value for a structure with a different cross-section than the four structures defined by Van der Meer. He first tested two reference structures (two structures defined by Van der Meer) for which similar P-values were found as in the original tests. The third structure tested by Kik was a structure with a new cross-section, see Figure 10. The structure consists of an impermeable core, two filter layers and an armour layer. The grading of the rock used is $d_{85}/d_{15} \leq 1.5$.

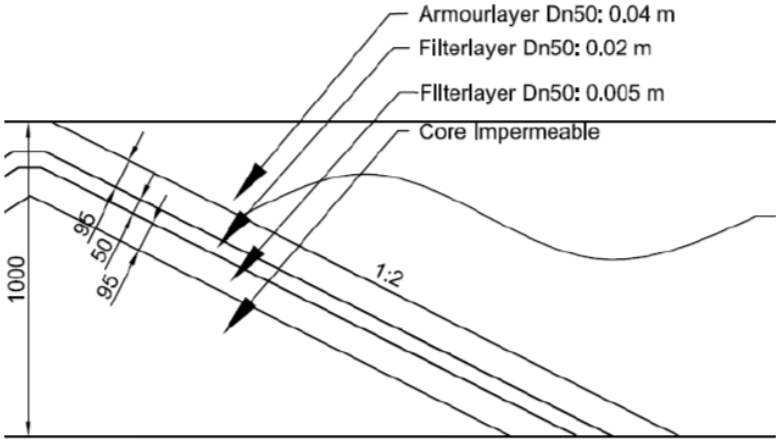

Figure 10 – The third tested structure by Kik. (Kik, 2011)

The test matrix of Kik can be found in Table 3. Due to limitations of the flume and time limits, only one wave height was tested for every structure and the angle of the slope was not changed. The main focus of the tests of Kik was to vary the Iribarren number, by changing the wave steepness through the wave period. The wave steepness was varied between approximately 1% and 5%, since in real-life the steepness of waves attacking a breakwater is almost always in between those values.

Test nr.	Structure	$P\ [-]$	$H_s\ [m]$	$T_m\ [s]$	$T_p\ [s]$	Steepness $[-]$	Expected damage
1	I	0.5	0.15	1.39	1.82	4.97%	3.5
2	I	0.5	0.15	1.8	2.35	2.97%	6.6
3	I	0.5	0.15	2.22	2.90	1.95%	10.5
4	I	0.5	0.15	2.8	3.66	1.23%	5.9
5	I	0.5	0.15	3.3	4.31	0.88%	3.9
6	I	0.5	0.15	3.6	4.71	0.74%	3.1
7	II	0.1	0.10	1.13	1.48	5.02%	1.9
8	II	0.1	0.10	1.5	0.96	2.85%	3.9
9	II	0.1	0.10	1.8	2.35	1.98%	6.2
10	II	0.1	0.10	2.4	3.14	1.11%	5.4
11	II	0.1	0.10	2.9	3.79	0.76%	4.9
12	II	0.1	0.10	3.4	4.44	0.55%	4.6
13	III	0.3?	0.13	1.3	1.70	4.93%	2.7
14	III	0.3?	0.13	1.7	2.22	2.88%	5.3
15	III	0.3?	0.13	2.3	3.01	1.57%	11.3
16	III	0.3?	0.13	2.8	3.66	1.06%	8.4
17	III	0.3?	0.13	3.2	4.18	0.81%	6.9
18	III	0.3?	0.13	3.6	4.71	0.64%	5.8

Table 3 - Test program of tests by (Kik, 2011)

By comparing the measured and calculated damage, and reducing the root mean squared error between these two, a P-value of 0.37 was found for the new structure cross-section. However, since the number of tests conducted on this structure is limited, especially with respect to different wave heights and slope angles, Kik advises to use a conservative value of $P = 0.35$ for the structure cross-section. Kik varied the Iribarren number directly and fitted the Van der Meer-formula to find a value for P, where Van der Meer used damage curves based on multiple measurements with varying wave steepness.

2.1.3 Research by Kluwen (Kluwen, 2012)

In her thesis, Kluwen researched the influence of the thickness of the second filter layer on the notional permeability of a structure. She did so by testing three structures: a structure with the same cross-section as structure 3 of Kik (model 3A), a structure with the same cross-section but a thicker second filter layer (model 4) and a structure with a calculated P-value of 0.45, consisting of an armour layer, filter layer and permeable core (model 5), see Figure 11 for the tested cross-sections.

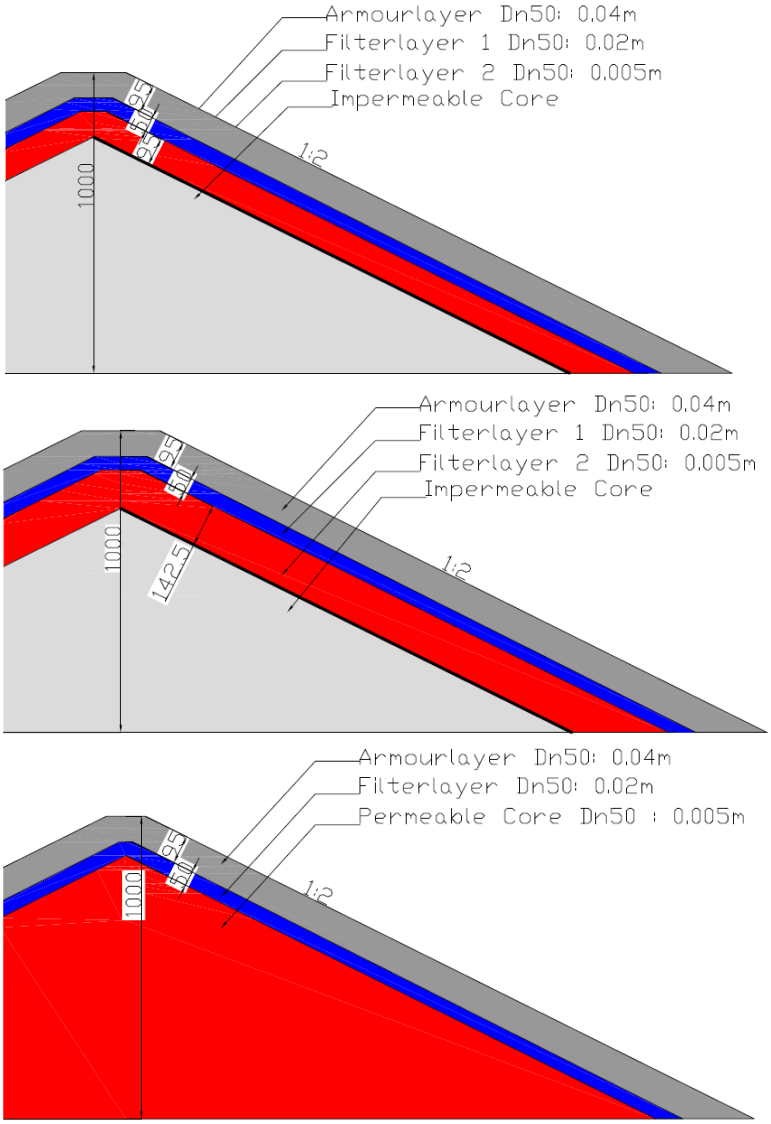

Figure 11 - From top to bottom: model 3A, model 4 and model 5 of Kluwen. (Kluwen, 2012)

A total of 51 tests were performed, see Table 4 for a summary of the test program. The notional permeability, P, is calculated for the structures using the "root mean square equation" as described by Kik. For model 3A (the structure of Kik), a P-value of 0.38 was found. For model 4, the measured damage figures were too low to calculate a value for P. And for model 5, the calculated P-value is 0.45.

Structure	Model 3A	Model 4	Model 5
H_s	0.12	0.08 - 0.16	0.08 – 0.16
T_m	1.10 – 4.90	1.30, 1.70, 2.15, 3.00	1.30, 1.70, 2.15, 3.00
Steepness	0.32% - 6.36%	0.57% - 6.07%	0.57% - 6.07%
ξ_m	1.98 – 8.83	2.03 – 6.62	2.03 – 6.62
$\cot\alpha$	2	2	2
Δ	1.62	1.62	1.62
N	3000	3000	3000
D_{n50}	0.04	0.04	0.04

Table 4 - Test program of tests by (Kluwen, 2012)

2.1.4 Research by Van der Neut (Van der Neut, 2015)

Van der Neut performed research to create a better understanding of the physical processes behind the notional permeability by analysing the results of some of the original physical model tests of (Van der Meer, 1988) using the numerical model IH-2VOF. IH-2VOF gives the pressures and velocities inside the structure as output. Based on literature, a hypothesis was made about the variables on which the notional permeability is dependent. These variables are transformed in four dimensionless Π terms, using the Buckingham Π theorem. These four dimensionless Π terms are:

- $\Pi_1 = \frac{u}{ngT}$ (=Acceleration parameter)
- $\Pi_2 = \frac{n^2\Delta p}{\rho u^2}$ (= Euler number)
- $\Pi_3 = \frac{uT}{nD}$ (= Keulegan-Carpenter number)
- $\Pi_4 = \frac{uD}{\nu(1-n)}$ (= Reynolds number)

In the research the Π terms are measured at three locations along the slope: $2.5\ H_s$ below the initial water level, $1.5\ H_s$ below the initial water level and $0.5\ H_s$ below the initial water level. The calculations for the Π terms are done in four directions: the horizontal (x), the vertical (y) and normal and parallel to the slope, see Figure 12.

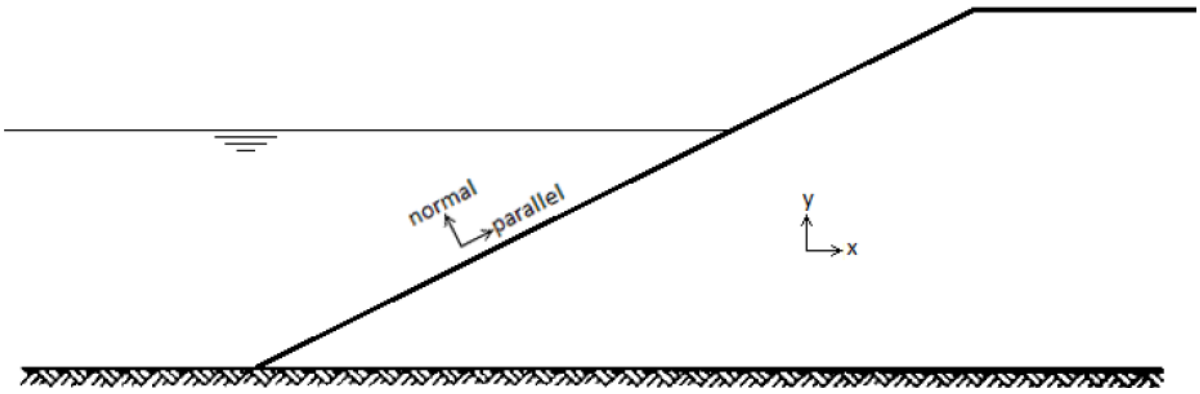

Figure 12 – Coordinate systems of Van der Neut. (Van der Neut, 2015)

In the research it is concluded that the Π terms are best measured $0.5\ H_s$ below the initial water level, inside the armour layer and in a normal direction to the front slope of the structure. In this case all four Π terms show a positive correlation with P.

These correlations are translated to functional relationships, based on curve fitting of the achieved data, where the P-values is allowed to vary under different hydraulic conditions. There is a functional relationship for every Π term:

$$P = 3.1 \cdot 10^2 \left| \frac{u_{\perp,min}}{ngT_{u_\perp}} \right|^{1.6} \tag{3}$$

$$P = 4.1 \cdot 10^7 \left| \frac{n^2}{\rho} \left(\frac{\Delta p}{u^2} \right)_{\perp,min} \right|^{11.2} \tag{4}$$

$$P = 0.1 \left| \frac{u_{\perp,min} T_{u_\perp}}{nD} \right|^{0.9} \tag{5}$$

$$P = 7.2 \cdot 10^{-5} \left| \frac{u_{\perp,min} D}{\nu(1-n)} \right|^{1.1} \tag{6}$$

The standard deviations for all the separate predictions of P is 0.18, which is quite significant. The accuracy of these predictions is likely to improve when more data points are added. This means that in order to improve the accuracy of the predictions, one or more intermediate structures have to be physically tested and the method described in the thesis of (Van der Neut, 2015) has to be repeated.

In his conclusions, Van der Neut stated that P has a large influence on the armour layer stability and that P is not only dependent on structural parameters, but on hydraulic parameters as well. Furthermore, he stresses that P should be used as a variable for optimal damage prediction and should vary under different hydraulic conditions.

2.1.5 Research by Franken (Franken, 2016)

Franken investigated methods for the prediction of P based on the flow of water into the core and the reflection coefficient of the structure. He used the numerical model IH-2VOF to determine this flow of water into the core and the reflection coefficient for a range of structures for varying wave conditions. Predictions of P are made using linear interpolation between structures with known P-values. A total of 12 structures are simulated with IH-2VOF for 8 different wave conditions per structure (4 different regular wave spectra and 4 different irregular wave spectra). The flow of water into the core could only be calculated for regular waves, while the reflection coefficient was calculated for both regular as irregular waves.

Franken concluded that linear interpolation between known P-structures yields accurate results for prediction of P based on the flow of water into the core. In the prediction of P using the reflection coefficient, a spread in outcomes is noticed. In some cases, this spread caused the interpolation to fail and thus no P-value could be predicted. Franken stated that the choice of wave periods has a small influence on the predictions. Interpolation using the flow of water into the core gives more robust results (a clearer trend and less scatter) compared to interpolation using the reflection coefficient. Furthermore, Franken found out that the prediction of P followed an expected trend for varying the thickness and filter stone diameter of the second filter (the layer between the filter layer and an impermeable core). For an increase in thicknesses and an increase in filter stone diameter, P increases as well, see Figure 13 and Figure 14.

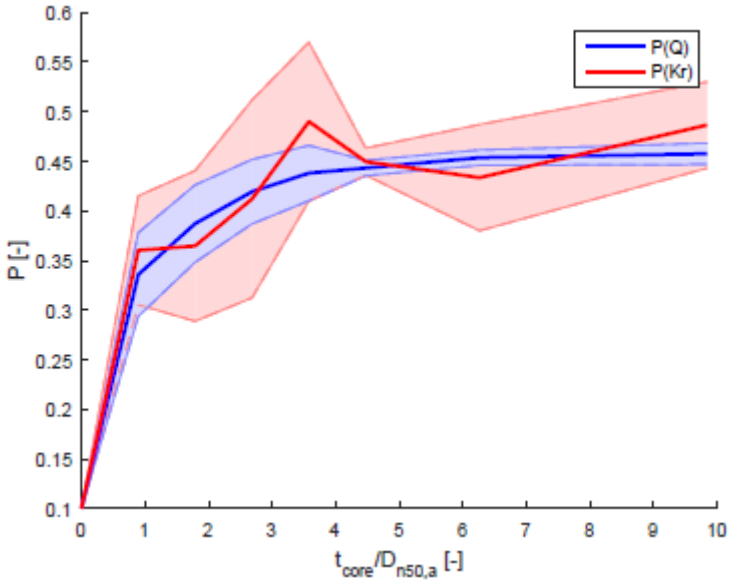

Figure 13 - Relation of P with the thickness of the second filter layer (t_{core} in the plot). (Franken, 2016)

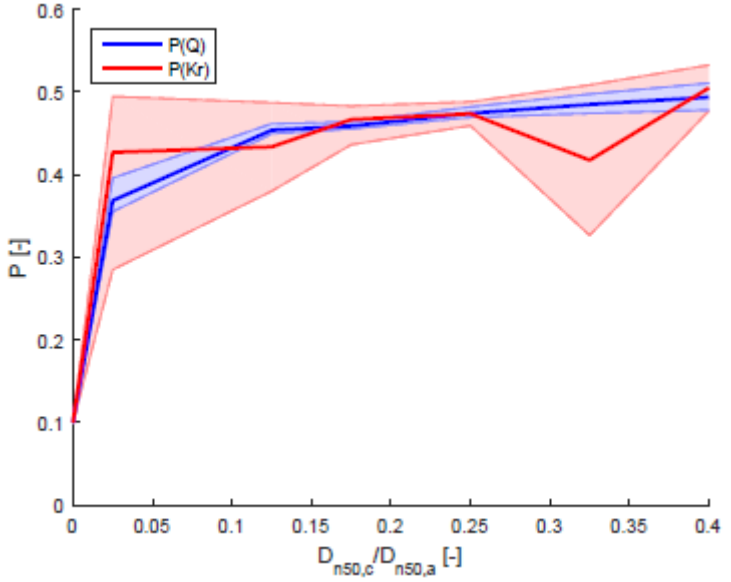

Figure 14 - Relation of P with the filter stone diameter of the second filter layer ($D_{n50,c}$ in the plot). (Franken, 2016)

A general relation for P as a function of the thickness of the second filter layer and the diameter of the armour stones and the filter stones of the second filter layer is found:

$$P = 0.1 + 0.3\left(\frac{D_{n50,f2}}{D_{n50,a}}\right)^{0.15}\left(\log\left(\frac{t_{f2}}{D_{n50,a}} + 1\right)\right)^{0.3} \quad (7)$$

Furthermore, Franken stated that variations in the porous media input parameters (n, α, β and γ) for the second filter layer of the structure have little influence on the flow into the core and the reflection coefficient, and thus on P.

2.2 General related literature

2.2.1 Waves2Foam / OpenFoam in general

In this thesis the numerical model of OpenFoam is used. OpenFoam is an open-source computational fluid dynamics (CFD) library and contains, amongst others, a method for solving free surface Newtonian flows. It does so by using the Reynolds averaged Navier-Stokes equations coupled with a volume of fluid method. In (Jacobsen et al., 2012) a generic wave generation an absorption method is described and demonstrated.

The governing equations for the combined flow of air and water are the Reynolds averaged Navies-Stokes (RANS) equations, equation (8), coupled with the continuity equation for incompressible flows (the volume of fluid method / VOF), equation (9).

$$\frac{\partial \rho \mathbf{u}}{\partial t} + \nabla \cdot [\rho \mathbf{u}\mathbf{u}^{\mathrm{T}}] = -\nabla p^{*} - \mathbf{g} \cdot \mathbf{x} \nabla \rho + \nabla \cdot [\mu \nabla \mathbf{u} + \rho \boldsymbol{\tau}] + \sigma_T \kappa_\gamma \nabla \gamma \tag{8}$$

$$\nabla \cdot \mathbf{u} = 0 \tag{9}$$

In these formulas, $\boldsymbol{\tau}$ is the specific Reynolds stress tensor as defined in equation (10) and $\nabla = (\partial/\partial x,\ \partial/\partial y,\ \partial/\partial z)^T$.

$$\boldsymbol{\tau} = \frac{2}{\rho}\mu_t \mathbf{S} - \frac{2}{3} k \mathbf{I} \tag{10}$$

The equations are solved simultaneously for the water and the air in the numerical model, where the fluids are tracked using a scalar field γ. $\gamma = 0$ means that the cell consists of air and $\gamma = 1$ means that the cell consists of water. For intermediate values for γ, the cell consists of a mixture of water and air. The distribution of γ is modelled by the advection equation:

$$\frac{\partial \gamma}{\partial t} + \nabla \cdot [\mathbf{u}\gamma] + \nabla \cdot [\mathbf{u}_{\mathrm{r}} \gamma (1-\gamma)] = 0 \tag{11}$$

Using γ, the spatial variation in any fluid property can be expresses through the weighting:

$$\Phi = \gamma \Phi_{water} + (1-\gamma)\Phi_{air} \tag{12}$$

Where Φ can be any fluid property. Turbulence becomes important in case of wave breaking and in that case is modelled using a $k-\omega$ closure model as described in (Jacobsen et al., 2012).

In this thesis, porous structures are modelled in OpenFoam and for these porous structures resistance coefficients are used based on the Darcy-Forchheimer flow resistance, see also section 2.2.4. As pointed out in (Jensen, Jacobsen, & Christensen, 2014) and (Jacobsen, van Gent, & Wolters, 2015), the resistance coefficients obtained in e.g. the work by (Van Gent, 1995) describe the bulk resistance over the permeable structure. In this bulk resistance, all dissipative effects are included, so also turbulence. This means that including a turbulence model in the numerical simulation will cause dual dissipation in the porous structures unless the resistance coefficients are modified, which is outside the scope of this thesis. Therefore, no turbulence model is applied in the numerical simulations.

2.2.2 Coupling OceanWave3D with OpenFoam

The waves used in the simulations in this thesis are computed with the fully nonlinear potential wave solver OceanWave3D (Engsig-Karup, Bingham, & Lindberg, 2009) and are one-way coupled to OpenFoam/waves2Foam (Jacobsen et al., 2012) through the interface described in (Paulsen, Bredmose, & Bingham, 2014).

This interface is a relaxation zone where the target solution, ψ_{target}, is given by the potential flow solver. In the relaxation zone, the velocity field, ($\boldsymbol{u}_H$,w), and the water volume fraction, γ, are at each step updated according to formula (13):

$$\psi = (1-\chi)\psi_{target} + \chi\psi_{com}, \qquad \psi \in \{\boldsymbol{u}_H, w, \gamma\} \tag{13}$$

The parameter, ψ_{com}, is the numerically computed quantities modelled by OpenFoam. The weight factor, χ, is defined by equation (14):

$$\chi(\xi) = 1 - \frac{\exp(\xi^{\beta}) - 1}{\exp(1) - 1} \tag{14}$$

Where $\xi \in [0; 1]$ is a local coordinate, which is zero at the OpenFoam side of the relaxation zone and one at the side away form the OpenFoam domain. β, is a shape factor in this case and is set to $\beta = 3.5$ by default. The inner domain (OpenFoam domain) has more grid cells in vertical direction than the outer domain (OceanWave3D domain), therefore does the value from χ_{target} have to interpolated onto the grid of the inner domain.

2.2.3 Damage profile of the armour layer of a breakwater

The damage profile of the armour layer of a breakwater due to wave loading is S-shaped, see Figure 15. This damage profile is an equilibrium profile after an n number of waves (normally 1000 to 3000 waves). It is not known what the location is of the first armour stone that is eroded, with other words: it is not known where the erosion of the armour layer starts. E.g. it could be that the erosion starts in the top part of the erosion area and progresses downwards, or that the erosion starts in the bottom part of the erosion area and progresses upwards. However, it could also be that the erosions starts right in the middle of the erosion area and progresses in both directions (upwards and downwards).

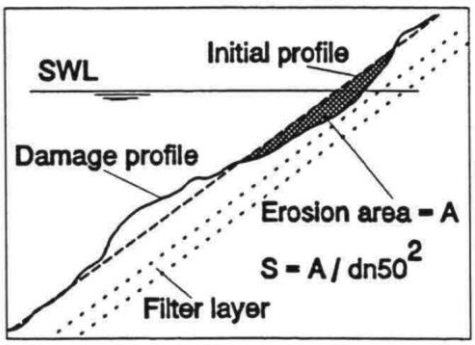

Figure 15 – Damage profile due to wave loading. (Schiereck & Verhagen, 2016)

(Hofland et al., 2017) studied the armour damage with physical model testing. A breakwater with a slope of 1:2 was loaded with 1000 irregular waves after which the damage profile was measured. The results of two of the test series is shown in Figure 16. From these results it

can be seen that the erosion area is from approximately minus 1.5 significant wave height below the still water level up till at least 1 significant wave height above the still water level.

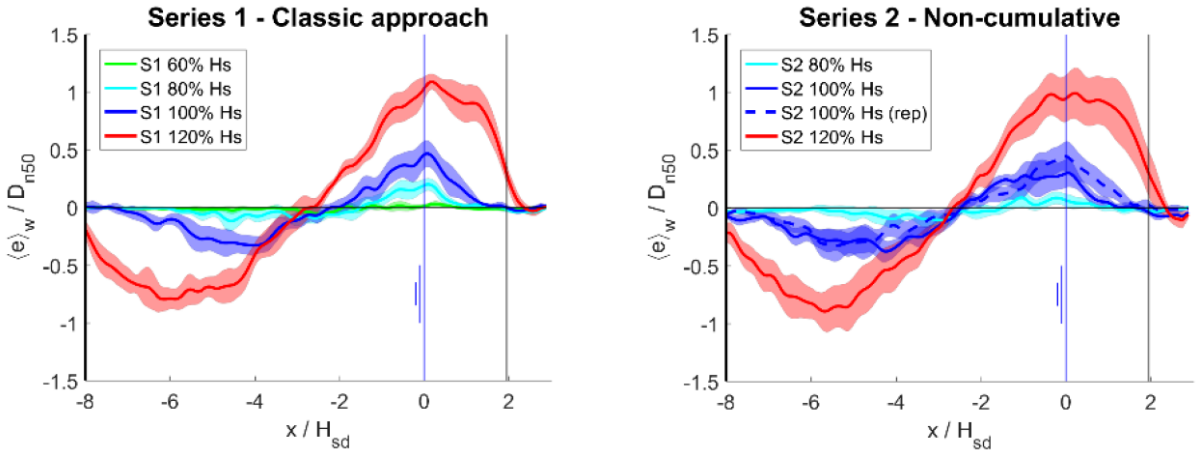

Figure 16 – Width-averaged erosion profile for the first two test series with confidence band. x is the horizontal cross-shore coordinate, with its origin at the waterline. (Hofland et al., 2017)

2.2.4 Forchheimer equation, parameters and KC-value

Porous flow through a porous layer is described by the extended Forchheimer formula, as defined by (Van Gent, 1993):

$$i = \frac{1}{\rho g}\frac{\partial p}{\partial x} = a u_f + b u_f |u_f| + c\frac{\partial u_f}{\partial t} \tag{15}$$

Where a, b and c are the resistance coefficients:

$$a = \alpha \frac{(1-n)^2}{n^3}\frac{\nu}{g\, d_{n50}^2} \tag{16}$$

$$b = \beta\left(1 + \frac{7.5}{KC}\right)\frac{1-n}{n^3}\frac{1}{g\, d_{n50}} \qquad with \quad KC = \frac{u_m T}{n d_{n50}} \tag{17}$$

$$c = \frac{1 + \frac{1-n}{n}\left(0.85 - \frac{0.015}{Ac}\right)}{ng} \qquad with \quad Ac = \frac{u_m}{ngT} > \frac{0.015}{\frac{n}{1-n} + 0.85} \tag{18}$$

Where u_m is the maximum oscillating velocity. The dimensionless coefficients α and β have to be determined experimentally. According to (Schiereck & Verhagen, 2016), values of $\alpha = 1000$ and $\beta = 1.1$ can be used as a first estimate, these values are also proposed by (Van Gent, 1995).

(Jensen et al., 2014) investigated the porous media equations and resistance coefficients for coastal structures. In the research constant values for the resistance coefficients for a broad range of flow conditions were recommended based on new calibrations: $\alpha = 500$ and $\beta = 2.0$.

The relation between measured filter velocity and pressure gradient for various materials is plotted in (Schiereck & Verhagen, 2016), see Figure 17. The graph is double logarithmic and shows that the flow in fine material is laminar since the relation between i and u_f is linear. This means that the relation between the pressure gradient and the velocity is dominated by the first term on the right hand side of equation (15). For rock, the slope is 1:2 on the double logarithmic scale, meaning that the relation between the pressure gradient and the flow velocity is quadratic and that the second term in the right hand side of equation (15) is dominant.

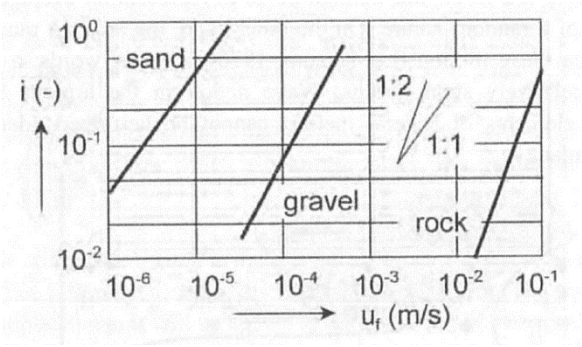

Figure 17 - Relation between filter velocity and gradient for various materials. (Schiereck & Verhagen, 2016)

Since u_m is unknown in the numerical simulations in this thesis, a different approach to determine the Keulegan-Carpenter number (KC-number) has to be used. According to (Jacobsen et al., 2015), a pragmatic approach to calculate the KC-number based on the incident wave field and shallow water theory is:

$$KC = \frac{H_{m0}}{2}\sqrt{\frac{g}{h}}\frac{T_p}{d_{50}} \tag{19}$$

2.2.5 Estimating porosity of a porous layer

One of the properties of the porous layers in a breakwater that has to be modelled is the porosity. In the Rock Manual, (CIRIA, CUR, & CETMEF, 2007), the formulas (20) and (21) are given, which can be used to predict the porosity of a layer of bulk-placed granular material.

$$n = \frac{e}{1+e} \tag{20}$$

$$e = \frac{1}{90}(e_o)\arctan(0.645 n_{RRD}) \tag{21}$$

Where e is the void ratio given by the volume of voids divided by the volume of solids. e_o is the void ratio associated with single-size particles of different shapes, see Table 5. n_{RRD} is the uniformity coefficient which can be calculated for any grading using formula (22).

Shape of fragments	Cube-like	Elongated	Flat	Typical mechanically crushed	Smooth sand and pebbles	Steel balls
Single-size void ratio, e_o	0.88-0.92	0.93-0.96	1.00-1.03	0.92-0.96	0.65-0.80	0.52-0.61

Table 5 – Typical values for the void ratio associated with single-size particles of different shapes. (CIRIA et al., 2007)

$$n_{RRD} = \log\left(\frac{ln(1-y_{NUL})}{ln(1-y_{NLL})}\right)\Big/\log\left({}^{NUL}/_{NLL}\right) \tag{22}$$

2.3 Conclusion of literature study

At this moment there are two methods to predict the notional permeability, the P-value, of a breakwater structure. The first method is described and developed by Van der Neut, section 2.1.4. The standard deviation for the prediction of P with this method is 0.18 which is significant.

The second method is the method developed by Franken, using the flow of water into the core, section 2.1.5. In his thesis, Franken was only able to calculate this flow of water into the core for regular waves. This means that the method using the flow of water into the core is not validated for irregular waves, while in practice breakwaters are always loaded by irregular waves. Franken also developed a method which can be used for irregular waves, using the reflection of the structure. The results of this method showed a lot of scatter, which can be seen in Figure 13 and Figure 14. This spread in outcomes in some cases caused the interpolation to fail and thus no P-value could be predicted.

Franken used interpolation between structures with known P-values to predict the P-value of structures with unknown P-values. It can be concluded that interpolating between structures with known P-values works well, but the accuracy and applicability of the method can be improved by using different parameters for the interpolation. Therefore, new methods will have to be developed using interpolation between structures with known P-values but using different parameters in the interpolation. The parameters used should be hydraulic parameters that influence rock stability in general.

Furthermore, both Franken and Van der Neut used the numerical model of IH2-VOF for their research on the notional permeability. Recently a lot of developments are going on for the simulation of rubble mound structures with OpenFoam, therefore a prediction method using OpenFoam is searched for.

3 Methodology

In this chapter, the methodology of the research is discussed. The research is structured in 4 steps:

1. Desk study to define the hydraulic loading parameters
2. Model validation for the selection of the hydraulic loading parameters
3. Determine prediction method for the notional permeability
4. Sensitivity analysis of the preferred prediction method

Each step will be discussed in their own section below.

3.1 Step I: Desk study to define the hydraulic loading parameters

Step I of the research is to search for hydraulic parameters that influence rock stability in general. The idea is that hydraulic parameters that influence rock stability, might also influence the stability of the armour stones of a breakwater. The search for these parameters is based on different stability concepts for rock stability. These stability concepts are used for different kind of rock structures in water. The found hydraulic parameters are called the hydraulic loading parameters. For every hydraulic loading parameter is checked if OpenFoam is able to simulate the parameter at all. Whether OpenFoam simulates the hydraulic loading parameter correct will be investigated in step II.

3.2 Step II: Model validation for the selection of the hydraulic loading parameters

Step II of the methodology is to investigate whether OpenFoam simulates the hydraulic loading parameters correct. With other words, OpenFoam is validated for simulating the hydraulic loading parameters. This is done by recreating a physical model test performed by Markus Muttray, (Muttray, 2000), in OpenFoam. The physical model tests of Muttray are chosen for the validation since during the tests, one of the hydraulic loading parameters is measured on several locations inside the breakwater and the data of these tests was available. After this chapter it will be concluded which hydraulic loading parameters seem to be simulated correctly in OpenFoam and can be used as a comparison parameter for the prediction of P in step III.

3.3 Step III: Determine prediction method for the notional permeability

Step III is to predict the notional permeability based on the hydraulic loading parameters that are simulated correctly in OpenFoam. The idea is that the notional permeability for the structure of interest is predicted by interpolating the values of the hydraulic loading parameter for the structure of interest between the values for the hydraulic loading parameters of the three structures tested by Van der Meer, since from these three structures the notional permeability is known. To test this prediction method, one of the structures tested by (Kik, 2011) is simulated in OpenFoam, together with the three structures of Van der Meer, in order to see if the notional permeability can be predicted.

Since the simulations will be with irregular waves, the results of the simulations are also irregular. The stability of the armour layer material is largely determined by the biggest and/or longest wave, therefore the maximum simulated values of the hydraulic loading parameters are of interest for the prediction of the notional permeability. However, since the results of the

simulations will be irregular, the maximum values will show some randomness and/or spikiness. Therefore, from the hydraulic loading parameters the 2% exceedance values in time will used to predict the P-values.

The first step of the prediction method (step III.a) is to simulate the three structures tested by Van der Meer with OpenFoam, as well as the structure of interest (with unknown P-value). All structures are simulated for the same hydraulic conditions and with the same numerical parameters, only the structures itself are different in the simulations. In these simulations, a row of pressure probes has to be implemented on the surface of the armour layer and on the interface between the armour layer and the filter layer. The structure of Van der Meer with a notional permeability of 0.6 does not have a filter layer, so there is no interface between the armour layer and the filter layer. In order to calculate and integrate over the hydraulic loading parameters, for the structure of Van der Meer with a P-value of 0.6, the second row of pressure probes is located on the same location with respect to the surface of the front slope as for the other three structures. Every pressure probe along the slope of the armour layer has an accompanying pressure probe on the interface of the filter layer. These pressure probe pairs are positioned such that they can measure flow velocity differences and pressure differences perpendicular to the armour slope.

The second step of the prediction method (step III.b) is to calculate the values for the hydraulic loading parameter for every construction from the results of the OpenFoam simulations. How the values of these hydraulic loading parameters are calculated is explained in chapter 6 and not in this chapter, since the choice on hydraulic loading parameters is depending on the results of step I and step II.

When the values of the hydraulic loading parameter of the structures is known, they are made relative to the biggest of these values. This is the third step of the prediction method (step III.c). The largest value of the hydraulic loading parameter will be for the structure with $P = 0.1$ or $P = 0.6$, depending on what the hydraulic loading parameter is.

The fourth step of the prediction method (step III.d) is to interpolate the relative value of the hydraulic loading parameter of the structure with unknown P-value between the other structures and predict the corresponding P-value. Figure 18 gives a schematic representation of the concept of the prediction method.

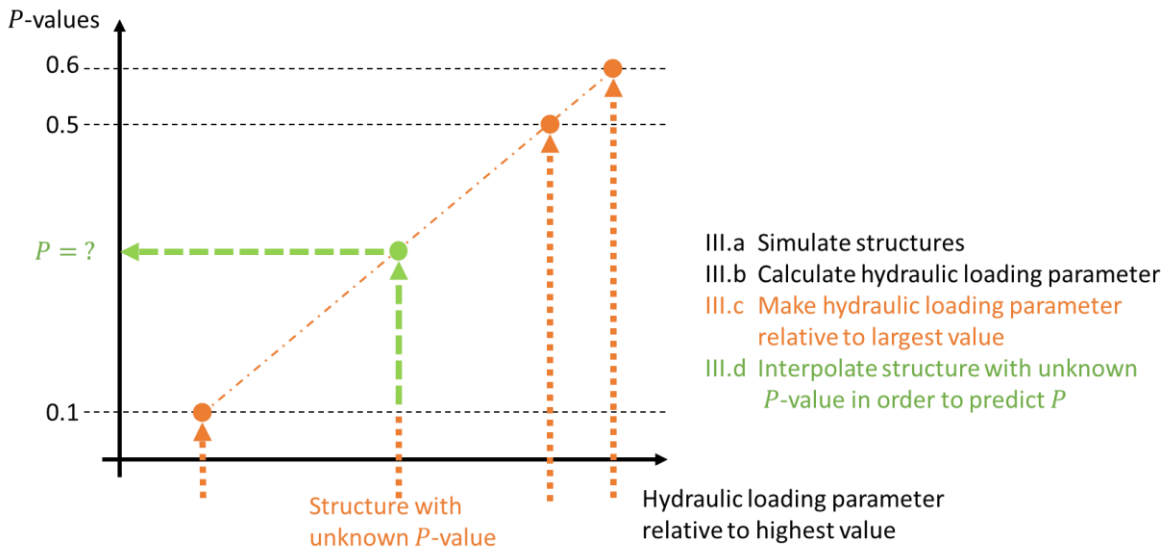

Figure 18 - Concept of the method to predict the notional permeability

At the end of this step, a conclusion is made on which hydraulic loading parameter is best to use for the prediction of the notional permeability of breakwater structures.

3.4 Step IV: Sensitivity analysis of the preferred prediction method

Step IV of the methodology is investigate how sensitive the preferred prediction method is for a change in input parameters. The sensitivity is analysed for a change in the following parameters:

- Wave conditions
- Porosity of the porous layers
- Applied Forchheimer parameters

The wave conditions are changed because both (Van der Neut, 2015) and (Franken, 2016) found that the wave conditions have influence on the notional permeability. Therefore, it is interesting to check the sensitivity of the prediction method on a change in wave conditions. In step III, the steepness of the average wave is 2.4%. In the sensitivity analysis this will be changed to 1.5% and to 5.3%, because all waves occurring in design situations have a steepness between approximately 1% and 5%. The waves with a steepness of 2.4% and 1.5% are surging waves, while the waves with a steepness of 5.3% are plunging waves.

The porosity of the porous layers is changed since the notional permeability represents the permeability of the breakwater structure and the porosity of porous layers for an in-situ breakwater can never be designed or calculated with 100% certainty. The porosity of the porous layers of the structure of Kik in step III are estimated with formula (20) and a rock grading of $d_{85}/d_{15} = 1.5$. This corresponds with a porosity of the porous layers of $n = 0.44$. In the sensitivity analysis, the porosity of all the porous layers is changed to a value of $n = 0.48$ and a value of $n = 0.40$, corresponding to a rock grading of respectively $d_{85}/d_{15} =$ close to 1 and $d_{85}/d_{15} \approx 2.25$. Also the porosity of the porous layers of the structures of Van der Meer are varied, since for these structures the exact porosity is not known, only the rock grading, but the porosity is dependent on more than just the rock grading.

The applied Forchheimer parameters are varied since different values for these parameters are given in various literature pieces but the influence of changing the Forchheimer parameters on the hydraulic loading parameters is not yet investigated. The applied Forchheimer parameters in step III are the Forchheimer parameters advised by (Van Gent, 1995): $\alpha = 1000$ and $\beta = 1.1$. In the sensitivity analysis these values are changed to the values advised by (Jensen et al., 2014): $\alpha = 500$ and $\beta = 2.0$.

3.5 Proposed engineering approach

After the four steps, there is proposed how the prediction method can be applied in the design process of a breakwater: a so-called engineering approach.

4 Step I: Desk study to define the hydraulic loading parameters

In this chapter, different stability concepts for rock stability are discussed and parameters that might be interesting to use as a hydraulic loading parameter in the prediction of the notional permeability are selected. The first paragraph of this section gives an introduction to the different stability concepts, the following paragraphs each elaborate on one of these stability concepts. The last paragraph holds a summary of the possible parameters on which the stability concepts are based and a selection of the parameters that might be interesting to use as hydraulic loading parameter for the prediction of the notional permeability.

4.1 Introduction to stability concepts

There are different stability concepts for structural response to hydraulic loading. The stability concepts taken into account in this chapter are all described in (CIRIA et al., 2007). The following hydraulic loading variables and parameters can be used to practically describe the structural response of armour stones in breakwaters and form the basis for these stability concepts:

- Specific discharge, q, across a structure ($m^3/s\,per\,m$)
- Shear stress, τ (N/m^2), or non-dimensional shear stress, ψ (–), or the shear velocity, u_* (m/s)
- Velocity, either depth-averaged, U, or local, u (m/s)
- (differences in) water level, h, or head, H (m)
- Wave height, H, e.g. the significant wave height, H_s, in front of a breakwater (m)

As stated in (CIRIA et al., 2007), the viscous forces on the particle surface can be neglected for coarse sediments. This means that the viscous forces can be ignored for armour stones, since these are way bigger than coarse sediment.

The resistance of the armour stones regarding stability comes from the variables:

- Characteristic size or diameter of the stone, D, the nominal diameter, D_n, or the median nominal diameter, D_{n50} of the armourstone (m)
- Relative buoyant density of rock, Δ (–), which is defined as:

$$\Delta = \frac{\rho_r - \rho_w}{\rho_w} = \frac{\rho_r}{\rho_w} - 1 \tag{23}$$

In which:

ρ_r = Apparent mass density of the rock $[kg/m^3]$
ρ_w = Mass density of water $[kg/m^3]$

The apparent mass density of rock is the mass density of rock that may have water in its pores, so like it is used in hydraulic structures. According to (CIRIA et al., 2007), the layer porosity, n_v (–), as well as the permeability of the rock structure are also resistance parameters that play a role in the structural response to waves and currents but to a lesser extent. Often, the loading and resistance parameters are combined in non-dimensional numbers (e.g. Shields parameters, Izbash parameters, Stability number).

There are two basic stability concepts: the critical shear stability concept and the critical velocity concept. From these two stability concepts, other criteria can be derived in terms of mobility or stability numbers. Table 6 shows an overview of the various stability concepts and the relation with structure types and stability formulae for design.

Stability Concept	Stability parameter	Structure types
Velocity	Izbash number, $U^2/(2g\Delta D)$	Bed and bank protection, near-bed structures, toe and scour protection
Shear stress	Shields parameter, ψ_{cr}	Bed and bank protection, spillways and outlets, rockfill closure dams
Hydraulic head	$H/(\Delta D)$	Dams, sills, weirs
Discharge	$q/\sqrt{[g(\Delta D)^3]}$	Rockfill closure dams, sills, weirs
Wave height	Stability number, $H_s/(\Delta D)$	Rock armour layers, concrete armour layers, toe and scour protection

Table 6 - Stability concepts and the relation with structure types and stability formulae for design (CIRIA et al., 2007)

Every stability concept is discussed in their own section below.

4.2 Velocity stability concept

The velocity stability concept is the simplest concept and is the most straightforward: the initiation of motion of material occurs when the flow velocity exceeds the critical flow velocity. However, selection of a proper representative velocity is key for this stability concept. When the velocity stability design concept is used, normally the depth averaged velocity, U, is used. For the application of the velocity stability concept on the design of breakwater armour stability, it is quite hard to determine the depth-averaged velocity above the armour layer, especially since the flow velocity is not expected to have a logarithmic fully developed flow profile. However, with the use of OpenFoam, the local flow velocity above the armour stones can be determined, which can be linked to a critical flow velocity above the armour layer. It is however not yet known how well OpenFoam calculates these values, nor is this critical flow velocity known. Besides, the existing formulae that are based on the velocity stability concept, are all empirical formulae and are not suitable for the case of flow velocities due to wave run-up or run-down. Although the existing formulas are not suitable for determining the stability of armour stones of a breakwater under wave loading, there is a clear link between armour stone stability and the occurring maximum flow velocity.

4.3 Shear stress stability concept

The shear stress concept works with the basic grain mechanisms. When the occurring shear stress, due to an unidirectionally steady flow, is higher than the critical shear stress, the motion of material is initiated. The occurring shear stress and the critical shear stress are represented by the Shields parameter, ψ, and the critical Shields parameter, ψ_{cr}.

For this concept, the velocity profile on top of the stones has to be transferred into shear stress. For stationary unidirectional flow with developed turbulance, this can be done using equation (24):

$$\tau_c = \rho_w g \frac{U^2}{C^2} \tag{24}$$

In which:

U = The depth-averaged current velocity $[m/s]$

The shear stress can be written in non-dimensional form, ψ, using formula (25):

$$\psi = \frac{\tau}{(\rho_r - \rho_w)gD} \tag{25}$$

To use these equations in case of wave attack perpendicular to a slope (like for a breakwater), a correction factor for wave run-up and run-down has to be applied. For a description of these factors and how to calculate them is referred to page 550 of the rock manual, (CIRIA et al., 2007).

Unfortunately, the wave run-up and run-down cannot be regarded as an unidirectional flow. (Komar & Miller, 1974) showed that if the shear stress for oscillatory flow due to waves is calculated using the concept of the wave friction factor according to (Jonsson, 1966), the initial motion in unsteady flow is in reasonable agreement with the Shields curve for unidirectional flow. However, the wave run-up and run-down is also not an oscillatory movement, it is more an irregular movement. Determining the shear stress for irregular flow is not possible and the model OpenFoam is also not able to determine the shear stresses, only the flow velocities. There clearly is a link between the shear stress and the flow velocities, and there is also clearly a link between shear stress and rock stability. Therefore it is assumed that, based on the shear stress stability concept, the flow velocities right above the armour layer might be interesting to use as comparative quantity for the prediction of the notional permeability.

4.4 Hydraulic head stability concept

The hydraulic head stability concept uses a stability factor based on the head difference. It is normally only used for dams, sills and weirs, where a water level difference is present. The hydraulic head stability criterion for through-flow dams is empirically determined by (Prajapati, 1981) to be:

$$\frac{H}{\Delta D_{n50}} = 2.78 + 0.71\frac{h_b}{\Delta D_{n50}} \tag{26}$$

In which:

H = Upstream water level relative to dam crest ($H < 0$ for through-flow) $[m]$

h_b = Tailwater depth downstream of dam or sill, relative to dam crest ($h_b < 0$ when below dam crest) see Figure 19 $[m]$

This stability concept is not directly applicable to a breakwater under wave loading. However, it is clear that there is a relation between the head difference between the inside and the outside of a structure and the stability of the armour layer. There clearly is a link between head difference, or pressure difference, and armour stone stability. Therefore it is assumed that, based on the hydraulic head stability concept, the head difference over the armour layer might be interesting to use as comparative quantity for the prediction of the notional permeability based on the hydraulic head stability concept.

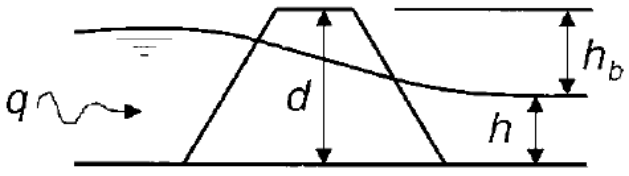

Figure 19 - Definition of parameters h_b and h

4.5 Discharge stability concept

The critical discharge stability concept links the stability of an armour layer with the flow of water through an armour layer (in outward direction). It is normally only used for dams, sills and weirs, where the flow through the structure is caused by a water level difference. So basically it is an variation on the hydraulic head stability concept. (Prajapati, 1981) investigated the discharge stability concept for flow through porous dams and found the following empirical relationship:

$$\frac{q}{\sqrt{g(\Delta D_{n50})^3}} = 0.55\left(\frac{h}{\Delta D_{n50}}\right)^{0.32} \tag{27}$$

In which:

q = Total discharge through the dam $[m^3/s/m]$

h = Actual tailwater depth, see Figure 19 $[m]$

This stability concept is not directly applicable to a breakwater under wave loading. However, it is clear that there is a relation between the discharge of water from the inside of a structure towards the outside and the stability of the armour layer. Therefore it is assumed that, based on the discharge stability concept, the discharge of water through the armour layer can be used as comparative quantity for the prediction of the notional permeability.

4.6 Wave height stability concept

The wave height stability concept is based on a stability number:

$$N_s = \frac{H_s}{\Delta D_{n50}} \leq K_1^a K_2^b K_3^c \ldots \tag{28}$$

In which:

N_s = Stability number $[-]$

H_s = Significant wave height $[m]$

K_1^a, K_2^b, K_3^c, etc = Factors depending on all kind of parameters influencing the stability $[-]$

The factors in the right hand side of equation (28) have been researched extensively, with a couple of empirical relationships as a result. As already discussed in section 1.1 of the introduction, the most common used empirical formulas are the formula of Hudson (Hudson, 1959) and the formulas of Van der Meer (Van der Meer, 1988). The porosity and packing density of the rock is not included in these formulas, although these parameters might influence the armour stability. A lower porosity might lead to a higher stability, but a higher porosity might also lead to a higher stability, due to an increase in energy dissipation in the armour layer. However, a higher porosity might also lead to a lower stability due to the reduction in interlocking and/or friction between the rocks. The formula of Van der Meer is discussed in more detail in section 2.1.1. Since the existing design formulas for armour stability of rubble mound breakwaters (which include the notional permeability) are all based on the wave height stability concept and the significant wave height is an input parameter in OpenFoam, no comparative quantity for prediction of the notional permeability based on this stability concept is found.

4.7 Summary of stability concepts and selection of hydraulic loading parameters

To summarize, the studied stability concepts and the resulting possible interesting comparative quantities for prediction of the notional permeability based on these stability concepts are shown in Table 7.

Stability concept	Comparative quantity
Velocity	Flow velocity on top of the armour stones, $u_{\parallel}$
Shear stress	Flow velocity on top of the armour stones, $u_{\parallel}$
Hydraulic head	Water pressure difference $\Delta p_{\perp}$, or head difference over the armour layer
Discharge	Discharge through armour layer (in outward direction), $q_{\perp}$
Wave height	None

Table 7 - Stability concepts and the resulting possible interesting comparative quantities for prediction of the notional permeability based on these stability concepts

As can be seen in Table 7, there are three comparative quantities that might be interesting for the prediction of the notional permeability:

- The wave induced water pressure difference over the armour layer, $\Delta p_{\perp}$
- The discharge through the armour layer perpendicular to the front slope, $q_{\perp}$ or $Q_{\perp}$
- The flow velocity on top of the armour stones (parallel to the slope), $u_{\parallel}$

These comparative quantities are called the three hydraulic loading parameters. In the next chapter, OpenFoam is validated for the simulation of these hydraulic loading parameters.

5 Step II: Model validation

5.1 Introduction

In this chapter validation simulations are conducted with OpenFoam. The goal of this validation is to see which of the selected hydraulic loading parameters (as described in the previous chapter) can be simulated correctly in OpenFoam. The simulation of the hydraulic loading parameter with OpenFoam is checked by simulating a physical model test in OpenFoam and compare the results of these two tests. The physical model test which is simulated is a test performed by Muttray, (Muttray, 2000). Muttray tested a breakwater structure for several wave conditions. He measured the wave run-up along the front slope of the structure and the wave induced water pressure on several locations inside the structure and on the front slope of the structure. For details on the tests of Muttray (amongst others: the model set-up, type of measurements, test program, etc), please refer to Appendix A.

5.2 Numerical model set-up

The structure which is modelled in OpenFoam is shown in Figure 20. The structure is modelled on a sloping foreshore of 1:50. The parameters of the porous layers of the structure are shown in Table 8. When possible, the applied parameters are set to the same values as used in the physical model tests by Muttray. The structure in the physical model test had an armour layer which consisted of concrete elements, Accropodes. In OpenFoam it is not possible (and not necessary) to define whether a porous layer is made out of rocks or concrete elements. All the relevant parameters of the Accropodes (like the porosity of the armour layer, the equivalent armour stone diameter, D_{eq}, and the values for the α, β and γ parameters were given by (Muttray, 2000)). Two changes are made in the schematization of the structure in the numerical model: the numerical model does not have a crown wall element and the connection between the toe structure and the armour layer is slightly different. These changes were made due to local numerical stability issues and have no influence on the results off the simulation, see Appendix A and Appendix B. Furthermore, from the toe structure of the physical model test, only the d_{50} was given in (Muttray, 2000). For the porosity, γ, α and β-values of the toe structure the same values as those for the armour layer are taken.

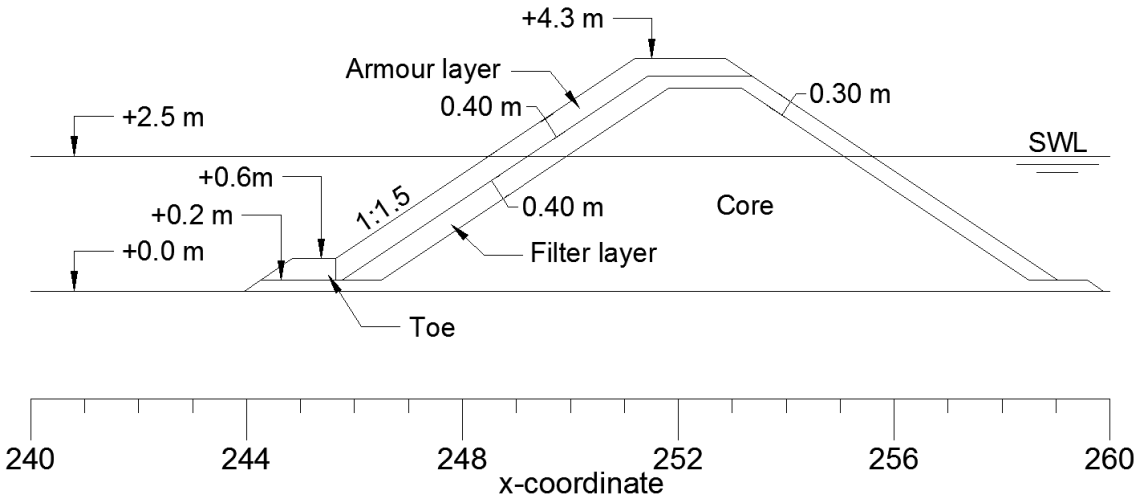

Figure 20 - Schematic cross-section of the breakwater construction modelled in OpenFoam

Porous layer:	Porosity	KC-value	γ-value	d_{50}	α	β
Armour layer	0.510	23.78	0.52	0.257	305.0	1.27
Filter layer	0.394	67.91	0.43	0.090	305.0	1.27
Core	0.388	197.15	0.00	0.031	1007.0	0.63
Toe	0.510	20.37	0.52	0.300	305.0	1.27

Table 8 - Porous layer parameters used in OpenFoam model

The water depth is $4.5\,m$ in front of the foreshore and $2.5\,m$ on top of the foreshore. The incoming waves are regular waves with a wave height of $0.85\,m$ and a wave period of $6.0\,s$. This corresponds to a wave length of $36.51\,m$ in the deep part and a wave length of $28.32\,m$ on top of the foreshore. The incoming waves have an Iribarren number of $\xi = 4.37$, thus the incoming waves are surging. The waves are computed with OceanWave3D and are coupled to OpenFoam/waves2Foam as described in section 2.2.2.

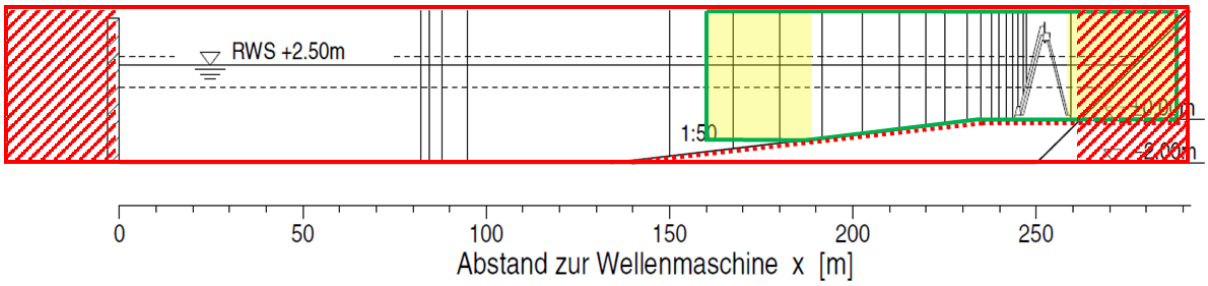

Figure 21 - Domain of the OceanWave3D model (red box) and the OpenFoam model (green box)

Figure 21 shows the domain of the OceanWave3D model and the OpenFoam Model. The domain of the OceanWave3D model is shown in red. The red hatched areas are the wave generation zone (left) and the pressure dampening zone (right) in OceanWave3D and the red dashed line is the bottom profile implemented in OceanWave3D to mimic the foreshore. The domain of the OpenFoam model is shown in green. The yellow boxes show the relaxation zones of the OpenFoam model. The wave generation zone, pressure dampening zone and relaxation zones all have the same length of $30\,m$, which is approximately equal to one wavelength.

The OceanWave3D simulation only has a grid size in x-direction and a number of layers in y-direction. The number of vertical layers is kept to the default value of 9 layers. According to (26th ITTC Specialist Committee on CFD in Marine Hydronamics, 2011), at least 40 grid cells are required to resolve the shortest wave length (at least 20 grid points for irregular waves). This results in a maximum grid size in x-direction, Δx, of $0.71\,m$. According to (Bingham & Zhang, 2007), a resolution of 15 – 20 grid cells per wavelength are adequate for general purpose applications. This results in a maximum grid size in x-direction, Δx, of $1.89 - 1.42\,m$. Since the OceanWave3D calculation is not computational demanding, a grid size of $\Delta x = 0.5\,m$ is chosen for the OceanWave3D part of the simulation.

The OpenFoam simulation has a 2D grid, so the grid size in both x-direction, Δx, as well as in y-direction, Δy, has to be chosen. Again, the maximum grid size in x-direction is, depending on which literature is followed, between $0.71\,m$ and $1.89\,m$. However, according to (26th ITTC Specialist Committee on CFD in Marine Hydronamics, 2011), an orthogonal grid should be used to resolve a free surface, with other words, the aspect ratio $\left(\frac{\Delta x}{\Delta y}\right)$ should be 1. This means that the maximum grid size in y-direction is normative.

According to (26th ITTC Specialist Committee on CFD in Marine Hydronamics, 2011), no less than 20 grid points in vertical direction should be used where the free surface is expected. With other words, the maximum grid size in y-direction, Δy, should be smaller than $\frac{H}{20}$. This results in a grid size in y-direction of $\Delta y \leq \frac{0.85}{20} = 0.0425\ m$. Since the grid should be orthogonal, a grid size of $\Delta x = \Delta y = 0.04\ m$ is used as a start in the OpenFoam domain.

As can be seen in Figure 21, the domain of the OpenFoam model is not rectangular, due to the sloping foreshore. The connection of the OpenFoam model with the OceanWave3D model is positioned halfway the slope (approximately 1 wavelength in front of the crest of the foreshore) and is positioned horizontally, while the bottom of the flume is sloped. This was the result of one of the optimizations of the OpenFoam model, see Appendix A and Appendix B. Another result of this optimization was the use of a grid which is varying in size. Along the part of the OpenFoam domain where the bottom is sloping upwards, the grid changes in size from a grid with $\Delta y = \Delta x = 0.04\ m$ towards a grid with $\Delta y = \Delta x \approx 0.035\ m$. A schematization of how such a grid looks like is given in Figure 22. It is clear that the cells are becoming skewed on the sloping part of the breakwater. In practice, this skewness is limited (it is exaggerated in Figure 22). This skewness does not have influence on the model results, see Appendix B. Table 9 shows the used grid sizes and the number of grid cells per wave length or wave height.

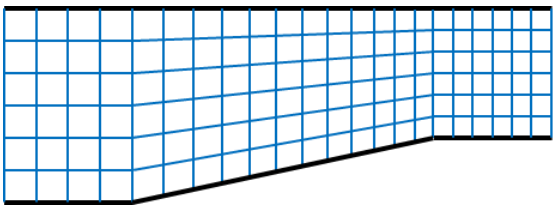

Figure 22 - grid schematization of varying grid size along sloping part of domain

Model	$\Delta x\ [m]$	Grid cells per L_0	Grid cells per L close to the structure	$\Delta y\ [m]$	Grid cells per H
OceanWave3D	0.5	73	57	–	–
OpenFoam	0.040 – 0.035	913	809	0.040 – 0.035	21 – 24

Table 9 – Grid sizes and number of grid cells per wave length or wave height.

To compare the measurements of the physical model tests with the results from the OpenFoam simulations, a number of measurement instruments is set-up in the numerical model. A total of 19 wave gauges is included in the OpenFoam model, these wave gauges are positioned on the same locations in the numerical flume as there were wave gauges in the physical model tests. These locations are both in front of the structure, in the structure and behind the structure. Besides these wave gauges, a total of 34 pressure probes are installed inside the breakwater structure. Again, the locations of the pressure probes correspond with the locations of pressure probes in the physical model test, see Figure 29 in section 5.3.5 for the global location of these pressure probes. Furthermore, three wave run-up gauges are installed in the OpenFoam model: one on top of the armour layer, one on top of the filter layer and one just beneath the filter layer. For more information on the set up of the numerical model and the exact location of the wave gauges, pressure probes and wave run-up gauges, see Appendix A.

5.3 Results

The results of the model validation are divided in six parts: a spectrum analysis, a reflection analysis, comparison of the wave gauges, comparison of the wave run-up, comparison of the measured pressures and comparison of the pressure lines. The first three parts, the spectrum analysis, reflection analysis and wave gauge comparison, are to check whether the test is reproduced correctly. The last three parts, the comparison of the wave run-up, comparison of the measured pressures and comparison of the pressure lines, are to see which hydraulic loading parameters are modelled correct in OpenFoam. The most important results are summarized in this chapter, for the full results is referred to Appendix A.

5.3.1 Spectrum analysis

For both the OpenFoam simulation and the measurements of (Muttray, 2000), a variance density spectrum of the waves is created. The spectrum can be created for every wave gauge but is mostly only interesting for locations in front of the breakwater structure. All spectra in front of the structure are quite similar and show the same comparison, therefore only one spectrum is shown in this chapter, see Figure 23. The peaks of the two spectra can be found for the same frequencies, which indicate that the waves are modelled correctly in the numerical model. For a full analysis of the spectrum is referred to Appendix A. From the spectrum analysis it can be concluded that the incoming waves of the physical model test are simulated correctly in OpenFoam.

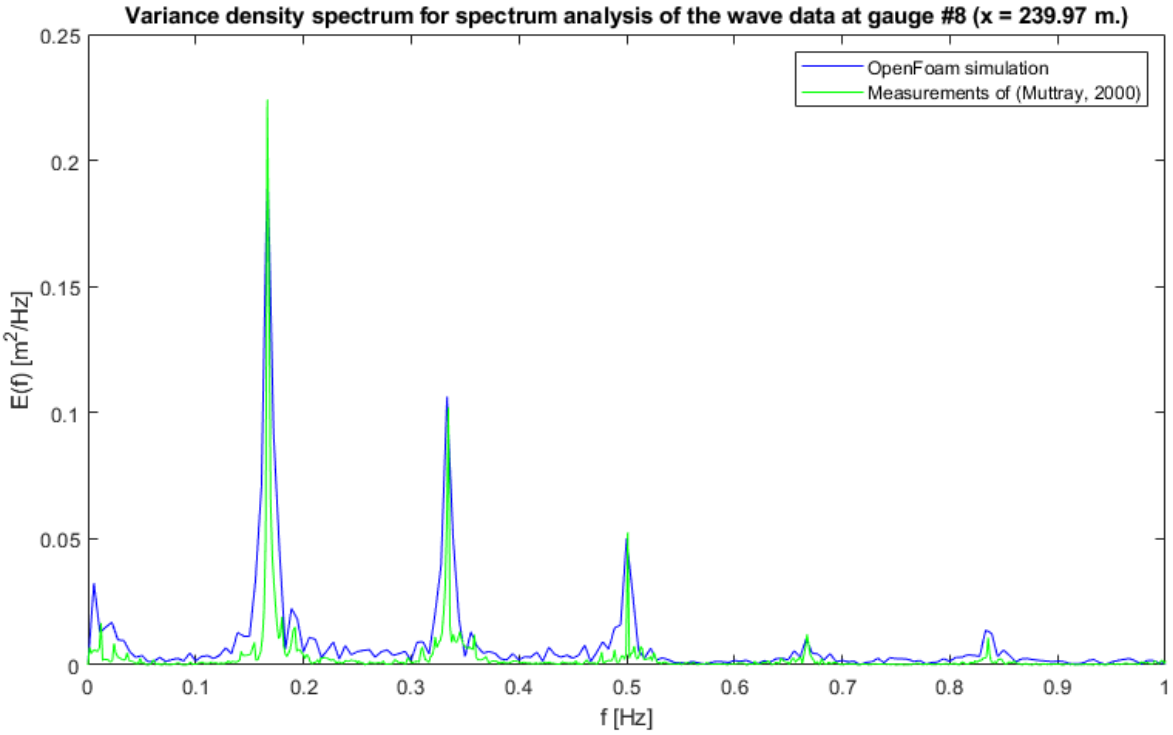

Figure 23 - Variance density spectrum at a location in front of the breakwater structure ($x = 239.97$)

5.3.2 Reflection analysis

To check if the structure is modelled correctly in OpenFoam, the reflection of the structure is compared with the reflection of the structure in the physical model test. This is done by performing a reflection analysis, following the method described in (Zelt & Skjelbreia, 1993). With this method, a reflection analysis can be done with any number of wave gauges (2 wave gauges or more) and the surface elevation due to the incoming and reflected waves can be calculated at any arbitrary position. According to (Zelt & Skjelbreia, 1993), the accuracy increases with using more wave gauges, especially for broad band wave spectra. The wave spectra of the OpenFoam simulation and of the test of (Muttray, 2000) is not a broad band wave spectra and thus has increasing the number of wave gauges limited advantage, therefore three wave gauges are used for the reflection analysis. The reflection analysis is done for both the OpenFoam simulation as for the measurements of (Muttray, 2000). The results of the reflection analysis is given in Figure 24 and Figure 25.

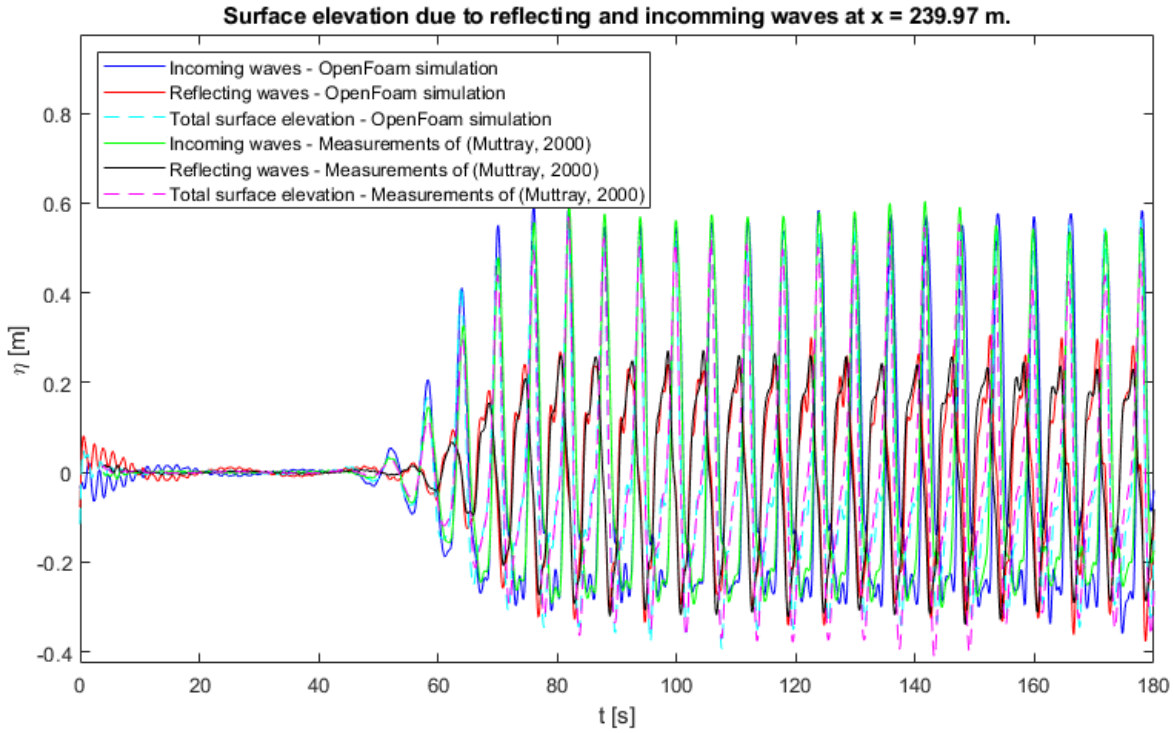

Figure 24 - Surface elevation due to reflecting and incoming waves at $x = 239.97$

When looking to the results, it can be seen that the reflection of the OpenFoam simulation matches the reflection in the test of (Muttray, 2000) very well. Also when Figure 25 is compared with Figure 26 (the results of a wave gauge at the same location), it can be seen that the reflection analysis is carried out correctly, since the sum of the incoming and reflected waves match the surface elevation measured by the wave gauges for both the OpenFoam simulation as the test of (Muttray, 2000). The result of this reflection analysis in combination with the result of the spectrum analysis indicate that the structure and the incoming waves are modelled correctly.

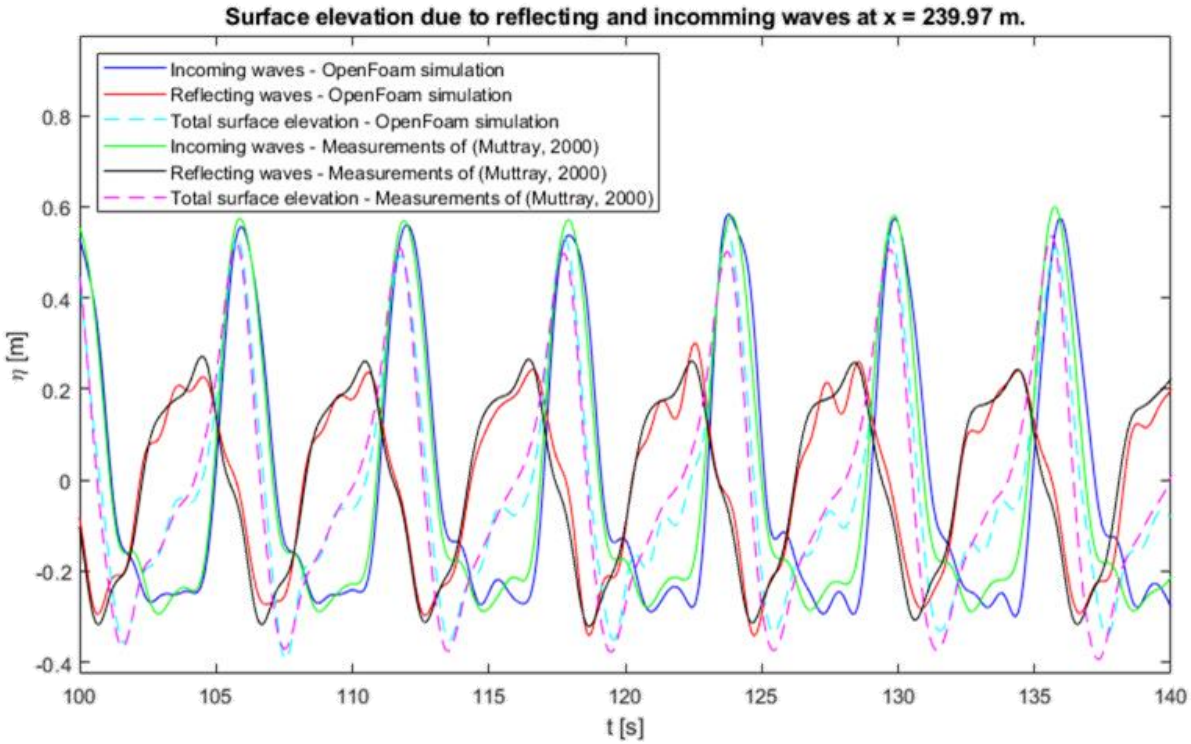

Figure 25 - Surface elevation due to reflecting and incoming waves at $x = 239.97$ (for $100 < t < 140$)

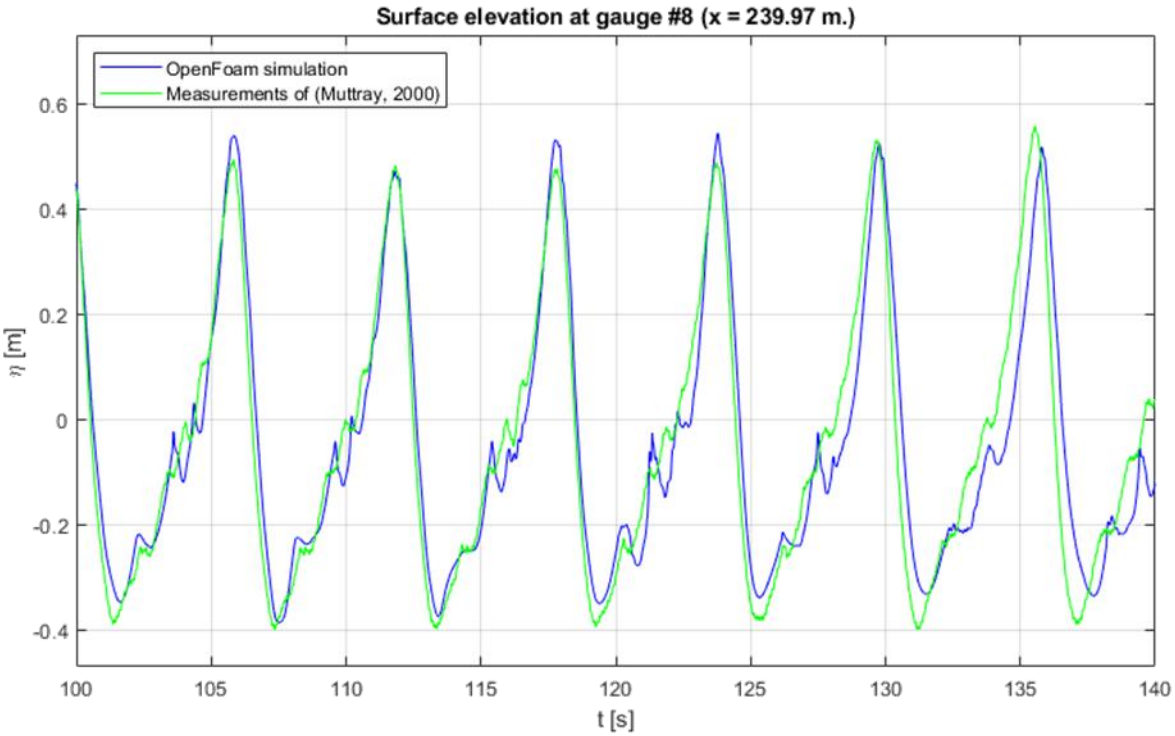

Figure 26 - Surface elevation comparison at gauge #8 ($x = 239.97$) (for $100 < t < 140$)

5.3.3 Wave gauge comparison

The surface elevation of the OpenFoam simulation is compared with the measurements in the physical model test by (Muttray, 2000) on 19 points. The measurements on the first 15 points show a good agreement, see for example Figure 26, which shows the comparison at wave gauge #8. The surface elevation in the OpenFoam simulation has the same order of magnitude as the measurements of the physical model test of (Muttray, 2000) and the shape of the graphs is more or less similar.

At the gauge #16 (at $x = 251.27$, which is just on the crest of the breakwater structure), a high peak of surface level elevation occurs in the OpenFoam results around $t = 85\ s$ (the moment in time the first fully developed wave reaches this point). Why this peak occurs is not fully understood by the author of this thesis but it is suspected that it is some kind of spin-up effect. This measured peaks does not seem to have an influence on other results.

From wave gauge #16 till wave gauge #19 (all positioned under or behind the crest of the breakwater structure) there is an amplitude difference between the measured and the simulated water level elevation, moreover, a set-up of water can be noted. This set-up of water level probably dampens the surface level elevation in the measurements of the physical model test. Both the water level set-up as the dampening of the amplitude increases when progressing towards the rear side of the structure. In Figure 27, the water level set-up in the measurements of the physical model test can be seen clearly. In the OpenFoam simulations, this water level set-up does not occur since the water level is kept at the still water level behind the structure by means of a relaxation zone. See Appendix A for a full comparison of all the wave gauges.

The water level set-up in and behind the structure has an influence on the pressures in the physical model test. Since the water level set-up is negligibly small near the front slope of the structure, it is expected not to have an influence on the measured quantities near the front slope. The hydraulic loading parameters for which OpenFoam is checked, all are measured around this front slope. Therefore it is safe to say that despite this set-up of water level inside and behind the structure, the results of the physical model test can still be used to validate the simulation of the hydraulic loading parameters in OpenFoam.

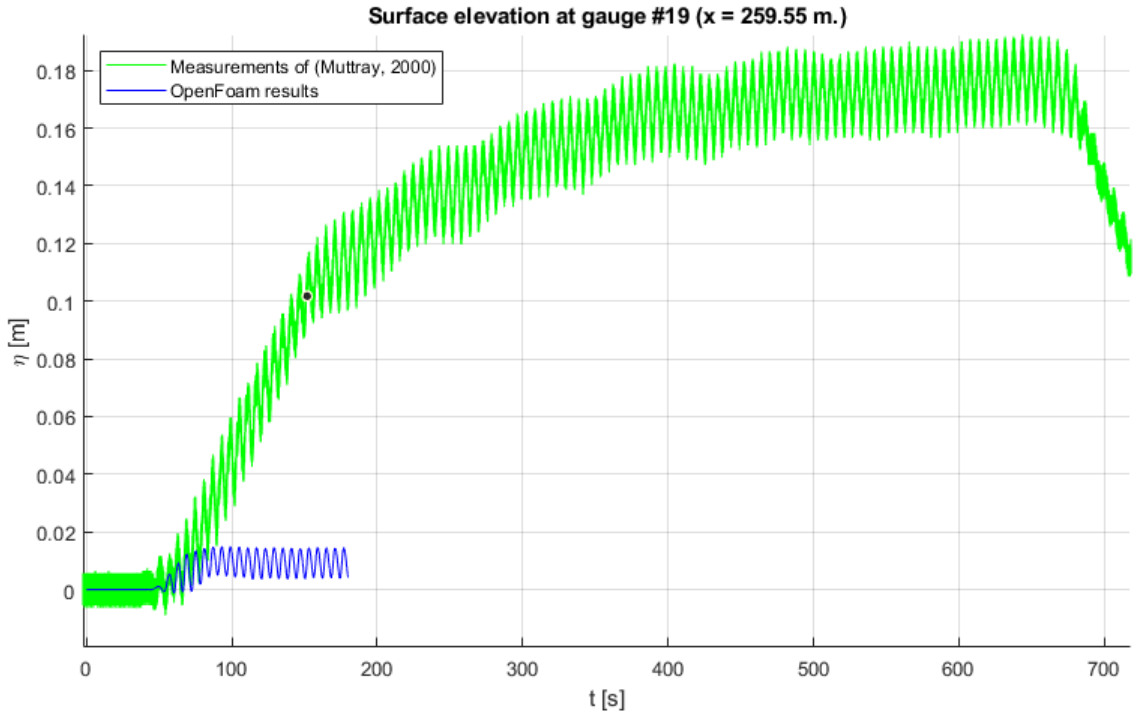

Figure 27 - Surface elevation comparison at gauge #19
(zoomed out to see the trend in the measurements of (Muttray, 2000))

5.3.4 Wave run-up comparison

Figure 28 shows the vertical level of the wave run-up over the armour slope for both the OpenFoam simulation as the measurements of (Muttray, 2000). As can be seen, both the peaks and the throughs of the results from the numerical simulation are not on the same level as the measurements of the physical model test. A possible explanation is given below.

The difference in maximum wave run-up level might be explained by the fact that the roughness of the front slope cannot be included in the OpenFoam model. Therefore the wave run-up is overestimated by the OpenFoam model. By tweaking the Forchheimer parameters of the armour layer, the maximum wave run-up level could be manipulated to match the measured wave run-up level. However, changing the Forchheimer parameters will also influence the flow velocities and pressure distributions through the armour layer, which is unwanted.

Furthermore, the difference in the maximum wave run-down level and the wave run-up level might be related to the used measuring techniques. When waves run down the front slope and the next waves arrives, some rather turbulent processes happen. In these processes the water is mixed with air which raises doubts about the accuracy of the measurements of the physical model test. In OpenFoam this mixing with air does not happen since turbulence is only modeled in the porous layers, see section 2.2.1 of the literature study. This might be an explanation for the difference in maximum wave run-up and maximum wave run-down.

Besides, the entire top of the armour layer is not modeled correctly, in reality it is a rough surface while in OpenFoam it is modelled as a smooth surface. Furthermore is the position of the wave run up gauge in the physical model test very unsure. This raises doubt about the simulation of the wave run-up and run-down and the simulation of the flow velocity on top of the armour layer, parallel to the slope. The influence on the pressure measurement on top of the armour layer will be discussed in the next section, the pressure probe comparison.

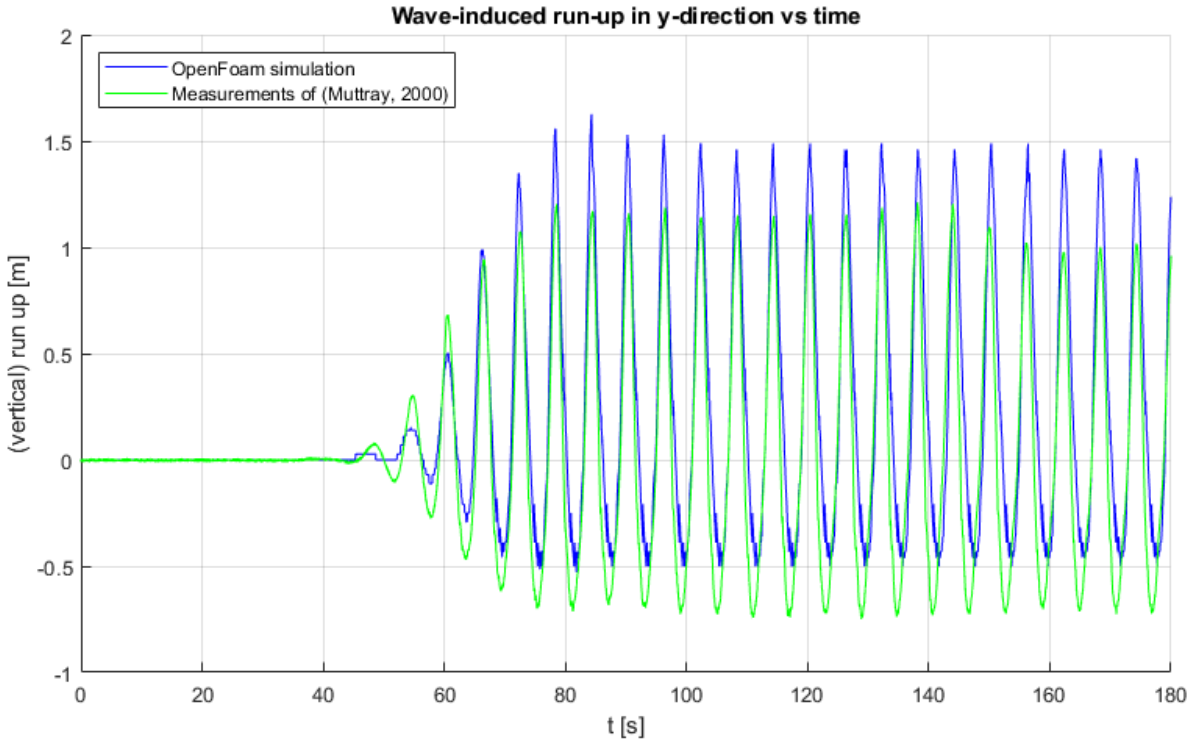

Figure 28 - Measured and simulated wave run-up (in y-direction) over the front slope of the breakwater structure

5.3.5 Pressure probe comparison

In the physical model tests, (Muttray, 2000) used quite a lot of pressure sensors (or pressure probes) to measure the wave induced pressure in the breakwater structure. The locations of the pressure sensors (the Druckmeßdosen) are shown in Figure 29. The exact coordinates of the pressure probes can be found in Appendix A.

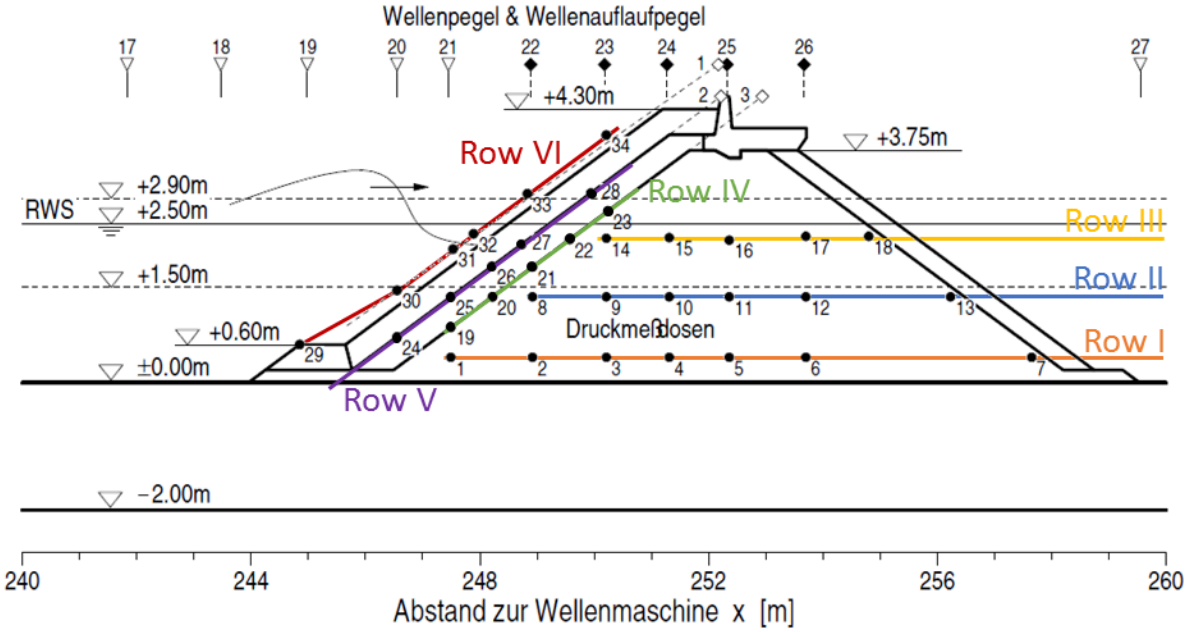

Figure 29 - location of the pressure sensors (Druckmeßdosen) in the physical model of (Muttray, 2000)

The pressure probes can be divided in six rows. Three horizontal rows:

Row I. Pressure probes 1, 2, 3, 4, 5, 6 and 7
Row II. Pressure probes 8, 9, 10, 11, 12 and 13
Row III. Pressure probes 14, 15, 16, 17 and 18

And three rows parallel to the front slope:

Row IV. Pressure probes 19, 20, 21, 22 and 23
Row V. Pressure probes 24, 25, 26, 27 and 28
Row VI. Pressure probes 29, 30, 31, 32, 33 and 34

The results from the OpenFoam simulation are compared with the measurements of the physical model tests. Since the hydraulic loading parameters are all located around the front slope of the structure, only the results of Row IV, V and VI are discussed in this chapter. The results of Row I, II and III are analyzed in detail in Appendix A.

Row IV, Row V and Row VI show the same pattern, when comparing the results of the OpenFoam simulation with the measurements of the physical model test. For the probes below the still water level (so the probes below $y = 2.5$) the wave induced pressure simulated in OpenFoam matches the measured pressure well, see e.g. probe #25, Figure 30. However, when looking at the probes above the still water level (probes #23, #28, #33 and #34), the wave induced pressure simulated in OpenFoam has much higher peaks than the measured pressure in the physical model tests, see e.g. probe #33 in Figure 31.

The author of this thesis suspects that the high peaks in pressure are due to flow velocity of the run-up. When wave run-up is progressing along the slope, the thickness of the water layer decreases but the flow velocity increases. Since the measurement probe is precisely on the interface of the front slope, only a very small layer of water with high velocities could result in high measured pressures. In the physical model tests, this is not measured since the pressure

sensors in the physical model tests are protected by a casing which have a significant influence on the flow. Besides, the wave run-up is not correctly modeled by OpenFoam, the wave run-up is higher in OpenFoam than in the physical model tests (due to the lack of roughness of the front slope and the lack of turbulence in the water, see section 5.3.4). This causes higher pressure in the part of the wave run-up zone above the still water level.

The simulated pressure in probes #31 and #32 (e.g. Figure 32 for the results of probe #32) in the OpenFoam simulation do not quite match the pressure measured by (Muttray, 2000). The simulated pressures drop to a zero value while the results of the physical model tests have a quite flat trough in these parts of the plots. This is due to the fact that probe #31 and probe #32 are sometimes underwater and sometimes lie dry. The lines of the OpenFoam measurements only show the pressure when the probes are underwater, so when the probes lie dry, a measurement value of 0 is shown. In the physical model tests, the probes keep showing a constant value when the probe falls dry.

From the pressure probe comparison it can be concluded that the wave induced pressure is modelled correctly for the area around the front slope, beneath the still water level. The wave induced pressures around the front slope, above the still water level seem to be not correct. In the prediction methods, only the relative values of the pressures around the front slope are regarded and between these values is interpolated in order to predict a P-value. Since all structures are modelled for exactly the same wave signal, it is expected that the relative error in the pressures around the front slope above the still water is approximately the same. The effect of these errors is canceled out by the interpolation of the values, and thus it is expected that the errors in the pressures above the still water level have no influence on the results of the prediction methods.

The flow velocities through the porous layers are not measured in the physical model tests of Muttray. However, the flow velocities through the porous layers are a consequence of the pressure difference over these layers. Since the pressure is correctly modelled around the armour and filter layer below the still water level, it is concluded that the flow velocities are also correctly modelled below the still water level. The flow velocities above the still water seem to be not correct. In one of the prediction methods, the flow velocities perpendicular to the front slope are used to calculate the discharge through the armour layer. There is only looked at the relative values of the discharge through the armour layer, between these values is interpolated in order to predict a P-value. Since all structures are modelled for exactly the same wave signal, it is expected that the relative error in the discharge through the armour layer above the still water is approximately the same. The effect of these errors is canceled out by the interpolation of the values, and thus it is expected that the errors in the flow velocities above the still water level have no influence on the results of the prediction method.

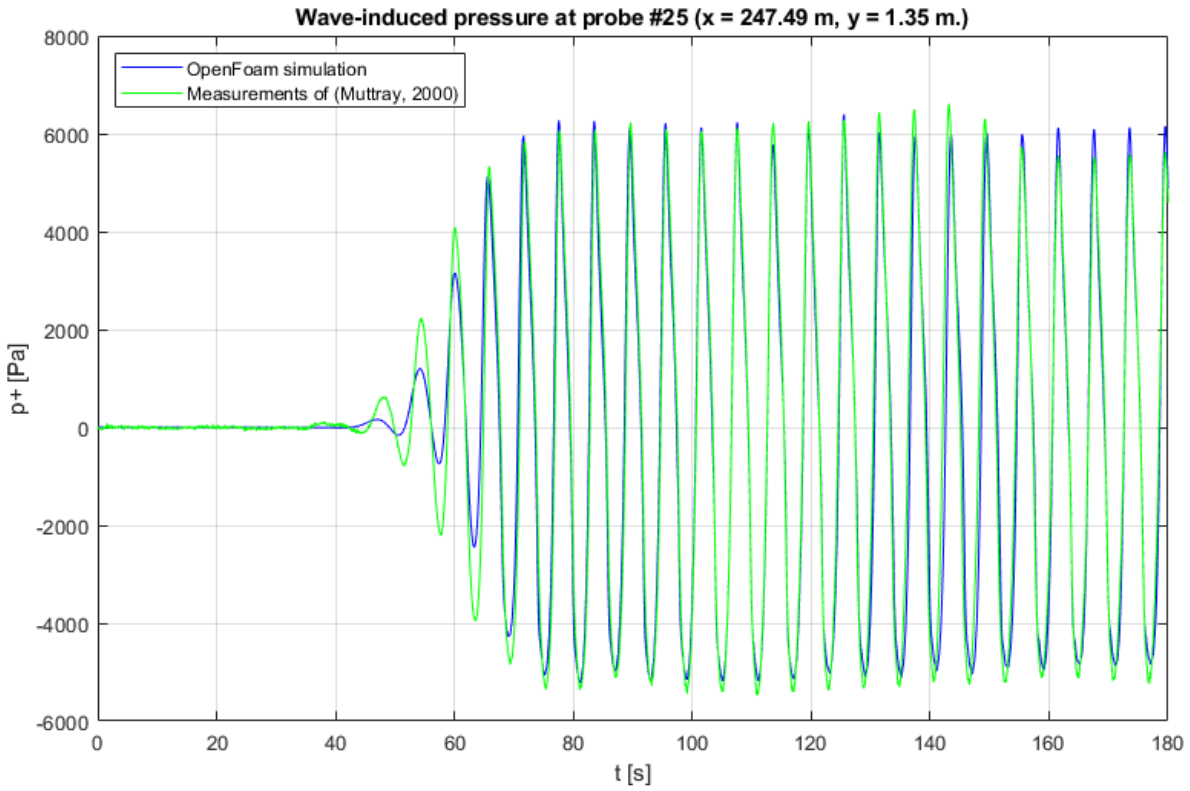

Figure 30 - Measured and simulated pressure in pressure probe #25 ($x = 247.49\ m$, $y = 1.35\ m$)

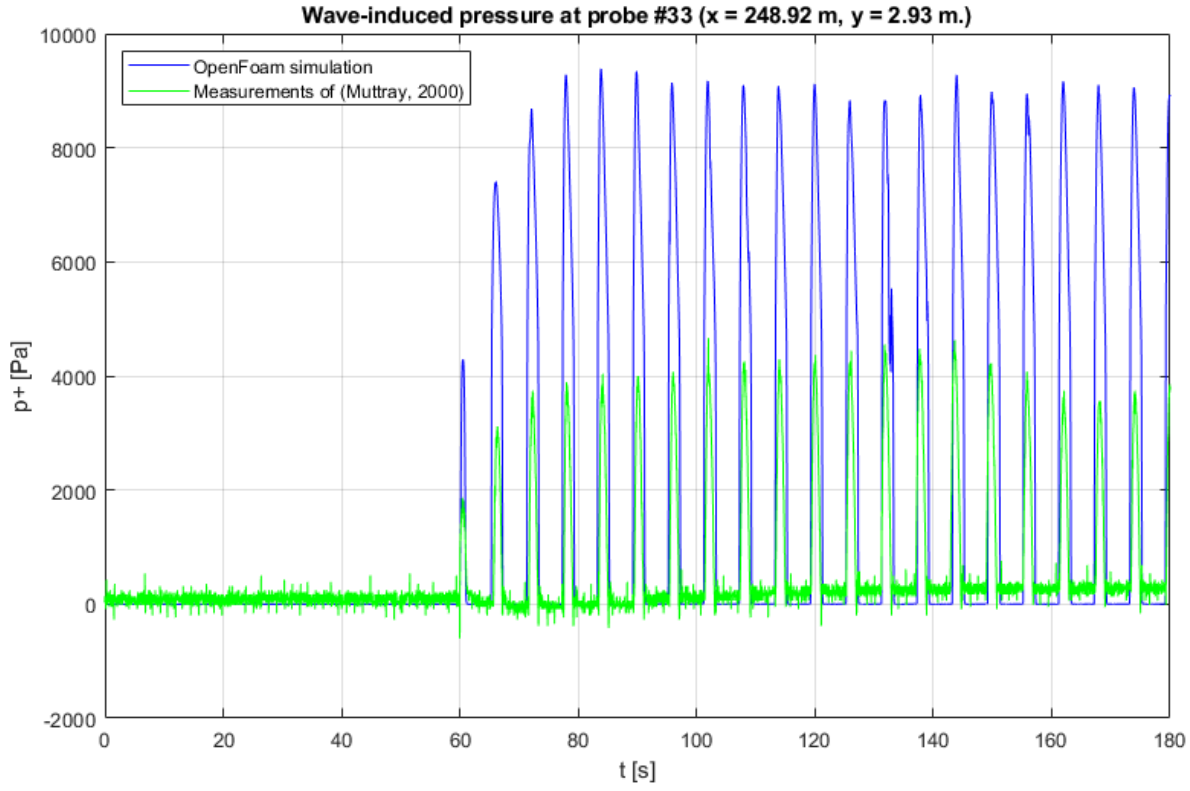

Figure 31 - Measured and simulated pressure in pressure probe #33 ($x = 248.92\ m$, $y = 2.93\ m$)

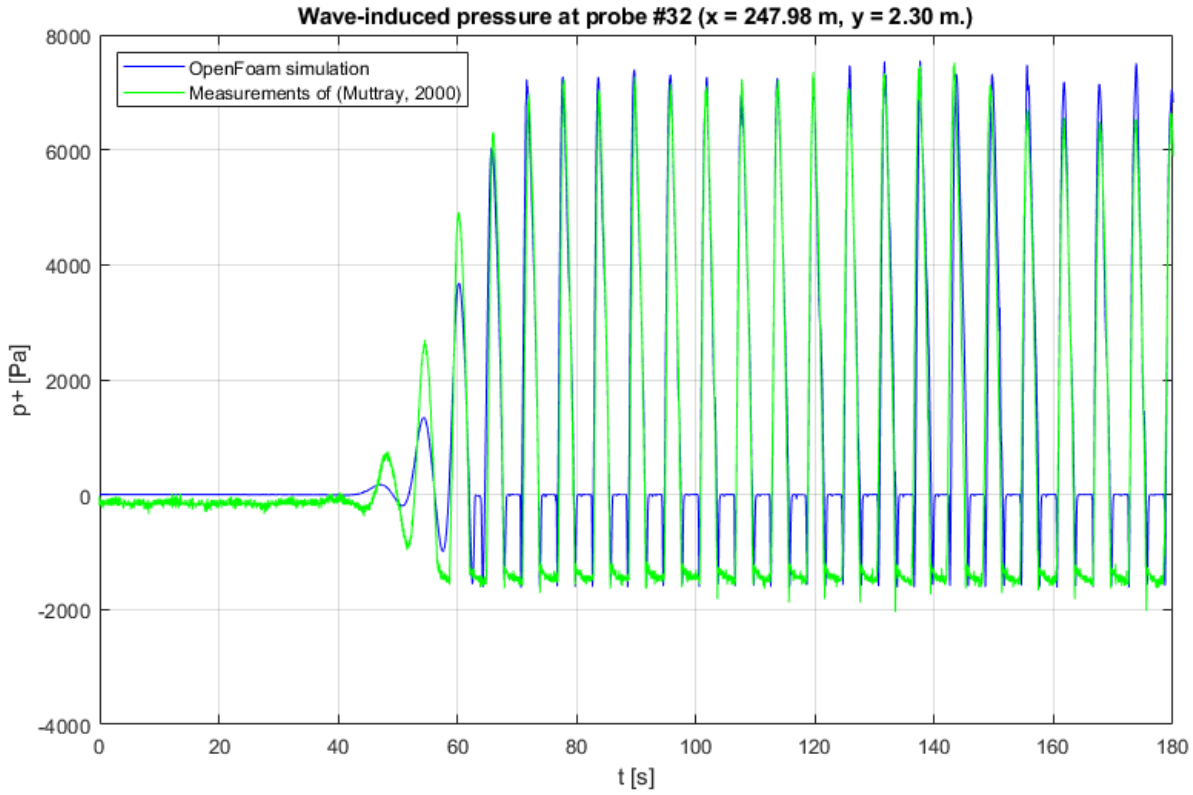

Figure 32 - Measured and simulated pressure in pressure probe #32 ($x = 247.98\ m$, $y = 2.30\ m$)

5.3.6 Pressure lines comparison

In his PhD thesis, (Muttray, 2000) included the pressure lines of test nr. 020694-01 on certain moments in time: $t(R_{u,max})$, $t(R_{u,max}) + 0.13T$, $t(R_{u,max}) + 0.31T$, $t(R_{u,max}) + 0.44T$, $t(R_{u,max}) + 0.75T$ and $t(R_{u,max}) + 0.94T$. These pressure lines were calculated by interpolating the pressures over the six lines described in the previous section and then interpolating the pressures in vertical direction to create the pressure field.

With OpenFoam the same kind of plots can be made. OpenFoam calculates the complete pressure field for every timestep and saves this output for every output moment in time. In theory this gives a more accurate pressure field since the results of the pressure sensors do not have to be interpolated. In the OpenFoam simulation, output was saved every 0.5 seconds of simulation time (for the last 15 seconds of simulation). Unfortunately, these times are not equal to the exact moments in time on which (Muttray, 2000) created the pressure lines plots. Therefore the results of the moments closes in time are compared with the pressure lines included in the PhD thesis of (Muttray, 2000).

Figure 33 and Figure 34 show the pressure lines of (Muttray, 2000) and the pressure lines simulated with OpenFoam for respectively $t = t(R_{u,max})$ and $t = t(R_{u,max}) + 0.03T$. The pressure lines for the other moments in time are compared in Appendix A. Even though the results are not on the exact same time but slightly off, the results look very good. It is clear that the pressure lines from the OpenFoam simulation follow the same pattern as the lines measured by (Muttray, 2000).

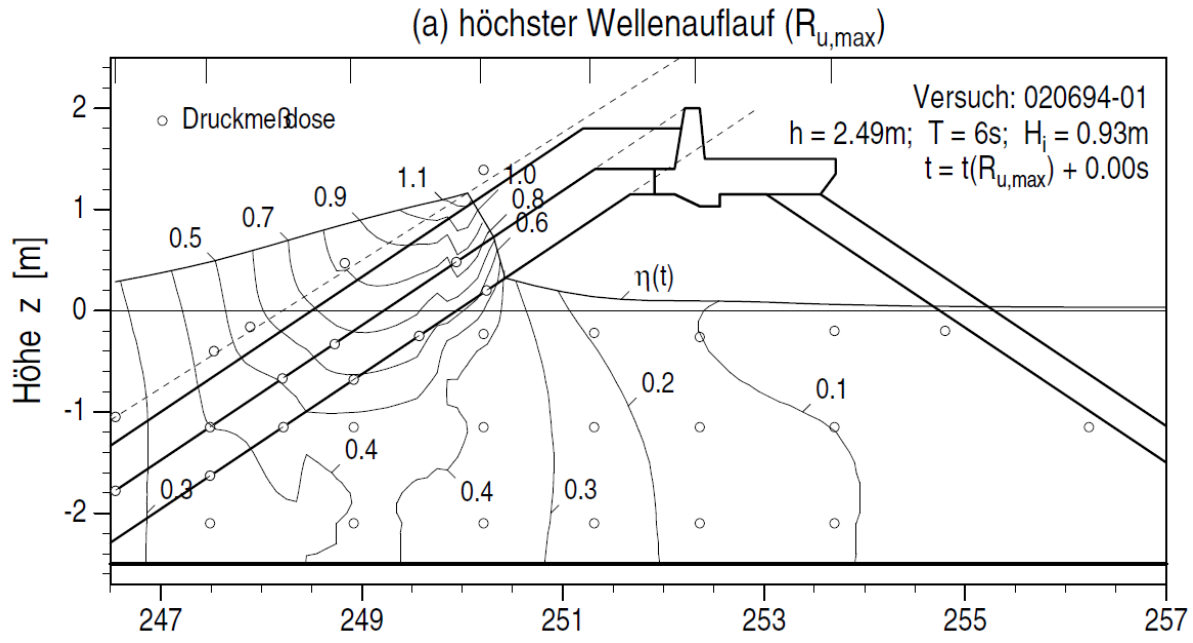

Figure 33 - Pressure lines $\left(\frac{p}{\rho g}\right)$ by (Muttray, 2000) at $t = t(R_{u,max})$

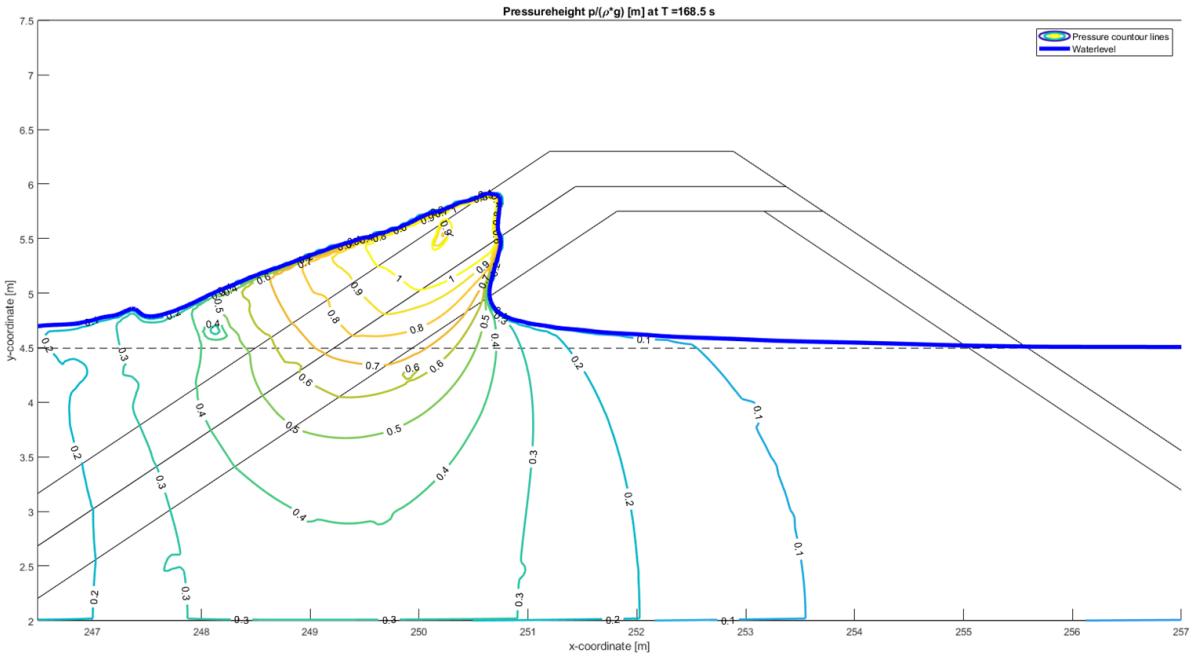

Figure 34 – Simulated pressure lines $\left(\frac{p}{\rho g}\right)$ at $t = 168.5\ s\ (\approx t(R_{u,max}) + 0.03T)$

5.4 Discussion and conclusion

The result of this reflection analysis in combination with the result of the spectrum analysis indicate that the structure and the incoming waves are modelled correctly in OpenFoam.

In the physical model tests, water setup at the rear side of the breakwater occurs. In the numerical simulation with OpenFoam, this water setup does not happen. This is due to the fact that in the OpenFoam simulation the water level at the rear side of the breakwater is kept constant by means of a relaxation zone. Although not validated, it is assumed that removing this relaxation zone on the rear of the breakwater and making the area behind the structure the same size as the area behind the breakwater in the physical model tests, will eliminate the effects due to this water set-up. Therefore the following conclusions are drawn.

The pressures around and inside a breakwater structure is simulated accurately by OpenFoam for the part of the breakwater that is below the still water level. Above the still water level, some peaks in the wave induced water pressure occur which are not measured in physical model tests. Although not measured in the physical model tests, the simulated flow velocities inside of the breakwater seem to be modelled accurate as well in OpenFoam, since the flow velocities inside porous layers are a consequence of the pressure gradient inside these layers and these pressures are modelled correctly.

The flow velocity on top of the armour layer could not be validated for the OpenFoam model with the available data. A clear difference in wave run-up and run-down between the physical model test and the numerical model test is noted which suggests that the flow velocity on top of the armour layer is not simulated correctly since this flow velocity is related to the wave run-up and run-down.

In the prediction methods, there is only looked at the relative values of the pressures around the front slope and the relative values of the discharge through the armour layer. The flow velocities perpendicular to the front slope are used to calculate the discharge through the armour layer. There is interpolated between these relative values in order to predict a P-value. Since all structures are modelled for exactly the same wave signal, it is expected that the relative error in the pressures around the front slope above the still water level and the relative error in the discharge through the armour layer above the still water level are approximately the same for each structure. The effect of these errors is canceled out by the interpolation of the values, and thus it is expected that the errors in the pressures above the still water level have no influence on the results of the prediction methods.

One condition for these conclusions is the grid resolution. The same number of cells per wave height have to be used in the simulations, see Table 9, since changes in grid size might have effect of the outcomes.

The consequence of these conclusions is that it was decided to not investigate the flow velocity on top of the armour stones as possible hydraulic loading parameter for the prediction of P. The remaining hydraulic loading parameters are:

- The wave induced water pressure difference over the armour layer, $\Delta p_{\perp}$
- The discharge through the armour layer perpendicular to the front slope, $q_{\perp}$ or $Q_{\perp}$

6 Calculation method of hydraulic loading parameters

6.1 Introduction

In this chapter, it is explained how the values for the selected and validated hydraulic loading parameters are calculated. The hydraulic loading parameter of the wave induced water pressure difference ($\Delta p_{\perp}$) is split into two prediction methods, one for the local pressure difference, $\Delta p_{\perp,loc}$, (looking at a single point in space) and one for the total pressure difference, $\Delta p_{\perp,tot}$,(integrated along the front slope of the structure in space). The prediction method using the discharge as hydraulic loading parameter, $Q_{\perp,tot}$, is also integrated along the front slope of the structure in space. For all three prediction methods, the 2% exceedance value of the hydraulic loading parameter is taken in time. The calculation of the hydraulic loading parameters is discussed on the next pages, each hydraulic loading parameter in its own section. The MATLAB scripts used to calculate the values for the hydraulic loading parameters can be found in Appendix D.

6.2 Linear or quadratic interpolation

The prediction method uses interpolation between the found values of the hydraulic loading parameters for the different structures to predict a value for the notional permeability, see Figure 35 summarizing the concept of the prediction methods. To keep the concept of the prediction methods relatively simple, the idea is that the notional permeability of the structures is linearly dependent on the initiation of motion of the armour stones. The armour stones start to move when the de-stabilizing force on the armour stones is bigger than the stabilizing forces. The de-stabilizing forces are the result of pressure differences. This would mean that the prediction of the notional permeability is linearly related to the pressure difference over the armour layer, and thus linear interpolation can be used for the prediction methods which use the pressure difference over the armour layer as hydraulic loading parameter.

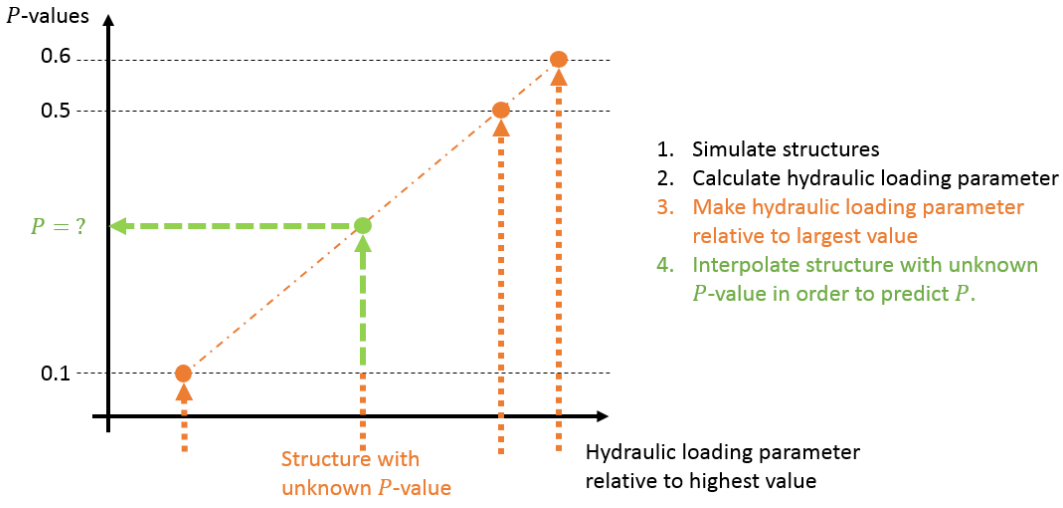

Figure 35 - Concept of the method to predict the notional permeability

According to (Schiereck & Verhagen, 2016), the relation between pressure gradient and the flow velocity is quadratic for flow and pressures in rock, see also section 2.2.4. Following the same reasoning this means that the flow velocity is quadratic related to the prediction of the notional permeability and thus quadratic interpolation can be used for the prediction method which uses the discharge through the armour layer as hydraulic loading parameter.

6.3 Local wave induced pressure difference over the armour layer ($\Delta p_{\perp,loc,2\%}$)

The local wave induced water pressure difference over the armour layer is determined by following the steps shown in Figure 36. For all the pressure probe pairs, the resulting wave induced water pressure is calculated for every timestep of the simulation. For all these time series of resulting pressures, the 2% exceedance value is calculated. From these 2% exceedance values, the maximum value is taken as the hydraulic loading parameter.

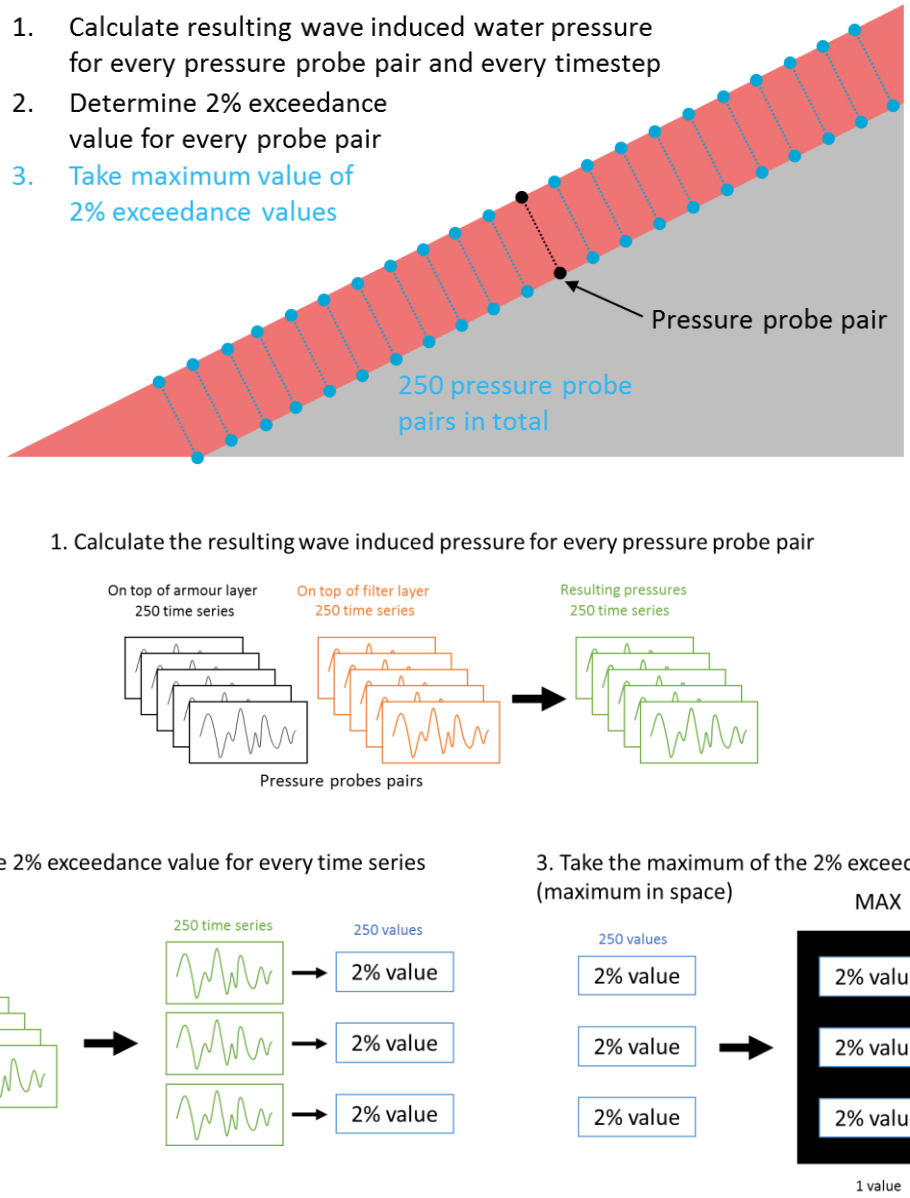

Figure 36 - Steps taken to calculate the value of $\Delta p\_(\perp, loc, 2\%)$

6.4 Total wave induced pressure difference over the armour layer ($\Delta p_{\perp,tot,2\%}$)

The total wave induced water pressure difference over the armour layer is determined by following the steps shown in Figure 37. For the pressure probe pairs, the resulting wave induced water pressure is calculated for every timestep of the simulation. For every time step of the simulation, the total wave induced pressure is calculated by interpolating the resulting wave induced pressure over the front slope of the structure from a level of $3\ H_s$ beneath the still water level upward till a level above the maximum run-up level. The lower level is chosen because erosion on the front slope of a breakwater occurs from approximately $1.5\ H_s$ below the still water level till approximately $1\ H_s$ above the still water level, see also section 2.2.3 of the literature study and section 11.4.1 of the recommendations. To make sure all pressures that might contribute to this erosion are taken into account a relative safe area is selected: from a level of $3\ H_s$ below the still water level till well above the maximum wave run-up level. The result is a time series of the total wave induced water pressure over the armour layer. From this time series the 2% exceedance value is taken as the hydraulic loading parameter.

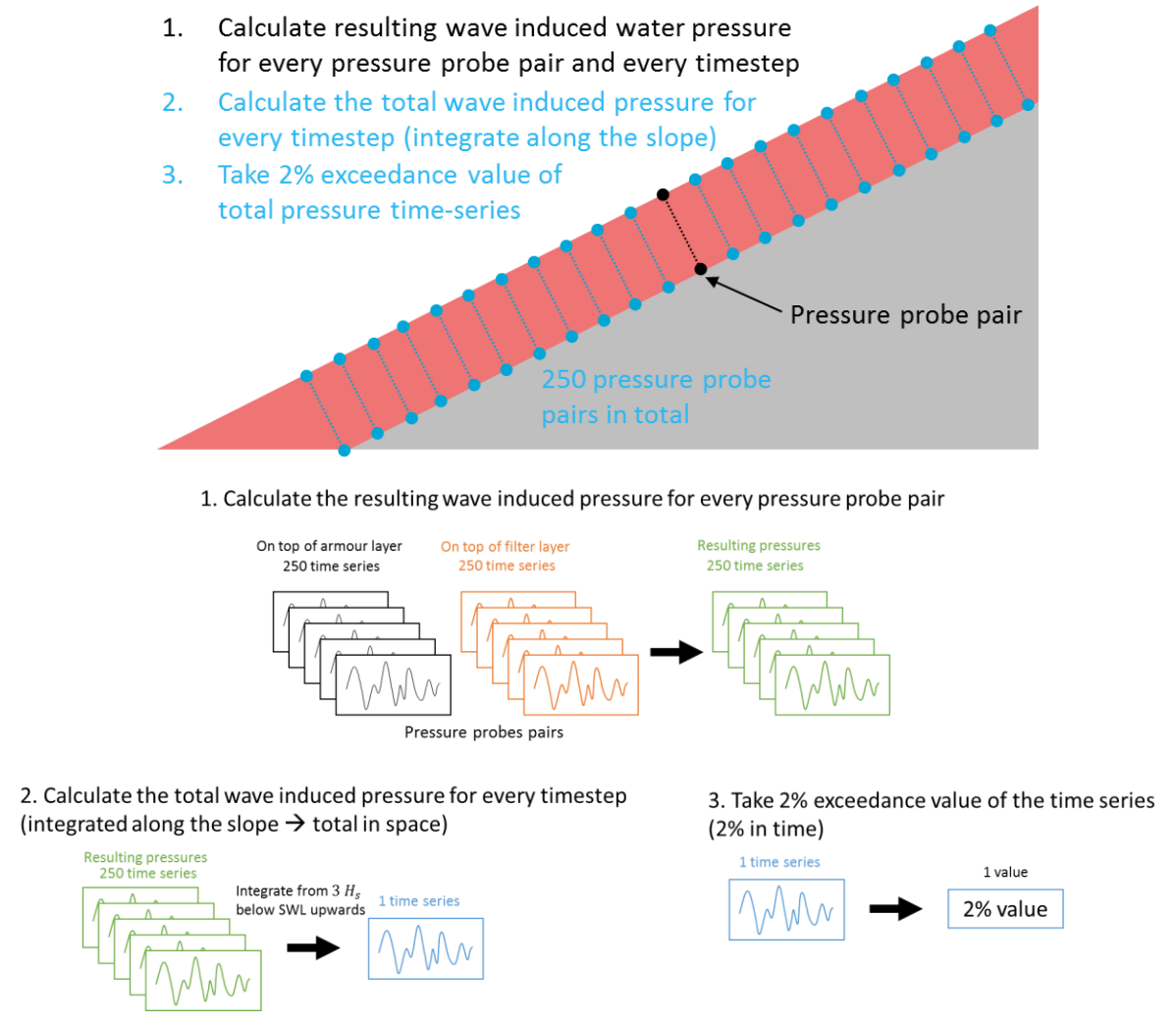

Figure 37 - Steps taken to calculate the value of $\Delta p_{\perp,tot,2\%}$

6.5 The wave induced discharge through the armour layer ($Q_{\perp,tot,2\%}$)

The discharge through the armour layer in outward direction is calculated by following the steps shown in Figure 38. The flow velocities are measured in OpenFoam by the (pressure) probes. For every pressure probe pair, the resulting flow velocity perpendicular to the armour layer is calculated for every timestep of the simulation. Since the structure is simulated in 2D, the resulting flow velocity perpendicular to the armour layer is equal to the discharge through armour layer per running meter of breakwater and per meter along the slope of the armour layer. The total discharge through the armour layer is calculated by interpolating the discharge over the front slope of the structure from a level of $3\ H_s$ beneath the still water level upward till a level above the maximum run-up level. The lower level is chosen because erosion on the front slope of a breakwater occurs from approximately $1.5\ H_s$ below the still water level till approximately $1\ H_s$ above the still water level, see also section 2.2.3 of the literature study and section 11.4.1 of the recommendations. To make sure all pressures that might contribute to this erosion are taken into account a relative safe area is selected: from a level of $3\ H_s$ below the still water level till well above the maximum wave run-up level. The results is a time series of the total discharge through the armour layer. From this time series the 2% exceedance value is taken as the hydraulic loading parameter.

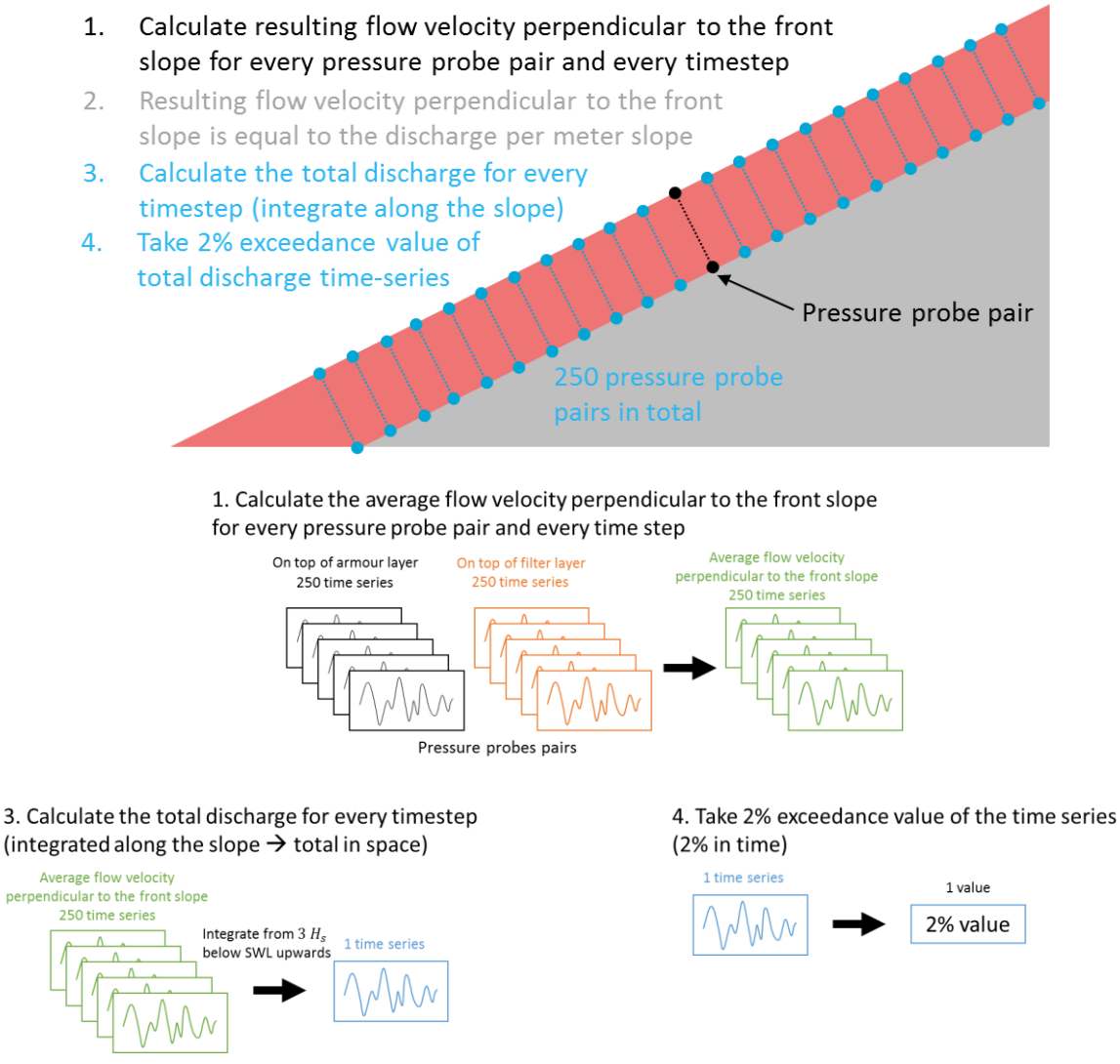

Figure 38 - Steps taken to calculate the value of $Q_{\perp,tot,2\%}$

7 Step III: Determine prediction method for the notional permeability

7.1 Introduction

In this chapter, the notional permeability of one of the structures tested by (Kik, 2011) is predicted following the steps described in chapter 3.3. The notional permeability is predicted using three hydraulic loading parameters: $\Delta p_{\perp,loc,2\%}$, $\Delta p_{\perp,tot,2\%}$ and $Q_{\perp,tot,2\%}$. How the values for these hydraulic loading parameters are calculated for the different prediction methods is discussed in chapter 6. In section 6.2 of chapter 6 is also discussed whether linear or quadratic interpolation is used in the prediction methods.

7.2 Numerical model set-up

This section discusses the set-up of the numerical models used to predict the notional permeability of one of the structures of (Kik, 2011).

7.2.1 Structures

The structure cross-sections are schematically drawn in Figure 39 till Figure 42.

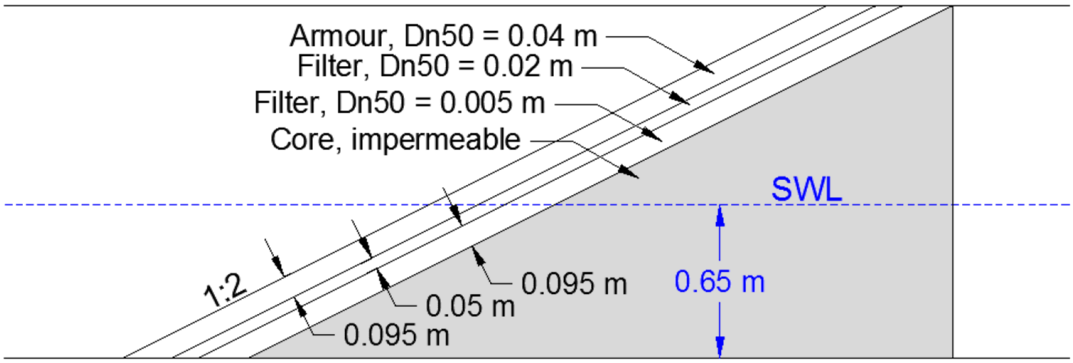

Figure 39 – Structure 1, tested by (Kik, 2011) and (Kluwen, 2012) to have a P-value of approximately 0.37 – 0.38

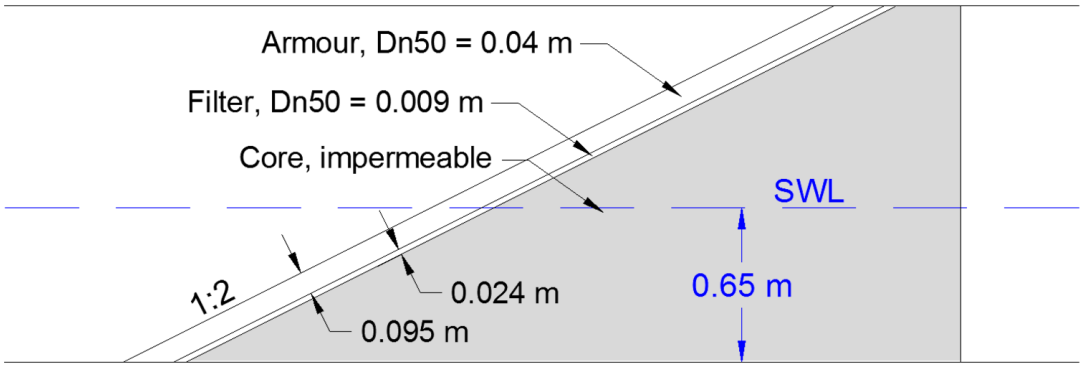

Figure 40 - Structure 2, tested by (Van der Meer, 1988) to have a P-value of 0.1

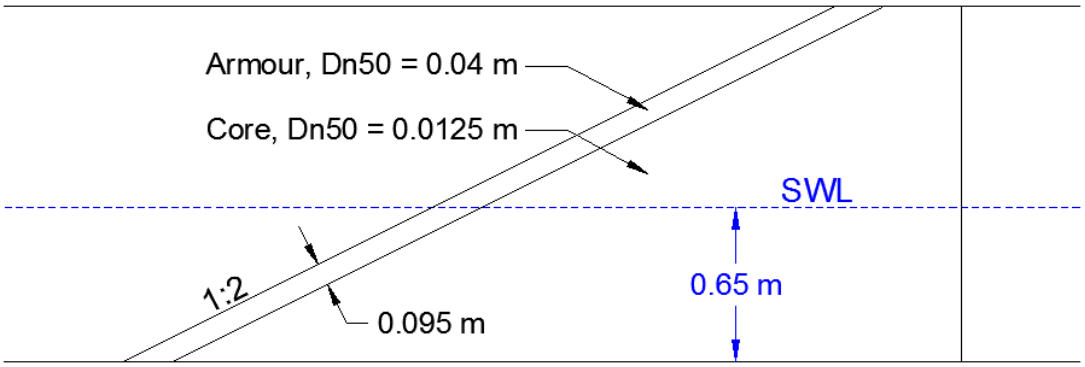

Figure 41 - Structure 3, tested by (Van der Meer, 1988) to have a P-value of 0.5

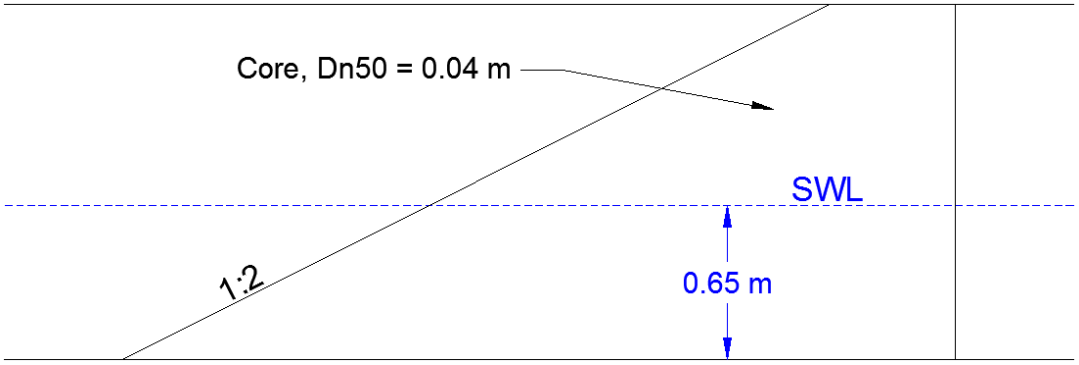

Figure 42 - Structure 4, tested by (Van der Meer, 1988) to have a P-value of 0.6

In all simulations of the prediction method, the front slope is on the same distance from the relaxation zone on the left boundary. The toe of the structures is at $x = 45.46\ m$. Because there is only interest in the armour on the front slope of the structures and not in the crest, the structures are created such that the crest of the structures is well above the maximum run-up level. The properties of the porous layers are included in Table 10 till Table 13 for respectively structure 1 till 4. The porosity of the armour layer of structure 1 is estimated using formulas (20), (21) and (22) and the grain sizes used by (Kik, 2011), see also section 2.1.2 of the literature study. The porosity for all porous layers of the four structures is set to this value.

Structure 1	n [–]	KC-value [–]	γ-value [–]	D_{n50} $[m]$	D_{50} $[m]$	α [–]	β [–]
Armour layer	0.44	16	0.34	0.04	0.0476	1000	1.1
Filter layer 1 (top)	0.44	32	0.34	0.02	0.0238	1000	1.1
Filter layer 2 (lower)	0.44	128	0.34	0.005	0.00595	1000	1.1
Core	Impermeable, cut out with SnappyHexMesh						

Table 10 - Properties of the porous layers of structure 1

Structure 2	n [–]	KC-value [–]	γ-value [–]	D_{n50} $[m]$	D_{50} $[m]$	α [–]	β [–]
Armour layer	0.461	16	0.34	0.04	0.0476	1000	1.1
Filter layer	0.396	71	0.34	0.009	0.0107	1000	1.1
Core	Impermeable, cut out with SnappyHexMesh						

Table 11 - Properties of the porous layers of structure 2

Structure 3	n [−]	KC-value [−]	γ-value [−]	D_{n50} [m]	D_{50} [m]	α [−]	β [−]
Armour layer	0.461	16	0.34	0.04	0.0476	1000	1.1
Core	0.441	51	0.34	0.0125	0.0149	1000	1.1

Table 12 - Properties of the porous layers of structure 3

Structure 4	n [−]	KC-value [−]	γ-value [−]	D_{n50} [m]	D_{50} [m]	α [−]	β [−]
Core	0.461	16	0.34	0.04	0.0476	1000	1.1

Table 13 - Properties of the porous layers of structure 4

7.2.2 Waves and water

In the simulations, the structures are forced by irregular waves of a Pierson-Moskowitz spectrum. The total simulation time is chosen such that approximately 500 waves reach the structure. The properties of the Pierson-Moskowitz spectrum is shown in Table 14. The Iribarren number of the mean incoming wave is 3.2 which means that the incoming waves are surging waves.

	H_{m0} [m]	T_{m0} [s]	T_p [s]	L_{m0} [m]	s [−]	ξ_m	T_{sim} [s]
Spectrum	0.13	2.3	3.01	5.33	2.4%	3.2	1175

Table 14 - Properties of the Pierson-Moskowitz spectrum used

The properties of the water in the OpenFoam models is set to common values. The water has a kinematic viscosity, ν, of $1.0 \cdot 10^{-6}\ m^2/s$ and a density, ρ_w, of $1000\ kg/m^3$.

7.2.3 Domain, grid size and timestep

The waves in the numerical simulation are generated with OceanWave3D and are coupled with OpenFoam as described in 2.2.2. The OceanWave3D model needs to have a bigger domain than the OpenFoam model. The OceanWave3D domain runs from $x = 0\ m$ till $x = 58.5\ m$ with a wave generation zone from $x = 0\ m$ till $x = 9m$ and a pressure dampening zone from $x = 49.5\ m$ till $x = 58.5\ m$. The OpenFoam domain runs from $x = 27\ m$ till $x = 53.5\ m$ with a relaxation zone from $x = 27$ till $x = 36$ and a relaxation zone from $x = 49$ till $x = 53.5$. The last of these two relaxation zones is only applied for the simulations of structures 3 and 4. This is due to the impermeable core of structures 1 and 2, this impermeable core can only be modelled by OpenFoam when the impermeable layer is cut out of the computational domain by using SnappyHexMesh (a mesh cutting tool of OpenFoam). Cutting out the core shortens the domain since the core layer runs along the whole domain in y-direction, and therefore no relaxation zone on this side of the domain can be applied for structures 1 and 2.

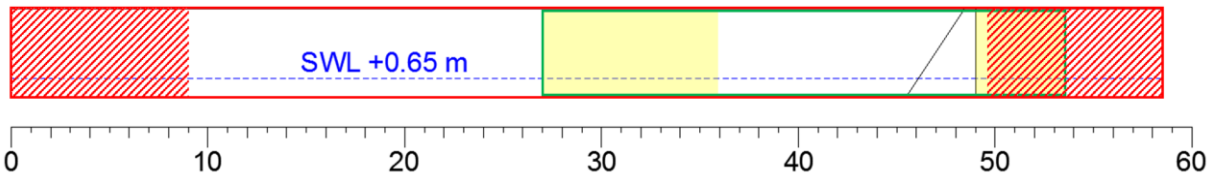

Figure 43 – Domain of the OceanWave3D model (red box) and the OpenFoam model (green box)

Figure 43 shows the domain of the OceanWave3D model and the OpenFoam model. The domain of the OceanWave3D model is shown in red. The red hatched areas are the wave generation zone (left) and the pressure dampening zone (right) in OceanWave3D. The domain of the OpenFoam model is shown in green. The yellow boxes show the relaxation zones of the OpenFoam model.

All the dimensions of the wave generation zones are chosen such that all wave generation zones and pressure dampening zones are at least 1 L_{m0} long and the relaxation zones are at least 0.5 L_{m0} long for the longest waves that will be applied in the thesis. These longest waves are part of the sensitivity analysis and will be described in chapter 8.2. Also a length of at least 1 L_{m0} is available between the relaxation zone, where the waves are transferred from OcenWave3D to OpenFoam, and the structure, so the incoming waves have time to develop. All these criteria are advised by (Jacobsen et al., 2012).

The OceanWave3D simulation only has a grid size in x-direction and a number of layers in y-direction. The number of vertical layers is kept to the default value of 9 layers. According to (26th ITTC Specialist Committee on CFD in Marine Hydronamics, 2011), at least 20 grid cells are required to resolve the shortest wave length for irregular waves. It is known that longer and bigger waves carry more wave energy and it is expected that the hydraulic loading parameters are correlated with the incoming wave energy. Therefore the average wave length is used as the shortest wave to resolve. This results in a maximum grid size in x-direction, Δx, of $0.123\,m$ for the shortest average waves applied in this thesis. These shortest average waves are part of the sensitivity analysis and will be described in chapter 8.2. According to (Bingham & Zhang, 2007), a resolution of 15 – 20 grid cells per wavelength are adequate for general purpose applications. This results in a maximum grid size in x-direction, Δx, of $0.164 - 0.123\,m$. Since the OceanWave3D calculation is not computational demanding, a grid size of $\Delta x = 0.1\,m$ is chosen for the OceanWave3D part of the simulation.

The OpenFoam simulation has a 2D grid, so the grid size in both x-direction, Δx, as well as in y-direction, Δy, has to be chosen. Again, the maximum grid size in x-direction is between $0.123\,m$ and $0.164\,m$. However, according to (26th ITTC Specialist Committee on CFD in Marine Hydronamics, 2011), an orthogonal grid should be used to resolve a free surface, with other words, the aspect ratio $\left(\frac{\Delta x}{\Delta y}\right)$ should be 1. This means that the maximum grid size in y-direction is normative.

According to (26th ITTC Specialist Committee on CFD in Marine Hydronamics, 2011), no less than 20 grid points in vertical direction should be used where the free surface is expected. With other words, the maximum grid size in y-direction, Δy, should be smaller than $\frac{H}{20}$. The formulas of Van der Meer show that the armour layer stability is strongly dependent on the bigger and longer waves. Therefore the higher waves are of way more interest. Therefore it is assumed that, in order to reduce the total number of grid cells, the grid size in y-direction should be smaller than $\frac{H_{1/100}}{20}$. This results in a grid size in y-direction of $\Delta y \leq \frac{1.67*0.13}{20} = 0.0109\,m$. Since the grid should be orthogonal, a grid size of $\Delta x = \Delta y = 0.01\,m$ is used in the OpenFoam domain. Table 15 shows the grid sizes and number of grid cells per wave length or wave height.

Model	$\Delta x\ [m]$	Grid cells per L_0	$\Delta y\ [m]$	Grid cells per H_{m0}	Grid cells per $H_{1/100}$
OceanWave3D	0.1	25 - 88	–	–	–
OpenFoam	0.01	250 - 880	0.01	13	22

Table 15 – Grid sizes and number of grid cells per wave length or wave height.

OpenFoam changes the timestep of the simulation automatically in order to limit the courant number. However, a beginning timestep has to be chosen. A limit for the timestep is the courant number, $C = \frac{u*\Delta t}{\Delta x}$, which has to be smaller than 1. As flow velocity, u, the wave speed of incoming waves is used, $u \approx 2.53\,\frac{m}{s}$ (calculated with linear wave theory for shallow water). This results in a maximum time step of $\Delta t \leq 0.004\,s$. Therefore a starting timestep of $\Delta t = 0.004\,s$ is chosen.

7.2.4 Wave gauges and pressure probes

On several locations in the OpenFoam simulation the surface level elevation is measured. Table 16 shows the locations of the wave gauges in the OpenFoam model.

Wave Gauge #	x-coordinate	Wave Gauge #	x-coordinate	Wave Gauge #	x-coordinate
1	37.0	4	43	7	46
2	39.0	5	44	8	47
3	41.0	6	45		

Table 16 - locations of the wave gauges in the OpenFoam model

Besides the wave gauges, two sets of pressure probes are included in the OpenFoam model to measure the pressure, flow velocity and the α-value along these lines. The α-value is used by OpenFoam to check if the cell consists of water or air. If $\alpha = 1$ the cell is filled with water, if $\alpha = 0$ the cell is filled with air. These lines each consist out of 250 pressure probes, evenly spaced along the lines. The locations of these pressure probe lines are located on the armour layer (line 1) and on the interface between the armour layer and the filter layer (line 2). The pressure probe lines are positioned in such a way that when an imaginary line is drawn from pressure probe X of pressure probe line 1 towards pressure probe X of pressure probe line 2, the imaginary line is perpendicular to the front slope. The coordinates of the lines are given in Table 17. The location of the pressure probe lines is shown by the red dashed line in Figure 44.

Pressure probe line #	Begin of pressure probe line		End of pressure probe line	
	x-coordinate	y-coordinate	x-coordinate	y-coordinate
1	45.9127	0.2247	48.4433	1.4900
2	45.9552	0.1397	48.4858	1.4050

Table 17 - locations of the pressure probe lines in the OpenFoam model

Note: structure 4 does not have a filter layer. In all the other four structures, the armour layer has the same thickness. In order to make a good comparison, the second pressure probe line for structure 4 is located on the same coordinates as the lines in structures 1, 2 and 3.

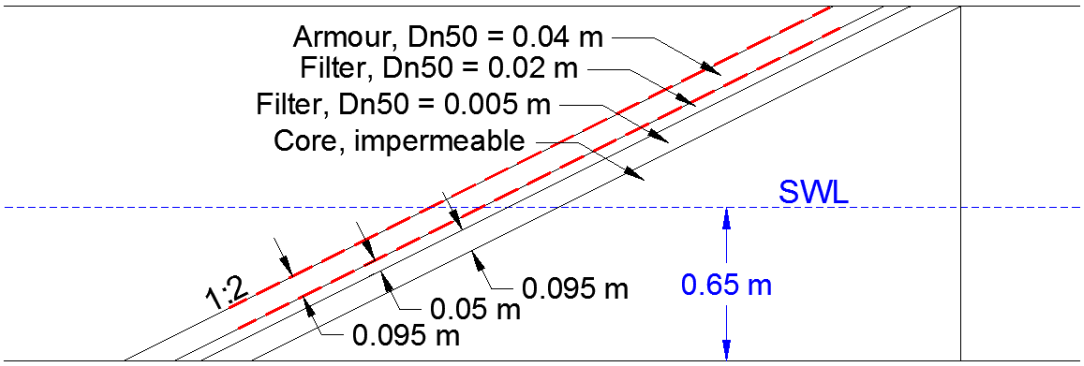

Figure 44 - Location of the pressure probe lines in the OpenFoam model (in structure 1)

7.3 Intermezzo: Influence of variation in P on the required rock grading

Some arbitrary calculations using the Van der Meer formula for plunging waves are made to investigate how much influence a change in P has on the required rock grading. When P is between 0.5 and 0.3, a reduction of P of 0.01 leads to an increase in the required M_{50} of approximately $2-4\ \%$ (depending on the wave conditions). This percentage becomes slightly lower when the P-value becomes lower, but is mainly governed by the wave conditions used in the Van der Meer Formulas. Translated in a rubble mound breakwater with a P-value of 0.4 and a required M_{50} of approximately $2500\ kg$ for the armour layer, a reduction of P of 0.01 lead to an increase in the required M_{50} of $65-100\ kg$. A reduction of P of 0.1 lead to an increase in the required M_{50} of $650-1100\ kg$.

Since the steps between the standard rock classes is quite big, a deviation of a few hundreds in a prediction of P does not have a lot of influence on the final required rock class. A deviation of one tenth in the prediction of P might have influence on the final required rock class. Therefore a deviation in predicted P-value of 0.03 is considered acceptable.

7.4 Results

In this part of the chapter, the results of the three prediction methods is included, each prediction method has its own section.

7.4.1 Local wave induced water pressure difference over the armour layer ($\Delta p_{\perp,loc,2\%}$)

Figure 45 shows the result of the prediction method for the notional permeability with the local wave induced water pressure difference over the armour layer ($\Delta p_{\perp,loc,2\%}$). The predicted P-value for structure 1 with this method is 0.31. The graph indicates that the linear fit for the prediction of P using pressure seems to be valid. Compared to the value found by (Kik, 2011), this method underestimates the P-value of the structure by 0.06 (approximately 15%).

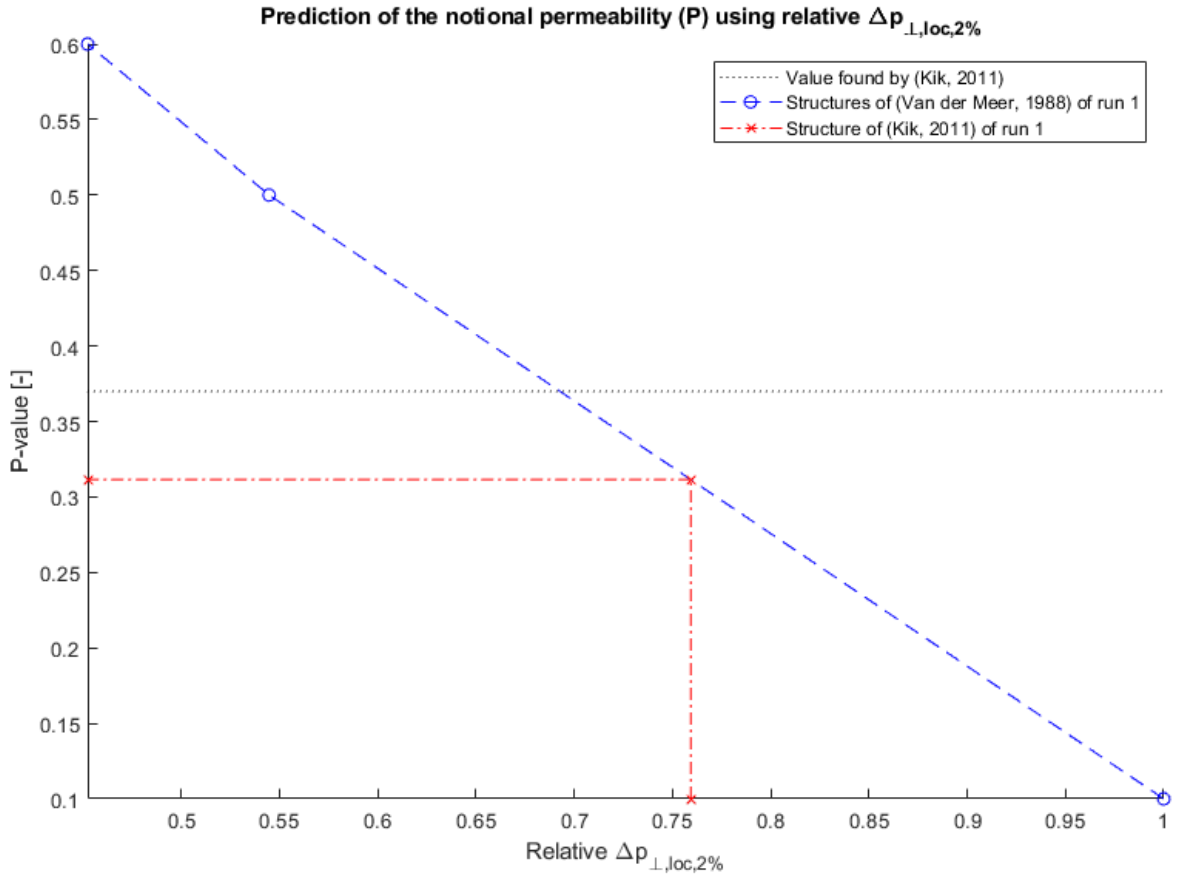

Figure 45 - Prediction of the notional permeability with the local wave induced pressure difference over the armour layer ($\Delta p_{\perp,loc,2\%}$)

7.4.2 Total wave induced water pressure difference over the armour layer ($\Delta p_{\perp,tot,2\%}$)

Figure 46 shows the result of the prediction method for the notional permeability with the total wave induced water pressure difference over the armour layer ($\Delta p_{\perp,tot,2\%}$). The predicted P-value for structure 1 with this method is 0.35. Also this graph indicates that the linear fit for the prediction of P using pressure seems to be valid. Compared to the value found by (Kik, 2011), this method underestimates the P-value of the structure by 0.02 (approximately 5%).

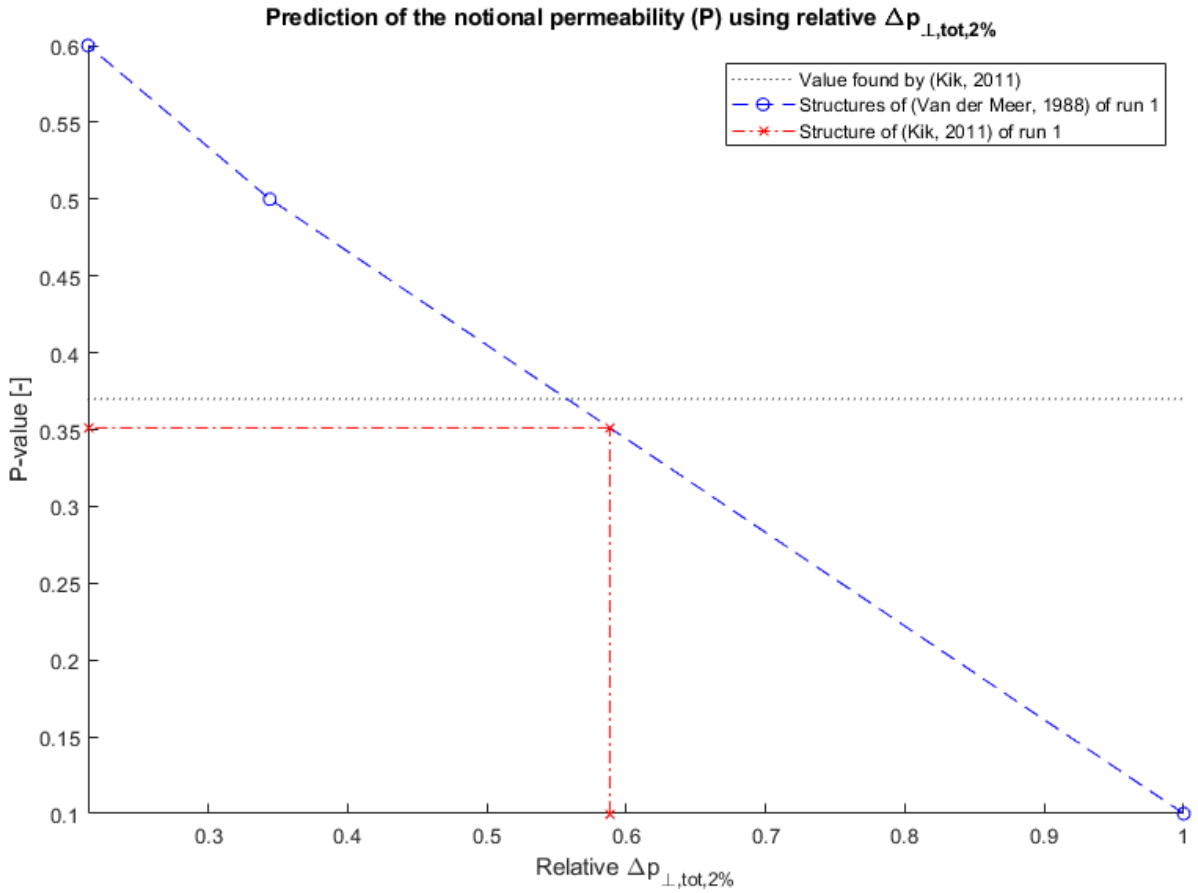

Figure 46 - Prediction of the notional permeability with the total wave induced pressure difference over the armour layer ($\Delta p_{\perp,tot,2\%}$)

7.4.3 The wave induced discharge through the armour layer ($Q_{\perp,tot,2\%}$)

Figure 47 shows the result of the prediction method for the notional permeability with the wave induced discharge through the armour layer ($Q_{\perp,tot,2\%}$). The predicted P-value for structure 1 with this method is 0.25. Compared to the value found by (Kik, 2011), this method underestimates the P-value of the structure by 0.12 (approximately 30%).

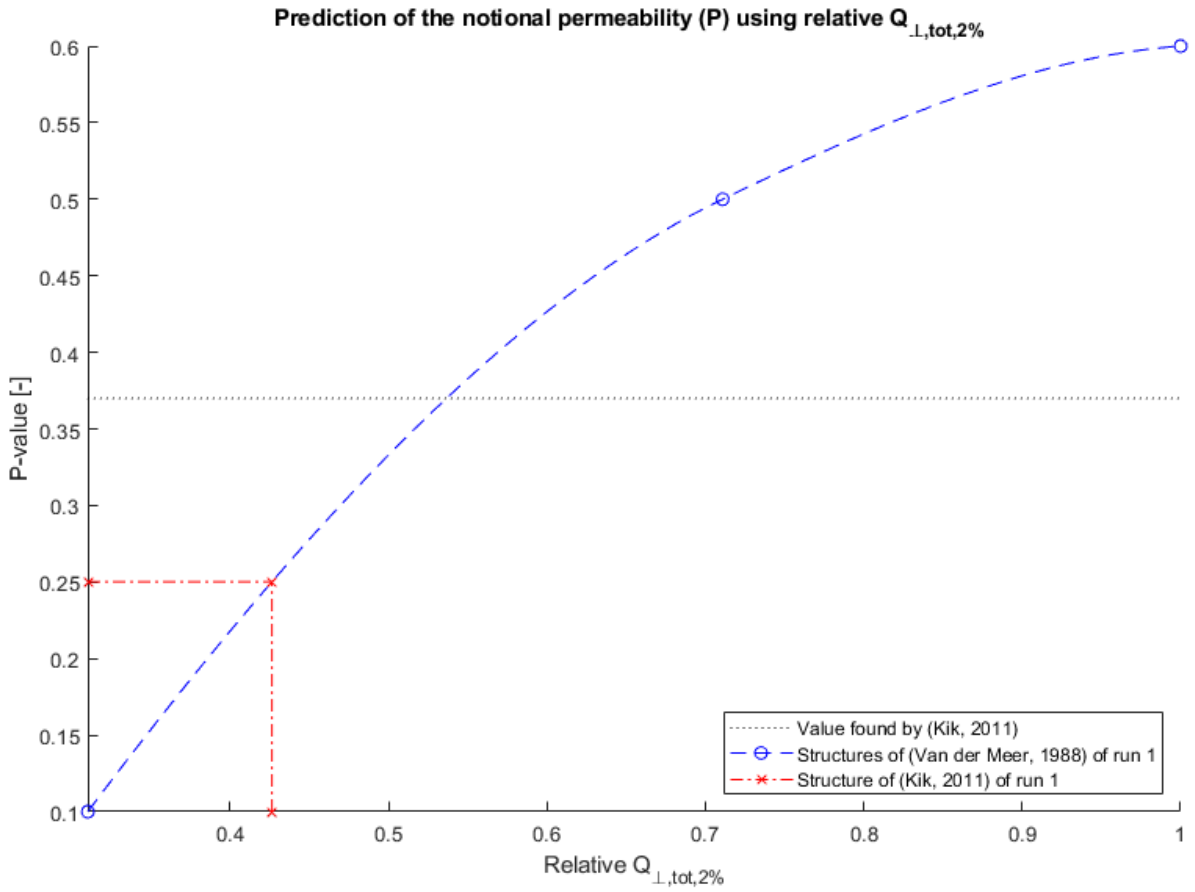

Figure 47 - Prediction of the notional permeability with the total wave induced discharge through the armour layer ($Q_{\perp,tot,2\%}$)

7.5 Discussion and conclusions

The prediction method using the total wave induced water pressure over the armour layer ($\Delta p_{\perp,tot}$) predicts a P-value closes to the P-value found by (Kik, 2011) and (Kluwen, 2012). The predicted P-value is 0.35 with this prediction method and (Kik, 2011) and (Kluwen, 2012) found a value of respectively 0.37 and 0.38 for structure 1. The prediction method using the local wave induced water pressure over the armour layer ($\Delta p_{\perp,loc}$), predicts the P-value a bit less well, with a value of 0.31. The prediction method using the total discharge ($Q_{\perp,tot}$) predicts the P-value even worse, with a value of 0.25. This indicates that the method using the total wave induced water pressure over the armour layer ($\Delta p_{\perp,tot,2\%}$) is the best method for predicting the notional permeability of a structure. The deviation in the predicted P-value using this method is 0.02, which is considered to be acceptable.

This method indicates that the notional permeability can be related to the total wave induced water pressure over the part of the armour layer where damage occurs. This sounds quite logical since the notional permeability is related to the total damage of the armour layer. And the total damage of the armour layer is related to the resulting force on the armour layer, which depends again on the resulting pressure on the armour layer. Therefore it is concluded that the prediction method using the total wave induced water pressure over the armour layer ($\Delta p_{\perp,tot}$) is the best prediction method for predicting the notional permeability.

8 Step IV: sensitivity analysis of the preferred prediction method

8.1 Introduction

The sensitivity of the prediction method for changes in the input parameters is investigated. The influence of changes in the hydraulic conditions, in the structural parameters and in the numerical parameters are of interest. In order to limit the number of parameters on which the sensitivity analysis is performed, for each of these three parameter types, one parameter is investigated. To limit the amount of work of the sensitivity analysis, only the influence of changes in parameters on the prediction method using the total wave induced water pressure over the armour layer ($\Delta p_{\perp,tot,2\%}$) is investigated. The following parameters are changed to investigate the sensitivity of the prediction method:

- Wave conditions (hydraulic parameter)
- Porosity of the porous layers (structural parameter)
- Applied Forchheimer parameters (numerical parameter)

The wave conditions are changed because both (Van der Neut, 2015) and (Franken, 2016) found that the wave conditions have influence on the notional permeability. The porosity of the porous layers is changed since the notional permeability represents the permeability of the breakwater structure and the porosity of porous layers for an in-situ breakwater can never be designed or calculated with 100% certainty. The applied Forchheimer parameters are varied since different values for these parameters are given in various literature pieces but the influence of changing these parameters is not investigated.

The porosities of the porous layers of the structures of Van der Meer (structures 2, 3 and 4) were not modelled correctly in the OpenFoam model tests for the sensitivity analysis. The modelled values for the porosity of all porous layers was set to a value of 0.44. This has influence on the validity of the predicted P-values in this chapter, however these predicted P-values are of no interest. Only the differences between the predicted P-values are of interest and it is assumed that the wrongly imposed porosities do not have a significant influence on these differences since the porosity is kept constant between the compared simulations (except for the sensitivity analysis on the porosity itself of course).

8.2 Numerical model set-up

The base model setup is described in section 7.2. This section discusses the changes in set-up of the numerical models for the sensitivity analysis. Each of the changed parameters is covered in their own section and in the last section a summarizing test matrix is included.

8.2.1 Change in wave conditions

A variation in the applied Pierson-Moskowitz spectra will be used to investigate the influence of the steepness of the incoming waves on the notional permeability. The original wave spectrum used had waves with an average steepness of 2.4%. As stated by (Kik, 2011), the waves that reach breakwaters in the real world have an average steepness ranging from approximately 1% till approximately 5%, therefore the wave period is changed to create steeper and less steep waves. Changing the steepness of the waves has influence on the Iribarren number, this means that the shorter waves are plunging waves, the longer waves are still surging. The total simulation time is still chosen such that approximately 500 waves reach the structure. The properties of the three Pierson-Moskowitz spectra are shown in Table 18.

	$H_{m0}\ [m]$	$T_{m0}\ [s]$	$T_p\ [s]$	$L_{m0}\ [m]$	$s\ [-]$	ξ_m	$T_{sim}\ [s]$
Original spectrum	0.13	2.3	3.01	5.33	2.4%	3.2	1175
Spectrum 2	0.13	1.3	1.70	2.46	5.3%	2.2	675
Spectrum 3	0.13	3.6	4.71	8.78	1.5%	4.1	1825

Table 18 - Properties of the Pierson-Moskowitz spectra used

The sensitivity analysis on a change in wave conditions makes use of sim numbers X.1, X.2 and X.3 (where X stands for the structure number) from the test matrix, Table 19.

8.2.2 Change in the porosity of the porous layers

To investigate the influence of a change in porosity of the porous layers in the simulated structures, the porosity of all porous layers of all structures (so both the structure of Kik as the structures of Van der Meer) is changed from a value of 0.44 to a value of 0.396 ($= -10\ \%$) and to a value of 0.484 ($= +10\%$). All the other properties of the porous layers are kept the same as described in section 7.2.1.

The sensitivity analysis on a change in the porosity of porous layers makes use of sim numbers X.1, X.4 and X.5 (where X stands for the structure number) from the test matrix, Table 19.

8.2.1 Change in applied Forchheimer parameters

The influence of the Forchheimer parameters is investigated by changing the Forchheimer parameter, α and β, for all porous layers in all structures. The Forchheimer parameters used in the prediction method were based on the values advised by (Van Gent, 1995): $\alpha = 1000$ and $\beta = 1.1$. In the sensitivity analysis, the Forchheimer parameters are changed towards the values advised by (Jensen et al., 2014): $\alpha = 500$ and $\beta = 2.0$.

The sensitivity analysis on a change in the applied Forchheimer parameters makes use of sim numbers X.1 and X.6 (where X stands for the structure number) from the test matrix, Table 19.

8.2.2 Test matrix sensitivity analysis

The simulations for the sensitivity analysis are summarized in Table 19, with all the changed parameters displayed in **bold**. The parameters that are indicated with a *, are changed to the value indicated in the table for every porous layer. Sim 1.0, 2.0, 3.0 and 4.0 are the simulations from step III, chapter 7.

Structure 1 ($P \approx 0.37$)								
Sim #	Name:	T_{m0} $[s]$	T_p $[s]$	L_{m0} $[m]$	n $[-]$*	α $[-]$*	β $[-]$*	T_{sim} $[s]$
1.0	Run1.0	2.3	3.01	5.33	0.440	1000	1.1	1175
1.1	Run1.1	2.3	3.01	5.33	0.440	1000	1.1	1175
1.2	Run1.2	**1.3**	**1.70**	**2.46**	0.440	1000	1.1	**675**
1.3	Run1.3	**3.6**	**4.71**	**8.78**	0.440	1000	1.1	**1825**
1.4	Run1.4	2.3	3.01	5.33	**0.396**	1000	1.1	1175
1.5	Run1.5	2.3	3.01	5.33	**0.484**	1000	1.1	1175
1.6	Run1.6	2.3	3.01	5.33	0.440	**500**	**2.0**	1175
Structure 2 ($P = 0.1$)								
Sim #	Name:	T_{m0} $[s]$	T_p $[s]$	L_{m0} $[m]$	n $[-]$*	α $[-]$*	β $[-]$*	T_{sim} $[s]$
2.0	Run2.0	2.3	3.01	5.33	Varies per layer	1000	1.1	1175
2.1	Run2.1	2.3	3.01	5.33	0.440	1000	1.1	1175
2.2	Run2.2	**1.3**	**1.70**	**2.46**	0.440	1000	1.1	**675**
2.3	Run2.3	**3.6**	**4.71**	**8.78**	0.440	1000	1.1	**1825**
2.4	Run2.4	2.3	3.01	5.33	**0.396**	1000	1.1	1175
2.5	Run2.5	2.3	3.01	5.33	**0.484**	1000	1.1	1175
2.6	Run2.6	2.3	3.01	5.33	0.440	**500**	**2.0**	1175
Structure 3 ($P = 0.5$)								
Sim #	Name:	T_{m0} $[s]$	T_p $[s]$	L_{m0} $[m]$	n $[-]$*	α $[-]$*	β $[-]$*	T_{sim} $[s]$
3.0	Run3.0	2.3	3.01	5.33	Varies per layer	1000	1.1	1175
3.1	Run3.1	2.3	3.01	5.33	0.440	1000	1.1	1175
3.2	Run3.2	**1.3**	**1.70**	**2.46**	0.440	1000	1.1	**675**
3.3	Run3.3	**3.6**	**4.71**	**8.78**	0.440	1000	1.1	**1825**
3.4	Run3.4	2.3	3.01	5.33	**0.396**	1000	1.1	1175
3.5	Run3.5	2.3	3.01	5.33	**0.484**	1000	1.1	1175
3.6	Run3.6	2.3	3.01	5.33	0.440	**500**	**2.0**	1175
Structure 4 ($P = 0.6$)								
Sim #	Name:	T_{m0} $[s]$	T_p $[s]$	L_{m0} $[m]$	n $[-]$*	α $[-]$*	β $[-]$*	T_{sim} $[s]$
4.0	Run4.0	2.3	3.01	5.33	Varies per layer	1000	1.1	1175
4.1	Run4.1	2.3	3.01	5.33	0.440	1000	1.1	1175
4.2	Run4.2	**1.3**	**1.70**	**2.46**	0.440	1000	1.1	**675**
4.3	Run4.3	**3.6**	**4.71**	**8.78**	0.440	1000	1.1	**1825**
4.4	Run4.4	2.3	3.01	5.33	**0.396**	1000	1.1	1175
4.5	Run4.5	2.3	3.01	5.33	**0.484**	1000	1.1	1175
4.6	Run4.6	2.3	3.01	5.33	0.440	**500**	**2.0**	1175

Table 19 – summary of simulations for sensitivity analysis, the changed parameters are displayed in **bold**.

8.3 Results

In this part of the chapter, the results of the sensitivity analysis is included, each parameter that is changed to investigate the sensitivity in its own section.

8.3.1 Change in wave conditions

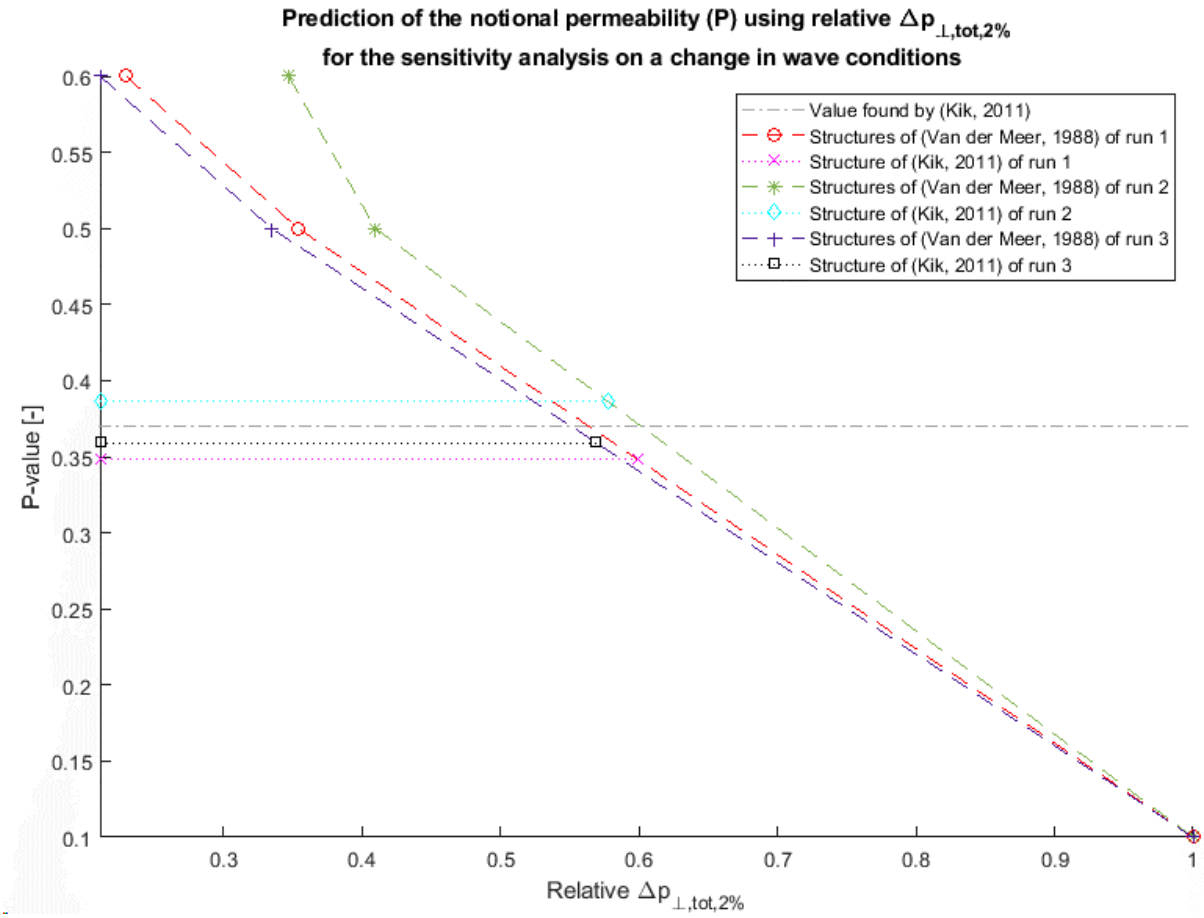

Figure 48 - Sensitivity analysis for different wave conditions, $\Delta p_{\perp,tot,2\%}$ relative to the value found in sim 2.X

Figure 48 shows the sensitivity on the wave conditions based on the prediction method which uses $\Delta p_{\perp,tot,2\%}$. The three dashed lines are the results of tests with the structures of Van der Meer for different wave conditions. The found values for $\Delta p_{\perp,tot,2\%}$ for the different simulations are all made relative to the found value for structure 2 for the same wave conditions (sim 2.X, where X is the wave spectrum number). The predicted P-values are shown in Table 20. This means a difference of 0.038 between the highest and the lowest predicted P-value.

The green dashed line (simulation runs with shorter waves, sim X.2) has a different shape compared to the other runs, this is probably due to the shape of the waves. The waves in simulation runs sim X.2 are with plunging waves, while the waves in simulation runs sim X.1 and sim X.3 are with surging waves. Besides, in the OceanWave3D simulations of the simulation runs sim X.2, the grid in x-direction is too coarse, see section 10.2.4 of the discussion.

	Structures of Van der Meer		
	RunX.1 ($T_p = 3.01$) (Red dashed line with circles)	RunX.2 ($T_p = 3.01$) (Green dashed line with asterisks)	RunX.3 ($T_p = 3.01$) (Blue dashed line with plusses)
Structure of Kik (magenta crosses, cyan diamonds and black squares)	0.348	0.386	0.359

Table 20 - predicted P-values for runs with different wave conditions

The required M_{50} for the armour layer will change when the wave conditions change, the relative small extra change in required M_{50} due to a slightly different P-value will be negligible compared to this.

8.3.2 Change in the porosity of the porous layers

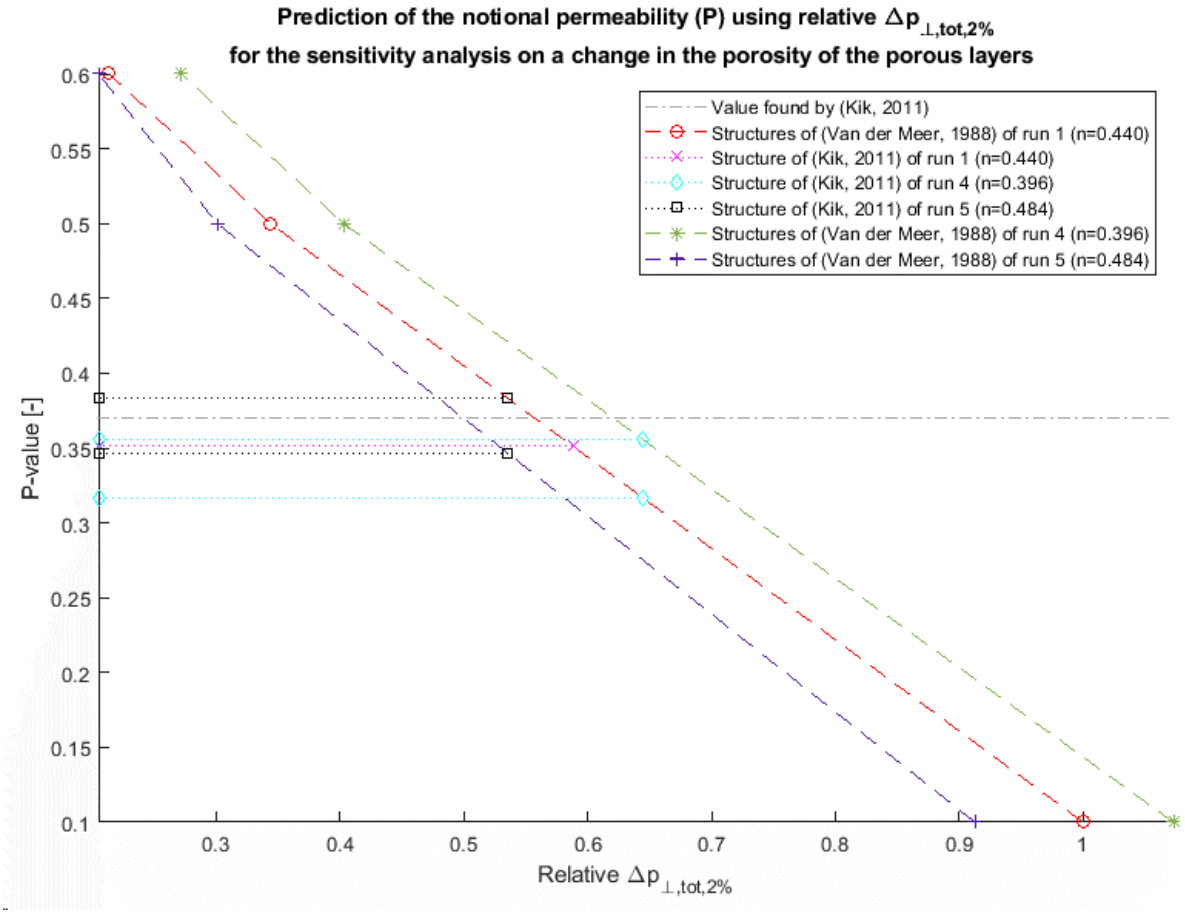

Figure 49 - Sensitivity analysis for different porosities of the porous layers

Figure 49 shows the sensitivity on the porosity of the porous layers based on the prediction method which uses $\Delta p_{\perp,tot,2\%}$. The three dashed lines are the results of tests with the structures of Van der Meer with different porosities for the porous layers. As described in section 8.1, the porosity for all porous layers is set to the same value in one structure. The found values for $\Delta p_{\perp,tot,2\%}$ for the different simulations are all made relative to the found value of sim 2.1 (structure of Van der Meer with a P-value of 0.1 and a porosity of the porous layers of $n = 0.44$). The black squares, magenta crosses and cyan diamonds represent the results of the simulations of structure 1 with different values for the porosity of the porous layers. Table 21 shows all the predicted P-values (the values of the dotted lines on the y-axis).

	Structures of Van der Meer		
Structures of Kik	RunX.1 ($n = 0.44$) (Red dashed line with circles)	RunX.4 ($n = 0.396$) (Green dashed line with asterisks)	RunX.5 ($n = 0.484$) (Blue dashed line with plusses)
Run1.1 ($\boldsymbol{n = 0.44}$) (magenta crosses)	0.351	-	-
Run1.4 ($\boldsymbol{n = 0.396}$) (cyan diamonds)	0.317	0.356	-
Run1.5 ($\boldsymbol{n = 0.484}$) (black squares)	0.383	-	0.347

Table 21 - predicted P-values for runs with different porosities of the porous layers

From Figure 49 and Table 21, two analysis can be done. The first one is when looking at the influence of changing the porosity of all porous layers in all structures, so looking at the black square on the blue line, the magenta cross on the red line and the cyan diamond on the green line. When looking at the predicted P-values for these three simulations (the diagonal from left top to right bottom in Table 21), it can be seen that changing the porosity of all porous layers in all structures has a negligible influence on the predicted P-value, the maximum difference is 0.011.

The second analysis which can be performed is by looking at the influence of changing the porosity of the porous layers of only structure 1, so looking at the black square, the magenta cross and the cyan diamond on the red line. When looking at the predicted P-value for these three simulations (the left column in Table 21), it can be seen that changing the porosity of the porous layers has quite an influence on the predicted P-value, the maximum difference is 0.066. However, there is a big difference between the used porosity values. Besides, a porosity value of 0.484 corresponds to a rock grading of d_{85}/d_{15} close to 1, which is unrealistically low (a rock grading of $d_{85}/d_{15} = 1$ means that the used rock is single-sized). The porosity value of 0.396 corresponds to a rock grading of approximately $d_{85}/d_{15} \approx 2.25$, which means that the rocks have quite a wide gradation. A grading of $d_{85}/d_{15} = 2.25$ (or higher) is common for rip-rap, often used in cores of rubble mound breakwaters, but not for armour layers. According to the rock manual, (CIRIA et al., 2007), in most cases, armourstone is narrow graded. Therefore it can be concluded that the sensitivity analysis for the porosity of the porous layers of structure 1 is carried out for a too low and a too high value of the porosity.

The following values should have been better to use in the sensitivity analysis for the porosity of structure 1:

- $n = 0.449$ corresponding to a grading value of $d_{85}/d_{15} \approx 1.4$
- $n = 0.434$ corresponding to a grading value of $d_{85}/d_{15} \approx 1.6$

Although not tested, it is expected that applying the values for the porosity suggested above will have an influence on the predicted P-value of no more than 0.02 (probably less). This suggests that the prediction method is not very sensitive for changes in the applied porosities of the porous layers of the tested structure. However, this is not tested and should be verified.

8.3.3 Change in applied Forchheimer parameters

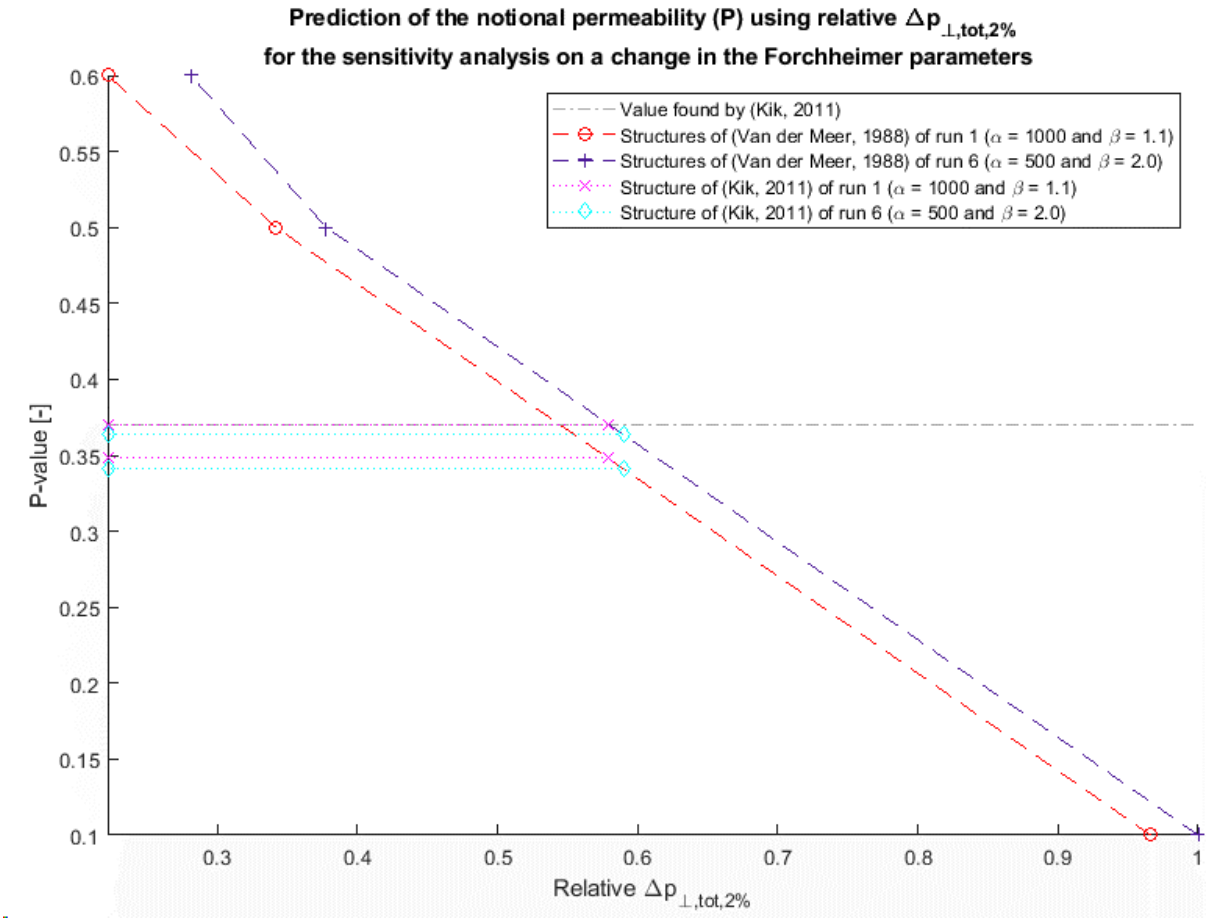

Figure 50 - Sensitivity analysis for different applied Forchheimer parameters

Figure 50 shows the sensitivity on the Forchheimer parameters based on the prediction method which uses $\Delta p_{\perp,tot,2\%}$. The two dashed lines are the results of tests with the structures of Van der Meer with different Forchheimer parameters. The found values for $\Delta p_{\perp,tot,2\%}$ for the different simulations are made relative to the found value of sim 2.1 (structure of Van der Meer with a P-value of 0.1 and a α-value of 1000 and a β-value of 1.1). The magenta crosses and cyan diamonds represent the results of the simulations of structure 1 with different values for the Forchheimer parameters. Table 22 shows all the predicted P-values (the values of the dotted lines on the y-axis).

	Structures of Van der Meer	
Structures of Kik	RunX.1 (Red dashed line with circles) ($\alpha = 1000$ and $\beta = 1.1$)	RunX.6 (Blue dashed line with plusses) ($\alpha = 500$ and $\beta = 2.0$)
Run1.1 (magenta crosses) ($\boldsymbol{\alpha = 1000}$ and $\boldsymbol{\beta = 1.1}$)	0.348	0.371
Run1.4 (cyan diamonds) ($\boldsymbol{\alpha = 500}$ and $\boldsymbol{\beta = 2.0}$)	0.341	0.363

Table 22 - predicted P-values for runs with different values of the Forchheimer parameters for the porous layers

When looking at Figure 50 and Table 22, it can be seen that the Forchheimer parameters applied in the modelling of the structures of Van der Meer (structure 2, 3 and 4), has only a small influence on the predicted P-value of the tested structure. This can be seen by comparing the rows of Table 22, the difference between the predicted values of P in these rows is approximately $0.022 - 0.023$.

The difference between the predicted values of P in the columns of Table 22 is $0.007 - 0.008$ which show that the Forchheimer parameters of the simulated structure is of little influence.

A maximum difference of 0.03 can be found between the highest and lowest predicted P-value, however this only happens when different Forchheimer parameters are applied for the new structure than for the structures of Van der Meer. It is advised to apply the same Forchheimer parameters for all structures.

8.4 Discussion and conclusions

Changing the period of the incoming spectra has a small influence on the predicted P-values. A difference of 0.038 was found between the highest and lowest predicted P-value. The required M_{50} for the armour layer will change when the wave conditions change, the relative small extra change in required M_{50} due to a slightly different P-value will be negligible compared to this. It is noted that the prediction with the shortest waves (sim X.2) results in the highest predicted P-value but the simulation with the longest waves (sim X.3) does not result in the lowest predicted P-value. This has probably something to do with the fact that the longer waves (sim X.3) are surging waves (as is in sim X.1) and the shortest waves (sim X.2) are plunging waves. The exact influence of this has to be investigated further. It can be concluded that changing the wave conditions has influence on the predicted P-value but since the wave conditions are also incorporated in the Van der Meer formulas, this influence is negligible compared to the required rock grading.

From the sensitivity analysis on a change in the porosity of the porous layers it can be seen that changing the porosity of all porous layers in all structures has a negligible influence on the predicted P-value with respect to the required rock grading.

For the sensitivity analysis for the porosity of the porous layers of the structure with unknown P-value, the applied porosity values are too high and too low. Although not confirmed by tests, it seems that the prediction method is not very sensitive for changes in the applied porosities of the porous layers of the structure with unknown P-value.

Changing the applied Forchheimer parameters has a small influence on the predicted P-values. Changes in the Forchheimer parameters used for the structures of Van der Meer are of a bigger influence than changes in the Forchheimer parameters used in the structure with unknown P-value. A maximum difference of 0.03 was found between the highest and lowest predicted P-value, however this only happens when different Forchheimer parameters are applied for the new structure than for the structures of Van der Meer. It is advised to apply the same Forchheimer parameters for all structures, in that case, the maximum difference of 0.023 was found. It is not known which values are best to use but the influence of the applied Forchheimer parameters on the predicted P-value is small. The advice is to use the values for the Forchheimer parameters advised by (Van Gent, 1995) ($\alpha = 1000$ and $\beta = 1.1$), since by using these values, the predicted P-value is slightly lower, which might lead to a higher required rock grading. Thus using the Forchheimer parameters advised by (Van Gent, 1995) is a bit more conservative.

9 Proposed engineering approach

In this chapter is discussed how the new method can be applied in the engineering approach. In the proposed engineering approach, the prediction method is used as it is described in this thesis to improve initial design of a breakwater. The proposed engineering approach is to follow the following steps:

1. Design a cross-section of a breakwater structure based on e.g. optimal use of available materials for which the P-value is unknown and, for now, (over-)estimate the armour layer by using the Van der Meer formulas and a conservative value for the P-value.

2. Simulate this designed structure and the three structures of Van der Meer for the governing design wave conditions with OpenFoam. See Appendix C on how to set-up such an OpenFoam model.

3. Predict the P-value of the designed structure using interpolation of the simulated total wave induced water pressure difference over the armour layer ($\Delta p_{\perp,tot,2\%}$)

4. Update the design of the armour layer with the Van der Meer formulas using the predicted P-value.

5. (optional) Re-simulate the updated design for the governing design wave conditions with OpenFoam, predict the P-value of the updated structure and update the design of the armour layer again with the Van der Meer formulas (This step is optional since it is expected that the optimization achieved in this step is limited).

6. Validate and optimize the design with physical model testing.

By applying this engineering approach, the design is optimized a bit before it is tested in physical model tests. The downside of this engineering approach is that for every breakwater design a new set of simulations has to be performed.

10 Discussion

The discussion is split in two parts, a part on the model validation and a part on the prediction of the notional permeability

10.1 Model validation

For the model validation there are four topics which are discussed in this section:

- The coupling of Oceanwave3D with OpenFoam
- Water set-up on the lee side of the breakwater
- Wave run-up and wave run-down
- Peaks in pressure measurements above the still water level

10.1.1 The coupling of OceanWave3D with OpenFoam

In the model validation, the OpenFoam domain is connected with the fully nonlinear potential wave solver OceanWave3D (Engsig-Karup et al., 2009) through the relaxation zone on the sloping foreshore. The bottom of the wave flume in the OpenFoam domain is not aligned with the bottom of the OceanWave3D domain in this relaxation zone (on the left side the difference is highest and the bottom are on the same level on the right side of the relaxation zone).

The relaxation zones work as described by (Paulsen et al., 2014), see section 2.2.2 of the literature study. This difference in bottom level leads to an error in the transmitted wave energy through the relaxation zone. However, since the target solution, χ_{target}, had to be interpolated between the grid points in vertical direction in the OceanWave3D domain onto the OpenFoam domain, and the difference in bottom level is smaller than this vertical grid size in the OceanWave3D domain, the error is very small. Besides, for every step of Δx in the OpenFoam domain, the velocity field and water fraction is calculated based on both the simulated values (with small errors) and the target solution. And when progressing to the OpenFoam side of the relaxation zone, the difference in bottom level becomes smaller which causes the error to become even smaller. Therefore the solutions of a simulation with the coupling in front of the sloping foreshore and the simulation with the coupling as it is used in the model validation case match quite well, see also Appendix B. Besides, the difference in bottom level is very small in comparison with the water depth.

However, even though this error is very small, there is an error, so for a 100% correct coupling of OceanWave3D with OpenFoam, a coupling in front of the sloping foreshore should be used, or the coupling on top of the sloping foreshore should be corrected. Fixing this coupling is not expected to have any significant influence on the found results.

10.1.2 Water set-up on the lee side of the breakwater

In the physical model tests which are used for the model validation, a set-up of water can be noted, see section 5.3.3. This water level set-up does have influence on the measured results but this water level set-up is not modelled in the OpenFoam model. For the validation of the hydraulic loading parameters, the influence of this water level set-up is negligible, since the hydraulic loading parameters are measured around the front slope and the water level set-up is negligible at this side of the structure but increases towards the lee side of the structure. What the precise influence of this water level set-up is on the measurements is not known. This means that in the model validation it is not known if the differences in the measured and simulated results are due to this water level set-up or something else, e.g. that OpenFoam does not simulate some processes correctly.

The effect of the water set-up on the lee side of the breakwater can be checked quite easily by simply changing the boundary condition on the lee side of the breakwater. A simulation of this water level set-up in OpenFoam suggests that the water level set-up is the cause of some the difference between the measured and simulated results (the results of this quick simulation are not included in this thesis report due to time limitations). More research has to be performed on this.

10.1.3 Wave run-up and wave run-down

As already discussed in section 5.3.4, there are doubts about the simulation of the wave run-up and the wave run-down in OpenFoam. This is due to the fact that in reality, the top of the armour layer is a rough surface, while in OpenFoam it is modelled as a smooth surface. Furthermore, it is not possible to implement the roughness of the front slope in the OpenFoam model and there is no turbulence model implied in the model. As described in 2.2.1, there is no turbulence model applied in the OpenFoam model because the resistance coefficients for the permeable structure include dissipation due to turbulence. Implying a turbulence model would require a lowering of the resistance coefficients. Furthermore, the position of the wave run up gauge in the physical model test, which is used for the model validation, is very unsure. More research should be performed on this in order to correctly model the wave run-up and run-down on a breakwater in OpenFoam.

10.1.4 Peaks in pressure measurements above the still water level

In the model validation, much higher peaks were observed in the wave induced pressure simulated by OpenFoam than in the measured pressure in the physical model tests, see section 5.3.5 and Appendix A. A possible explanation for this difference might be that the high peaks in pressure are due to the wave run-up and the measurement technique in the physical model tests. In the physical model tests the pressure sensors are protected by a casing which has influence on the flow and the measured pressure. Besides, the wave run-up is not correctly modeled by OpenFoam, the wave run-up is higher in OpenFoam than in the physical model tests, see 10.1.3. This causes higher pressure in the part of the wave run-up zone above the still water level. This is however not validated yet and should be investigated further.

10.2 Prediction of the notional permeability

For the prediction of the notional permeability, the following topics are discussed in this section:

- Duration of the pressure difference over the armour layer
- Peaks in pressure measurements above the still water level
- Sensitivity analysis
- Grid resolution in OceanWave3D
- Comparison with literature

10.2.1 Duration of the pressure difference over the armour layer

The value for $\Delta p_{\perp,tot,2\%}$ might be present for only a very short period of time, with a much lower value just before and right after this short period of time. The total duration of this period of time is not taken into account in the prediction methods. This means that it might be possible that the used value of $\Delta p_{\perp,tot,2\%}$ is not present long enough to initiate motion of the armour stones and thus will not cause any damage. Although the highest/shortest peaks are filtered by taking the 2% exceedance value in time for the total pressure difference over the armour layer, the values of $\Delta p_{\perp,tot,2\%}$ might still be sensible to outliers. Besides, the time step in the OpenFoam simulations might influence the 2% exceedance value in time. More research on the time influence on the predicted P-values should be performed.

10.2.2 Peaks in pressure measurements above the still water level

The peaks in pressure measurements above the still water level discussed in section 10.1.4 can also be observed in the simulations of the structures for the prediction of the notional permeability. The peaks occur in all simulated structures and the relative height for these peaks is the same for all simulations. These peaks might have influence on $\Delta p_{\perp,tot,2\%}$. However, the effect of these peaks on the predicted P-values is expected to be negligible since the P-values are predicted by means of interpolation and all the peaks with the same relative height are included in this interpolation for all structures.

10.2.3 Sensitivity analysis

In the sensitivity analysis, the sensitivity of the prediction method (using $\Delta p_{\perp,tot,2\%}$) on changes in the wave conditions is investigated. The wave conditions investigated differ in the steepness of the waves. The difference in this steepness is caused by changing the wave period of the incoming waves (and thus the wave length). A difference in wave steepness can also be caused by a change in wave height, this is not investigated but might have an influence on the prediction of P, because in that case the ratio of wave height with the rock diameter of the armour stones changes, as well as the ratio of the wave height with the water depth in front of the structure.

In the sensitivity analysis, the porosity of the porous layers is only changed for all the porous layers of a structure at once. The influence of changes in the porosity in between the porous layers of one single construction is not investigated. This might have an influence on the predicted P-values as well and should be investigated.

10.2.4 Grid size in OceanWave3D

In section 7.2.3 is stated that according to (26th ITTC Specialist Committee on CFD in Marine Hydronamics, 2011), at least 20 grid cells are required to resolve the shortest wave length for irregular waves. This is only correct for a 3rd or 4th order method, while OceanWave3D uses a 2nd order method. This means that for the OceanWave3D simulation at least 40 grid cells are required to resolve the shortest wave length for irregular waves. The chosen grid size in the OceanWave3D simulations was $\Delta x = 0.1\,m$, this corresponds with 53 grid cells per wave length for simulations sim X.0, sim X.1 and sim X.4 till sim X.6 (see Table 19 in section 8.2.2). For simulations sim X.3 the grid size corresponds with 88 grid cells per wave length and for simulations sim X.2, the grid size corresponds with 25 grid cells per wave length. From this it can be concluded that the results of simulations sim X.2 (the green dashed line in Figure 48 in section 8.3.1) might not be reliable since the grid size in x-direction is too big for the waves to resolve.

The same mistake is made for the model validation simulation. In section 5.2 is stated that according to (26th ITTC Specialist Committee on CFD in Marine Hydronamics, 2011), at least 40 grid cells are required to resolve the shortest wave length (at least 20 grid points for irregular waves). Again, this is only correct for a 3rd or 4th order method, while OceanWave3D uses a 2nd order method. This means that for the OceanWave3D simulation at least 80 grid cells are required to resolve the shortest wave length for regular waves. The chosen grid size in the OceanWave3D simulation was $\Delta x = 0.5\,m$. This corresponds to 73 grid cells per wave length. According to the criteria provided by (26th ITTC Specialist Committee on CFD in Marine Hydronamics, 2011), this is not enough. However, the grid size in x-direction is only slightly too big and the spectrum analysis, reflection analysis and wave gauge comparison show good comparison, therefore it is assumed that the error in the model validation is negligible.

In the OpenFoam domains the grid size in x-direction are determined by the grid size in y-direction since the grid cells are required to have an aspect ratio of 1 and thus this mistake is not made.

10.2.5 Comparison with literature

In their theses, (Van der Neut, 2015) and (Franken, 2016), concluded that the notional permeability of a structure is not only dependent on structural properties but also on hydraulic conditions. In the sensitivity analysis in this thesis it is found that changes in the hydraulic conditions do have some influence on the predicted P-value. The influence of this small change in the predicted value of P on the required M_{50} of the armour layer is negligible compared to the influence the change in hydraulic conditions has on the required M_{50} of the armour layer.

In his thesis, (Franken, 2016), concluded that variations in the porous media input parameters (n, α, β and γ) of the second filter layer, have little influence on the notional permeability of the structure.

In the sensitivity analysis in this thesis, the Forchheimer parameters of all porous layers are changed. It is found that changing these Forchheimer parameters does have little influence on the predicted P-value. In the sensitivity analysis in this thesis, the porosity of the porous layers is changed as well. It is found that changing the porosity of all porous layers in all structures has almost no influence on the predicted P-value. For the sensitivity of the porosity of the porous layers of the structure with unknown P-value, the applied porosity values are too high and too low. Although not confirmed by tests, it seems that the prediction method is not very sensitive for changes in the applied porosities of the porous layers of the structure with unknown P-value.

These two comparisons combined indicate that the prediction method (using $\Delta p_{\perp,tot,2\%}$) for the notional permeability is very robust and that the dependencies of the notional permeability in previous research are included in the prediction method developed in this thesis.

Furthermore, (Franken, 2016) found that varying the thickness of the second filter layer has a large influence on P. The influence of the thickness of the second filter layer on the predicted P-value is not investigated in this thesis. However, it is believed that the thickness of the second filter layer is the major structural parameters that can be used to change the P-value of a structure.

The prediction method developed in this thesis makes use of irregular waves. (Franken, 2016) developed two prediction methods, one which uses irregular waves and one which can only be used with regular waves. Although breakwaters are normally only attacked by irregular waves, it might be interesting to see whether the prediction method developed in this thesis can also be used with regular waves (with e.g. $H = H_{2\%}$), since this will strongly reduce the total simulation time.

11 Conclusions and recommendations

For the conclusions on this research, the research questions are answered, each in their own section. The research question is repeated before the answer is given to improve the readability of the conclusions. Furthermore, feedback on the research objectives is given and some recommendations are given for future research.

11.1 Answer to research question I

RESEARCH QUESTION I Which hydraulic parameters influence the armour stability of a rock armoured rubble mound breakwater, in which way do these parameters influence the armour stability and how well are these parameters simulated by the numerical model of OpenFoam?

There are several hydraulic parameters that influence the armour stability of a rock armoured rubble mound breakwater. Based on stability concepts for rock stability in general, it is found that the following hydraulic parameters have influence on the armour stability of a rock armoured rubble mound breakwater:

- The (wave induced) water pressure difference over the armour layer
- The discharge of water through the armour layer (in outward direction)
- The flow velocity on top of the armour stones, parallel to the front slope
- The shear stress on top of the armour stones, parallel to the front slope
- The incoming significant wave height

These hydraulic parameters result in forces on the rocks in the armour layer. When the hydraulic parameters are higher than a critical value or a stability factor, the rocks in the armour layer are set into motion which causes damage.

It is not possible to simulate shear stresses with OpenFoam. Besides, shear stress is a consequence of flow velocity. The incoming significant wave height is an input parameter in OpenFoam. Pressures and flow velocities can be modelled in OpenFoam and the discharge can be calculated with these flow velocities. The pressures around and inside a breakwater structure is simulated accurately by OpenFoam for the part of the breakwater that is below the still water level. Above the still water level, some peaks in the wave induced water pressure occur which are not measured in physical model tests, more research on this is required. Although not measured in the physical model tests, the simulated flow velocities inside of the breakwater seem to be modelled accurate as well in OpenFoam, since the flow velocities inside porous layers are a consequence of the pressure gradient inside these layers and these pressures are modelled correctly.

The flow velocity on top of the armour layer could not be validated for the OpenFoam model with the available data. A clear difference in wave run-up and run-down between the physical model test and the numerical model test is noted which suggests that the flow velocity on top of the armour layer is not simulated correctly since this flow velocity is related to the wave run-up and run-down.

11.2 Answer to research question II

RESEARCH QUESTION II What is an appropriate method, with the help of the numerical model OpenFoam, to predict the notional permeability for rubble mound breakwaters?

By appropriate method, a method which fulfils the following requirements is meant:

- The method should be practically applicable.
- There must be a clear link between the method and the physical processes that influence the armour stability of rock armour layers.

Inspired by the research of (Franken, 2016), interpolation between characteristic values is used to predict the notional permeability. From the hydraulic parameters found in answering the first research question, two are investigated for prediction of the notional permeability:

- The wave induced water pressure difference over the armour layer, $\Delta p_{\perp}$
- The discharge through the armour layer perpendicular to the front slope, $Q_{\perp}$

These two parameters are called the hydraulic loading parameters. The other hydraulic parameters cannot be simulated with OpenFoam, are an input parameter for OpenFoam or there are doubts about the accuracy of the simulated values of the parameter.

The hydraulic loading parameter of the wave induced water pressure difference is split into two prediction methods, one for the local pressure difference, $\Delta p_{\perp,loc}$, (looking at a single point in space) and one for the total pressure difference, $\Delta p_{\perp,tot}$, (integrated along the front slope of the structure in space). The prediction method using the discharge as hydraulic loading parameter is also integrated along the front slope of the structure in space. For all three prediction methods, the 2% exceedance value of the hydraulic loading parameter is taken in time.

The prediction methods are validated for a structure cross-section for which (Kik, 2011) found a P-value of 0.37 by means of physical model testing. A P-value of 0.38 was found by (Kluwen, 2012) for the same structure cross-section by means of more physical model testing.

The prediction method using the total wave induced water pressure over the armour layer, $\Delta p_{\perp,tot}$, predicts a P-value closes to the P-value found by (Kik, 2011) and (Kluwen, 2012). The predicted P-value is 0.35 with this prediction method. The prediction method using the local wave induced water pressure over the armour layer ($\Delta p_{\perp,loc}$) predicts the P-value a bit less well, with a predicted P-value of 0.31. The prediction method using the total discharge ($Q_{\perp,tot}$) predicts the P-value even worse, with a predicted P-value of 0.25.

Therefore, it is concluded that an appropriate method to predict the notional permeability is by interpolation of the total pressure over the armour layer ($\Delta p_{\perp,tot}$). The prediction method using the local pressure over the armour layer ($\Delta p_{\perp,loc}$) is less good and the prediction method using the total discharge ($Q_{\perp,tot}$) is even worse.

The predicted P-value is marginally sensitive for changes in the wave conditions and changes in the Forchheimer parameters. Changing the porosity of all porous layers in all structures has a negligible influence on the predicted P-value. And although not confirmed by tests, it seems that the prediction method is not very sensitive for changes in the applied porosities of the porous layers of the structure with unknown P-value. Therefore, the method seems to be a robust method and can be practically used in engineering projects, following the engineering approach as described in chapter 9.

11.3 Feedback on research objectives

The research objectives of this thesis were:

RESEARCH OBJECTIVE I The first goal of the thesis project is to give more insight in the hydraulic processes that influence the armour stability of a rock armoured breakwater.

RESEARCH OBJECTIVE II The second goal of the thesis project is to develop an engineering approach which can be used to predict a value for the notional permeability for rubble mound breakwaters based on the processes relevant for armour stability.

The first research objective has been achieved. From step I of the thesis, chapter 4, it is clear that flow velocity on top of the armour layer (and the accompanying shear stress), discharge through the armour layer and pressure difference over the armour layer influence the armour stability. How the relation between these hydraulic processes is and how the combination of these hydraulic processes exactly influence the armour stability has to researched further.

The second research objective has been achieved as well. In this thesis a prediction method is developed which can be used to predict the notional permeability for a rubble mound breakwater, based on one of the processes relevant for armour stability. In chapter 9, the prediction method is translated in an engineering approach.

11.4 Recommendations

The recommendations following from this thesis are divided in several categories, based on the intended purpose of the recommendation. The recommendations are divided in recommendations for:

- Improvements of the prediction of P
- Better understanding of armour layer stability
- Other applications of the method
- Improving breakwater simulation with OpenFoam

11.4.1 Improvements of the prediction of P

To improve the prediction method, more investigation has to be carried out on the exact effect of different wave conditions on the prediction of P, and then specifically the difference between plunging and surging waves. The results of the sensitivity analysis on the wave conditions indicate that this has influence on the predicted P-value.

The prediction method uses the value of $\Delta p_{\perp,tot,2\%}$ which is the 2% exceedance value in time of the total wave induced pressure difference over the front slope of the breakwater from a level of $3\ H_s$ below the still water level upward. This level was chosen to make sure that all pressures that might contribute to the erosion of the armour layer are taken into account. It is known that the erosion area is from a level of 1 a $1.5\ H_s$ below the still water level upward. This indicates that a too large area is taken into account which may cause some inaccuracies in the calculated value of $\Delta p_{\perp,tot,2\%}$. To further improve the prediction method, the exact area that has to be taken into account can be investigated further. By reducing this area, the postprocessing time might be reduced as well. Another way to reduce the post-processing time is to reduce the number of pressure probes applied per pressure probe line. It should however be investigated by how many the number of pressure probes per pressure probe line can be reduced without having significant effect on the predicted P-value.

The simulations in the prediction method take quite some time, up to a couple of days (depending amongst others, on the specifications of the computer is used for the simulation and the number of processor cores is applied). These simulations take so much time because 500 waves have to be simulated. If the number of waves required can be reduced, the total simulation time can be reduced. In theory at least 50 waves are required to get a 2% exceedance value, but this will definitely reduce the accuracy of the predicted P-value. Therefore, more investigations have to be carried out on the influence of reducing the required number of waves on the prediction of P.

Furthermore, it might also be interesting to see investigate whether the prediction method developed in this thesis can be used with regular waves (e.g. with $H = H_{2\%}$), since this will strongly reduce the total simulation time.

Another improvement of the prediction method might be to include the time influence on the prediction of P, see section 10.2.1. Furthermore some more research on the influence of a change in the porosity of porous layers might be useful, see 10.2.3.

The last recommendation for the improvement of the prediction of P, is to develop the prediction method further into a design graph which can be used for a quick estimation of the notional permeability. The graph links the notional permeability of a structure with the thickness of the second filter layer, t_{f2}, (the layer between the filter layer and an impermeable core) and a wave parameter, e.g. the wave length.

See Figure 51 for a schematic representation on how such a graph would look like. (Franken, 2016) created a similar type of graph based on the found predictions of P in his thesis. It should however be investigated which other parameters should be included in the definition of such a graph. One might think of parameters such as the diameter of the armour stones or the porosity of the filter layer to have some influence on the P-value as well.

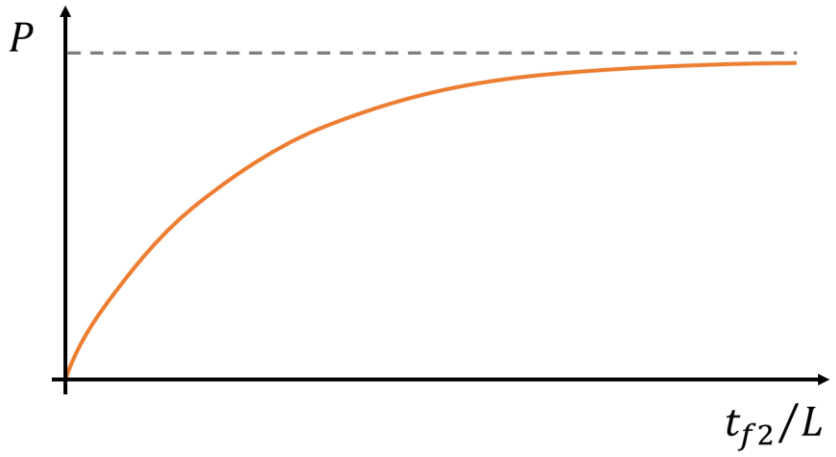

Figure 51 – Schematic representation of design graph

With such a design graph, a quick estimate can be made of the P-value of a breakwater cross-section based on the thickness of the second filter layer. Or, the other way around, a quick estimation on the required thickness of the second filter layer can be made to maintain a certain P-value for the structure. The downside is that it requires quite a lot of numerical simulations and analysis of these simulations to create such a graph. On the other hand, once such a graph is created, it will be a very valuable design tool.

11.4.2 Better understanding of armour layer stability

To create a better understanding of the armour layer stability, the correlation between the three hydraulic loading parameters defined in chapter 4 should be investigated. Since the stability of the armour stones is probably related to a combination of the pressures on the armour stones and the velocities (or discharges) around the armour stones.

11.4.3 Other applications of the method

The concept on which the prediction method developed in this thesis is based might also be applied for stability predictions of other hydraulic structures. An example for which the concept of linking the stability with the measured pressure might be applied is the design of breakwaters with an armour layer of concrete elements, e.g. Xbloc. The modelling of a breakwater with concrete elements seems to be correct in OpenFoam, as long as the values of the porosity, the equivalent rock diameter and the α, β and γ-parameters of the armour layer are known. The physical model test used to validate OpenFoam for the simulation of the hydraulic loading parameters was built with Accropods, see chapter 5. Numerical tests can be performed to create a graph like discussed in section 11.4.1 but now with the pressure reduction on the concrete elements as a function of the thickness of the filter layer. With such a graph an easy estimate can be made what the required size of the concrete element is.

11.4.4 Improving breakwater simulation with OpenFoam

As discussed in 5.3.4 and in 10.1.3, there are doubts about the simulation of the wave run-up and the wave run-down in OpenFoam. In order to improve the simulation of wave run-up and run-down in OpenFoam, it should be investigated if it is possible to include the roughness of the surface of the armour layer in the model or if it makes a difference if the surface of the armour layer is not simulated as a straight line, since the surface of the armour layer is never a straight, smooth surface. Furthermore should the application of a turbulence model in the OpenFoam simulation in combination with a porous structure be investigated further. Because, at this moment, when a porous structure is modelled in OpenFoam, no turbulence model should be applied since the dissipation due to turbulence is already included in the resistance coefficients for the porous layers. The wave run-up over the front slope of the breakwater can be manipulated by changing these resistance coefficients, however, this will influence the flow velocities and pressure distributions through the armour layer as well. More research should be performed on the influence of changing these resistance coefficients on the flow velocities and pressure distributions.

Another recommendation to improve the simulation of breakwaters with OpenFoam is to research the peaks in the measured pressure above the still water level as described in 10.1.4 and 10.2.2. These peaks might be a result of the wrong simulation of the wave run-up.

Further improvement of the simulation of breakwaters can be achieved by performing more numerical simulations like the model validation described in this thesis. The model validation described in chapter 5 is only carried out for one specific wave condition: regular waves with a constant wave height. The results of the model validation, section 5.3, in general show a good comparison with the measured data from the physical model tests of (Muttray, 2000). However, in order to validate that the good comparison is not a coincidence, and in order to find a relationship between the differences between the physical and numerical model results and the hydraulic conditions, different hydraulic conditions should be tested. Furthermore, for the same reasons, the model validation should also be carried out with irregular waves instead of regular waves. Besides, the water set-up on the lee side of the breakwater, as discussed in section 10.1.2, should be included as well.

Bibliography

26th ITTC Specialist Committee on CFD in Marine Hydronamics. (2011). *ITTC – Recommended Procedures and Guidelines - Practical Guidelines for Ship CFD Applications*. *ITTC – Recommended Procedures and Guidelines*. Retrieved from https://ittc.info/media/4196/75-03-02-03.pdf

Bingham, H. B., & Zhang, H. (2007). On the accuracy of finite-difference solutions for nonlinear water waves. *Journal of Engineering Mathematics*, *58*(1–4), 211–228. https://doi.org/10.1007/s10665-006-9108-4

CIRIA, CUR, & CETMEF. (2007). *The Rock Manual. The use of rock in hydrualic engineering (2nd edition)*. *Ciria C683*. C683, CIRIA, London.

Engsig-Karup, A. P., Bingham, H. B., & Lindberg, O. (2009). An efficient flexible-order model for 3D nonlinear water waves. *Journal of Computational Physics*, *228*(6), 2100–2118. https://doi.org/10.1016/j.jcp.2008.11.028

Franken, J. T. (2016). *On the predictability of the notional permeability of breakwaters as a function of core properties*. Delft University of Technology. Retrieved from https://repository.tudelft.nl/islandora/object/uuid:29e8291c-b84e-4500-b753-ac6c8b21ced0?collection=education

Hofland, B., Rosa-Santos, P., Taveira-Pinto, F., de Almeida Sousa, E., Lemos, R., Mendonça, A., & Juana Fortes, C. (2017). Measuring damage in physical model tests of rubble mounds. *Coasts, Marine Structures and Breakwaters 2017: Liverpool*, *11*(125). Retrieved from https://repository.tudelft.nl/islandora/object/uuid:9e71a06c-2d25-4f79-83f7-3375f4b34c34?collection=research

Hudson, R. Y. (1959). Laboratory investigation of rubble-mound breakwaters. *Journal of the Waterways and Harbors Division*, *85*, 93–121. Retrieved from http://www.sciencemag.org/cgi/doi/10.1126/science.1.3.84

Jacobsen, N. G., Fuhrman, D. R., & Fredsøe, J. (2012). A wave generation toolbox for the open-source CFD library: OpenFoam(R). *International Journal for Numerical Methods in Fluids*, *70*(9), 1073–1088. https://doi.org/10.1002/fld.2726

Jacobsen, N. G., van Gent, M. R. A., & Wolters, G. (2015). Numerical analysis of the interaction of irregular waves with two dimensional permeable coastal structures. *Coastal Engineering*, *102*, 13–29. https://doi.org/10.1016/j.coastaleng.2015.05.004

Jensen, B., Jacobsen, N. G., & Christensen, E. D. (2014). Investigations on the porous media equations and resistance coefficients for coastal structures. *Coastal Engineering*, *84*, 56–72. https://doi.org/10.1016/j.coastaleng.2013.11.004

Jonsson, I. G. (1966). Wave boundary layers and friction factors. *Proceedings of 10th Conference on Coastal Engineering, Tokyo, Japan*, *10*, 127–148.

Kik, R. (2011). *Notional permeability of breakwaters*. Delft University of Technology. Retrieved from https://repository.tudelft.nl/islandora/object/uuid%3A7591bcf7-139a-4b6c-b5c1-721c89dc1e38?collection=education

Kluwen, J. G. M. (2012). *Physical model tests On breakwaters*. Delft Univesity of Technology. Retrieved from https://repository.tudelft.nl/islandora/object/uuid%3Aee35f437-5c5f-4df3-b363-ca87c4e2f782?collection=education

Komar, P. D., & Miller, M. C. (1974). Sediment threshold under oscillatory waves. *Proc. 14th. Asce*

Coastal Engng. Conf. (Copenhagen), *2*, 756–775.

Le Méhauté, B. (1976). *An introduction to hydrodynamics and water waves* (viii). New York: Springer-Verlag.

Muttray, M. O. (2000). Wellenbewegung an und in einem geschütteten Wellenbrecher: Laborexperimente im Großmaßstab und theoretische Untersuchungen, 340. Retrieved from http://www.digibib.tu-bs.de/?docid=00001203

Paulsen, B. T., Bredmose, H., & Bingham, H. B. (2014). An efficient domain decomposition strategy for wave loads on surface piercing circular cylinders. *Coastal Engineering*, *86*, 57–76. https://doi.org/10.1016/j.coastaleng.2014.01.006

Prajapati, J. J. (1981). Model studies on through-flow rockfill structures. In *Proc 19th IAHR cong, New Delhi, 2-7 Feb.* Madrid.

Rabinovich, A. B. (2008). Seiches and Harbour Oscillations. In *Handbook of Coastal and Ocean Engineering* (p. 50). World Scientific.

Schiereck, G. J., & Verhagen, H. J. (2016). *Introduction to Bed, bank and shore protection* (2nd ed.). Delft, Netherlands: Delft Academic Press.

Van den Bos, J. P., & Verhagen, H. J. (2018). *Breakwater Design* (Edition 20). Delft, Netherlands.

Van den Bos, J. P., Verhagen, H. J., & Kuiper, C. (2015). Numerical modelling of wave reflection and transmission in vertical porous structures. Boston, USA: ASCE - COPRI. Retrieved from http://resolver.tudelft.nl/uuid:c0a57b0f-5ebf-49f7-a104-0359759e9547

Van der Meer, J. W. (1988). Rock Slopes and Gravel Beaches under Wave Attack. *PhD Thesis*, 214. https://doi.org/, Publication No. 396

Van der Neut, E. . M. (2015). *Analysis of the notional permeability of rubble mound breakwaters by means of a VOF model*. Delft University of Technology. Retrieved from https://repository.tudelft.nl/islandora/object/uuid%3A44ece14d-e307-424a-8f55-08d756c743b3?collection=education

Van Gent, M. R. A. (1993). *Stationary and oscillatory flow through coarse porous media* (Vol. 93). Delft, Netherlands. Retrieved from uuid:0408e897-5a3d-46a2-ae8c-75b49d990482

Van Gent, M. R. A. (1995). Porous Flow through Rubble-Mound Material. *Journal of Waterway, Port, Coastal, and Ocean Engineering*, *121*(3), 176–181. https://doi.org/doi: http://dx.doi.org/10.1061/(ASCE)0733-950X(1995)121:3(176)

Zelt, J. A., & Skjelbreia, J. E. (1993). Estimating Incident and Reflected Wave Fields Using an Arbitrary Number of Wave Gauges. In *Coastal Engineering 1992* (pp. 777–789). New York, NY: American Society of Civil Engineers. https://doi.org/10.1061/9780872629332.058

Appendix A.
Model validation simulation

A.1 Physical model test by Markus Muttray, (Muttray, 2000)

Markus Muttray performed physical model tests in order to investigate the wave motion and wave propagation at and inside a rubble mound breakwater. These processes have been investigated using large scale model tests in the Large Wave Flume, Hannover and relative simple theoretical models. For every part of the breakwater structure, the water surface elevations and the pore pressure oscillations have been studied (if possible).

A.1.1 Model set-up

The Large Wave Flume in Hannover has a length of $300\ m$, a width of $5\ m$ and a depth of $7\ m$. At $x = 250.7\ m$, the horizontal floor of the flume becomes a slope of $1{:}6$ (asphalt). The structure of the breakwater is located on a foreshore. The length of this foreshore is $100\ m$ and has a slope of $1{:}50$. The base point of this foreshore is at $x = 133.95\ m$, the top end of the foreshore is at $x = 233.95\ m$. The breakwater structure lies on a strong sand layer with a thickness of $2\ m$. In front of the breakwater structure lies a section of $10\ m$ with a flat bottom. See also Figure 52 for a schematic overview of the wave flume.

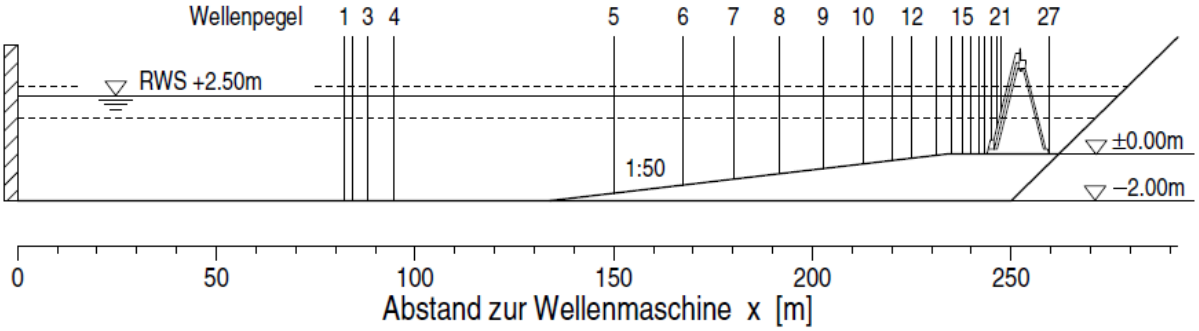

Figure 52 – Schematic overview of the wave flume. (Muttray, 2000)

The foreshore is made of sand with a grading of $d_{60}/d_{10} = 1.67$, a permeability of $2.6 \cdot 10^{-6} m/s$ and characteristic grain sizes of $d_{15} = 0.17\ mm$, $d_{50} = 0.22\ mm$ and $d_{85} = 0.30\ mm$. The breakwater can be divided in five parts: the core, the filter layers, the armour layer, the toe of the structure and the crown wall element, see Figure 53.

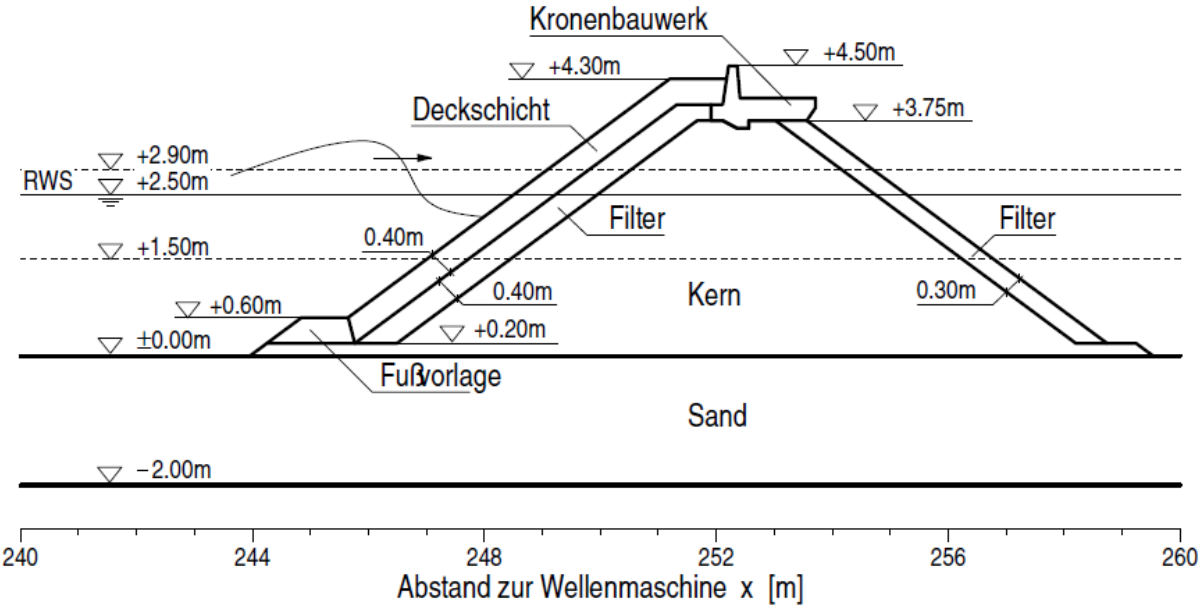

Figure 53 – schematic overview of the breakwater structure. (Muttray, 2000)mu

The front slope of the breakwater has a slope of $1:1.5$ and the width of the toe structure is $0.98\,m$. The armour layer consists of Accropods of Beton B35 (density of $2.35 \cdot 10^3 kg/m^3$) with a length of $36.8\,cm$ (length of the flat front), a volume of $17\,L$ and a mass of $40\,kg$. The Accropods are placed in a regular raster, in which the orientation of the blocks varies. The horizontal distance (in a row) between two raster points is $46.3\,cm$, the distance between two rows is $21.7\,cm$. This gives an average Accropoddensity of $9.95\,pcs/m^2$. The porosity of the armour layer is $n = 0.51$. The filter layer has a thickness of $40\,cm$ and a thickness of $30\,cm$ on the land side. The filter layer is made of rubble with a mass of $m_{50} = 1.95\,kg$ and a density of $2.64 \cdot 10^3\ kg/m^3$. The crest width of the core is $1.35\,m$ and a crest height is $3.75\,m$. The crown wall element has a height of $0.85\,m$ and the top of the crown wall lies $4.5\,m$ above the sand bed. The toe structure consists of rocks with a mass of $m_{50} = 80\,kg$ and a nominal diameter of $d_{n50} = 0.30\,m$. The toe structure is $60\,cm$ in height, $80\,cm$ in width and has a front slop of $1:1.5$. The theoretical base point of the breakwater is at $x = 244.75\,m$. See Table 23 for the properties of the used materials.

			Core material	Filter material	Armour element
Equivalent grain diameter [1]	d_{eq}	$[m]$	0.0385	0.112	0.319
Nominal grain diameter [2]	d_{n15}	$[m]$	0.023	0.069	-
	d_{n50}	$[m]$	0.031	0.090	0.257
	d_{n85}	$[m]$	0.040	0.109	-
Grading	d_{n60}/d_{n10}	$[-]$	1.51	1.58	-
Shape coefficient [3]	l_{max}/l_{min}	$[-]$	2.0	2.6	1.0
porosity	n	$[-]$	0.388	0.394	0.510

[1] $d_{eq} = (6m_{50}/\pi\rho_s)^{1/3}$

[2] $d_{ni} = (m_i/\rho_s)^{1/3}$

[3] $longest/shortest\ rock\ size$

Table 23 – Properties of the used materials

The resistance coefficients are determined as well for the armour layer, filter layer and core material, see Table 24.

Material for:	α $[-]$	β $[-]$	γ $[-]$	Laminar coeff. a $[s/m]$	% of resistance	Turbulence coeff. b $[s^2/m^2]$	% of resistance	Inertia coeff. c $[s^2/m]$	% of resistance
Armour	305.0	1.27	0.52	0.001	0	2.03	83-94	0.30	6-17
Filter	305.0	1.27	0.43	0.03	0.2	14.9	93-98	0.43	2-7
Core	1007.0	0.63	0.00	0.89	11	22.9	83-87	0.26	2-6

Table 24 – Resistance coefficients for the armour layer, filter layer and core material. (Muttray, 2000)

A.1.2 Measurements

On several locations in the physical model tests by (Muttray, 2000), the surface level elevation is measured, see Table 25. The locations of these wave gauges is also included in the schematic overview of the wave flume, Figure 52, the vertical lines represent the wave gauges.

Wave Gauge #	x-coordinate	Wave Gauge #	x-coordinate	Wave Gauge #	x-coordinate
1	82.18	10	212.67	19	244.98
2	84.37	11	219.98	20	246.55
3	88.03	12	224.99	21	247.45
4	94.81	13	231.23	22	248.89
5	149.97	14	235.00	23	250.18
6	167.44	15	237.69	24	251.27
7	180.12	16	239.97	25	252.32
8	191.67	17	241.83	26	253.67
9	202.68	18	243.47	27	259.55

Table 25 - locations of the wave gauges in the physical model test

The wave induced pressures are measured on several locations as well, using pressure probes. The locations of these pressure probes Table 26. The locations of the pressure probes with respect to the structure are shown in Figure 54.

Pressure probe #	x-coordinate	y-coordinate	Pressure probe #	x-coordinate	y-coordinate
1	247.49	2.40	18	254.80	4.30
2	248.92	2.40	19	247.49	2.87
3	250.21	2.40	20	248.22	3.35
4	251.31	2.40	21	248.92	3.82
5	252.36	2.40	22	249.64	4.30
6	253.70	2.40	23	250.21	4.68
7	257.65	2.40	24	246.55	2.72
8	248.92	3.35	25	247.49	3.35
9	250.21	3.35	26	248.21	3.83
10	251.31	3.35	27	248.92	4.30
11	252.36	3.35	28	250.21	5.16
12	253.70	3.35	29	244.85	2.60
13	256.23	3.35	30	246.55	3.35
14	250.21	4.30	31	247.49	3.98
15	251.31	4.30	32	247.98	4.30
16	252.36	4.30	33	248.92	4.93
17	253.70	4.30	34	250.21	5.79

Table 26 - locations of the pressure probes in the physical model test

The wave run-up is also measured in the simulations on three lines: on the armour layer, in between the armour layer and the filter layer and in between the filter layer and the core. The locations of these wave run-up gauges is shown in Table 27 and is also shown in Figure 54.

Wave run-up gauge	Location	Coordinates of base point		Angle $tan\ \alpha$ $[-]$
		x $[m]$	y $[m]$	
1	On top of the armour layer	245.65	2.60	1:1.58
2	Between armour and filter	245.87	2.20	1:1.50
3	Between filter and core	246.49	2.20	1:1.50

Table 27 - locations of the wave run-up gauges in the physical model

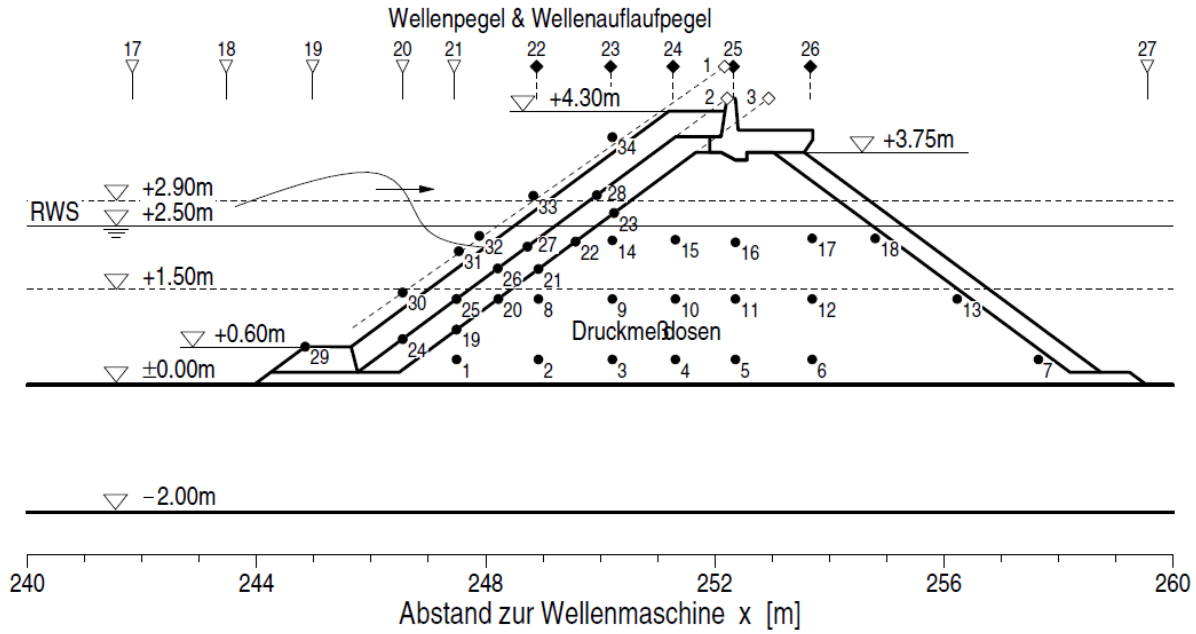

Figure 54 – location of the pressure probes (Druckmeßdosen) and wave run-up gauges. (Muttray, 2000)

A.1.3 Test program

Muttray performed multiple tests with regular waves and with irregular waves as well. In his tests, he varied the water level, the wave period and the wave height. The test program is shown in Table 28.

Water level	Wave period	Regular waves	Wave spectrum
h $[m]$	T or T_p $[s]$	Wave height H $[m]$	Wave height H_{m0} $[m]$
1.50	2	0.2; 0.3; 0.4	
	3	0.2; 0.4; 0.6	0.325
	4		0.325
	5	0.2; 0.4; 0.6	
2.50	4	0.25; 0.4; 0.55; 0.7; 0.85; 1.0	0.25; 0.4; 0.55; 0.7; 0.85
	5	0.25; 0.4; 0.55; 0.7; 0.85; 1.0	0.25; 0.4; 0.55; 0.7; 0.85; 1.0
	6	0.25; 0.4; 0.55; 0.7; 0.85; 1.0	0.25; 0.4; 0.55; 0.7; 0.85; 1.0
	8	0.25; 0.4; 0.55; 0.7; 0.85; 1.0	0.25; 0.4; 0.55; 0.7; 0.85; 1.0
	10	0.55	
2.90	3	0.25; 0.4; 0.55; 0.7	0.25; 0.4; 0.55
	4	0.25; 0.4; 0.55; 0.7	0.25; 0.4; 0.55; 0.7
	5	0.25; 0.4; 0.55; 0.7	0.25; 0.4; 0.55; 0.7
	6	0.25; 0.4; 0.55; 0.7	0.25; 0.4; 0.55; 0.7
	8	0.25; 0.4; 0.55; 0.7	0.25; 0.4; 0.55; 0.7
	10	0.25; 0.4; 0.55; 0.7	0.25; 0.4; 0.55

Table 28 – Test program of the physical model tests of Muttray. (Muttray, 2000)

A.2 Model set-up of model validation simulation

A.2.1 Structure

The structure which is modelled in the OpenFoam simulations is almost the same as in the physical model tests by (Muttray, 2000), see Figure 55 for the structure in the OpenFoam model.

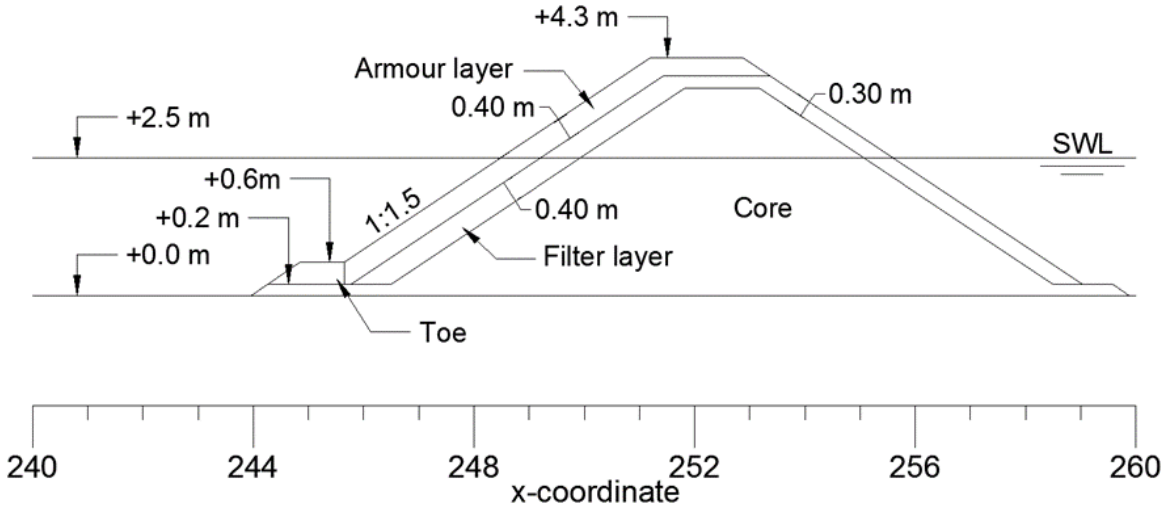

Figure 55 - Schematic cross-section of the breakwater construction modelled in OpenFoam

In both the physical as the numerical model lies the structure on a foreshore. The coordinates of the physical structure and the numerical model are the same except that the whole flume in the OpenFoam model is moved $30\,m$ in the positive x-direction due to the implementation of a relaxation zone on the left boundary. For simplicity, all coordinates in this appendix are in the same coordinate system as the physical model test by (Muttray, 2000). If the OpenFoam model is rebuild, add $30\,m$ to every x-coordinate in this appendix and add $2\,m$ to every y-coordinate in this appendix (OpenFoam does not allow negative coordinates and otherwise would the bottom of the numerical flume lie at $y = -2\,m$). The simulated structure in the numerical model is different compared to the model from the physical model tests in two parts:

1. The OpenFoam structure does not have a crown wall element while the physical model did have a crown wall element. This is due to the fact that the crown wall element did cause some trouble in the OpenFoam simulations. Therefore it was checked if the crown wall could be removed. Fortunately, removing the crown wall element did not cause significant changes in the model output, see Appendix B for details about this optimization.
2. The interface between the toe and the armour layer is vertical in the OpenFoam model which is not the case in the physical model. This was done because the coming together of four porous layers in one single point caused problems in the OpenFoam simulation as well. It is assumed that changing a small part of the toe into part of the armour layer does not have a significant influence on the simulation results. Especially since there is no difference in porosity, γ, α and β-value between the porous layers and only a small difference in D_{50} and KC-value (see Table 29).

Not all parameters are measured for the porous layers of the breakwater structure in the physical model tests. The parameters of the core, armour and filter layer are measured and included in the PhD Thesis report by (Muttray, 2000). Also the rock size of the toe construction is given. For the toe of the structure as well as the rear side armour layer, some parameters are missing. For the numerical model, these missing parameters are set to be the same as respectively the armour layer and the filter layer. It is assumed that doing this has no significant influence on the results of the numerical simulation, since the area of interest of the simulations

is not near these two porous layers (especially the rear side armour layer is not important at all). For the numerical model, the KC-values are calculated with formula (19), as described in section 2.2.4 of the literature study. Table 29 shows the porous layer parameters used in the OpenFoam model.

Porous layer:	Porosity	KC-value	γ-value	D_{50}	α	β
Armour layer	0.510	23.78	0.52	0.257	305.0	1.27
Filter layer	0.394	67.91	0.43	0.090	305.0	1.27
Core	0.388	197.15	0.00	0.031	1007.0	0.63
Toe	0.510	20.37	0.52	0.300	305.0	1.27
Rear side armour layer	0.394	67.91	0.43	0.090	305.0	1.27

Table 29 - Porous layer parameters in OpenFoam model

The foreshore in the OpenFoam model is created as an impermeable layer, while in the physical model test it is made of sand. It is assumed that simplifying this foreshore as non-permeable does not have an influence on the results of the numerical model, since the permeability of the foreshore in the physical model is very low.

A.2.2 Waves and water

Simulation number 020694-01 of (Muttray, 2000) is reproduced in OpenFoam. This simulation has a water depth in front of the foreshore of $4.5\ m$ and a water depth on top of the foreshore of $2.5\ m$. The waves modelled are regular waves with an incoming wave height of $0.85\ m$ and a wave period of $6.0\ s$, see Table 30 for a summary of the wave conditions.

Type of waves	h in front of the foreshore $[m]$	h on top of the foreshore $[m]$	$T\ [s]$	$H\ [m]$	$\xi\ [-]$
Regular waves	4.5	2.5	6.0	0.85	4.37

Table 30 - Wave conditions of test 020694-01 by (Muttray, 2000) and of the OpenFoam simulation

This test was selected for a couple of reasons:

- First of all, a choice between regular and irregular waves had to be made. Regular waves are more predictable than irregular waves and only approximately 10 regular waves are required to show a pattern. This means that numerical simulations with regular waves are way faster than simulations with irregular waves.
- The water depth of $2.5\ m$ was chosen simply because it is closest to the average water depth of the tests.
- The wave period of $T = 6\ s$ was chosen in combination with the wave height of $H = 0.85\ m$ because these waves are surging waves. Surging waves are well behaved in comparison with plunging waves and are easier to model in a numerical model.

The properties of the water in the OpenFoam model is set to the same values as the properties of the water in the physical model test by (Muttray, 2000). The water has a kinematic viscosity, ν, of $1.3 \cdot 10^{-6}\ m^2/s$ and a density, ρ_w, of $999.7\ kg/m^3$.

A.2.3 Domain and grid size

The waves in the numerical simulation are created with OceanWave3D and are coupled with OpenFoam. The OceanWave3D model needs to have a bigger domain as the OpenFoam model. The domains of these models are shown in Figure 56. The domain of the OceanWave3D model is shown in Red. The red hatched areas are the wave generation zone (left) and the pressure dampening zone (right) in OceanWave3D and the red dashed line is the bottom profile implemented in OpenFoam to mimic the foreshore. The domain of the OpenFoam model is shown in green. The yellow boxes show the relaxation zones of the

OpenFoam model. The wave generation zone, pressure dampening zone and relaxation zones all have the same length of $30\ m$, which is approximately equal to one wavelength.

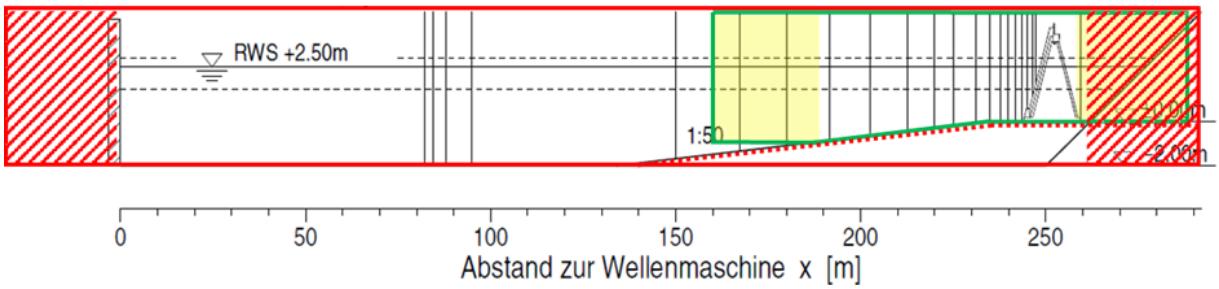

Figure 56 - Domain of the OceanWave3D model and the OpenFoam model

The OceanWave3D simulation only has a grid size in x-direction. According to (26th ITTC Specialist Committee on CFD in Marine Hydronamics, 2011), at least 40 grid cells are required to resolve the shortest wave length (at least 20 grid points for irregular waves). This results in a maximum grid size in x-direction, Δx, of $0.71\ m$. According to (Bingham & Zhang, 2007), a resolution of 15 – 20 grid cells per wavelength are adequate for general purpose applications. This results in a maximum grid size in x-direction, Δx, of $1.89 - 1.42\ m$. Since the OceanWave3D calculation is not computational demanding, a grid size of $\Delta x = 0.5\ m$ is chosen for the OceanWave3D part of the simulation.

The OpenFoam simulation has a 2D grid, so the grid size in both x-direction, Δx, as well as in y-direction, Δy, has to be chosen. Again, the maximum grid size in x-direction is, depending on which literature is followed, between $0.71\ m$ and $1.89\ m$.

According to (26th ITTC Specialist Committee on CFD in Marine Hydronamics, 2011), no less than 20 grid points in vertical direction should be used where the free surface is expected. With other words, the maximum grid size in y-direction, Δy, should be smaller than $\frac{H}{20}$. This results in an grid size in y-direction of $\Delta y \leq \frac{0.85}{20} = 0.0425\ m$. Also according to (26th ITTC Specialist Committee on CFD in Marine Hydronamics, 2011), an orthogonal grid should be used to resolve a free surface, with other words, the aspect ratio $\left(\frac{\Delta x}{\Delta y}\right)$ should be 1. Therefore a grid size of $\Delta x = \Delta y = 0.04\ m$ is used as a start in the OpenFoam domain.

As can be seen in Figure 56 is the domain of the OpenFoam model not rectangular, due to the sloping foreshore. The connection of the OpenFoam model with the OceanWave3D model is positioned halfway the slope (approximately 1 wavelength in front of the crest of the foreshore) and is positioned horizontally, while the bottom of the flume is sloped. This was the result of one of the optimizations of the OpenFoam model, see Appendix B. Another result of this optimization was the use of a grid which is varying in size. Along the part of the OpenFoam domain where the bottom is sloping upwards, the grid changes in size from a grid with $\Delta y = \Delta x = 0.04\ m$ towards a grid with $\Delta y = \Delta x \approx 0.035\ m$. A schematization of how such a grid looks like is given in Figure 57. It is clear that the cells are becoming skewed on the sloping part of the breakwater. In practice, this skewness is limited (it is exaggerated in Figure 57). It is assumed that this skewness does not have influence on the model results. OpenFoam changes the timestep of the simulation automatically in order to limit the courant number. However, a beginning timestep has to be chosen. A limit for the timestep is the courant number, $C = \frac{u * \Delta t}{\Delta x}$, which has to be smaller than 1. As flow velocity, u, the wave speed of incoming waves is used, $u \approx 4.72\ m/s$ (calculated with linear wave theory for shallow water). This results in a maximum time step of $\Delta t \leq 0.0085\ s$. Therefore a starting timestep of $\Delta t = 0.008\ s$ is chosen.

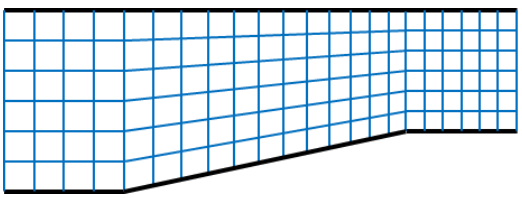

Figure 57 - grid schematization of varying grid size along sloping part of domain

A.2.4 Wave gauges and pressure probes

On several locations in the physical model tests the surface level elevation is measured. To compare these surface level elevations, they are measured on the same locations in OpenFoam as well. Table 31 shows the locations of the wave gauges in the OpenFoam model.

Wave Gauge #	x-coordinate	Wave Gauge #	x-coordinate	Wave Gauge #	x-coordinate
1	202.68	8	239.97	15	250.18
2	212.67	9	241.83	16	251.27
3	219.98	10	243.47	17	252.32
4	224.99	11	244.98	18	253.67
5	231.23	12	246.55	19	259.55
6	235.00	13	247.45		
7	237.69	14	248.89		

Table 31 - locations of the wave gauges in the OpenFoam model

In the OceanWave3D model also wave gauges are included. These wave gauges are only used in the optimization steps (Appendix B) and not in the analysis of the results, but the locations of these wave gauges are included in Table 32.

Wave Gauge #	x-coordinate	Wave Gauge #	x-coordinate	Wave Gauge #	x-coordinate
1	82.5	5	167.5	8	225
2	84.5	6	192	9	235
3	88.5	7	213	10	240
4	150				

Table 32 - locations of the wave gauges in the OceanWave3D model

Besides the surface level elevation, also the pressures and flow velocities are measured on several locations in the OpenFoam model by pressure probes. The locations of the pressure probes correspond to the locations of the pressure sensors in the physical model test by (Muttray, 2000). The locations of these pressure probes are included in Table 33. The locations of the pressure probes with respect to the structure are shown in Figure 54.

Pressure probe #	x-coordinate	y-coordinate	Pressure probe #	x-coordinate	y-coordinate
1	247.49	0.40	18	254.80	2.30
2	248.92	0.40	19	247.49	0.87
3	250.21	0.40	20	248.22	1.35
4	251.31	0.40	21	248.92	1.82
5	252.36	0.40	22	249.64	2.30
6	253.70	0.40	23	250.21	2.68
7	257.65	0.40	24	246.55	0.72
8	248.92	1.35	25	247.49	1.35
9	250.21	1.35	26	248.21	1.83
10	251.31	1.35	27	248.92	2.30
11	252.36	1.35	28	250.21	3.16
12	253.70	1.35	29	244.85	0.60
13	256.23	1.35	30	246.55	1.35
14	250.21	2.30	31	247.49	1.98
15	251.31	2.30	32	247.98	2.30
16	252.36	2.30	33	248.92	2.93
17	253.70	2.30	34	250.21	3.79

Table 33 - locations of the pressure probes in the OpenFoam model

Besides the pressure probes listed in Table 33, three sets of pressure probes are included in the OpenFoam model to measure the pressure, flow velocity and the α-value along these lines. The α-value is used by OpenFoam to check if the cell consists of water or air. If $\alpha = 1$ the cell is filled with water, if $\alpha = 0$ the cell is filled with air. These lines each consist out of 248 pressure probes, evenly spaced along the lines. The locations of these pressure probe lines are located on the armour layer (line 1), (on the interface between the armour layer and the filter layer (line 2) and on the interface between the filter layer and the core (line 3). The coordinates of the lines are given in Table 34.

Pressure probe line #	Begin of pressure probe line		End of pressure probe line	
	x-coordinate	y-coordinate	x-coordinate	y-coordinate
1	246.0485	0.8656	251.2000	4.3000
2	246.2703	0.5328	251.4219	3.9672
3	246.4922	0.2000	251.6438	3.6344

Table 34 - locations of the pressure probe lines in the OpenFoam model

A.3 Results of model validation simulation

In this chapter the simulation of the hydraulic loading parameter with OpenFoam is checked by comparing the results of the tests described in A.1 and A.2. First a spectrum analysis, a reflection analysis and a comparison of the wave gauges will be made in order to validate that the structure is modelled correctly in OpenFoam. Then a comparison is made between the wave run-up, the pressure probes and the pressure lines in order to conclude if OpenFoam is suitable for simulating the hydraulic loading parameters selected in chapter 4.

A.3.1 Spectrum analysis

For both the OpenFoam simulation and the measurements of (Muttray, 2000), a spectrum is created. The spectrum can be created for every wave gauge but is most interesting for locations in front of the breakwater structure. Since all spectra in front of the structure look quite similar, only one spectra is included in this report. Figure 58 shows the spectrum from gauge #8 ($x = 239.97$).

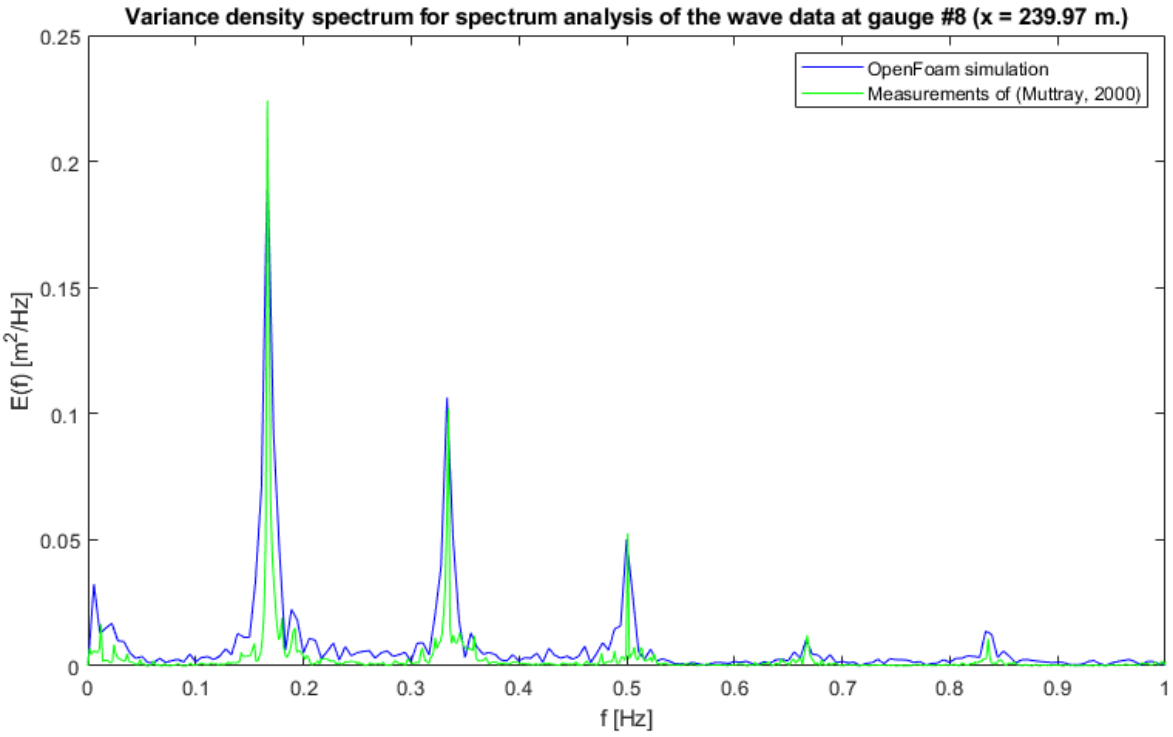

Figure 58 - Variance density spectrum at $x = 239.97$

The spectrum of the OpenFoam simulation and the spectrum of the measurements of Markus match quite well. In the spectra you see a big peak around a frequency, f, of 0.167, which is logical since this frequency equals the wave period, T, of 6 seconds. Two clear other peaks can be distinguished around $f = 0.333$ and $f = 0.499$ and some smaller peaks can be seen around the frequencies of 0.667 and 0.833. All these peaks are at frequencies which are multiples of the frequency of the highest peak. The peaks can be explained by looking into which wave theory is valid for the waves. The waves on location $x = 239.97$ in the OpenFoam simulation are in the 5th order stream function theory domain, see Figure 59 ($\frac{H}{gT^2} \approx 0.0025$ and $\frac{h}{gT^2} \approx 0.0071$, the red lines). Therefore it makes sense that there are five peaks in the spectrum (even though the last two are quite small). The peaks of the OpenFoam simulation are wider than the peaks of the measurements of the physical model test, this is due to the fact that the spectrum of the OpenFoam simulation is made from a time series of 180 seconds while the spectrum of the physical model test is made from a time series of 720 seconds.

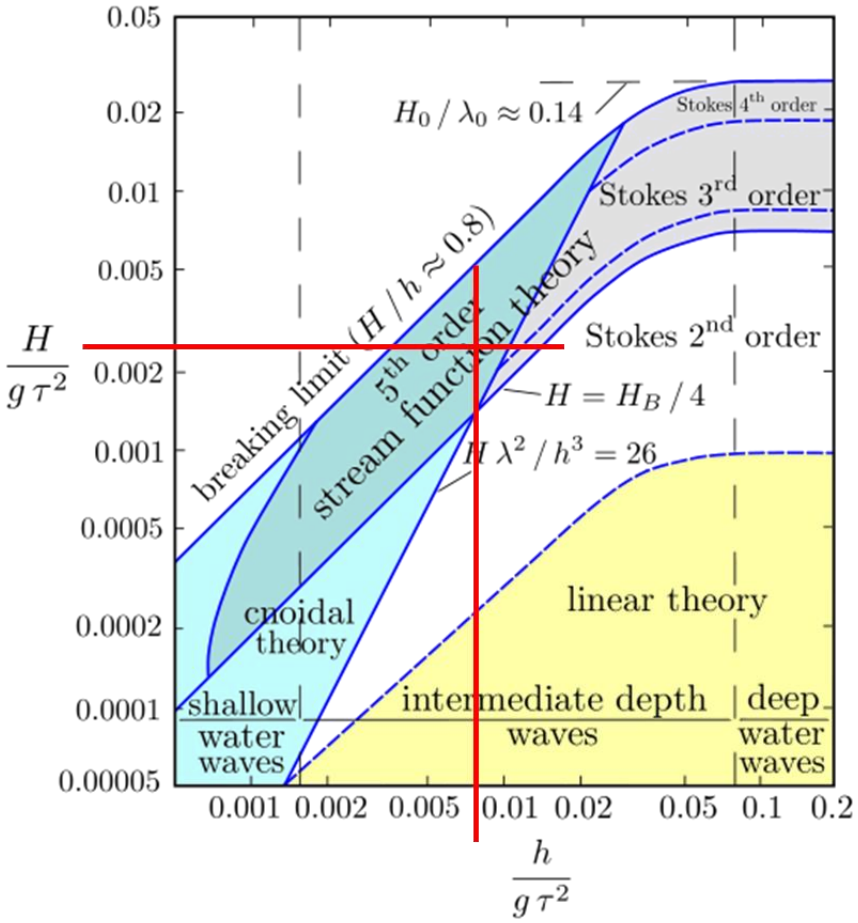

Figure 59 - Validity of several theories for periodic water waves, according to (Le Méhauté, 1976). The red lines represent the waves on wave gauge #8 ($x = 239.97$) in the OpenFoam simulation.

In Figure 58, there are also some peaks at the low frequencies ($0 < f < 0.05$), the waves that correspond to these frequencies are very long waves, or rather seiches. These seiches can be explained by looking into the period of free oscillation of the wave flume. When the wave flume is simplified as a rectangular flume with a water depth, h, of $4.5\ m$, the period of a free oscillation with one node is approximately 87 seconds, according to (Rabinovich, 2008). The period of a free oscillation with two nodes is approximately 43 seconds. When looking into the measurements of (Muttray, 2000) in Figure 60, you can recognize these two oscillations (see the red lines).

When looking into the spectrum of the measurements of (Muttray, 2000) in detail, these free oscillations can be recognized as well. A free oscillation with a period of 87 seconds results in a frequency of 0.01149. In the spectrum of the measurements of (Muttray, 2000), a small peak at a frequency of 0.01211 can be seen quite clearly (a frequency of 0.01211 corresponds to a wave period of 82.6 seconds). The difference between these two values can be explained by the simplification of the wave flume to a rectangular flume when the period of free oscillation of the flume is investigated. The actual flume has a sloping foreshore in the second half of the flume, which has an influence on the period of free oscillation of the flume.

In the spectrum of the measurements of (Muttray, 2000), a second peak can be spotted for a frequency of 0.02422 (a corresponding wave period of 41.3 seconds). This peak can be explained as the free oscillation of the flume with two nodes. When looking even closer to the spectrum at low frequencies, a smaller third and fourth peak can be spotted in this area, which represent the free oscillations of the flume with three and four nodes. These peaks are less clear in the spectrum of the OpenFoam simulation, this is due to the fact that the OpenFoam spectrum is based on a shorter timeseries.

From the spectrum analysis is can be concluded that the incoming waves of the physical model test are simulated correctly in OpenFoam.

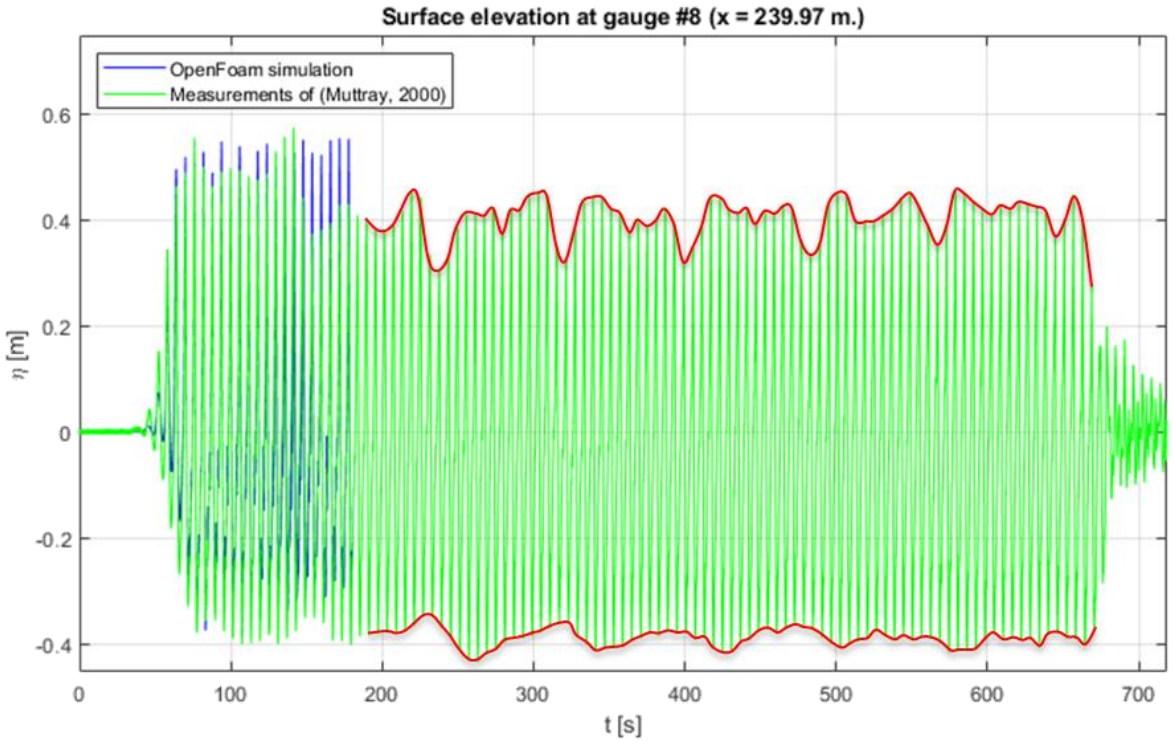

Figure 60 - Surface elevation comparison at gauge #8
(zoomed out to see the oscillations (red lines) in the measurements of (Muttray, 2000))

A.3.2 Reflection analysis

To check if the OpenFoam model does simulate the reflection of the incoming waves well, a reflection analysis is done following the method described in (Zelt & Skjelbreia, 1993). With this method, a reflection analysis can be done with any number of wave gauges (2 wave gauges or more) and the surface elevation due to the incoming and reflected waves can be calculated at any arbitrary position. According to (Zelt & Skjelbreia, 1993), the accuracy increases with using more wave gauges, especially for broad band wave spectra. The wave spectra of the OpenFoam simulation and of the test of (Muttray, 2000) is not a broad band wave spectra and thus has increasing the number of wave gauges limited advantage, therefore three wave gauges are used for the reflection analysis. The surface elevation due to the incoming and reflected waves are calculated for the position $x = 239.97$, because this is also the position wave gauge #8 and an extra check can be made to see if the sum of the incoming and reflected waves together give the same surface elevation as measured or simulated (to check if the reflection analysis is carried out correctly). The reflection analysis is done for both the OpenFoam simulation as for the measurements of (Muttray, 2000). The results of the reflection analysis is given in Figure 61 and Figure 62.

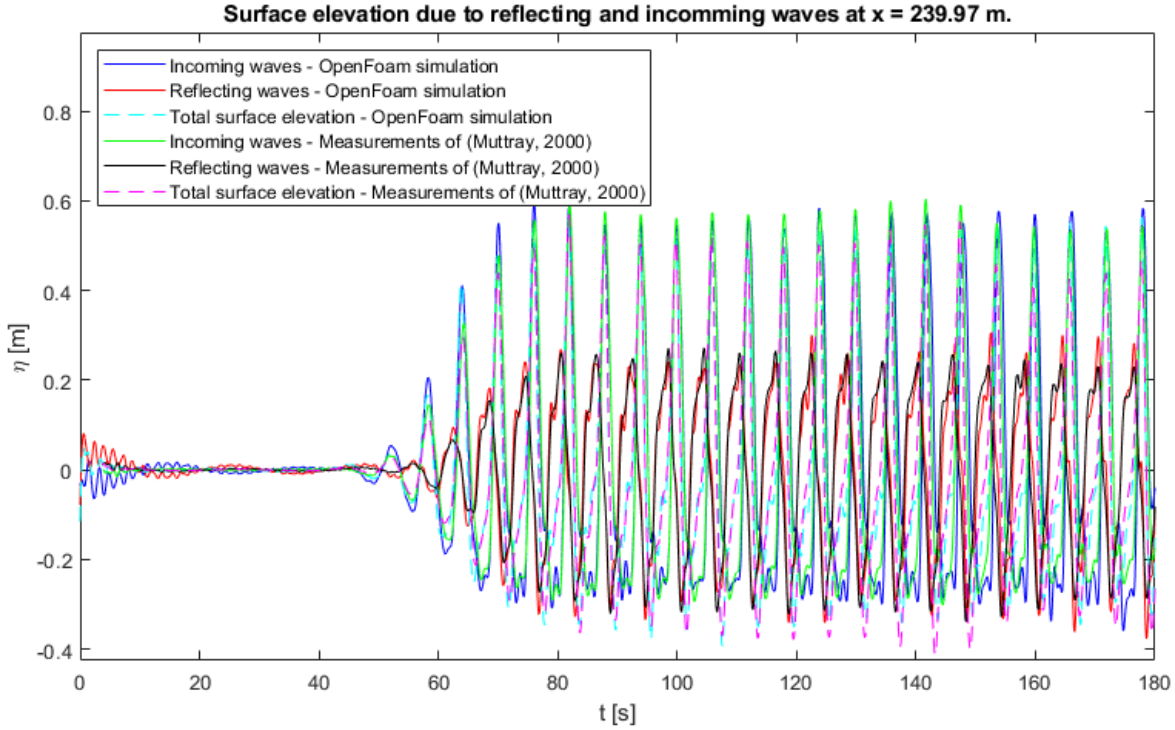

Figure 61 - Surface elevation due to reflecting and incoming waves at $x = 239.97$

When looking to the results, it can be seen that the reflection of the OpenFoam simulation matches the reflection in the test of (Muttray, 2000) very well. Also when Figure 62 is compared with Figure 63, it can be seen that the reflection analysis is carried out correctly, since the sum of the incoming and reflected waves match the surface elevation measured by the wave gauges for both the OpenFoam simulation as the test of (Muttray, 2000).

From the reflection analysis and the spectrum analysis is can be concluded that the incoming waves of the physical model test are simulated correctly in OpenFoam and that the structure of the physical model test is correctly implemented in the OpenFoam model.

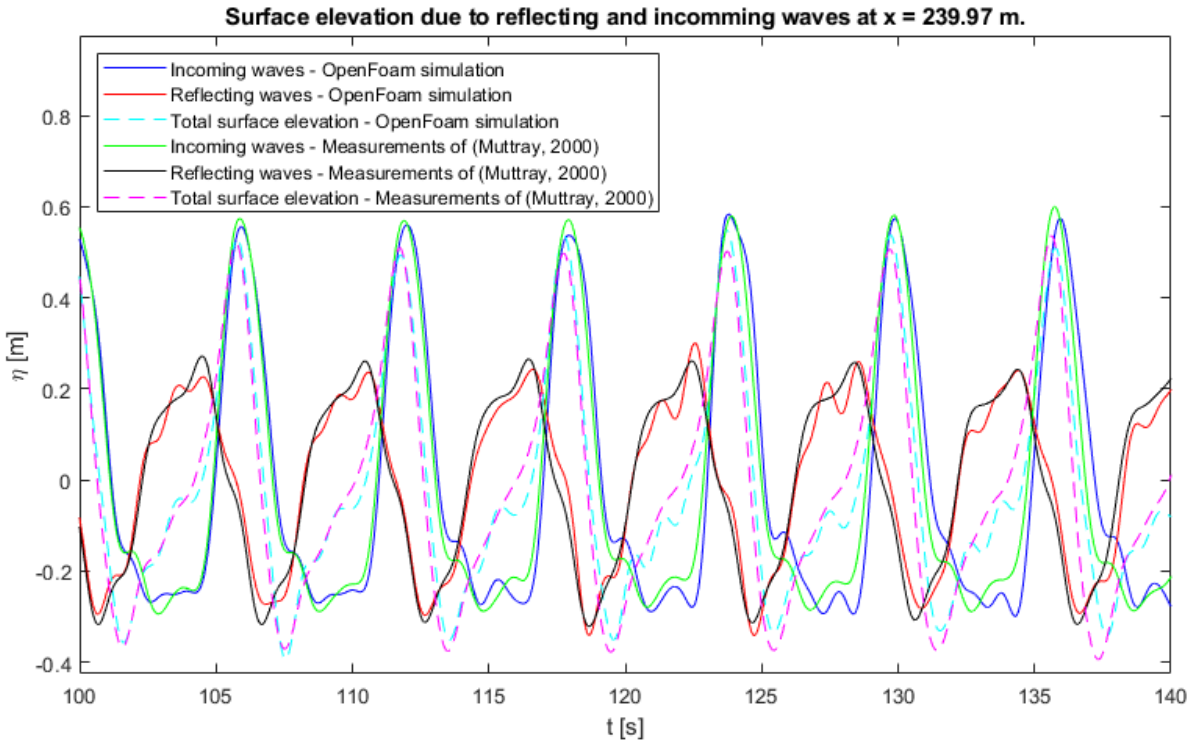

Figure 62 - Surface elevation due to reflecting and incoming waves at $x = 239.97$ (for $100 < t < 140$)

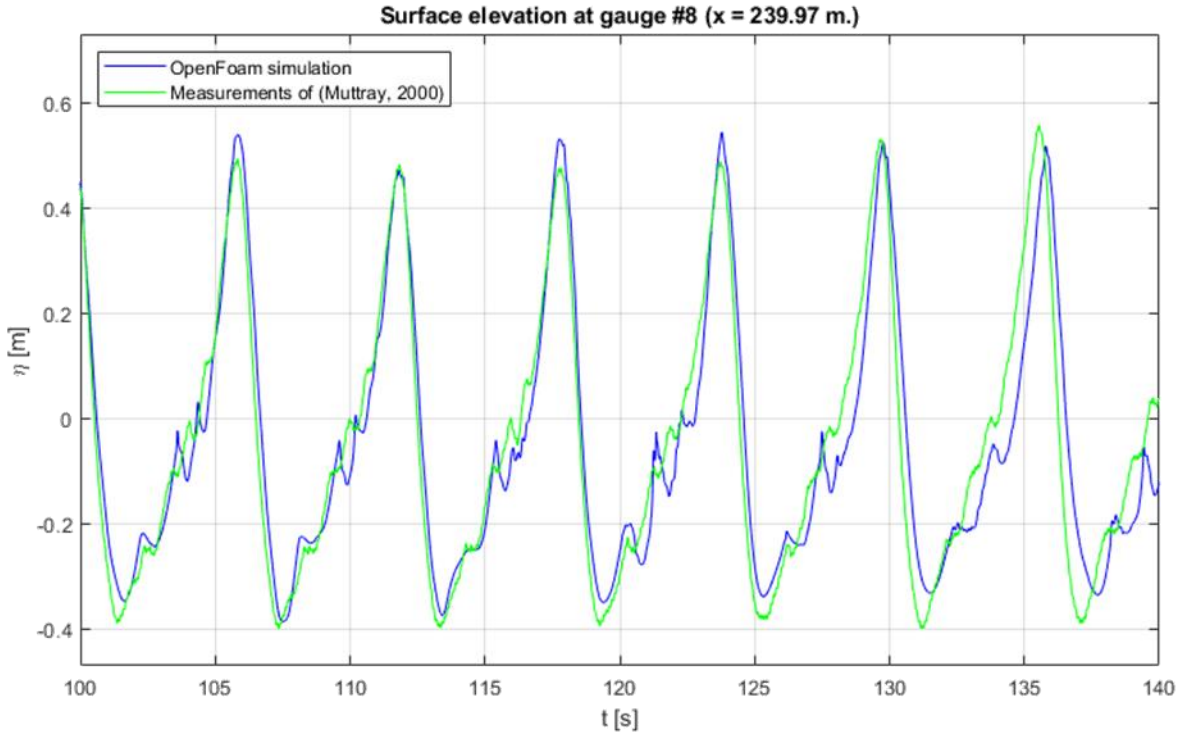

Figure 63 - Surface elevation comparison at gauge #8 (for $100 < t < 140$)

A.3.3 Wave gauge comparison

The results of the wave gauges in the OpenFoam simulation is compared with the measured surface elevation in the physical model test in Figure 64 till Figure 87.

All wave gauges till the wave gauge #16 at $x = 251.27$ show a good comparison, the surface elevation in the OpenFoam simulation has the same order of magnitude as the measurements of the physical model test of (Muttray, 2000) and the shape of the graphs is more or less similar. The measurements do however show some oscillations. The cause of these oscillations is discussed in the spectrum analysis, section A.3.1.

When looking at the gauge #16 at $x = 251.27$ (Figure 80), a high peak of surface level elevation occurs in the OpenFoam results around $t = 85\ s$. Why this peak occurs is not fully understood by the author of this thesis, however, when looking at the wave spectrum at this location (see Figure 81) a clear peak at a frequency, f, of 0.005 can be seen in the OpenFoam spectrum, which corresponds to a wave with a period of 180 seconds (the total simulation time) and is probably a result of the high wave around $t = 85\ s$.

Furthermore, from wave gauge #16 onward, there is an amplitude difference between the surface elevation from the OpenFoam case and the measurements of (Muttray, 2000). This means that the waves are damped less in the OpenFoam model than in the model of (Muttray, 2000). This can be explained by the set-up of water in the breakwater and on the lee side of the breakwater in the physical model test. See Figure 83, Figure 85 and Figure 87, from these figures this set-up can be seen (the trend in the graphs).

In the OpenFoam simulations, the set-up inside the breakwater structure is higher than behind the structure. This can be explained by the fact that behind the breakwater structure (from $x = 290$ onward) the water level is kept constant in the OpenFoam simulation due to the relaxation zone. From Figure 87 it can be seen clearly that in the simulation of (Muttray, 2000), the set-up is also present behind the breakwater structure. In the OpenFoam case, this is not the case due the aforementioned relaxation zone behind the breakwater structure.

The water level set-up in and behind the structure has influence on the pressures in the physical model test. Since the water level set-up is negligible small near the front slope of the structure, it does not have influence on the measured pressures near the front slope. The hydraulic loading parameters for which OpenFoam is checked, all are positioned around this front slope. Therefore it is safe to say that despite this set-up of water level inside and behind the structure, the results of the physical model test can still be used to validate the simulation of the hydraulic loading parameters in OpenFoam.

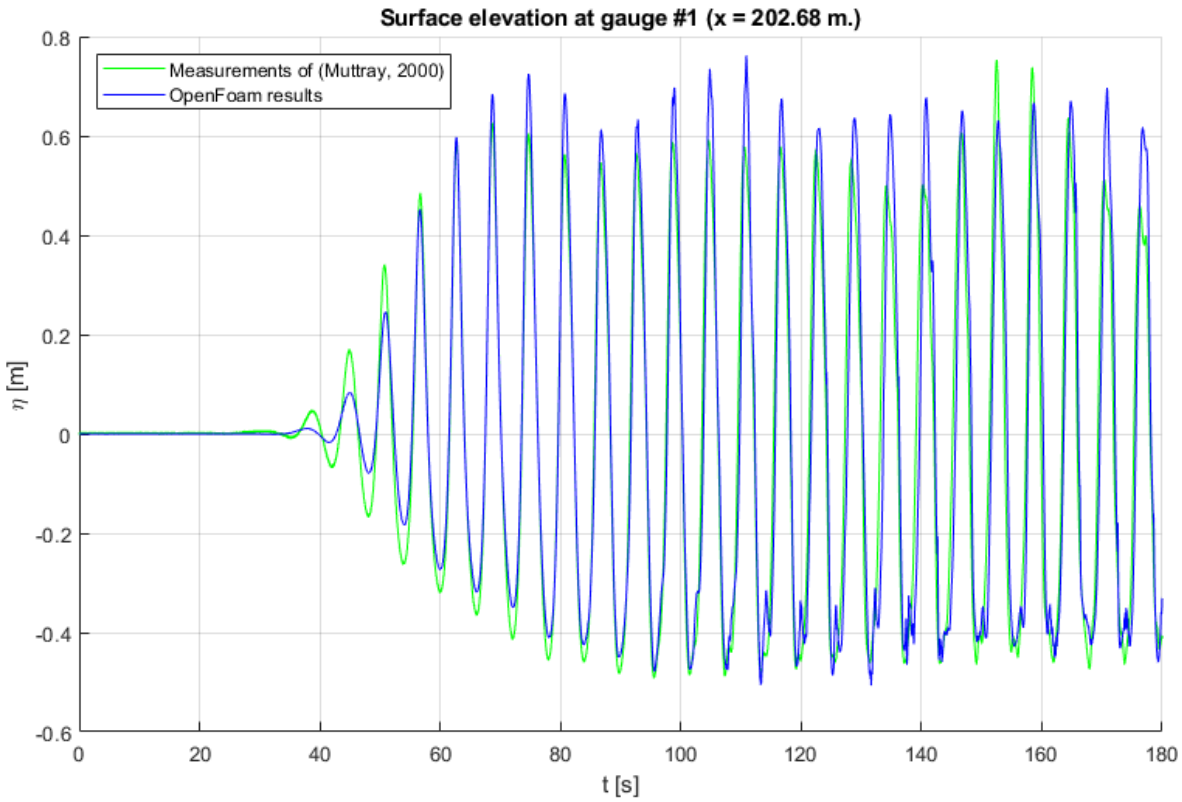

Figure 64 - Surface elevation comparison at gauge #1 ($x = 202.68$)

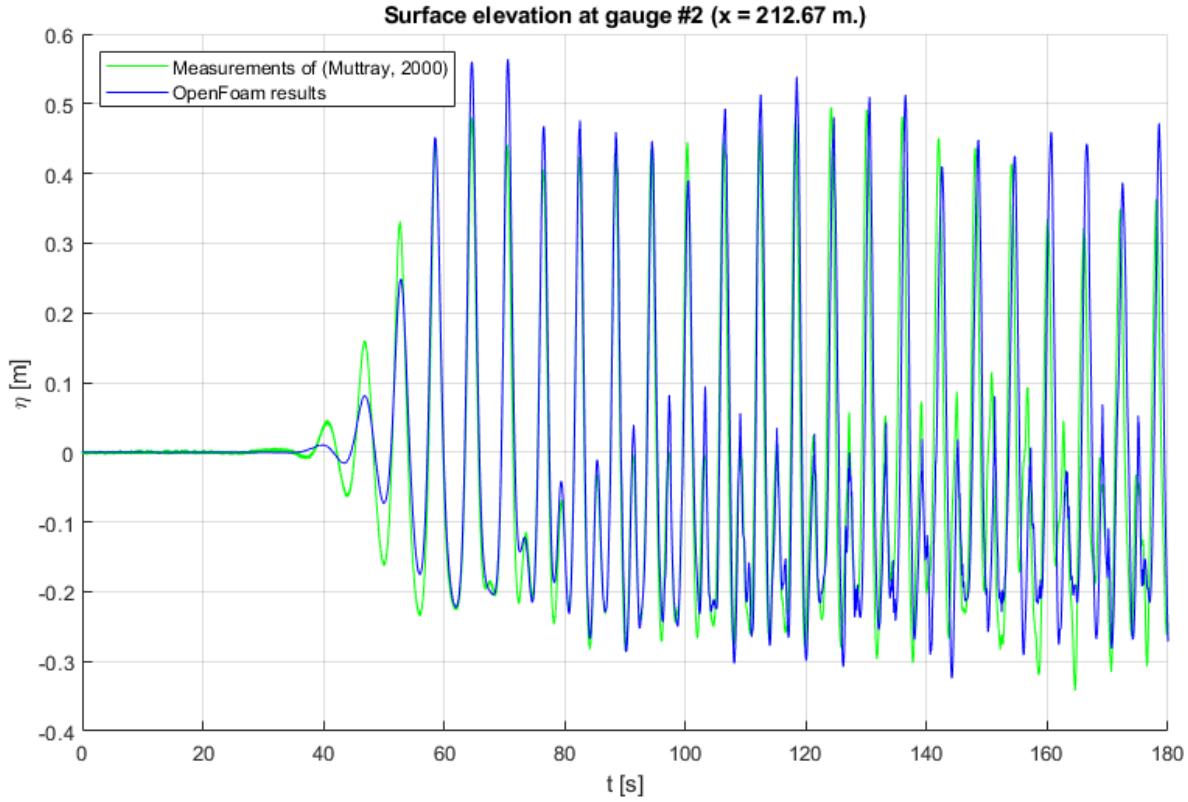

Figure 65 - Surface elevation comparison at gauge #2 ($x = 212.67$)

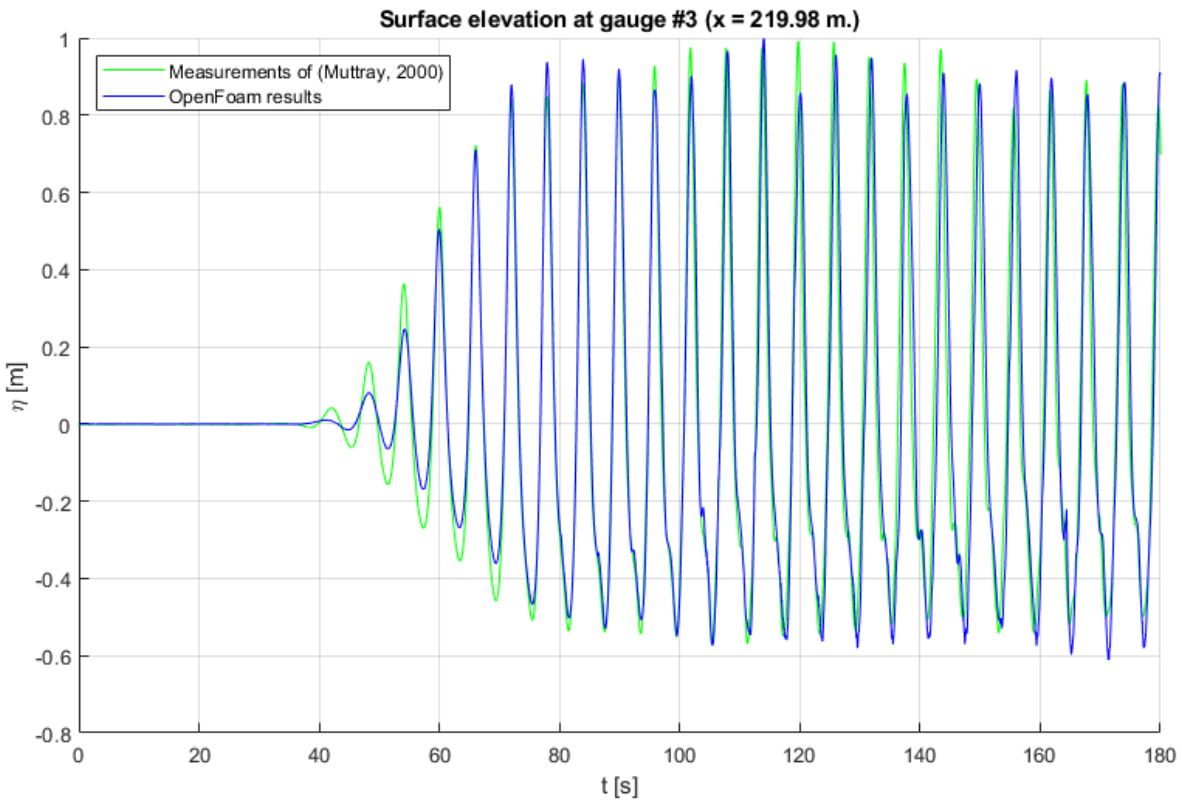

Figure 66 - Surface elevation comparison at gauge #3 ($x = 219.98$)

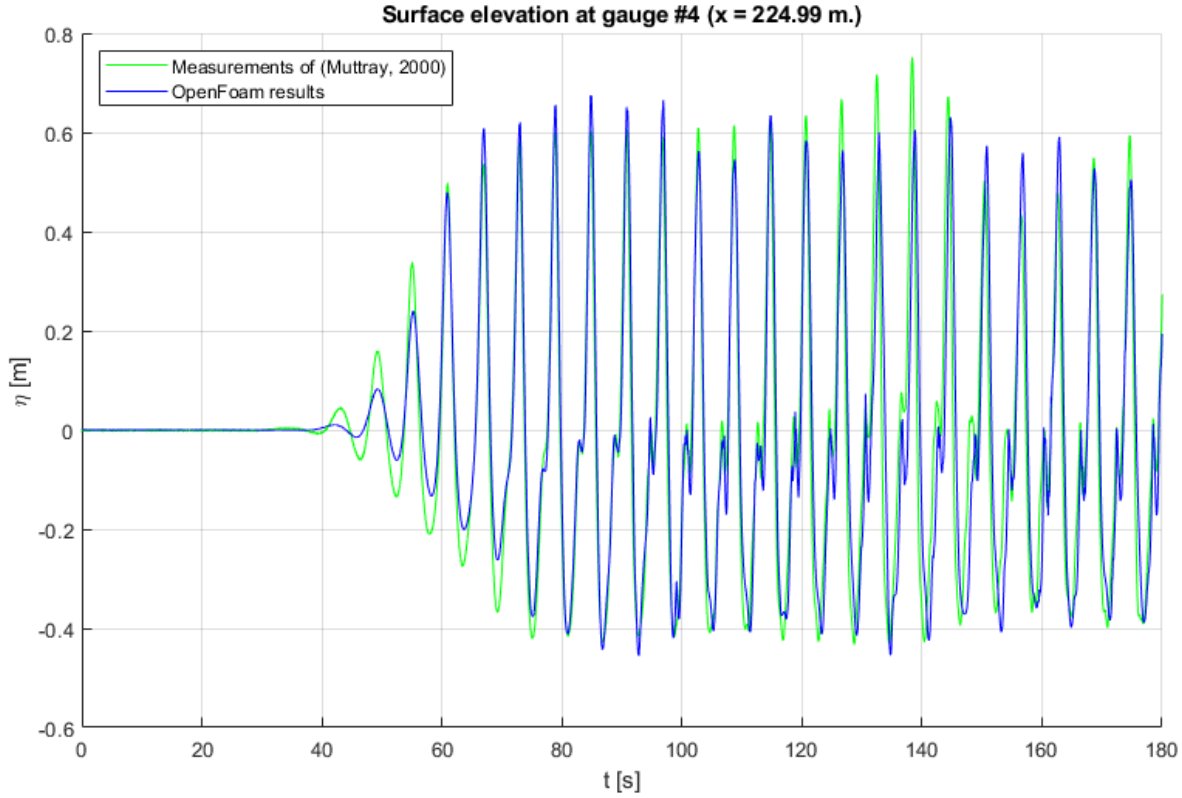

Figure 67 - Surface elevation comparison at gauge #4 ($x = 224.99$)

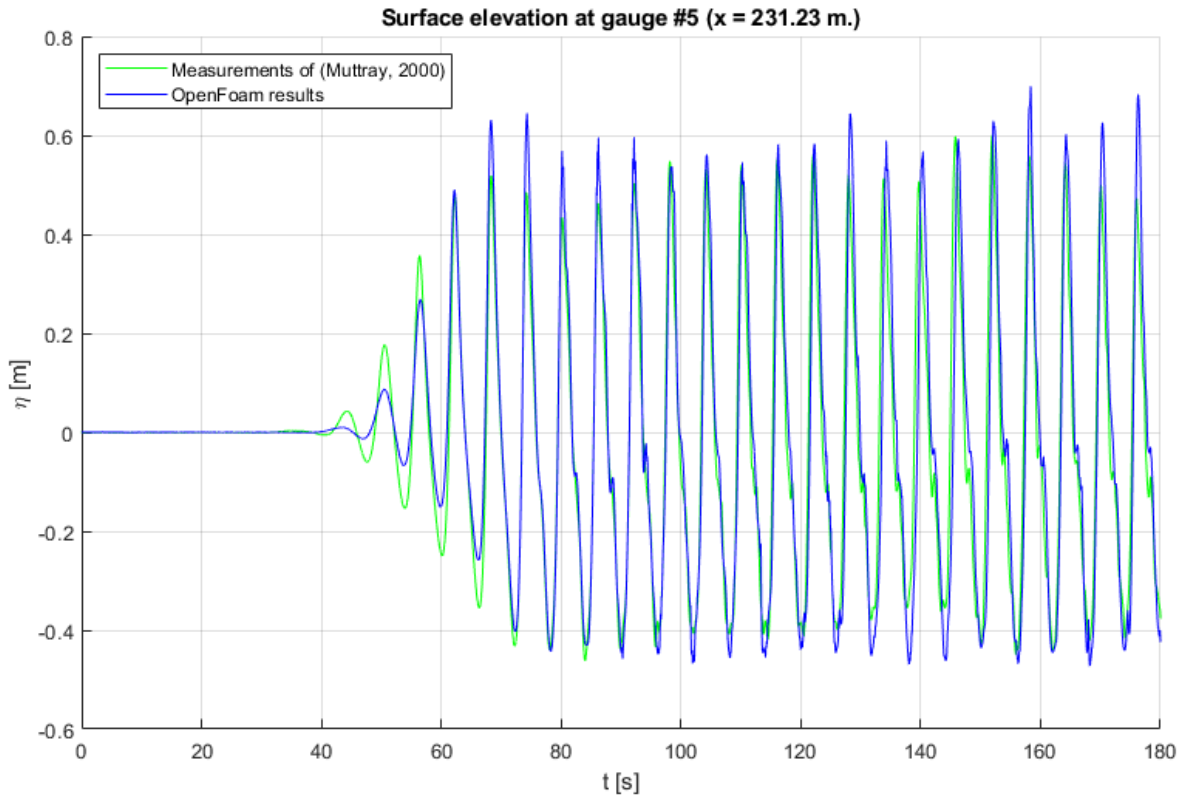

Figure 68 - Surface elevation comparison at gauge #5 ($x = 231.23$)

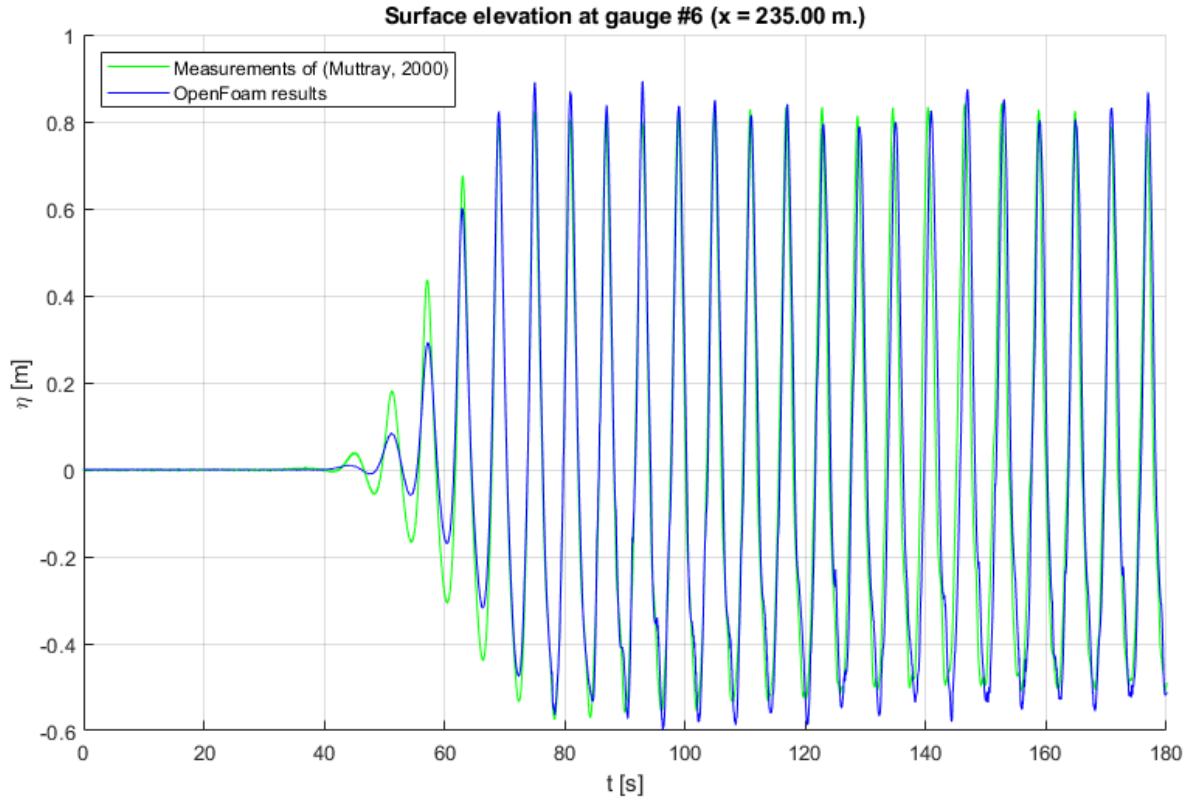

Figure 69 - Surface elevation comparison at gauge #6 ($x = 235.00$)

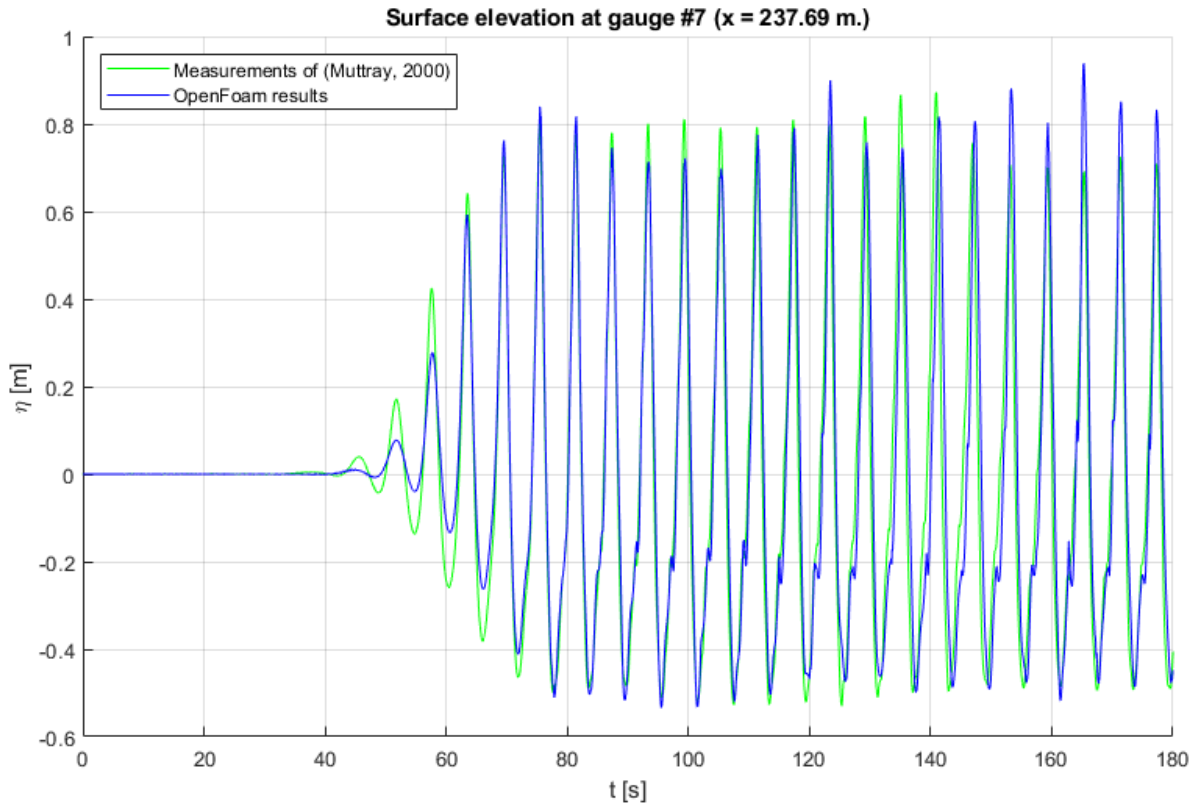

Figure 70 - Surface elevation comparison at gauge #7 ($x = 237.69$)

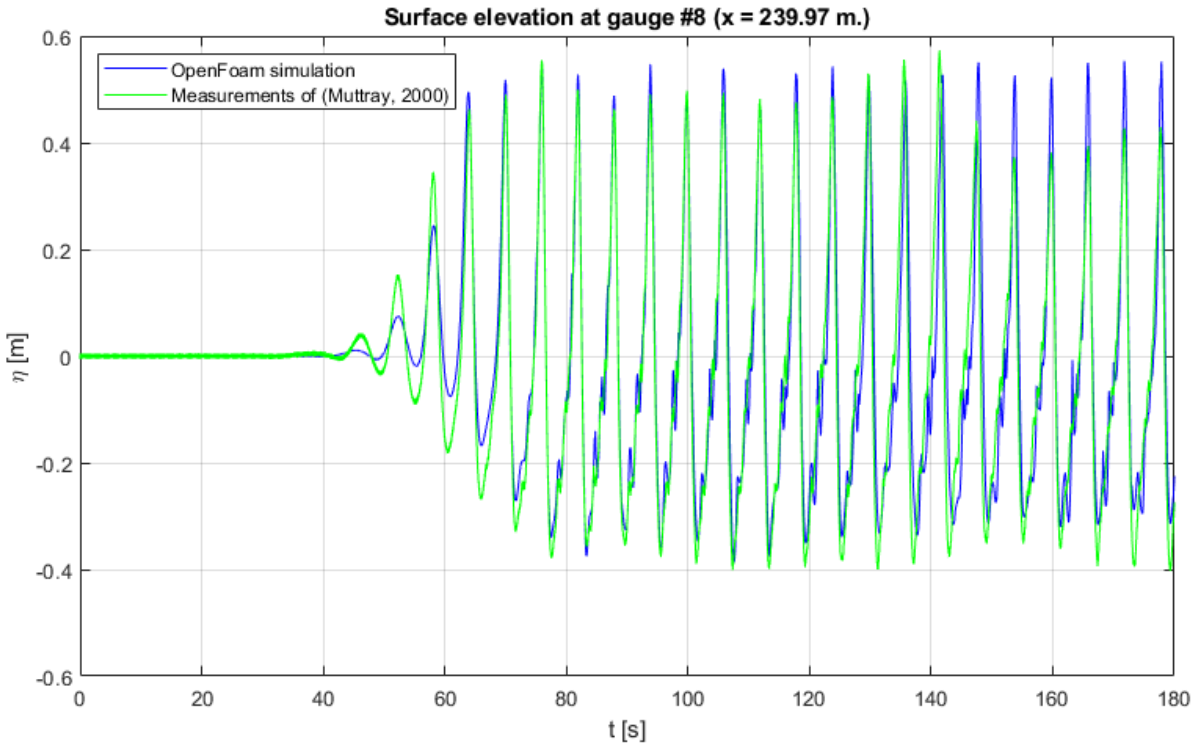

Figure 71 - Surface elevation comparison at gauge #8 ($x = 239.97$)
(On the flat part of the foreshore, in front of the structure)

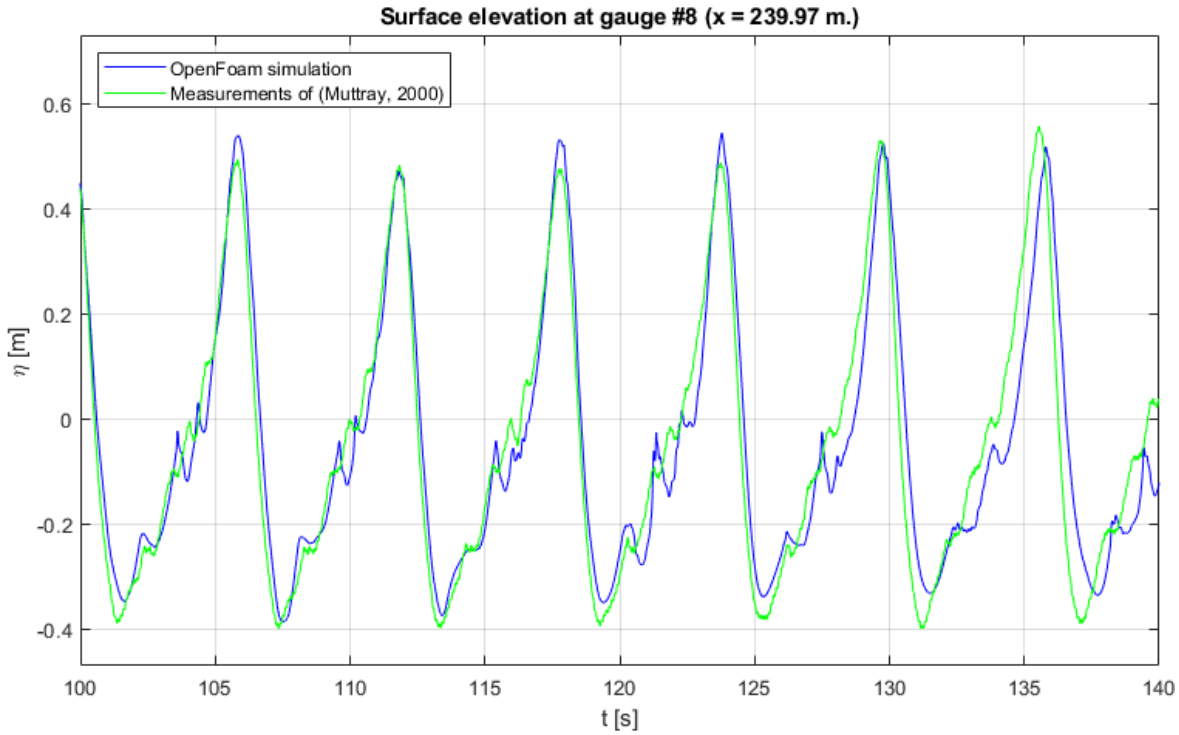

Figure 72 - Surface elevation comparison at gauge #8 (for $100 < t < 140$)

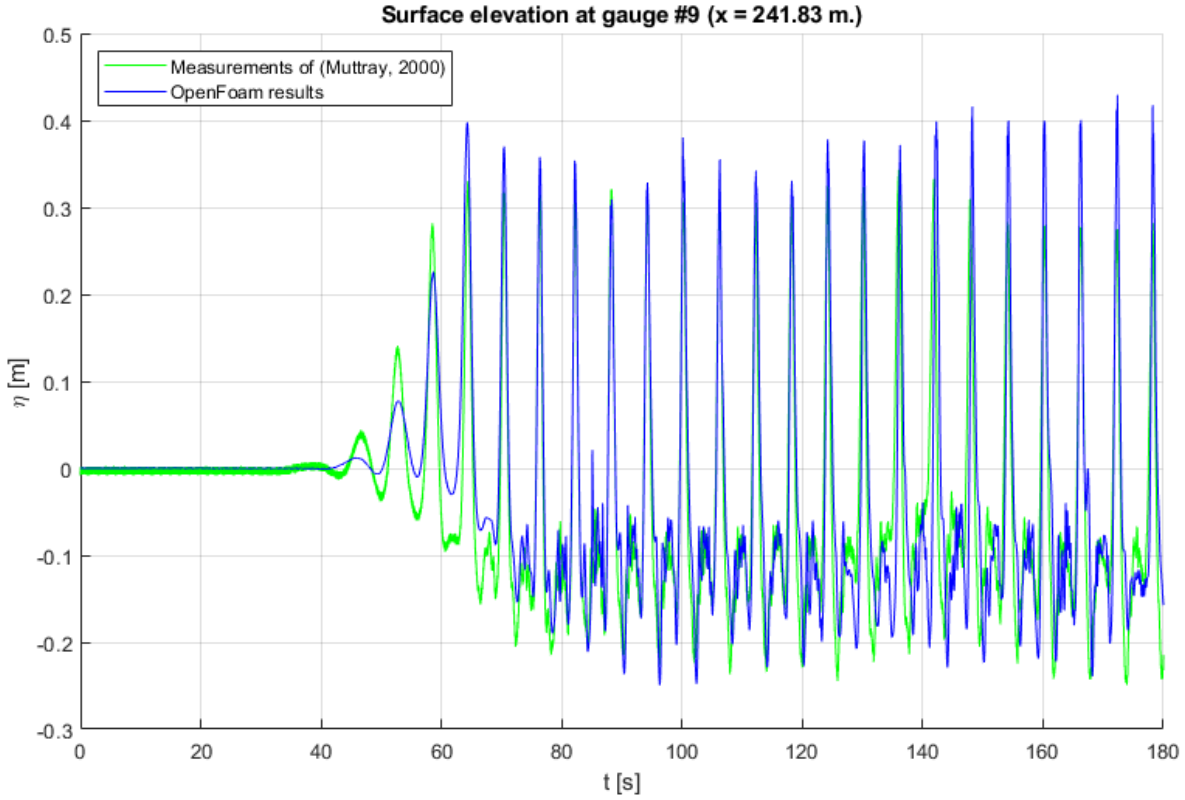

Figure 73 - Surface elevation comparison at gauge #9 ($x = 241.83$)

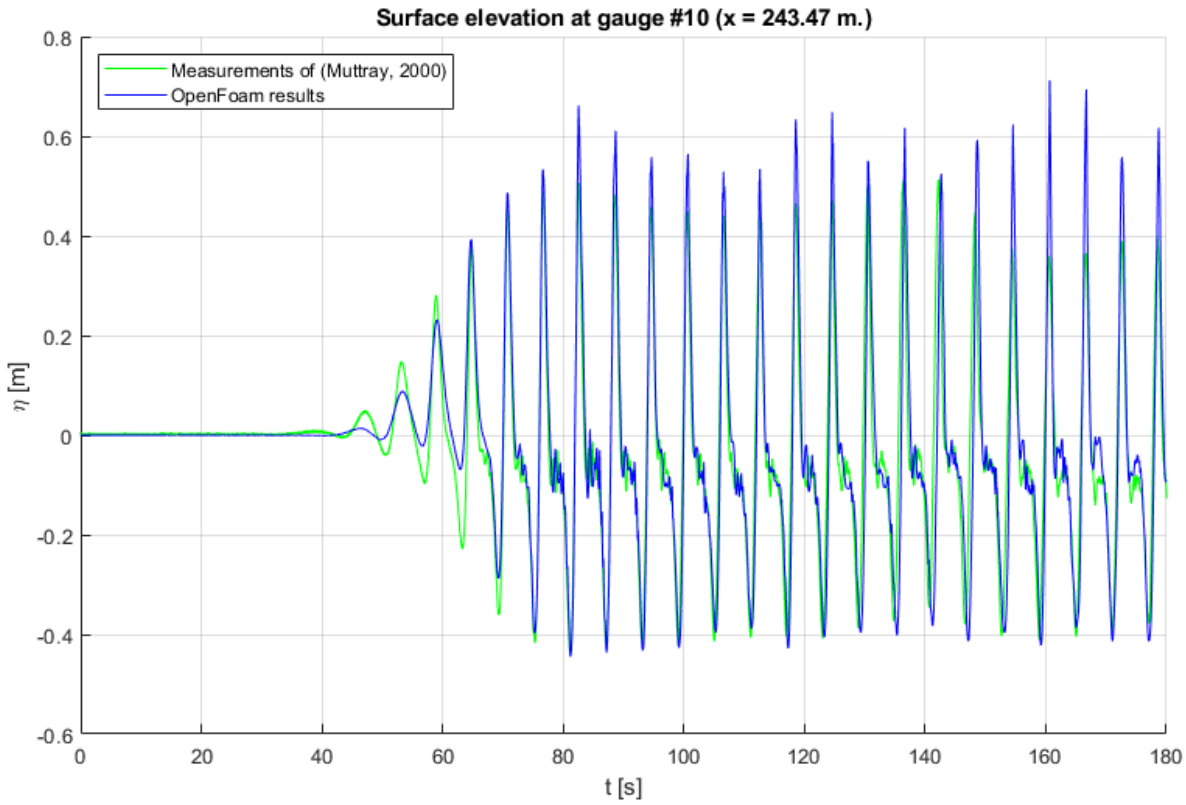

Figure 74 - Surface elevation comparison at gauge #10 ($x = 243.47$)

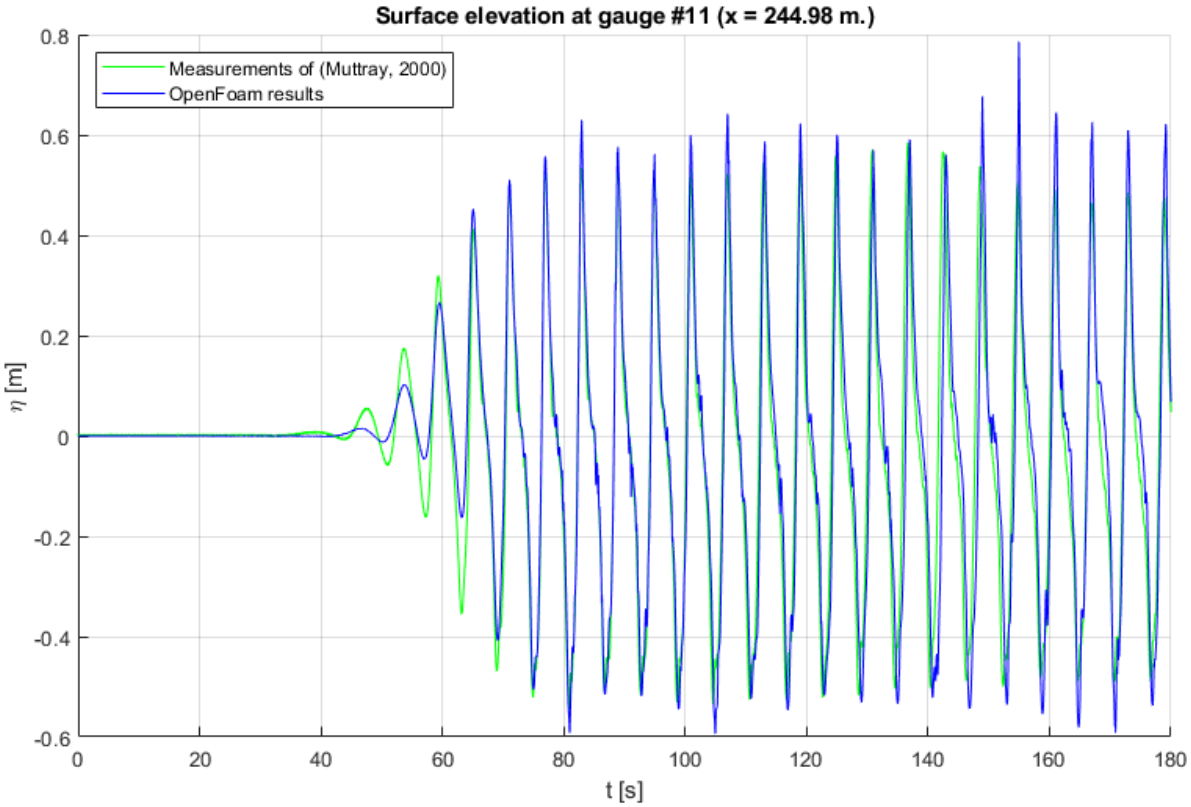

Figure 75 - Surface elevation comparison at gauge #11 ($x = 244.98$)

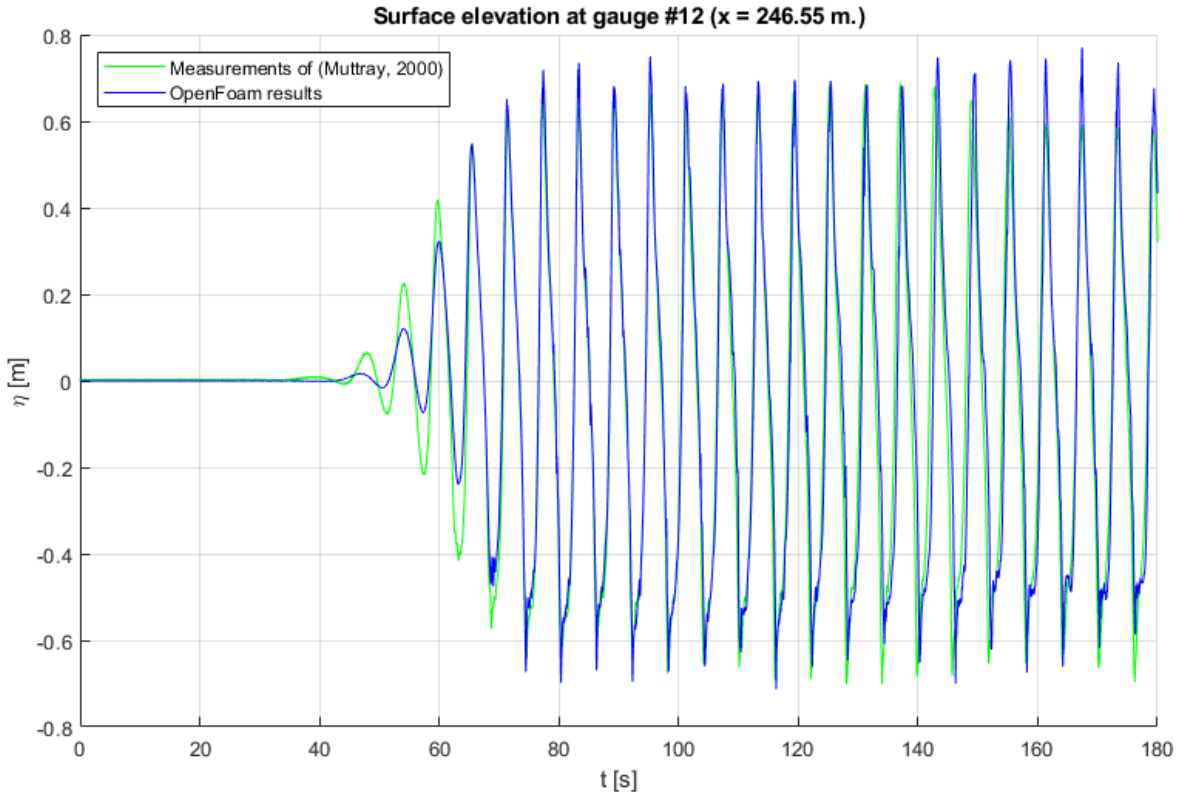

Figure 76 - Surface elevation comparison at gauge #12 ($x = 246.55$)

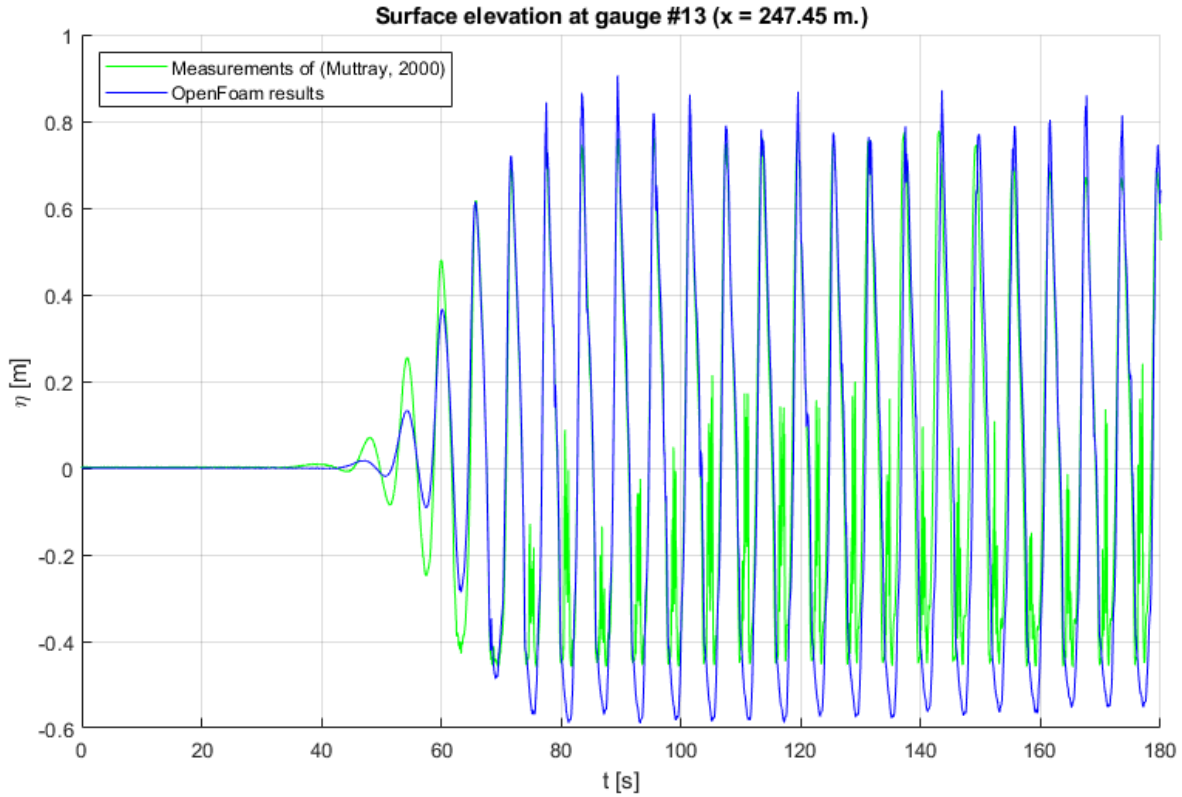

Figure 77 - Surface elevation comparison at gauge #13 ($x = 247.45$)

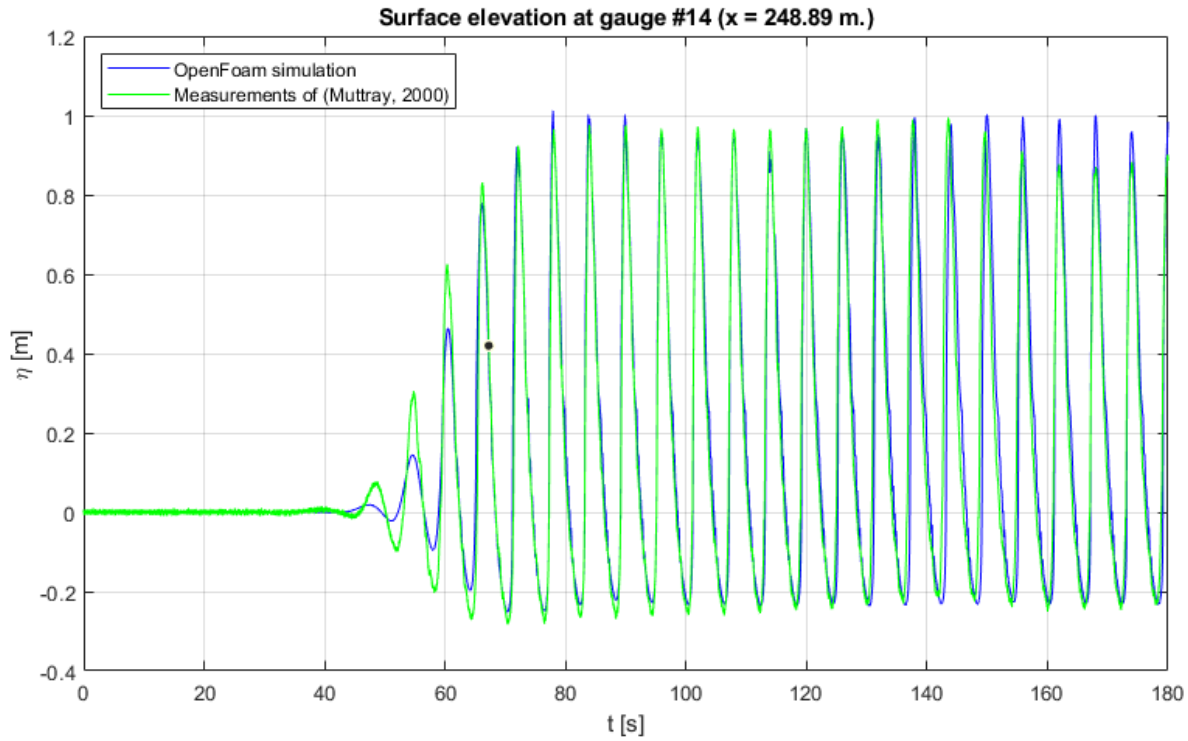

Figure 78 - Surface elevation comparison at gauge #14 ($x = 248.89$)
(In the middle of the front slope of the structure)

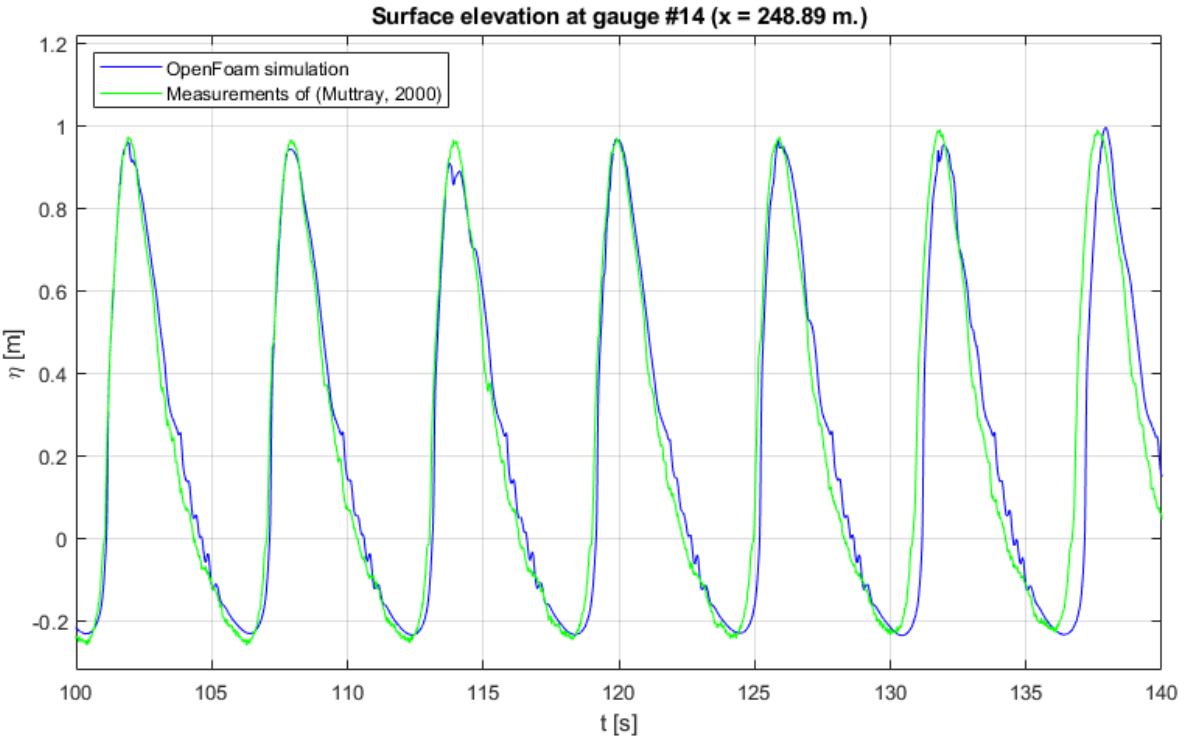

Figure 79 - Surface elevation comparison at gauge #14 (for $100 < t < 140$)

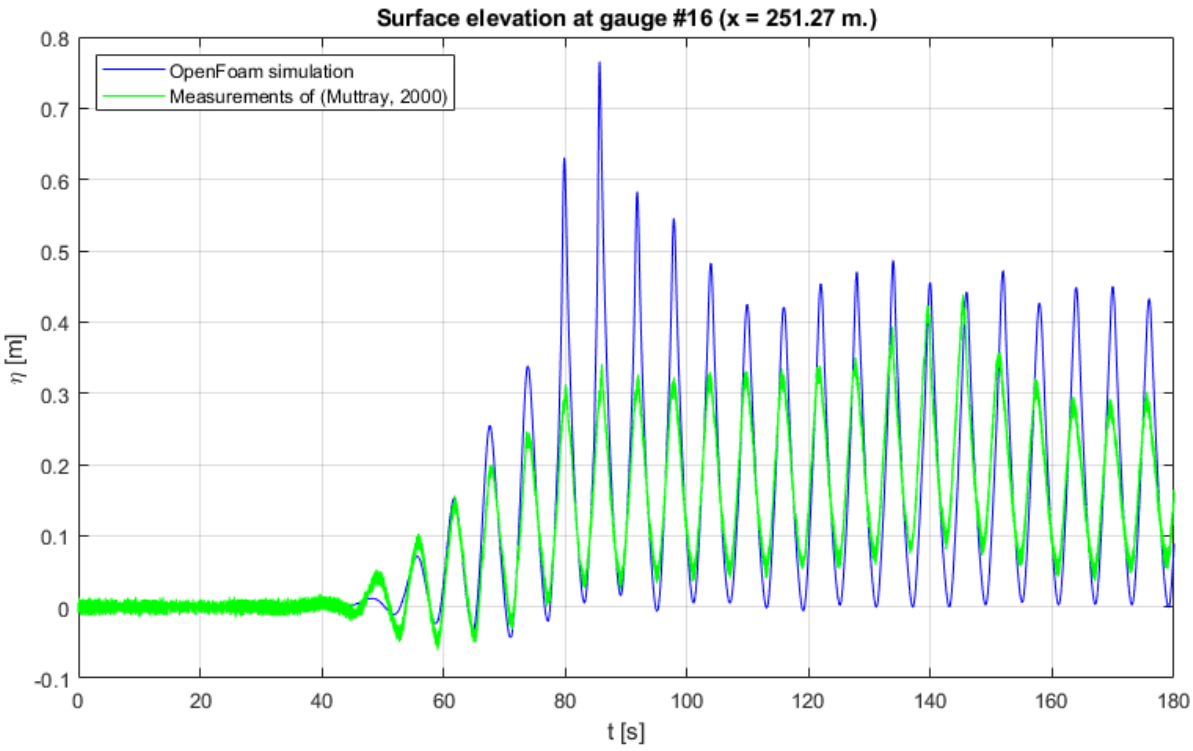

Figure 80 - Surface elevation comparison at gauge #16 ($x = 251.27$)
(Just in front of the crest of the structure)

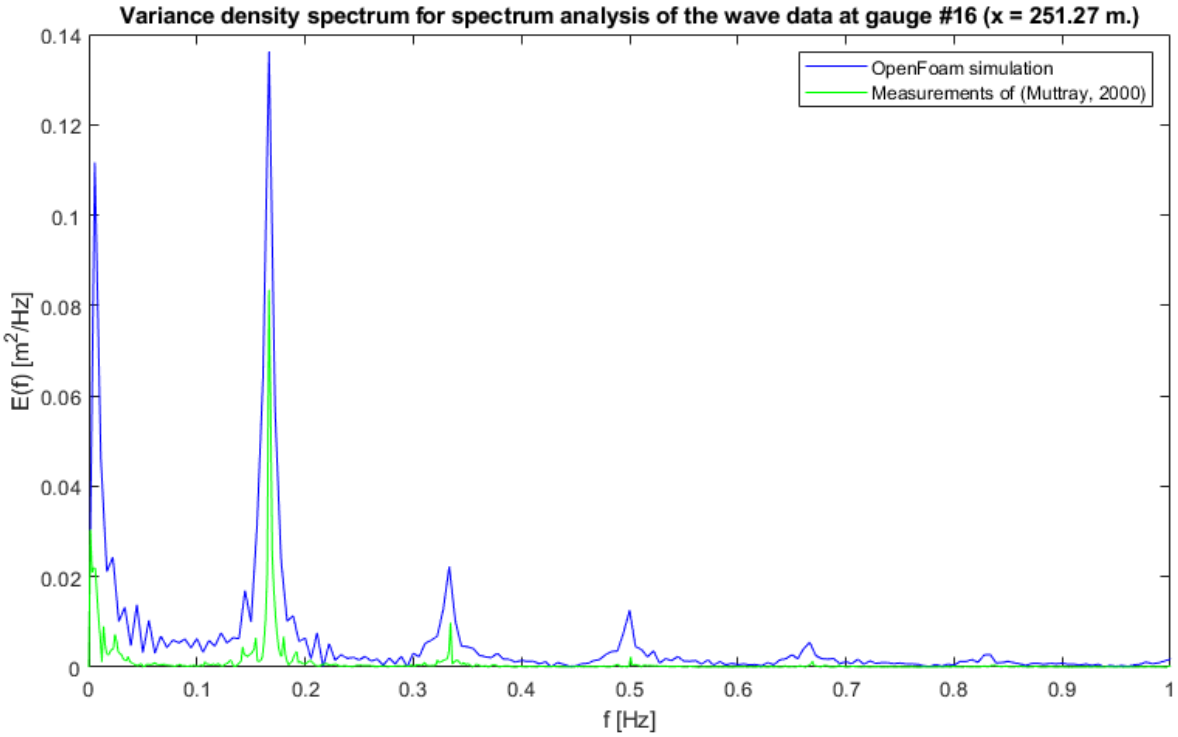

Figure 81 - Variance density spectra at gauge #16 $x = 251.27$

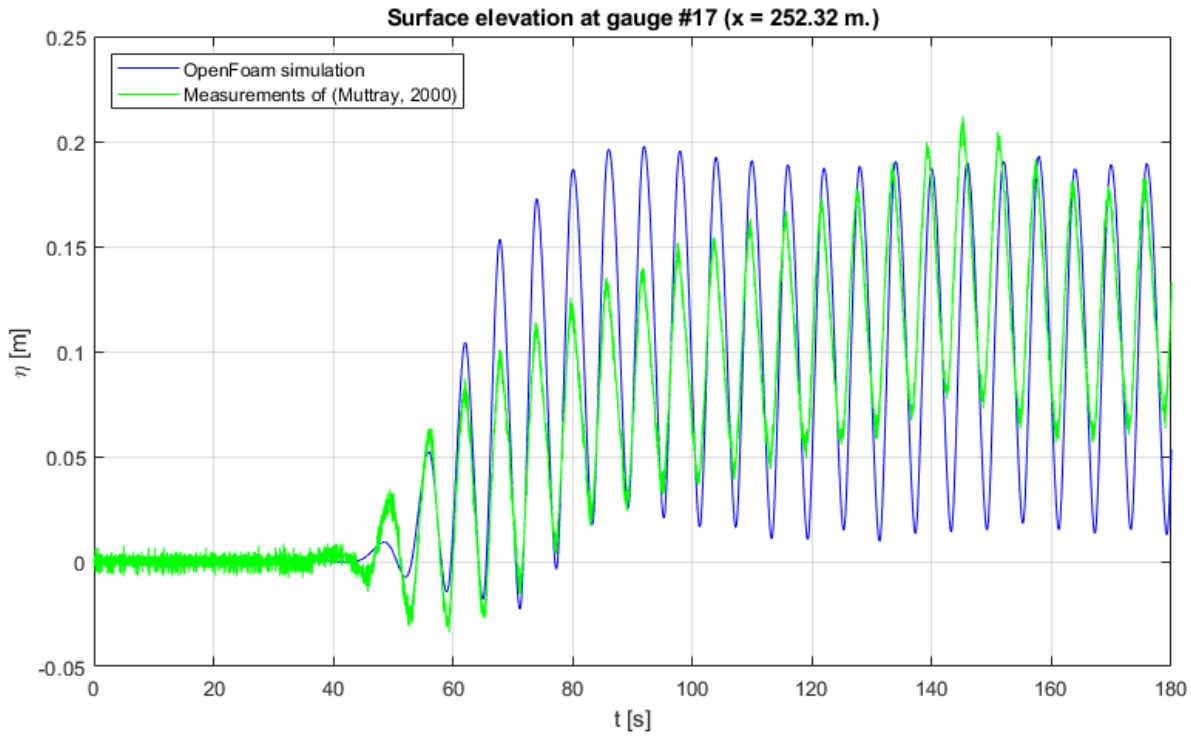

Figure 82 - Surface elevation comparison at gauge #17 ($x = 252.32$)
(In the middle of the crest of the structure)

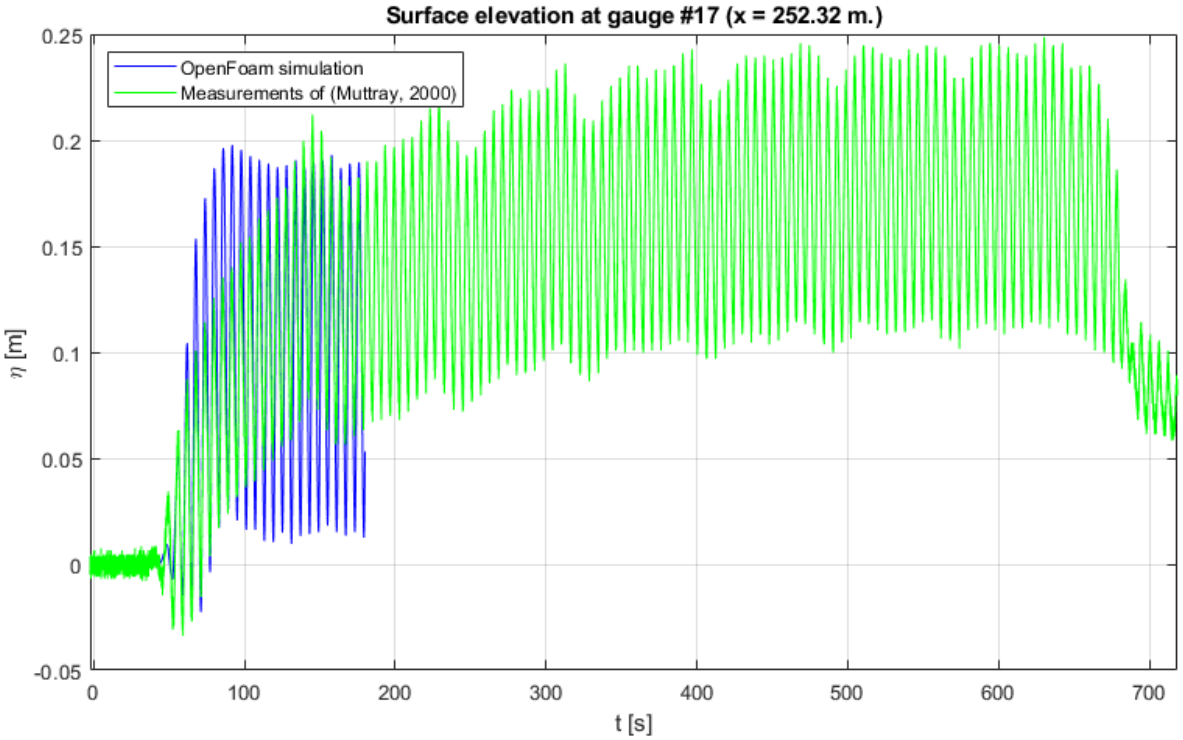

Figure 83 - Surface elevation comparison at gauge #17
(zoomed out to see the trend in the measurements of (Muttray, 2000))

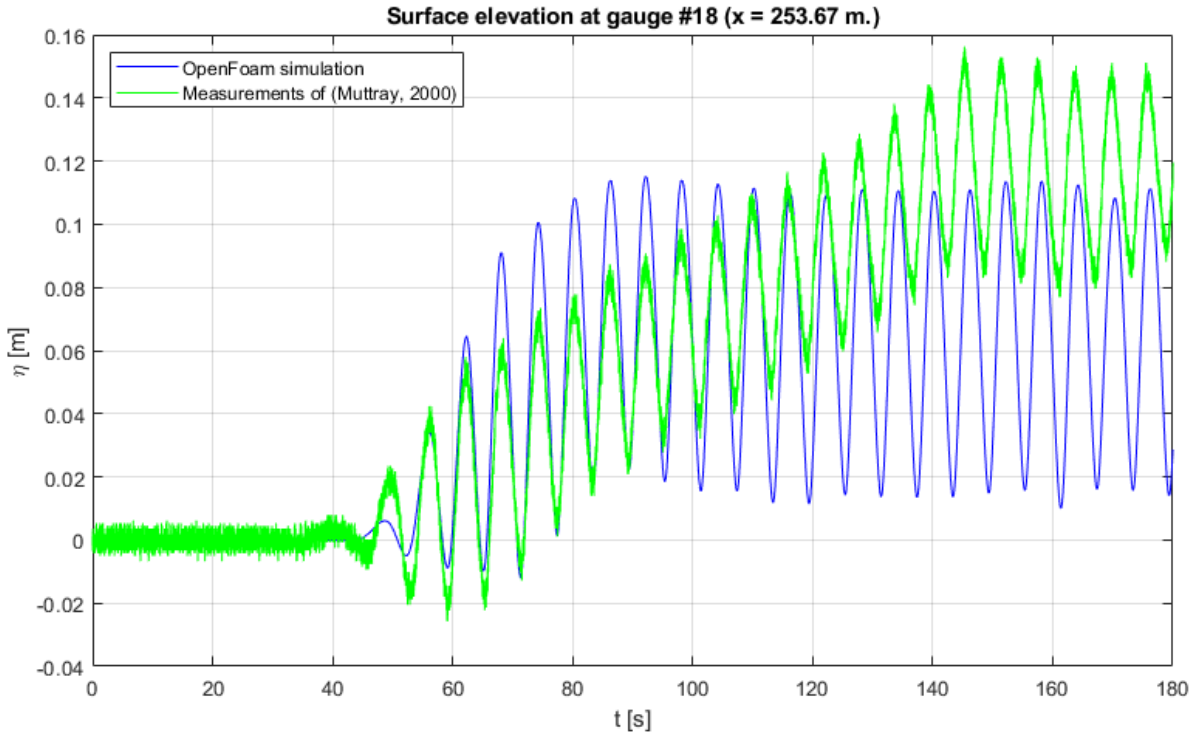

Figure 84 - Surface elevation comparison at gauge #18 ($x = 253.67$)
(Right after the crest of the structure)

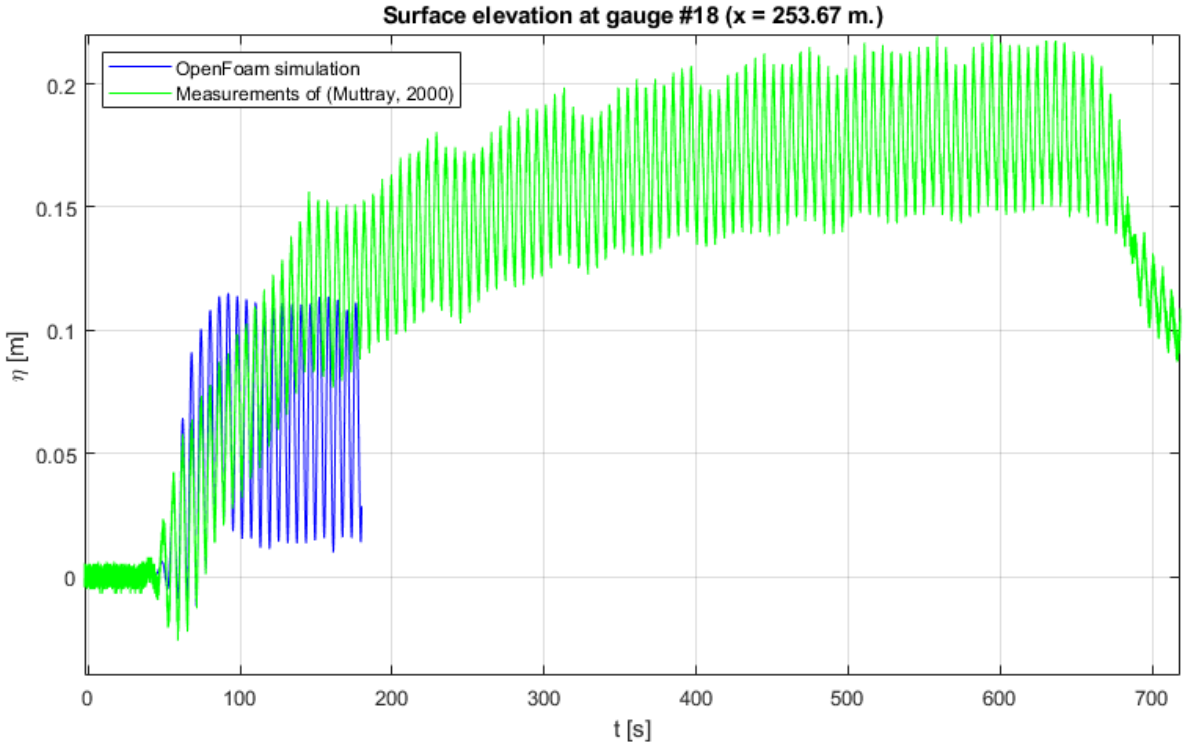

Figure 85 - Surface elevation comparison at gauge #18
(zoomed out to see the trend in the measurements of (Muttray, 2000))

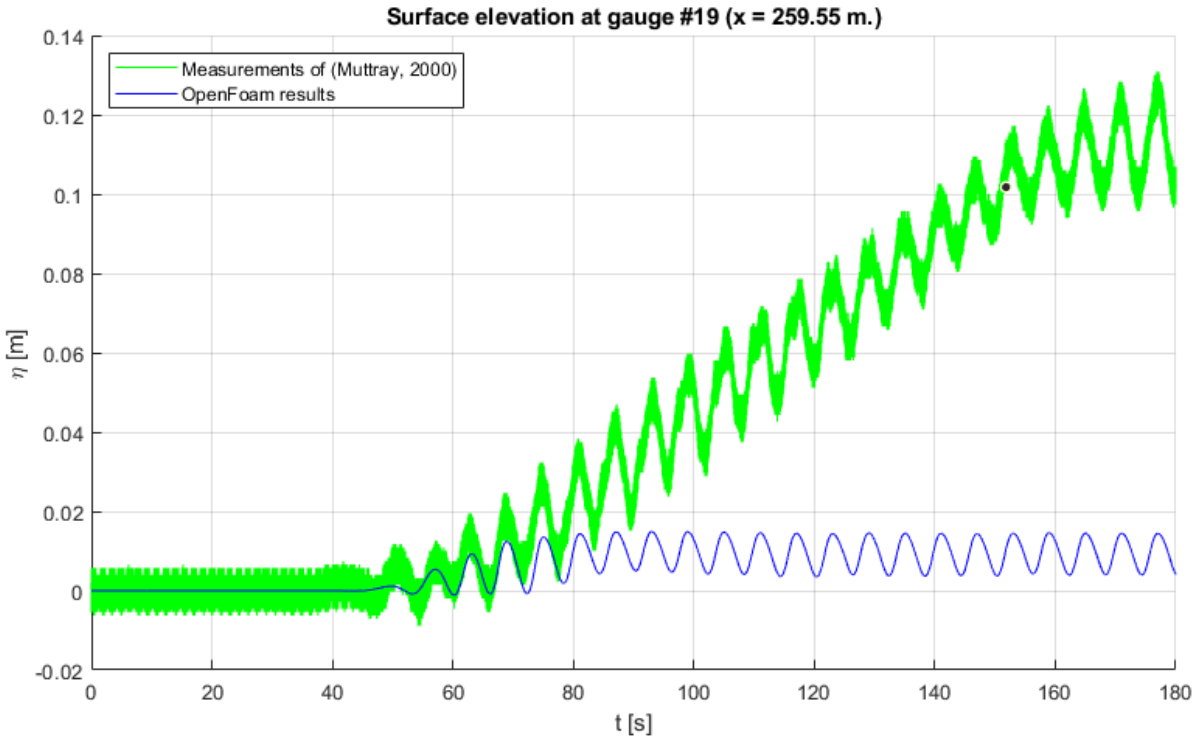

Figure 86 - Surface elevation comparison at gauge #19 ($x = 259.55$)
(Behind the structure)

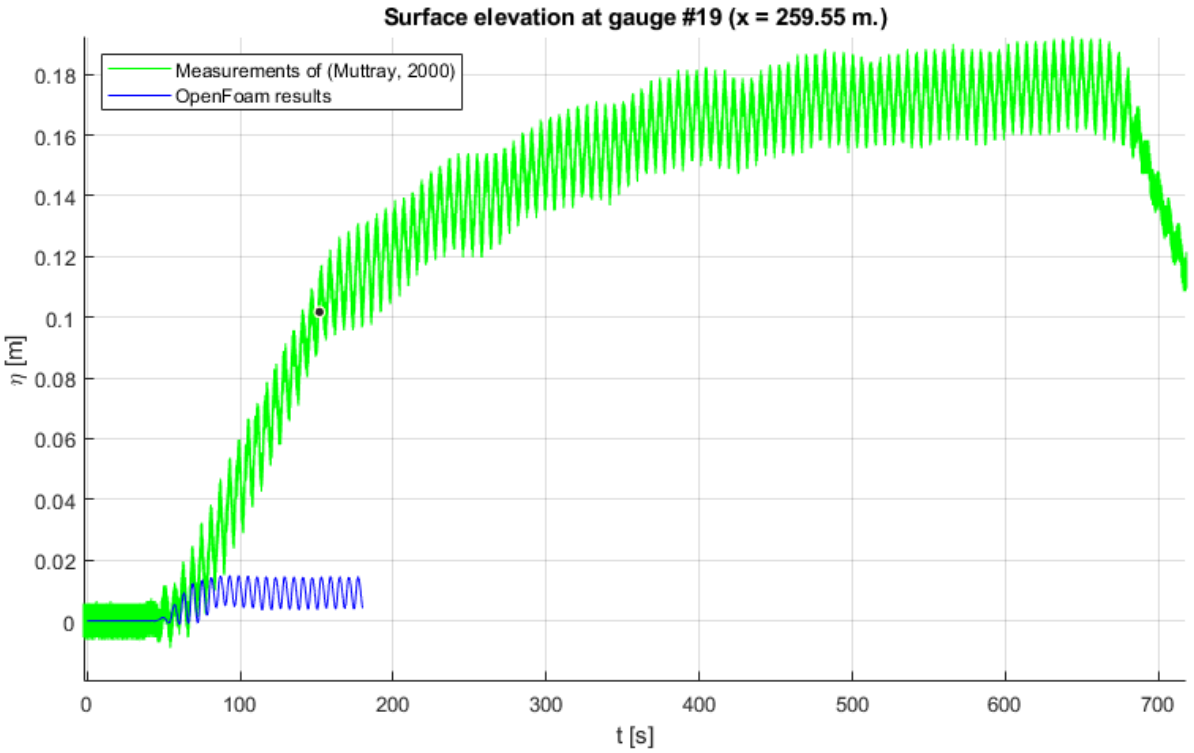

Figure 87 - Surface elevation comparison at gauge #19
(zoomed out to see the trend in the measurements of (Muttray, 2000))

A.3.4 Wave run-up comparison

Figure 88 shows the vertical level of the wave run-up over the armour slope for both the OpenFoam simulation as the measurements of (Muttray, 2000). As can be seen, both the peaks and the throughs of the results from the numerical simulation are not on the same level as the measurements of the physical model test. A possible explanation is given below.

The difference in maximum wave run-up level might be explained by the fact that the roughness of the front slope cannot be included in the OpenFoam model. Therefore the wave run-up is overestimated by the OpenFoam model. By tweaking the Forchheimer parameters of the armour layer, the maximum wave run-up level could be manipulated to match the measured wave run-up level. However, changing the Forchheimer parameters will also influence the flow velocities and pressure distributions through the armour layer, which is unwanted.

Furthermore, the difference in the maximum wave run-down level and the wave run-up level might be related to the used measuring techniques. When waves run down the front slope and the next waves arrives, some rather turbulent processes happen. In these processes the water is mixed with air which raises doubts about the accuracy of the measurements of the physical model test. In OpenFoam this mixing with air does not happen since turbulence is only modeled in the porous layers. This might be an explanation for the difference in maximum wave run-up and maximum wave run-down.

Besides, the entire top of the armour layer is not modeled correctly, in reality it is a rough surface while in OpenFoam it is modelled as a smooth surface. Furthermore is the position of the wave run up gauge in the physical model test very unsure. This raises doubt about the simulation of the flow velocity on top of the armour layer, parallel to the slope. The influence on the pressure measurement on top of the armour layer will be discussed in the next section, the pressure probe comparison.

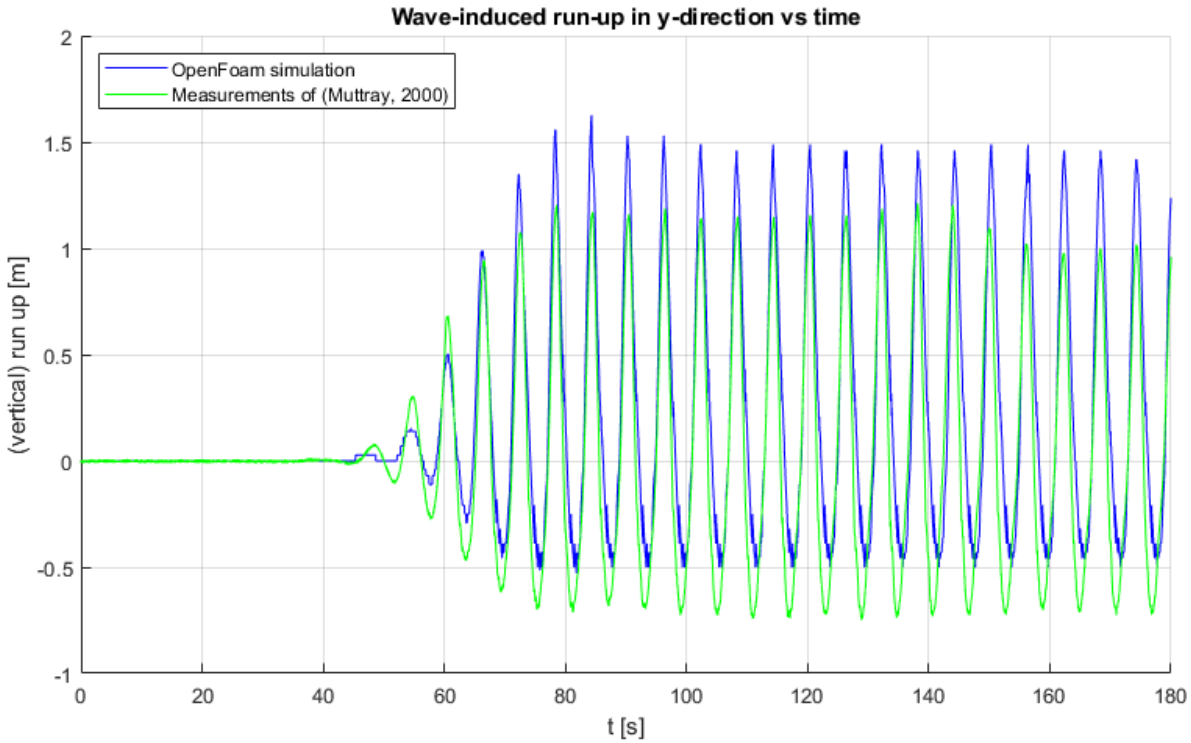

Figure 88 - Measured and simulated wave run-up (in y-direction) over the front slope of the breakwater structure

A.3.5 Pressure probe comparison

In the physical model tests, (Muttray, 2000) used quite a lot of pressure sensors (or pressure probes) to measure the wave induced pressure in the breakwater structure. The locations of the pressure sensors (the Druckmeßdosen) are shown in Figure 89. The exact coordinates of the pressure probes can be found in Table 26 in section A.1.2.

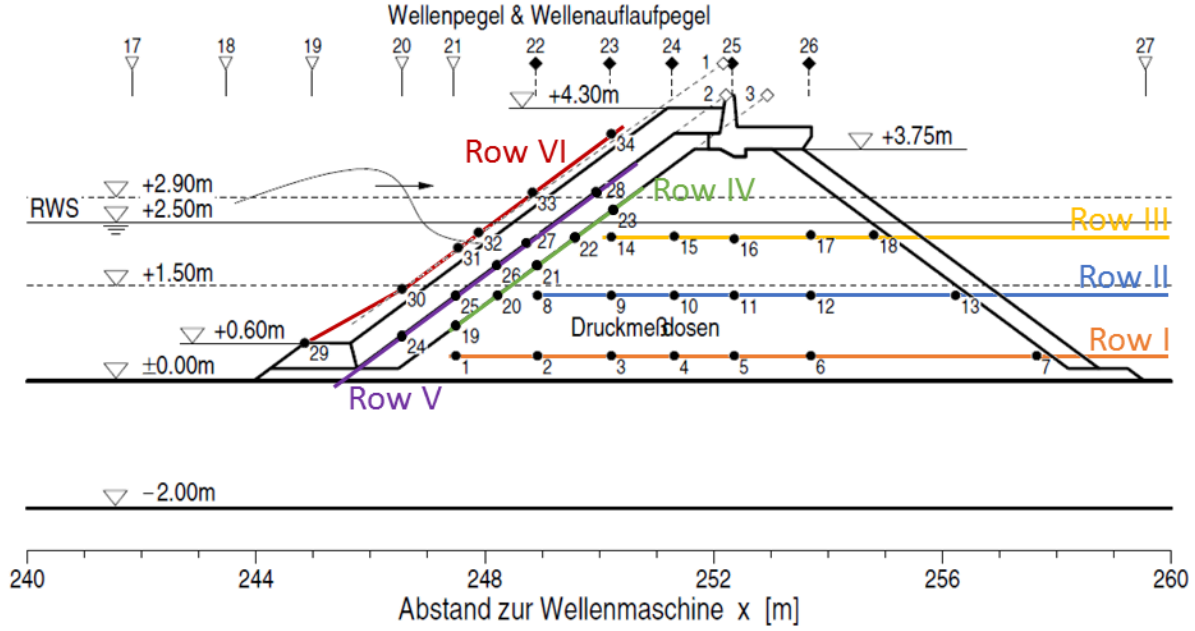

Figure 89 - location of the pressure sensors (Druckmeßdosen)

The pressure probes can be divided in six rows. Three horizontal rows:

Row I.	Pressure probes 1, 2, 3, 4, 5, 6 and 7	(Figure 90 till Figure 96)
Row II.	Pressure probes 8, 9, 10, 11, 12 and 13	(Figure 97 till Figure 102)
Row III.	Pressure probes 14, 15, 16, 17 and 18	(Figure 103 till Figure 107)

And three rows parallel to the front slope:

Row IV.	Pressure probes 19, 20, 21, 22 and 23	(Figure 108 till Figure 112)
Row V.	Pressure probes 24, 25, 26, 27 and 28	(Figure 113 till Figure 117)
Row VI.	Pressure probes 29, 30, 31, 32, 33 and 34	(Figure 118 till Figure 123)

The results from the OpenFoam simulation are compared with the measurements of the physical model tests. Row I, Row II and Row III show the same pattern. On the left side (near the front slope of the structure), the wave induced pressure simulated in OpenFoam matches the measured pressure quite well, see Figure 90, Figure 97, Figure 103 for the results of probes #1, #8 and #14. When moving along the row to the next probes, the amplitude of the simulated pressure is still approximately the same as the measured pressure, see e.g. Figure 91 and Figure 92, for the results of probes #2 and #3. However, when moving to probes in the middle or back section of the structure a trend in pressure measurements from the physical model test is noted, see e.g. Figure 94 and Figure 96 for the results of probes #5 and #7. On top of the pressure variation, the average pressure increases for these probes. This increase in average pressure becomes bigger when looking at probes further away from the front slope. This noted trend can be explained by the water level set-up on the backside of the breakwater structure. This water level set-up causes differences in water level elevations, which cause differences in wave induced pressure.

In Row III, the amplitude of the simulated wave induced pressures is a higher than in the amplitude of the measured pressures (approximately 15% at probe 14 to approximately 50% at probe 18) , e.g. see Figure 105 for the results of pressure probe #16. This can be explained by the difference in surface level elevation (see section A.3.3). When progressing through structure the incoming waves are dampened more in the physical model than in the OpenFoam model due to the water level set-up at the rear side of the breakwater in the physical model test. When the surface level elevation has a bigger amplitude, the amplitude of the measured pressure is also bigger. The influence of this amplitude difference in surface level elevation on the pressure reduces when moving down to pressure probes lower in the water column.

Row IV, Row V and Row VI show also the same pattern, when comparing the results of the OpenFoam simulation with the measurements of the physical model test. For the probes below the still water level (so the probes below $y = 2.5$) the wave induced pressure simulated in OpenFoam matches the measured pressure quite well, see e.g. probe #25, Figure 114. However, when looking at the probes above the still water level (so probes #23, #28, #33 and #34, respectively Figure 112, Figure 117, Figure 122 and Figure 123), the wave induced pressure simulated in OpenFoam has much higher peaks than the measured pressure in the physical model tests.

The author of this thesis suspects that the high peaks in pressure are due to flow velocity of the run-up. When wave run-up is progressing along the slope, the thickness of the water layer decreases but the flow velocity increases. Since the measurement probe is precisely on the interface of the front slope, only a very small layer of water with high velocities could result in high measured pressures. In the physical model tests, this is not measured since the pressure sensors in the physical model tests are protected by a casing which have a significant influence on the flow. Besides, the wave run-up is not correctly modeled by OpenFoam, the wave run-up is higher in OpenFoam than in the physical model tests (due to the lack of roughness of the front slope and the lack of turbulence in the water, see section A.3.4). This causes higher pressure in the part of the wave run-up zone above the still water level.

The simulated pressure in probes #31 and #32 (Figure 120 and Figure 121) in the OpenFoam simulation do not quite match the pressure measured by (Muttray, 2000). The simulated pressures drop to a zero value while the results of the physical model tests have a quite flat trough in these parts of the plots. This is due to the fact that probe #31 and probe #32 are sometimes underwater and sometimes lie dry. The lines of the OpenFoam measurements only show the pressure when the probes are underwater, so when the probes lie dry, a measurement value of 0 is shown. In the physical model tests, the probes keep showing a constant value when the probe falls dry.

From the pressure probe comparison it can be concluded that the wave induced pressure is modelled correctly for the area around the front slope, beneath the still water level. The wave induced pressures around the front slope, above the still water level seem to be not correct. In the prediction methods, there is only looked at the relative values of the pressures around the front slope and between these values is interpolated in order to predict a P-value. Since all structures are modelled for exactly the same wave signal, it is expected that the relative error in the pressures around the front slope above the still water is approximately the same. The effect of these errors is canceled out by the interpolation of the values, and thus it is expected that the errors in the pressures above the still water level have no influence on the prediction methods.

The flow velocities through the porous layers are not measured in the physical model tests of Muttray. However, the flow velocities through the porous layers are a consequence of the pressure difference over these layers. Since the pressure is correctly modelled around the armour and filter layer (below the still water level), it can be concluded that the flow velocities in this part are also correctly modelled.

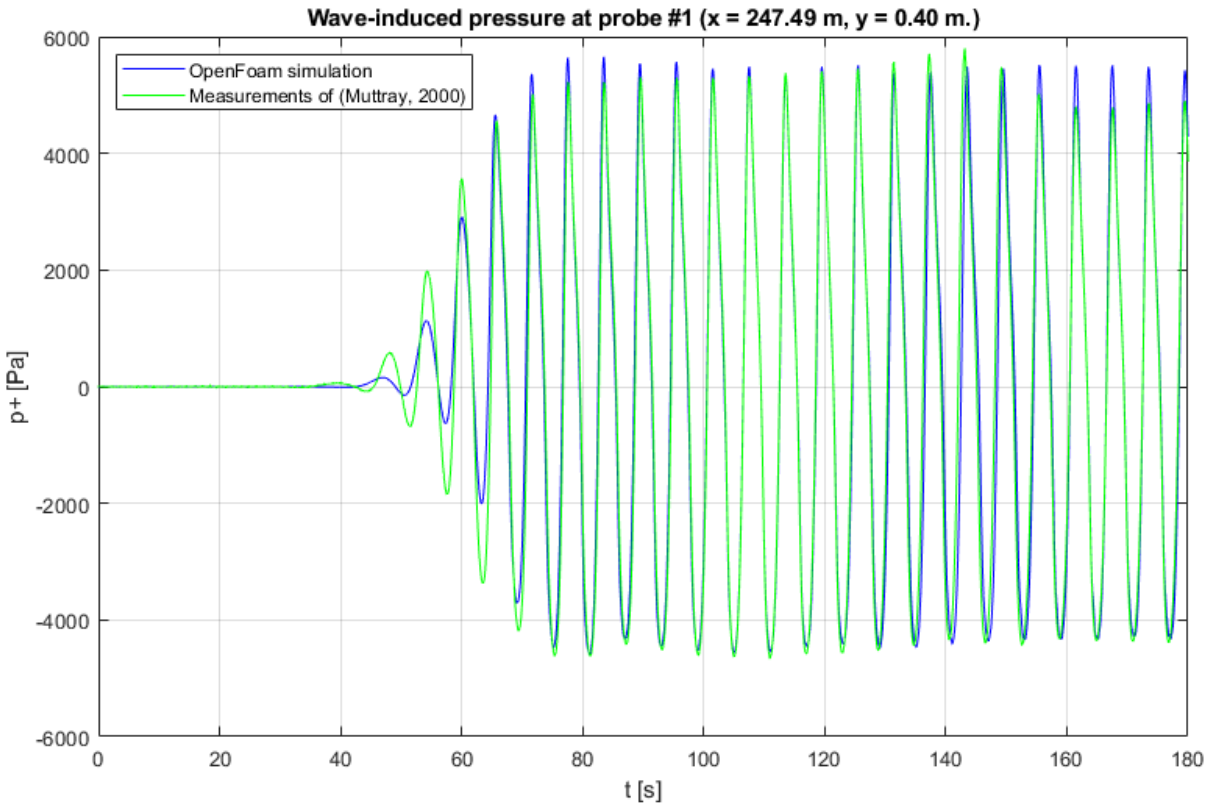

Figure 90 - Measured and simulated pressure in pressure probe #1 ($x = 247.49\ m$, $y = 0.40\ m$)

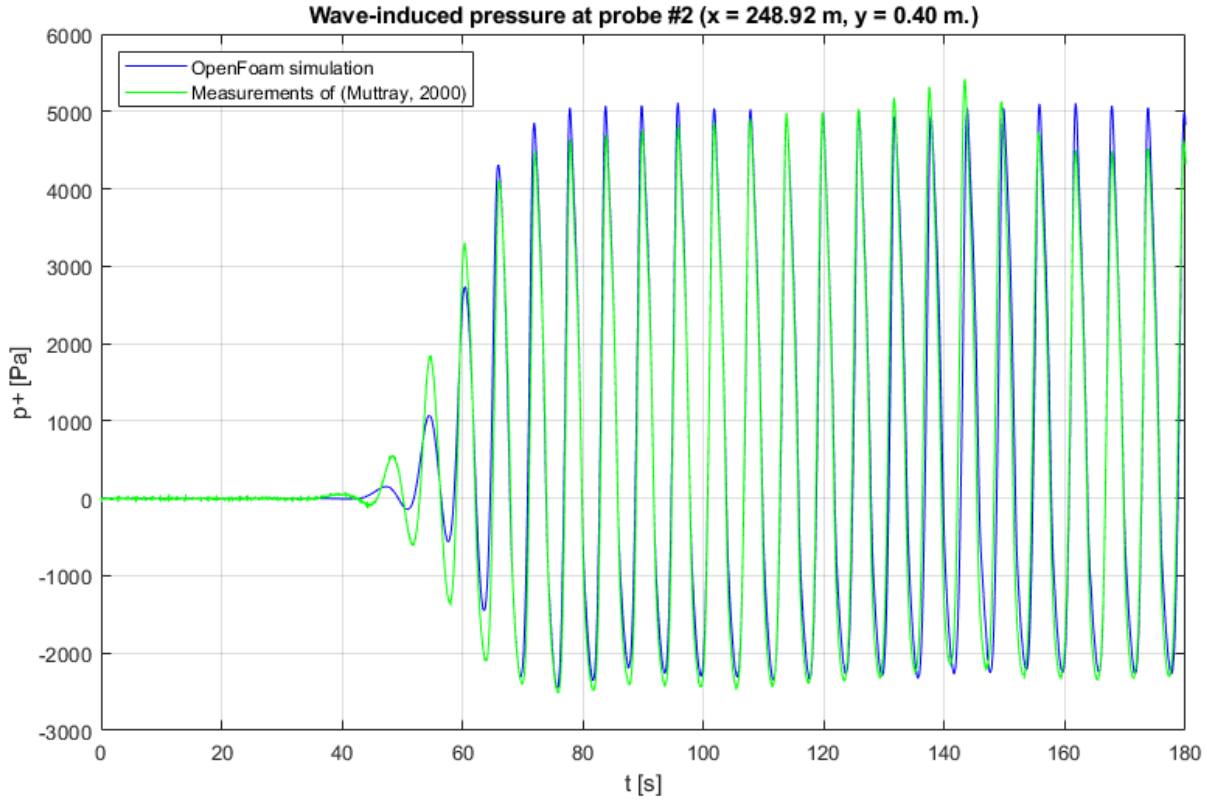

Figure 91 - Measured and simulated pressure in pressure probe #2 ($x = 248.92\ m$, $y = 0.40\ m$)

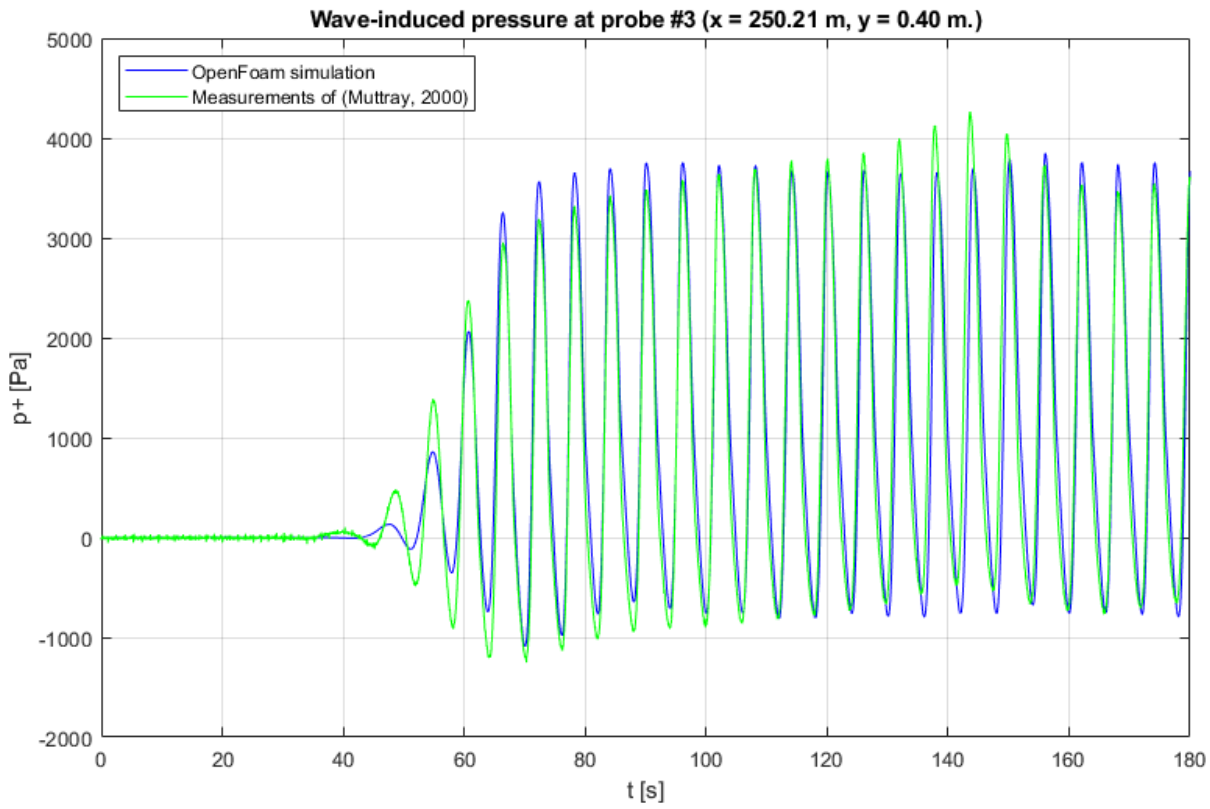

Figure 92 - Measured and simulated pressure in pressure probe #3 ($x = 250.21\ m$, $y = 0.40\ m$)

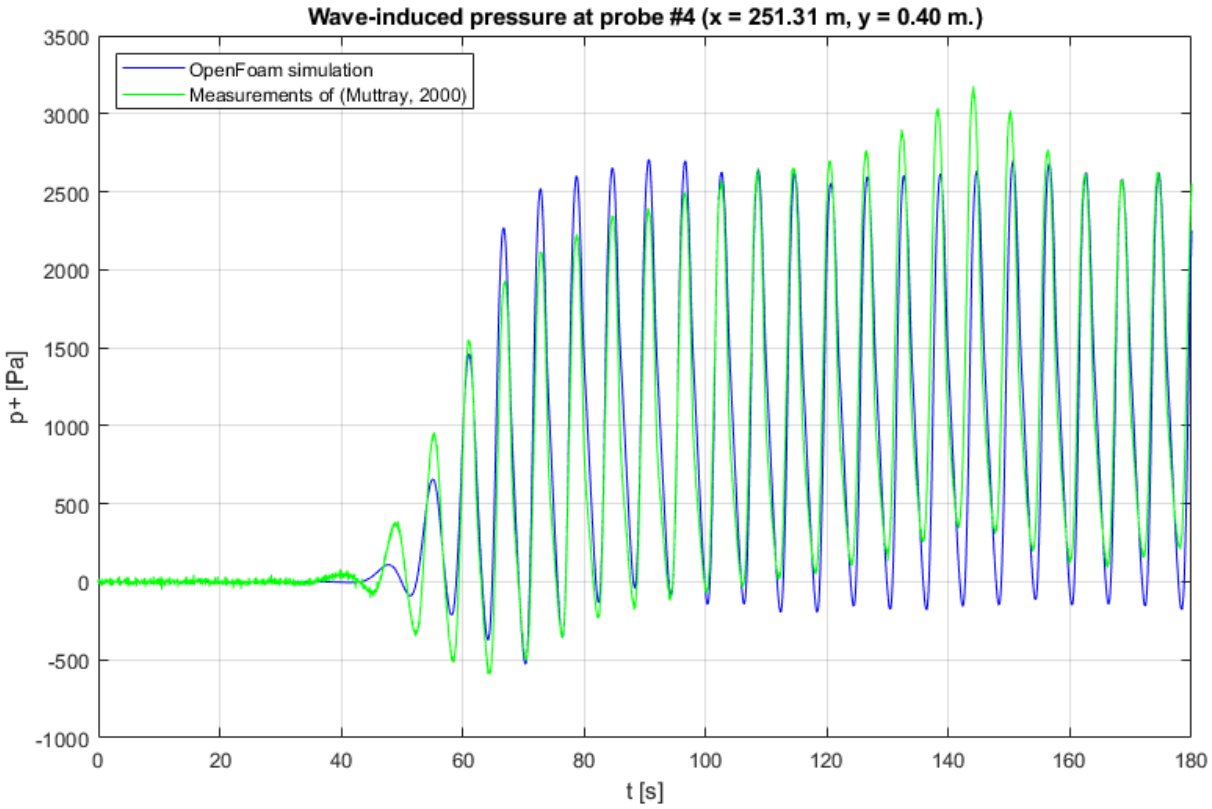

Figure 93 – Measured and simulated pressure in pressure probe #4 ($x = 251.31\ m$, $y = 0.40\ m$)

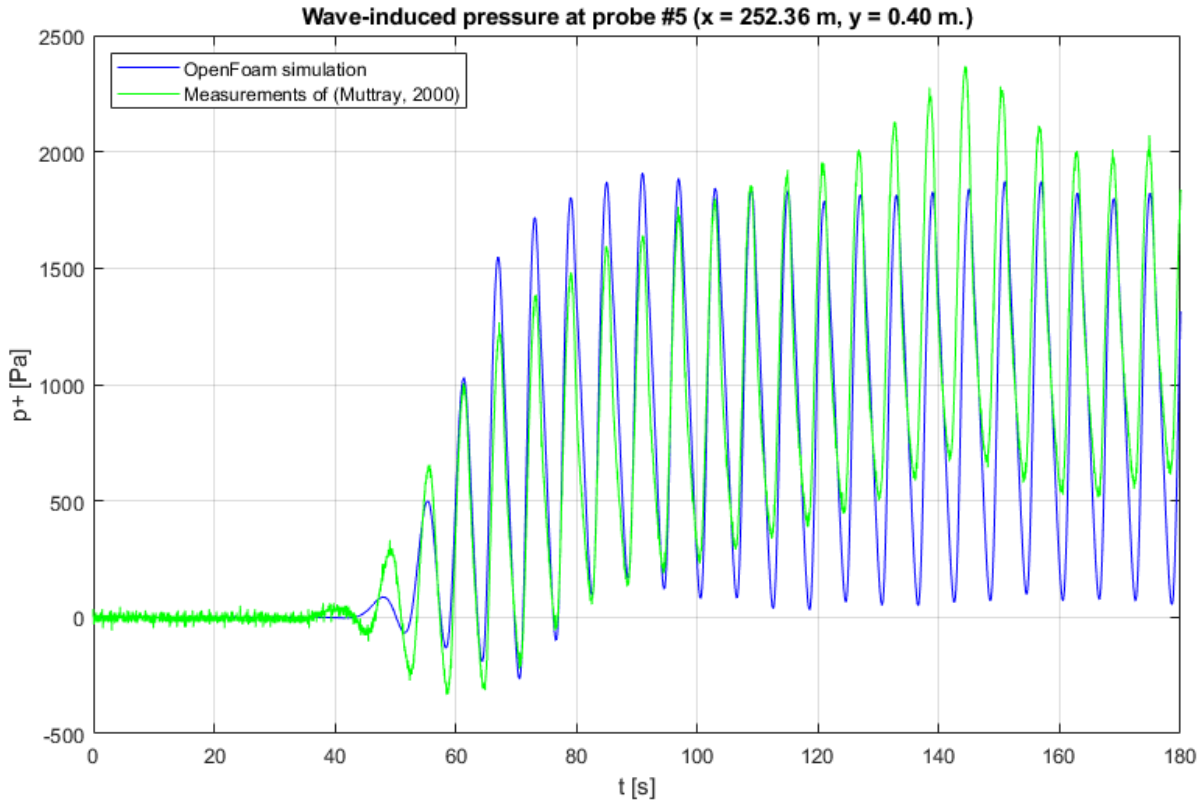

Figure 94 – Measured and simulated pressure in pressure probe #5 ($x = 252.36\ m$, $y = 0.40\ m$)

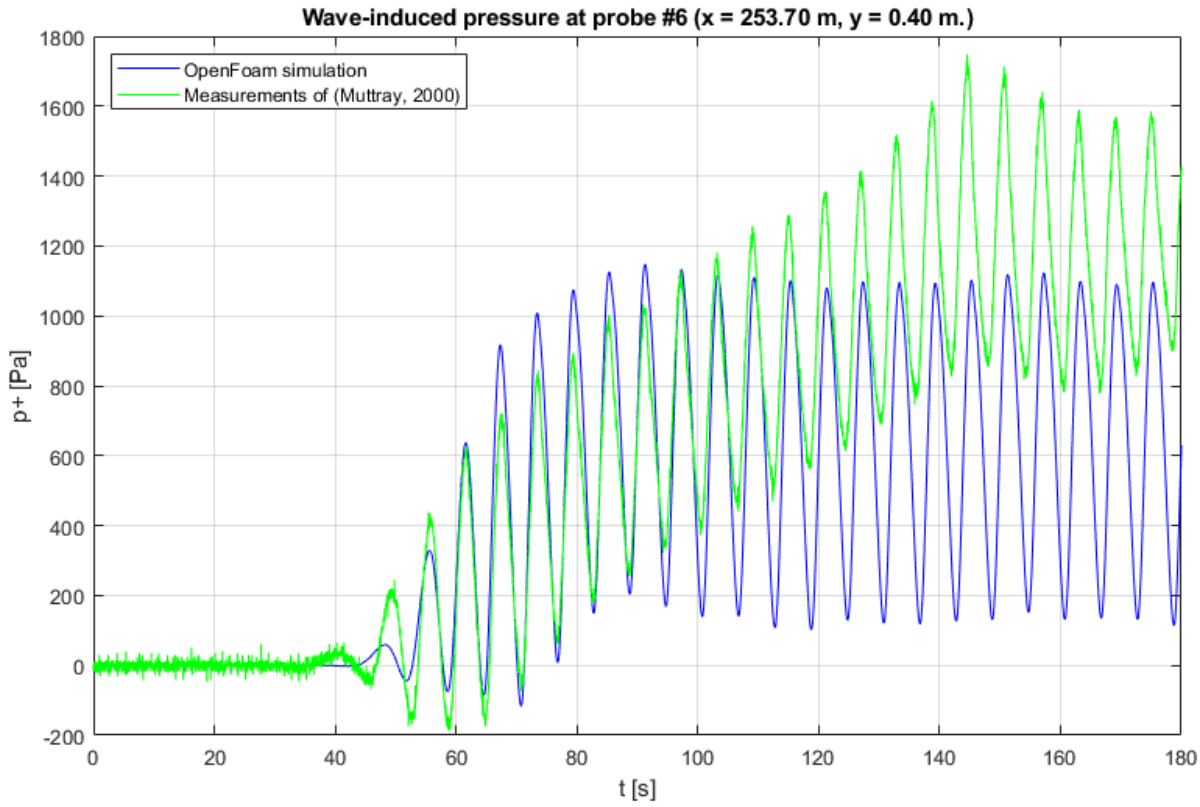

Figure 95 - Measured and simulated pressure in pressure probe #6 ($x = 253.70\ m$, $y = 0.40\ m$)

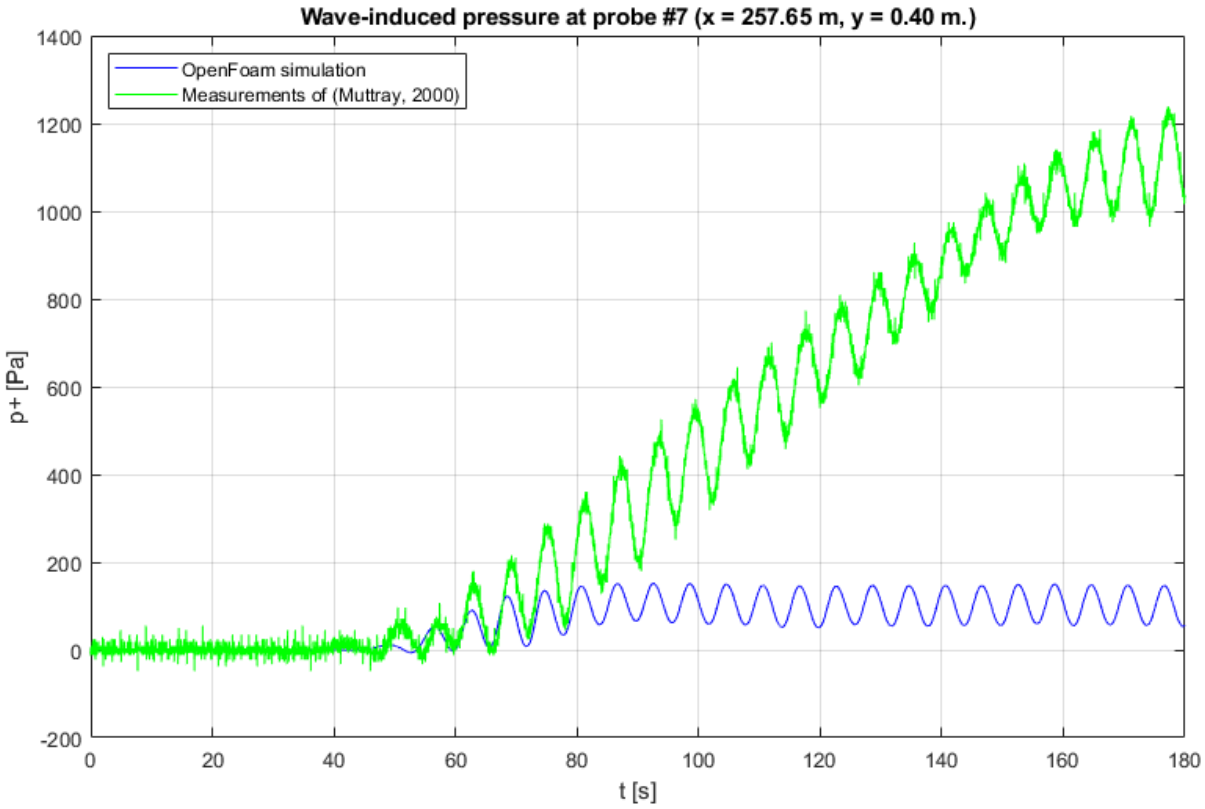

Figure 96 - Measured and simulated pressure in pressure probe #7 ($x = 257.65\ m$, $y = 0.40\ m$)

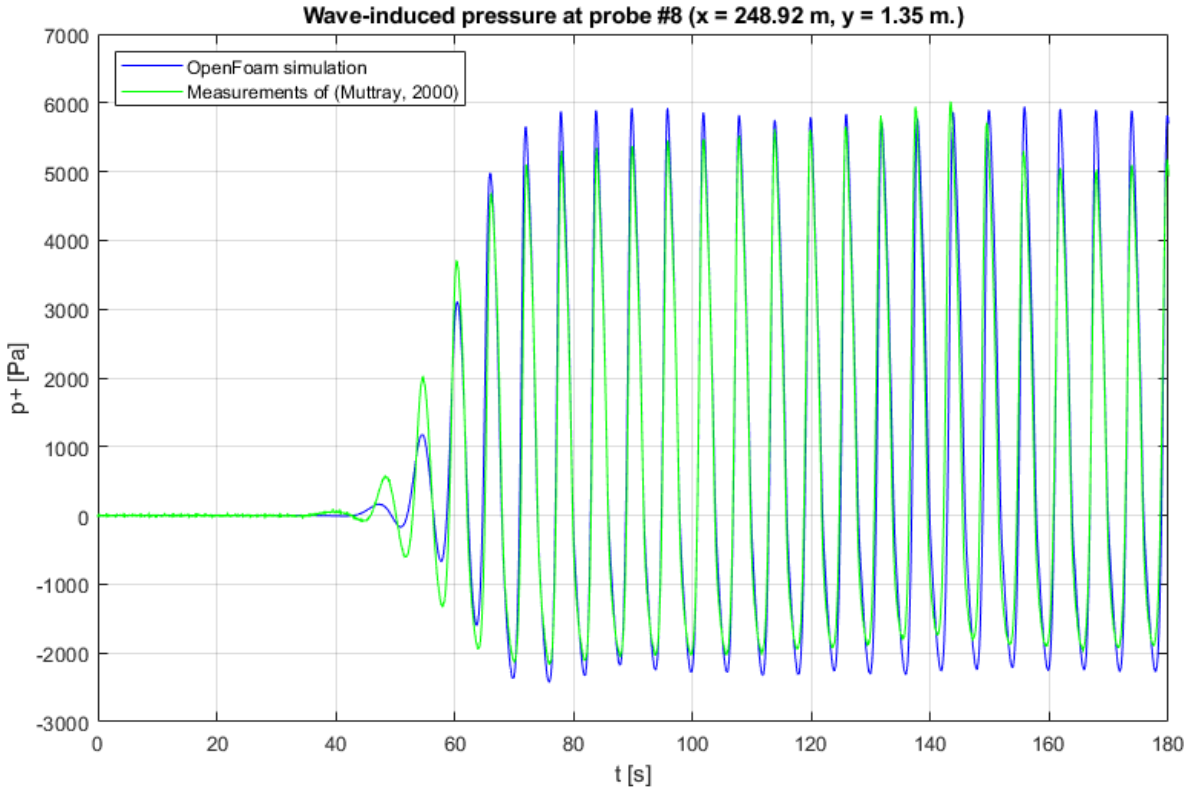

Figure 97 - Measured and simulated pressure in pressure probe #8 ($x = 248.92\ m$, $y = 1.35\ m$)

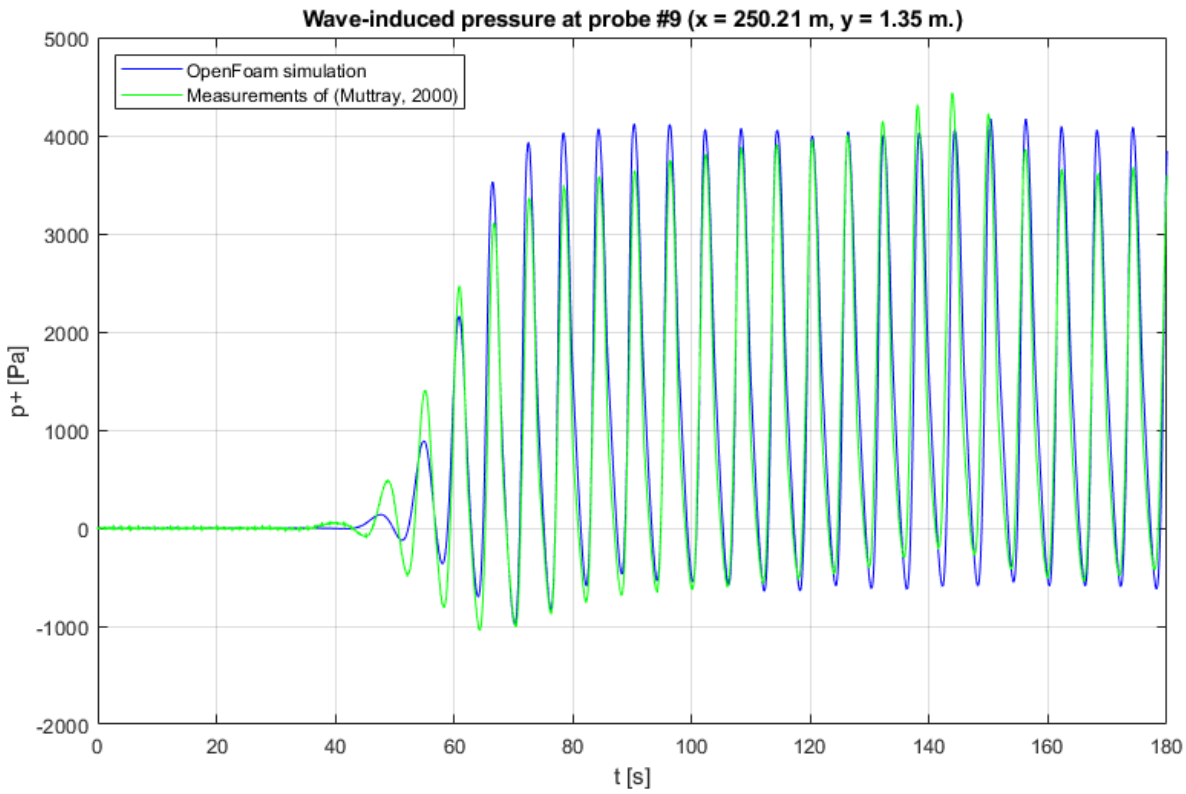

Figure 98 - Measured and simulated pressure in pressure probe #9 ($x = 250.21\ m$, $y = 1.35\ m$)

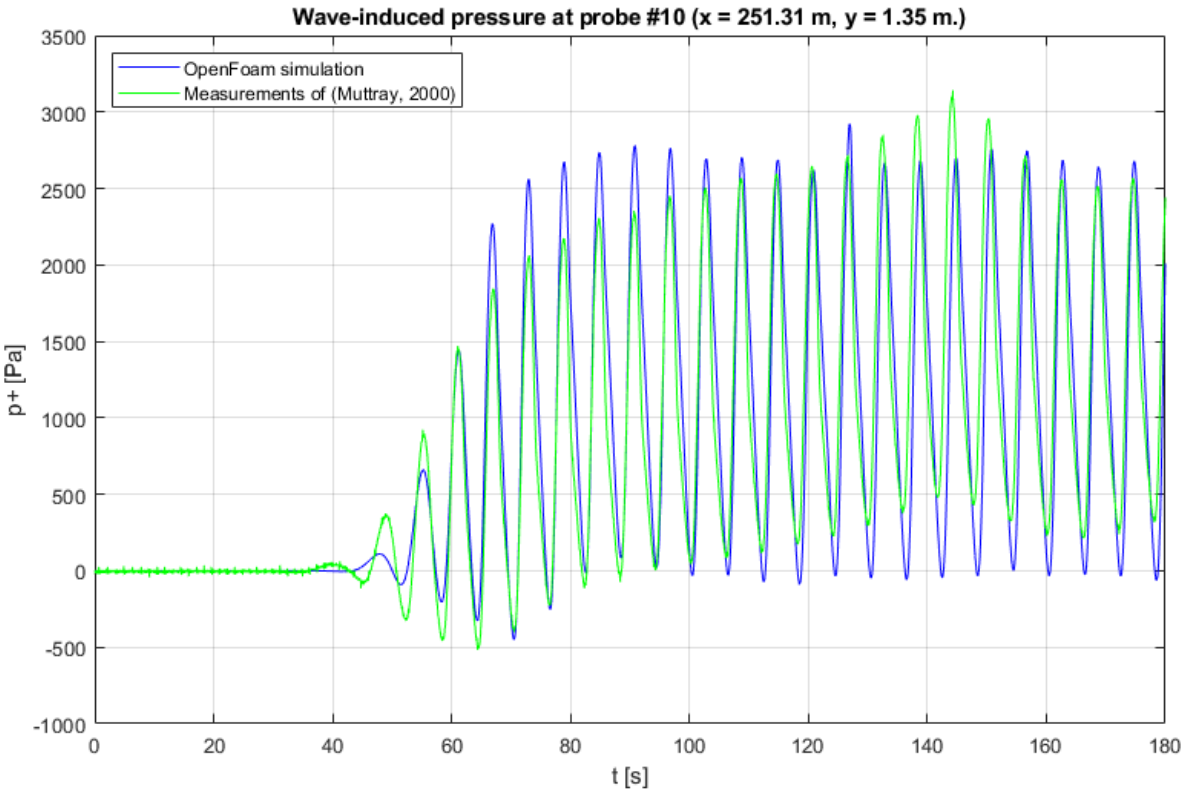

Figure 99 - Measured and simulated pressure in pressure probe #10 ($x = 251.31\ m$, $y = 1.35\ m$)

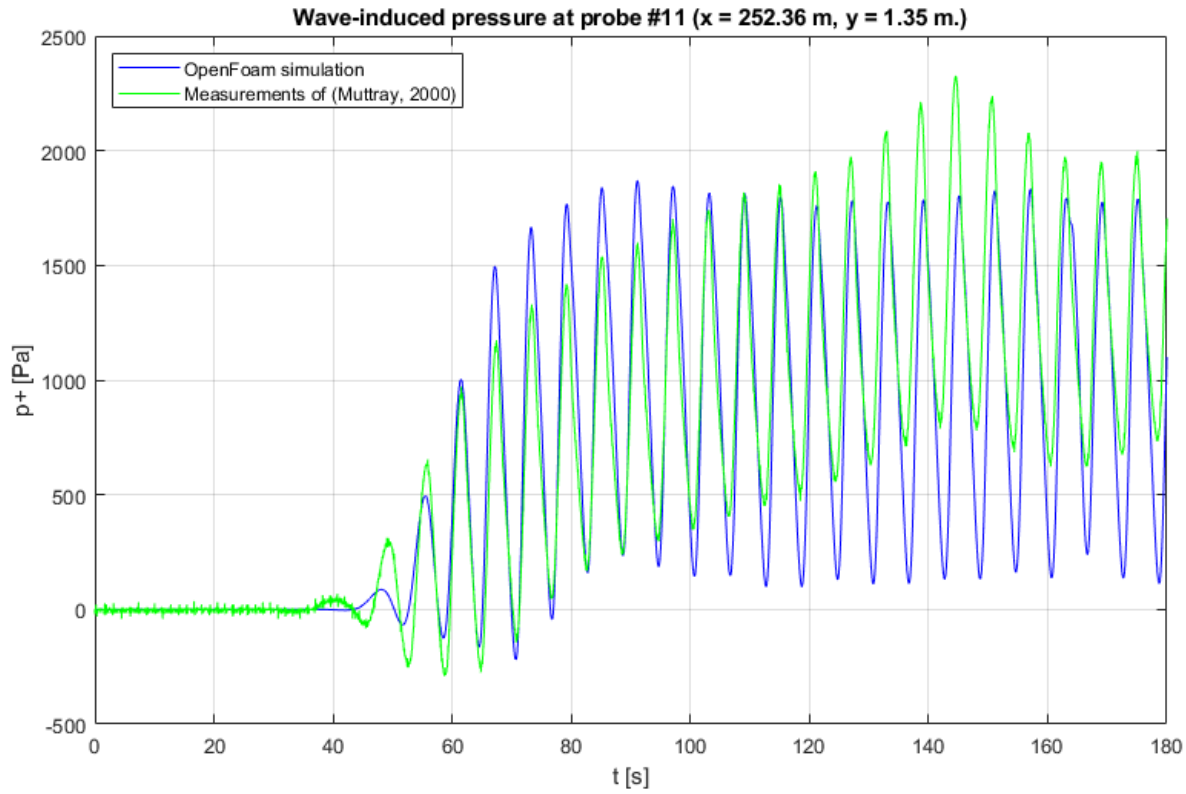

Figure 100 - Measured and simulated pressure in pressure probe #11 ($x = 252.36\ m$, $y = 1.35\ m$)

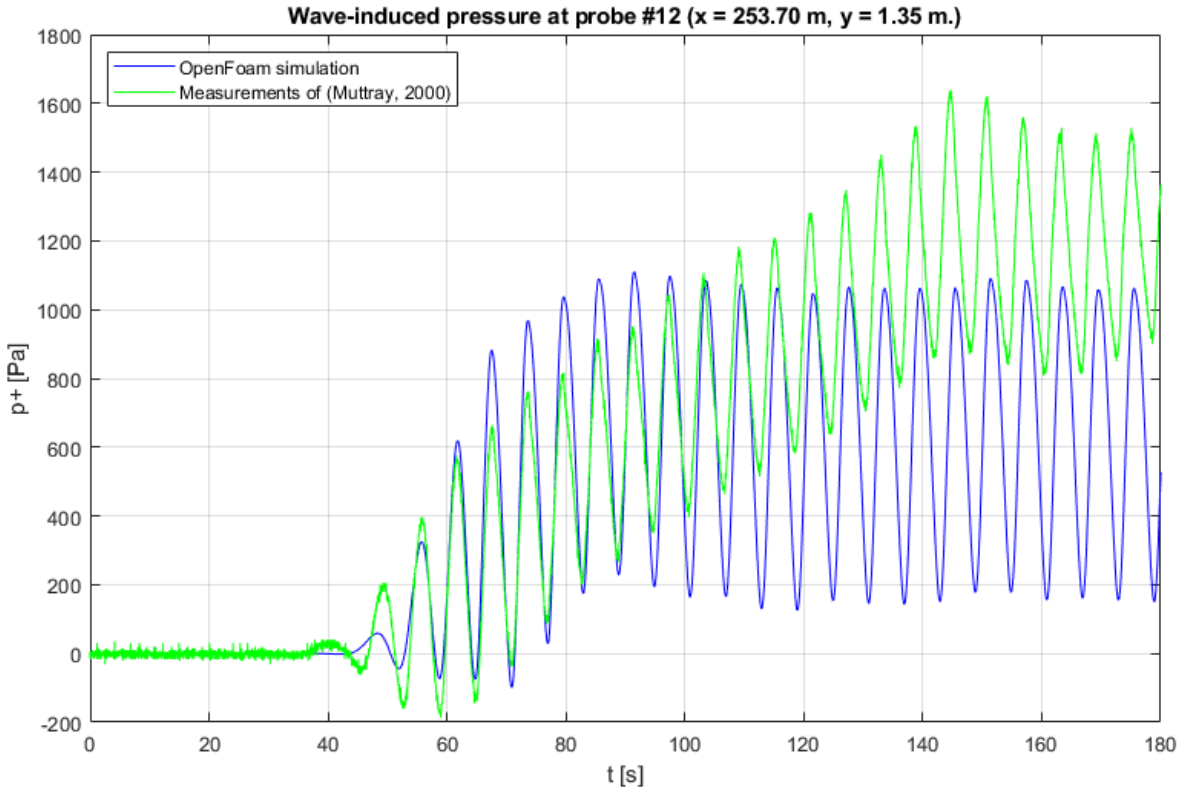

Figure 101 - Measured and simulated pressure in pressure probe #12 ($x = 253.70\ m$, $y = 1.35\ m$)

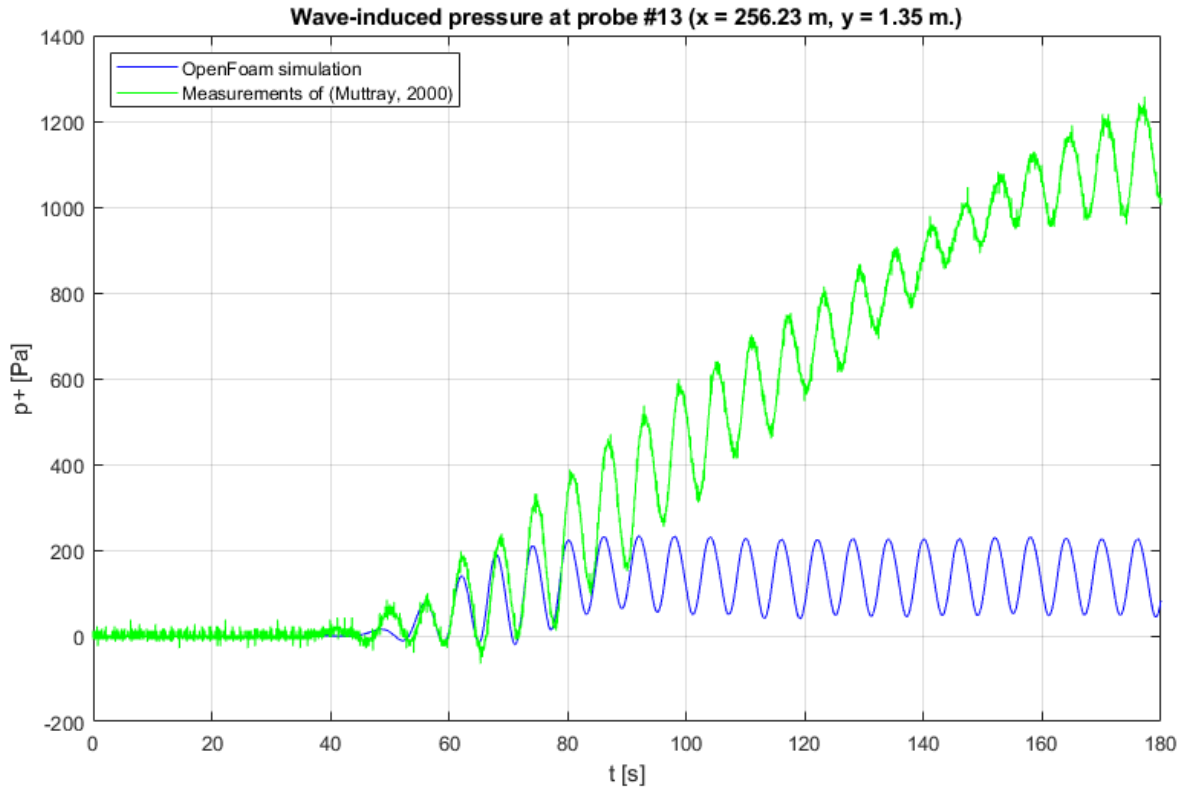

Figure 102 - Measured and simulated pressure in pressure probe #13 ($x = 256.23\ m$, $y = 1.35\ m$)

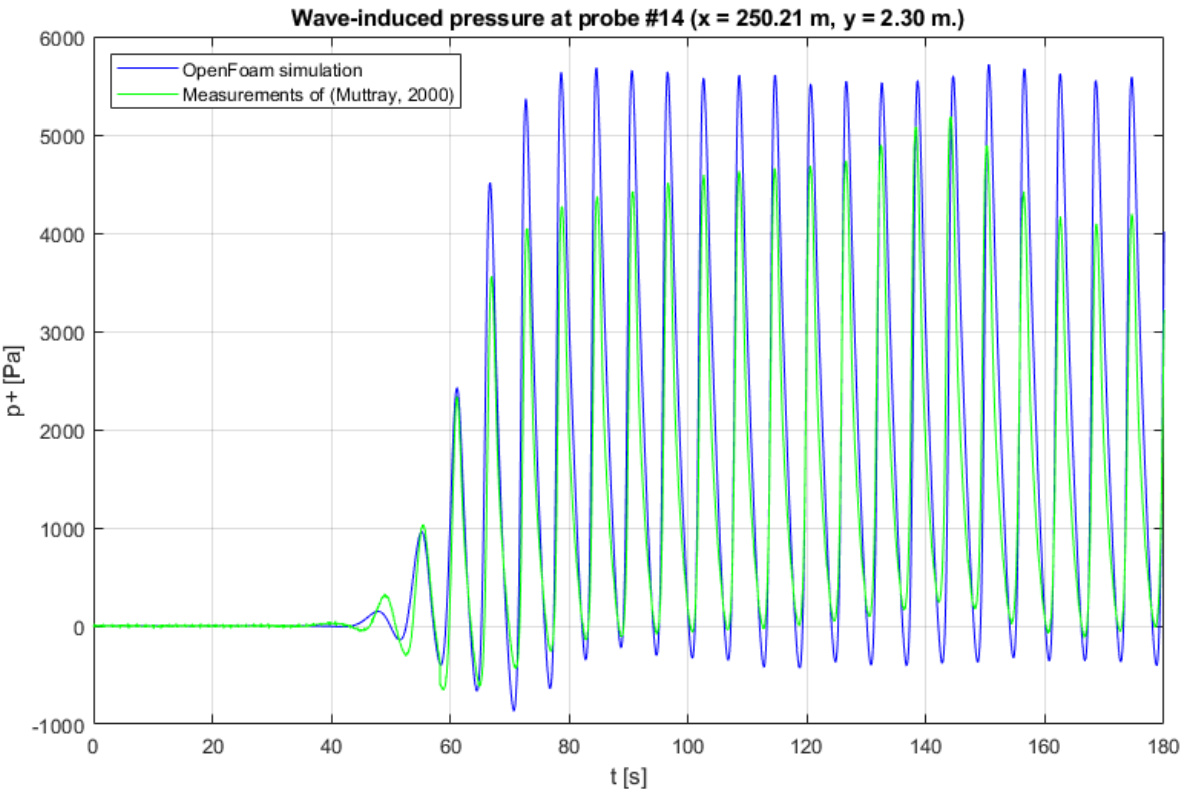

Figure 103 - Measured and simulated pressure in pressure probe #14 ($x = 250.21\ m$, $y = 2.30\ m$)

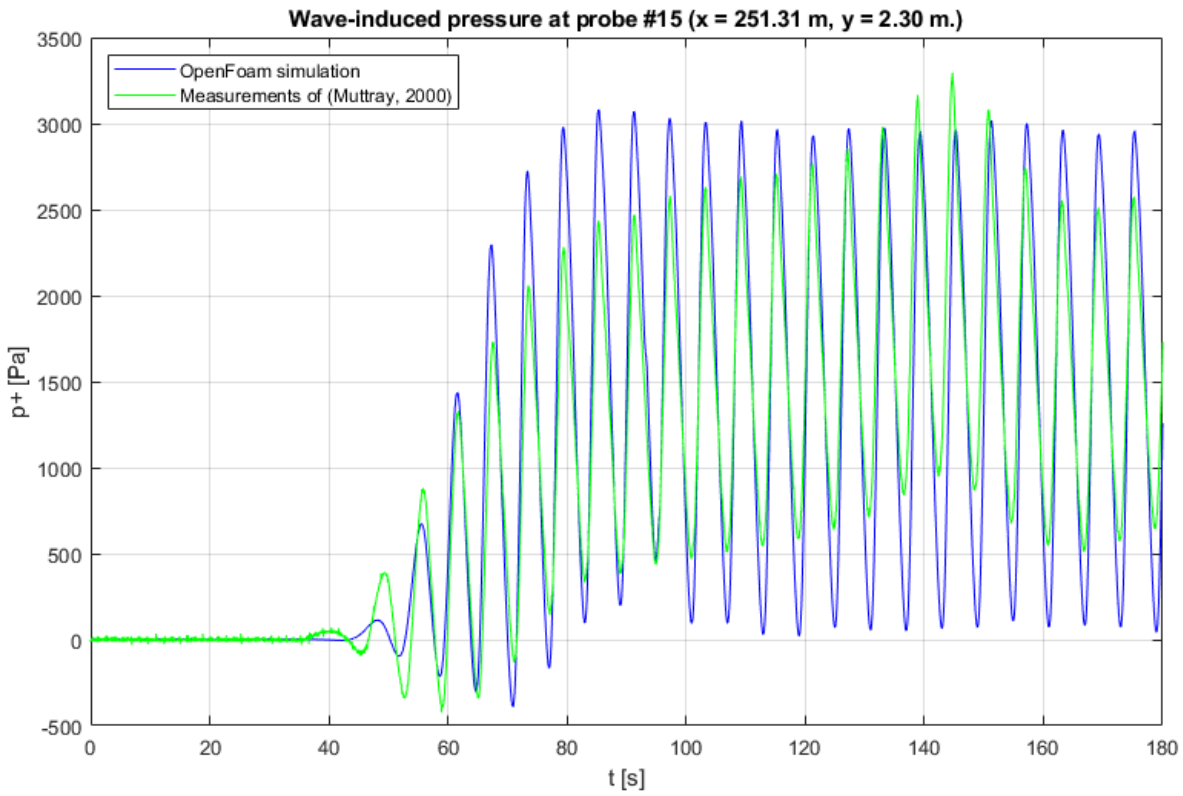

Figure 104 - Measured and simulated pressure in pressure probe #15 ($x = 251.31\ m$, $y = 2.30\ m$)

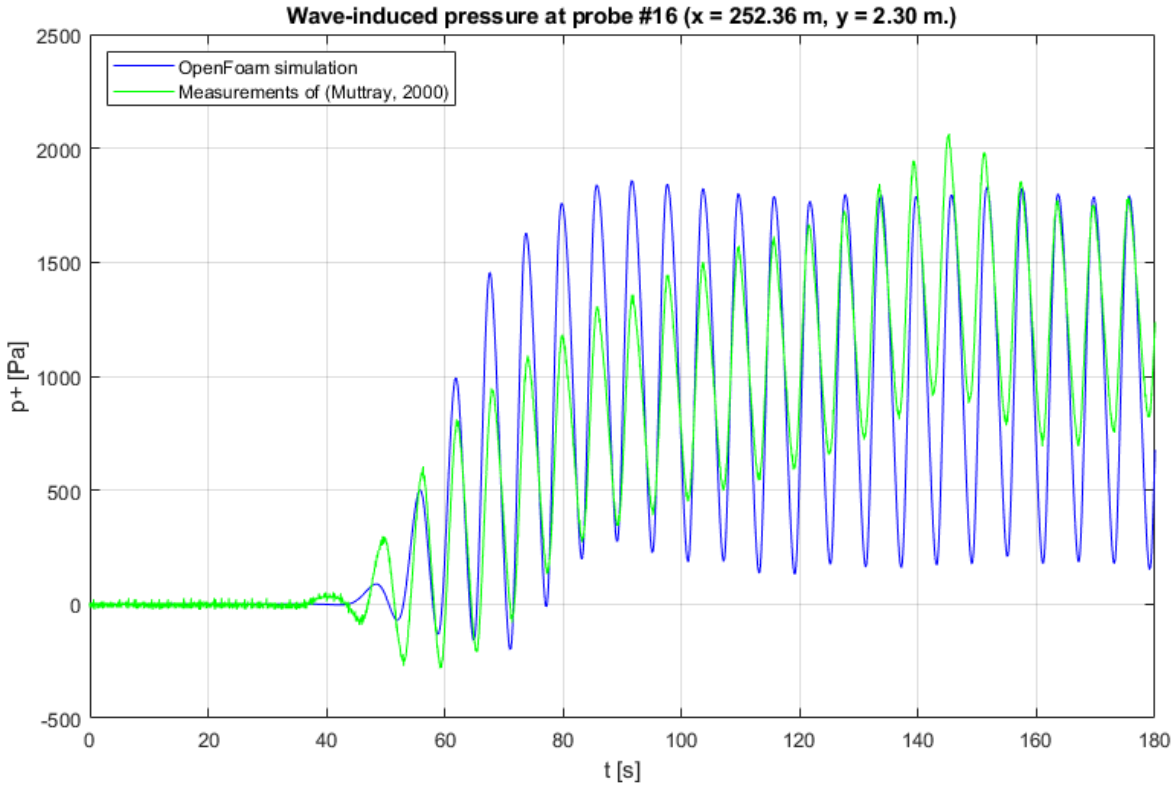

Figure 105 - Measured and simulated pressure in pressure probe #16 ($x = 252.36\ m$, $y = 2.30\ m$)

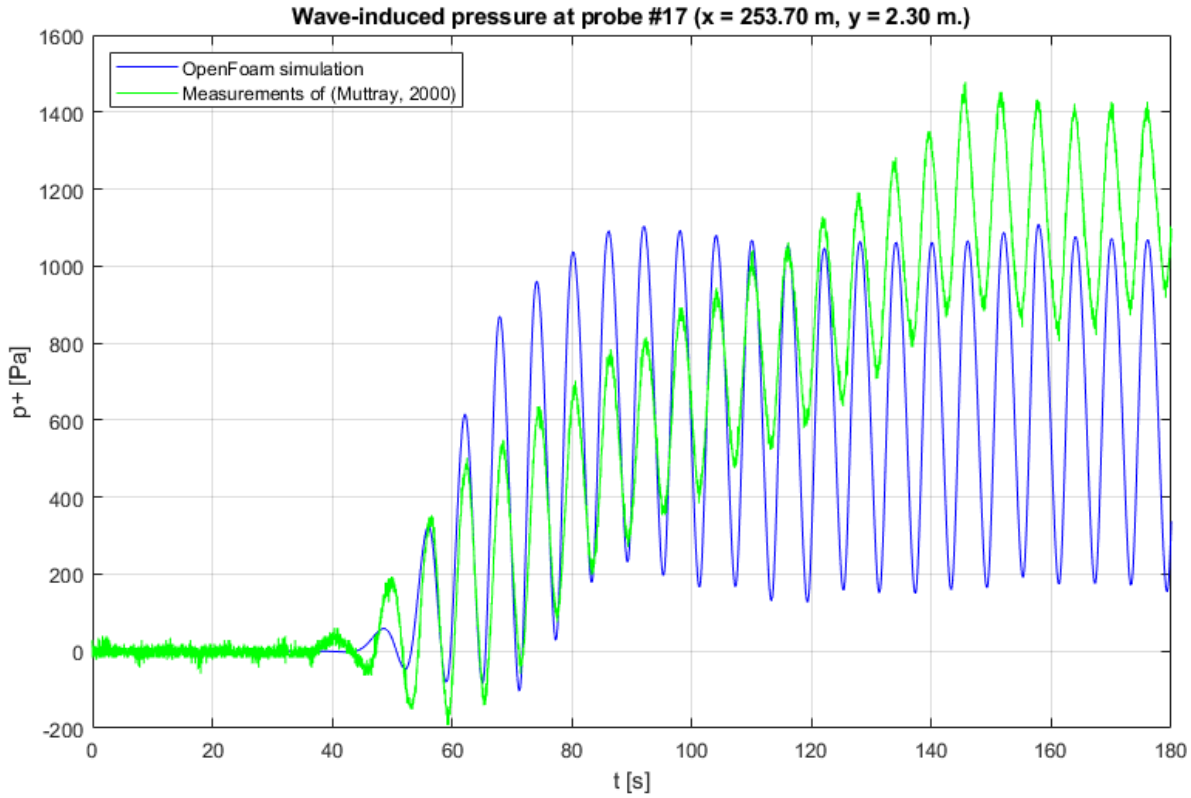

Figure 106 - Measured and simulated pressure in pressure probe #17 ($x = 253.70\ m$, $y = 2.30\ m$)

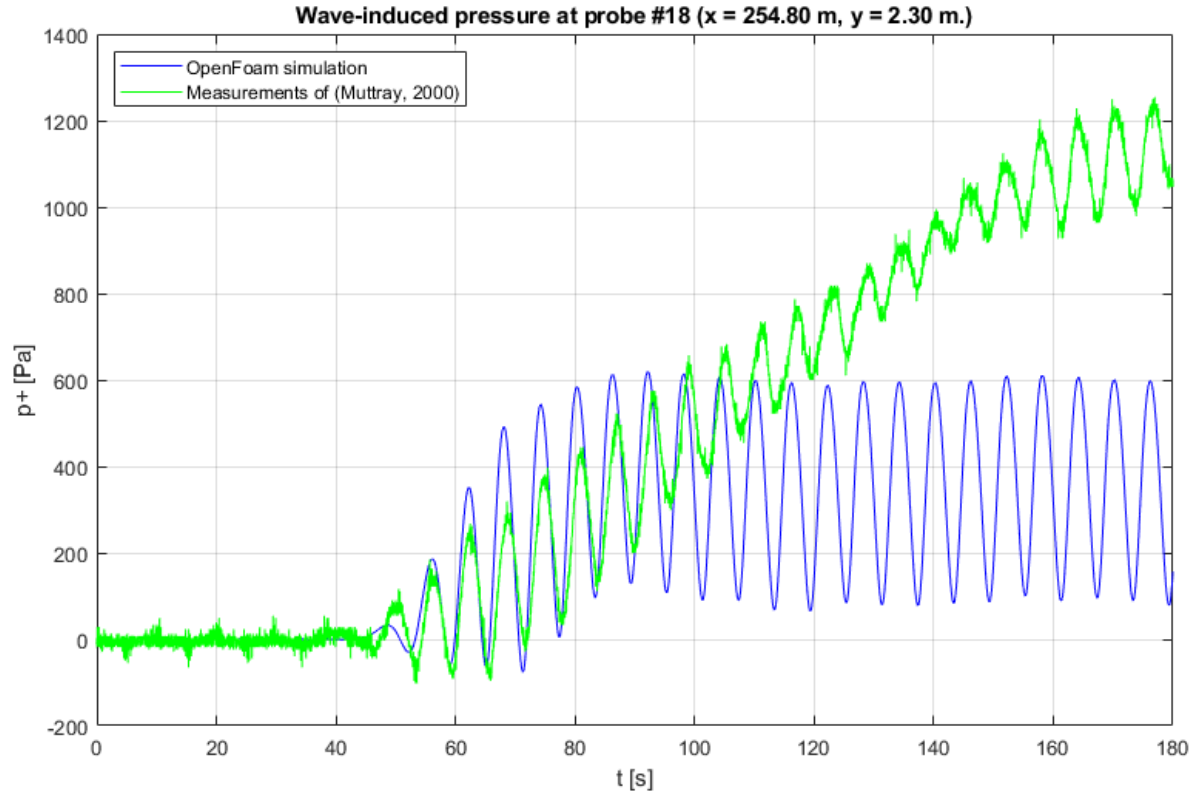

Figure 107 - Measured and simulated pressure in pressure probe #18 ($x = 254.80\ m$, $y = 2.30\ m$)

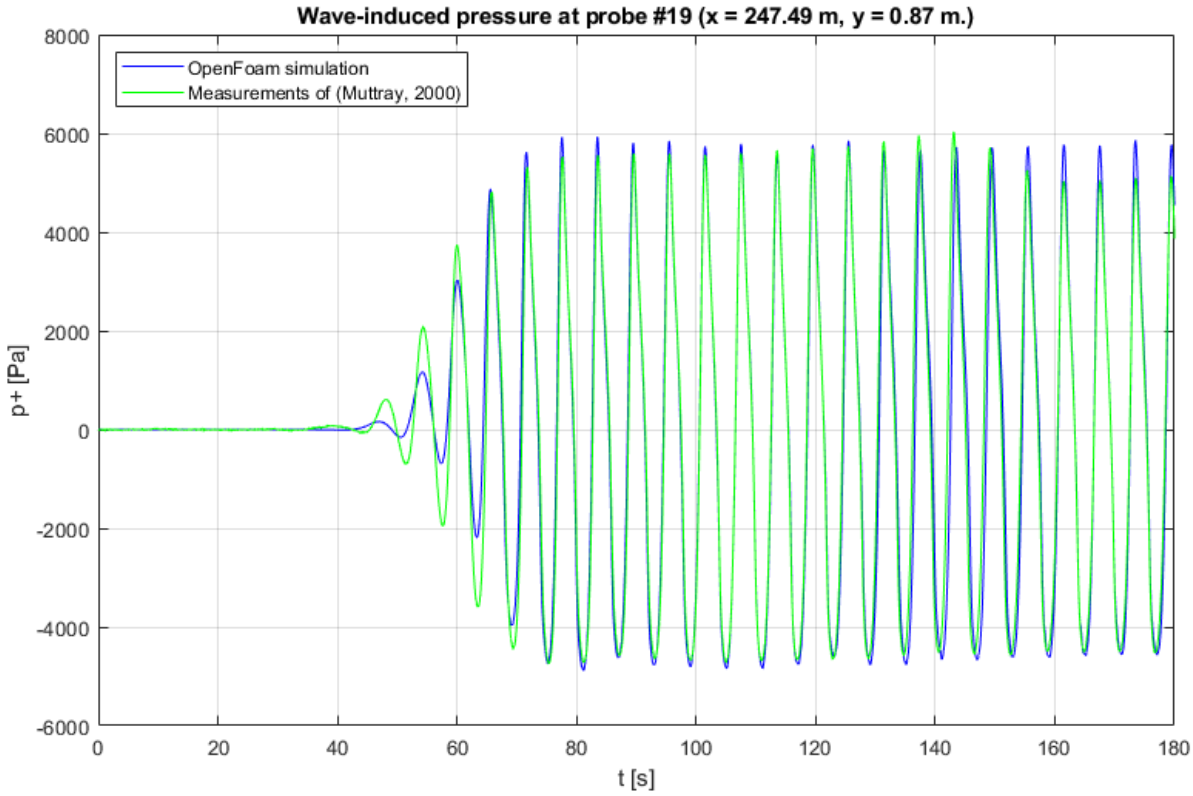

Figure 108 - Measured and simulated pressure in pressure probe #19 ($x = 247.49\ m$, $y = 0.87\ m$)

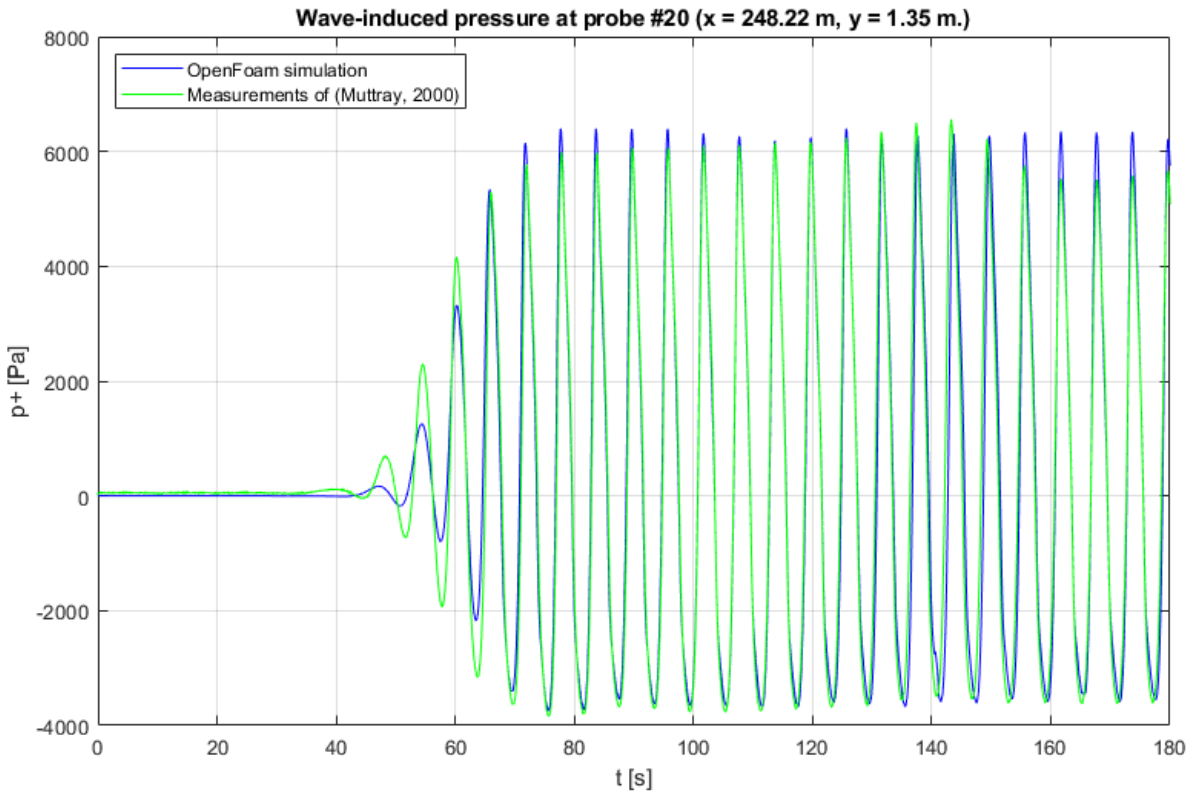

Figure 109 - Measured and simulated pressure in pressure probe #20 ($x = 248.22\ m$, $y = 1.35\ m$)

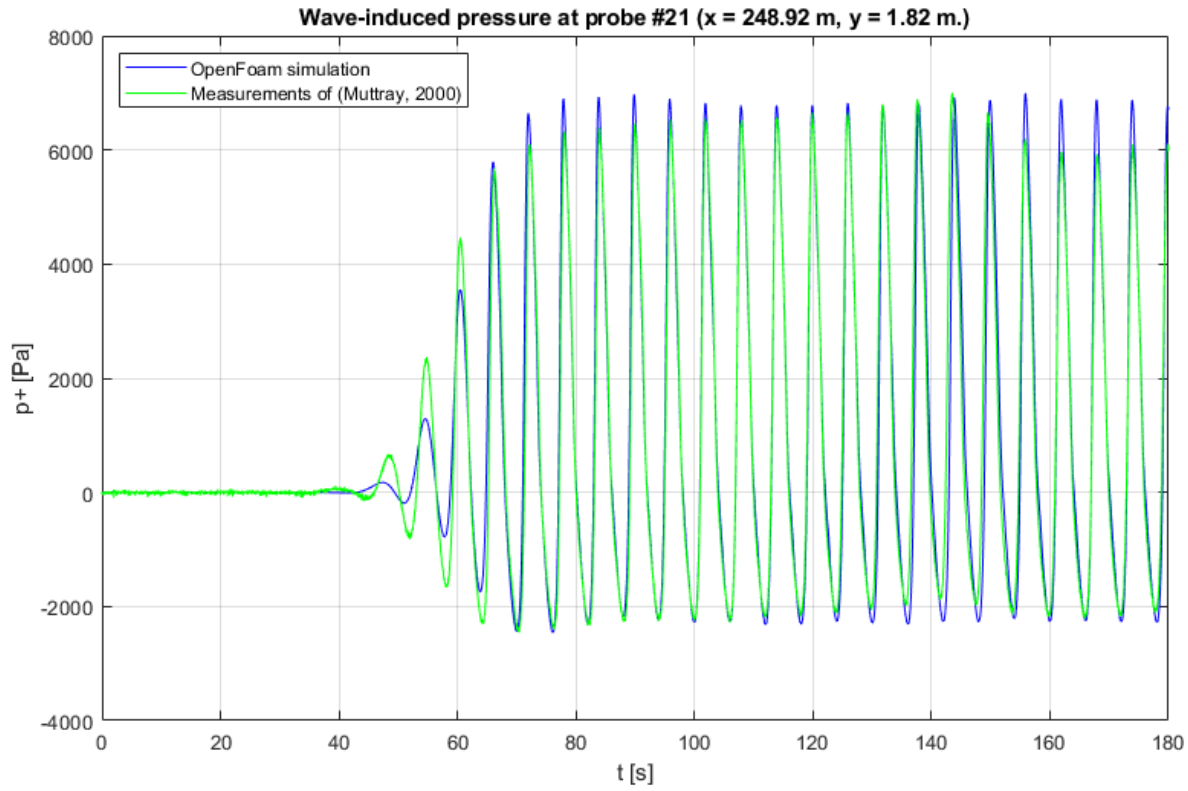

Figure 110 - Measured and simulated pressure in pressure probe #21 ($x = 248.92\ m$, $y = 1.82\ m$)

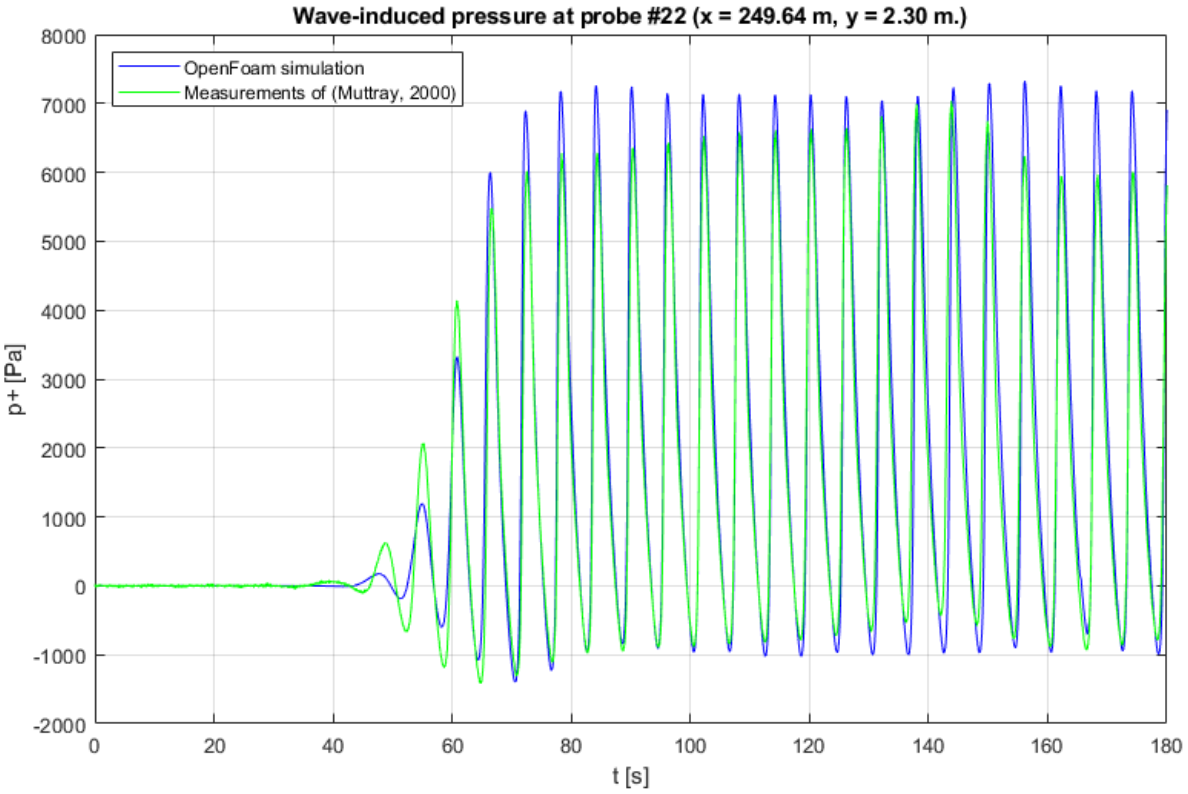

Figure 111 - Measured and simulated pressure in pressure probe #22 ($x = 249.64\ m$, $y = 2.30\ m$)

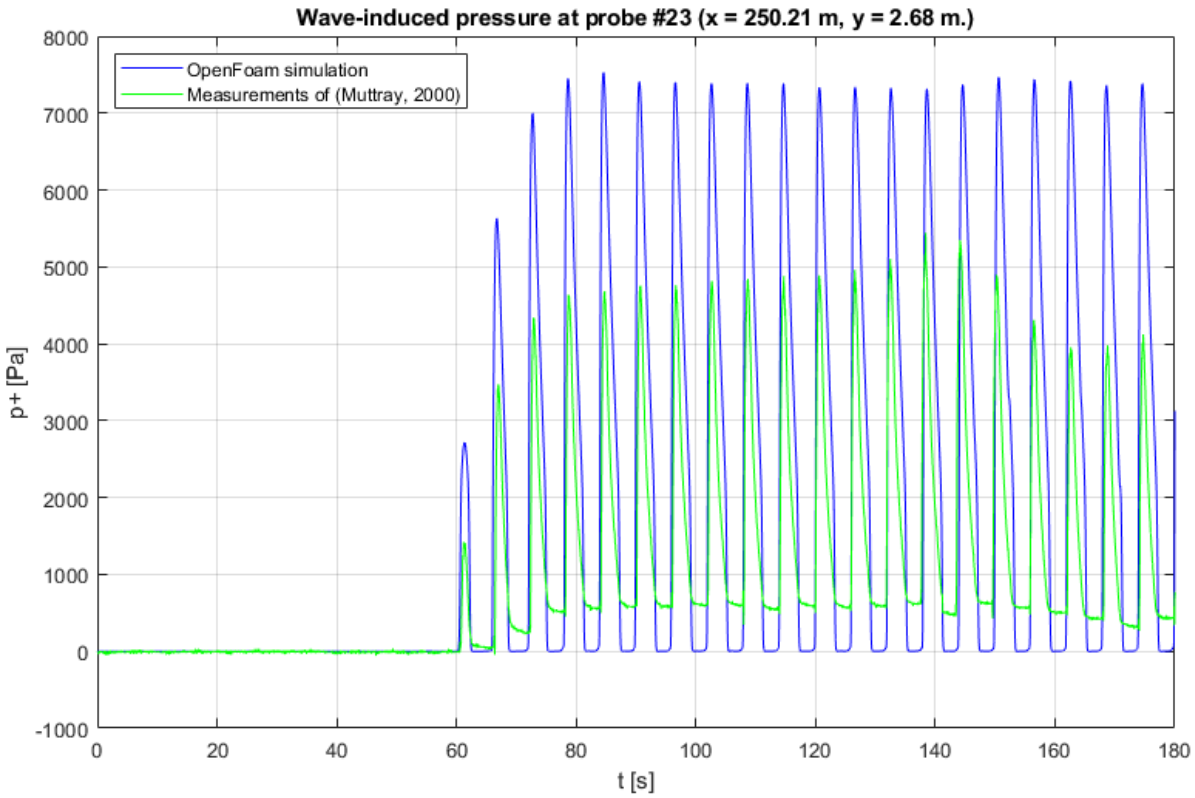

Figure 112 - Measured and simulated pressure in pressure probe #23 ($x = 250.21\ m$, $y = 2.68\ m$)

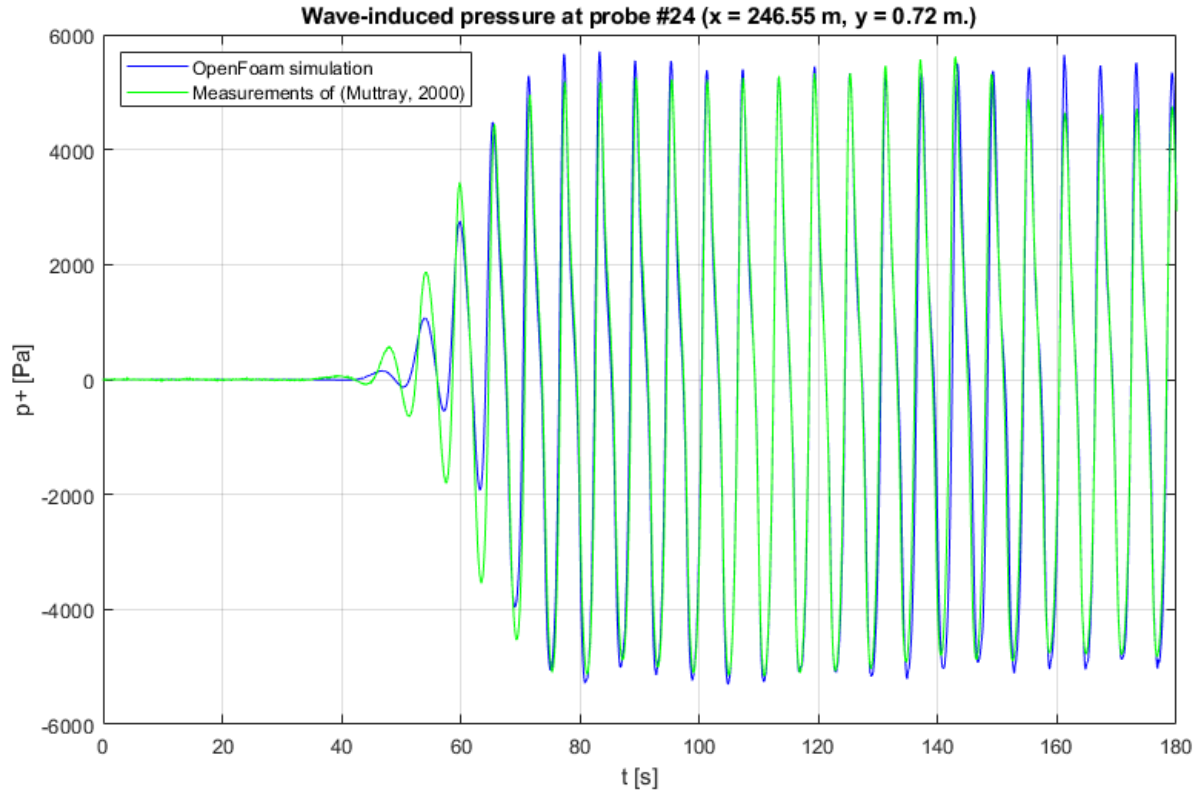

Figure 113 - Measured and simulated pressure in pressure probe #24 ($x = 246.55\ m$, $y = 0.72\ m$)

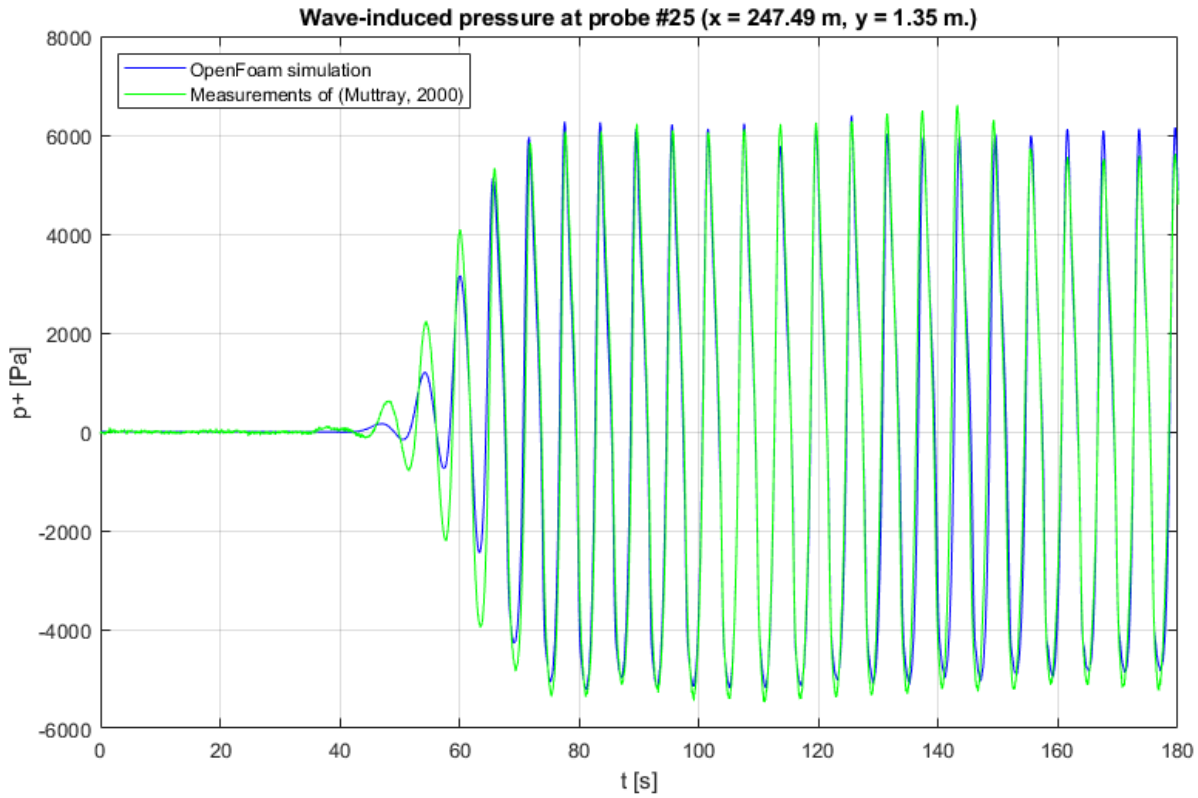

Figure 114 - Measured and simulated pressure in pressure probe #25 ($x = 247.49\ m$, $y = 1.35\ m$)

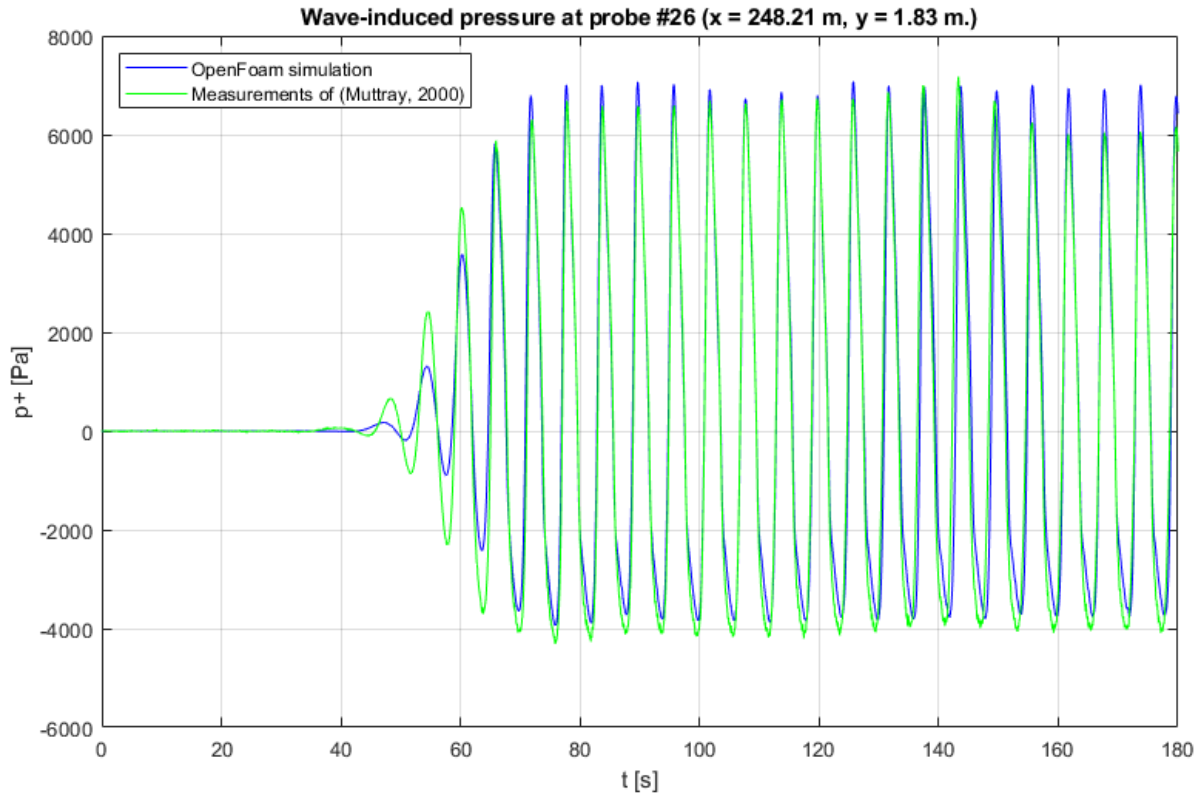

Figure 115 - Measured and simulated pressure in pressure probe #26 ($x = 248.21\ m$, $y = 1.83\ m$)

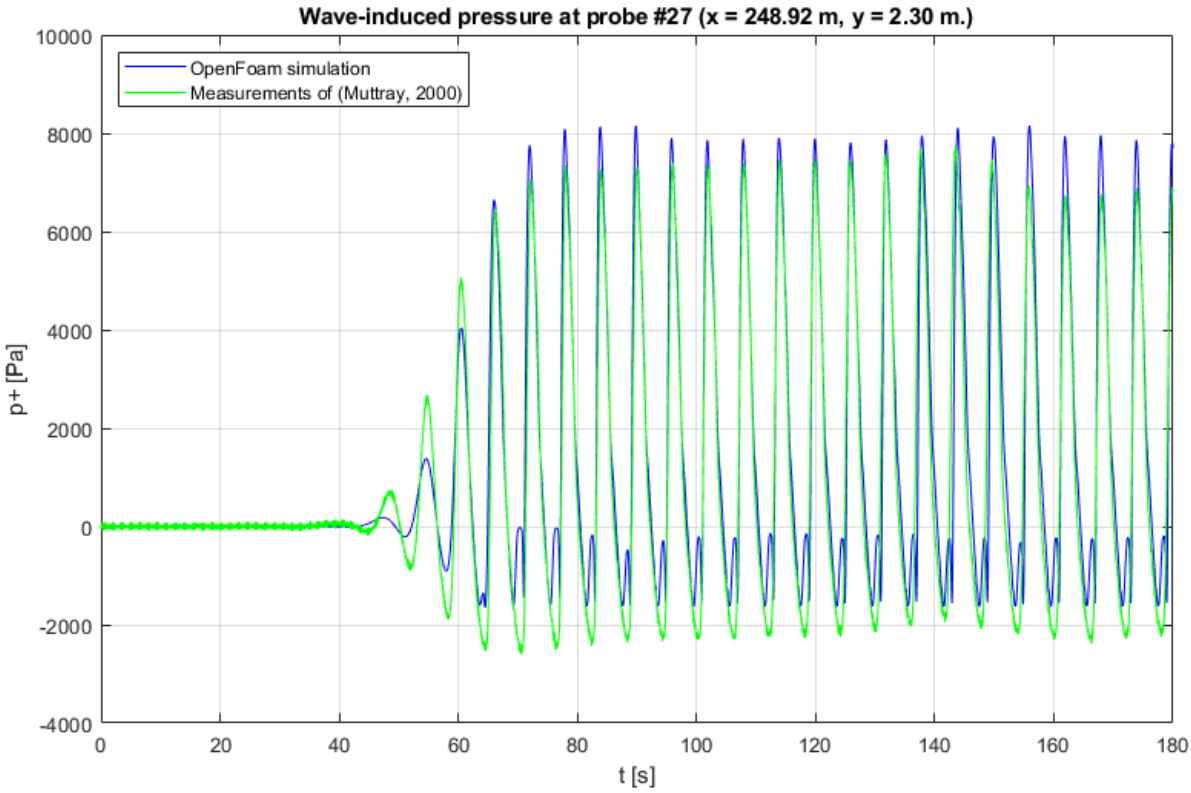

Figure 116 - Measured and simulated pressure in pressure probe #27 ($x = 248.92\ m$, $y = 2.30\ m$)

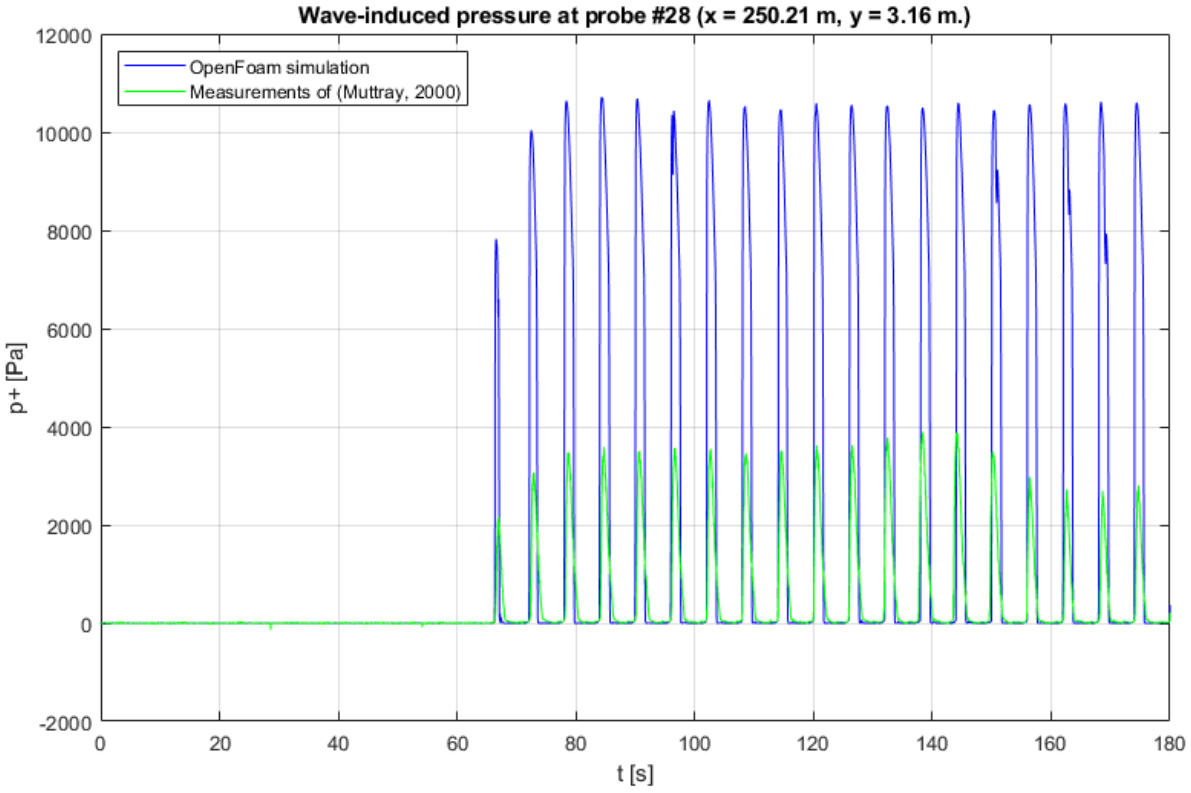

Figure 117 - Measured and simulated pressure in pressure probe #28 ($x = 250.21\ m$, $y = 3.16\ m$)

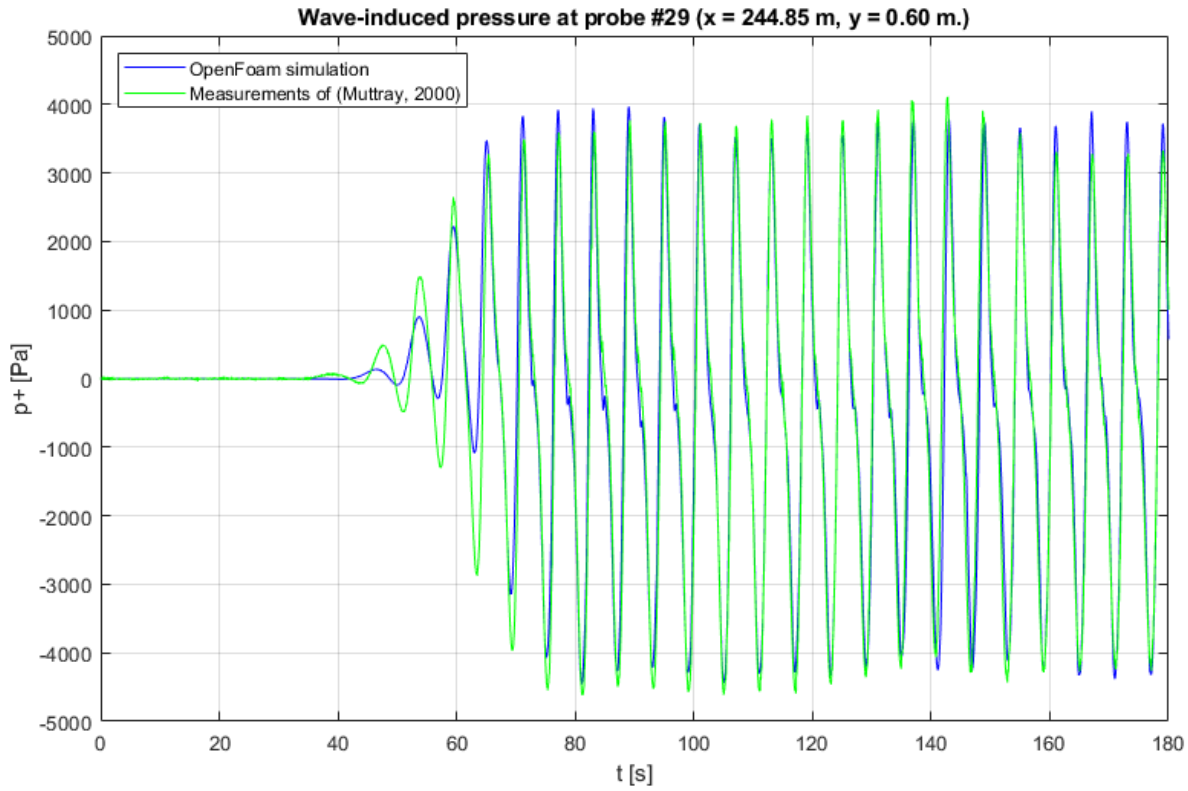

Figure 118 - Measured and simulated pressure in pressure probe #29 ($x = 244.85\ m$, $y = 0.60\ m$)

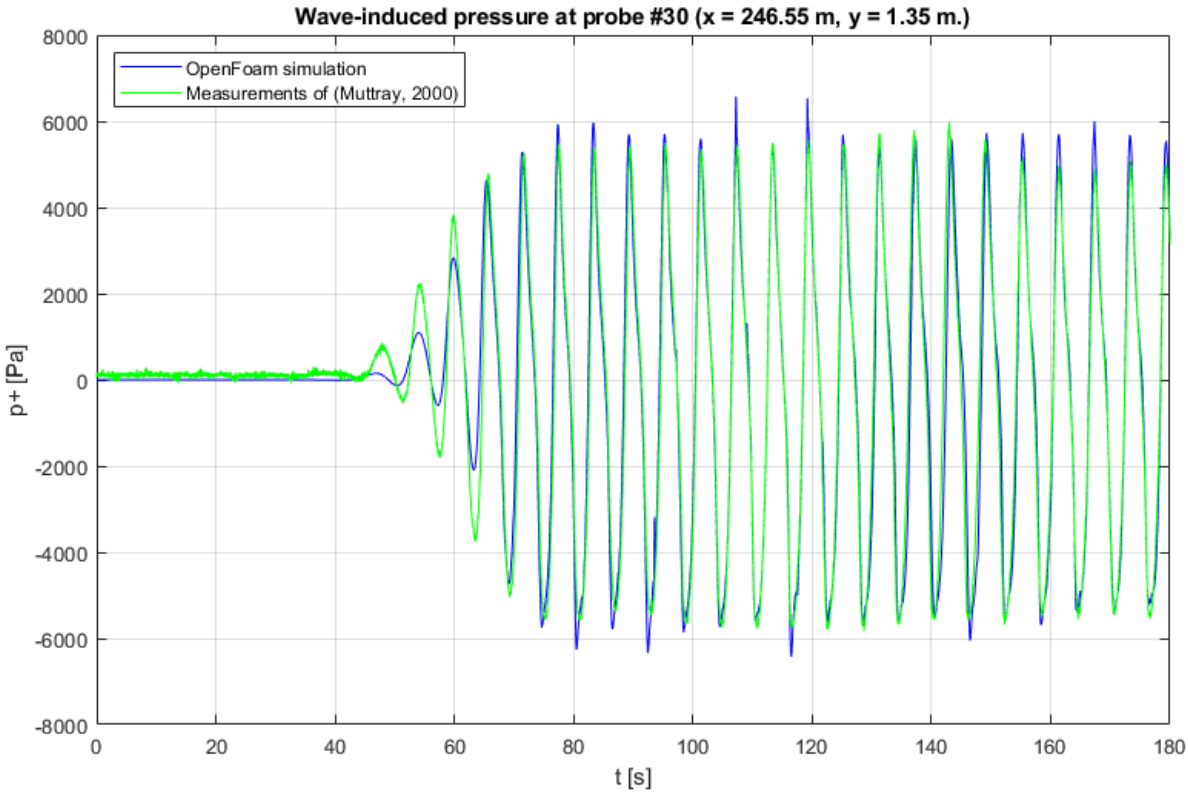

Figure 119 - Measured and simulated pressure in pressure probe #30 ($x = 246.55\ m$, $y = 1.35\ m$)

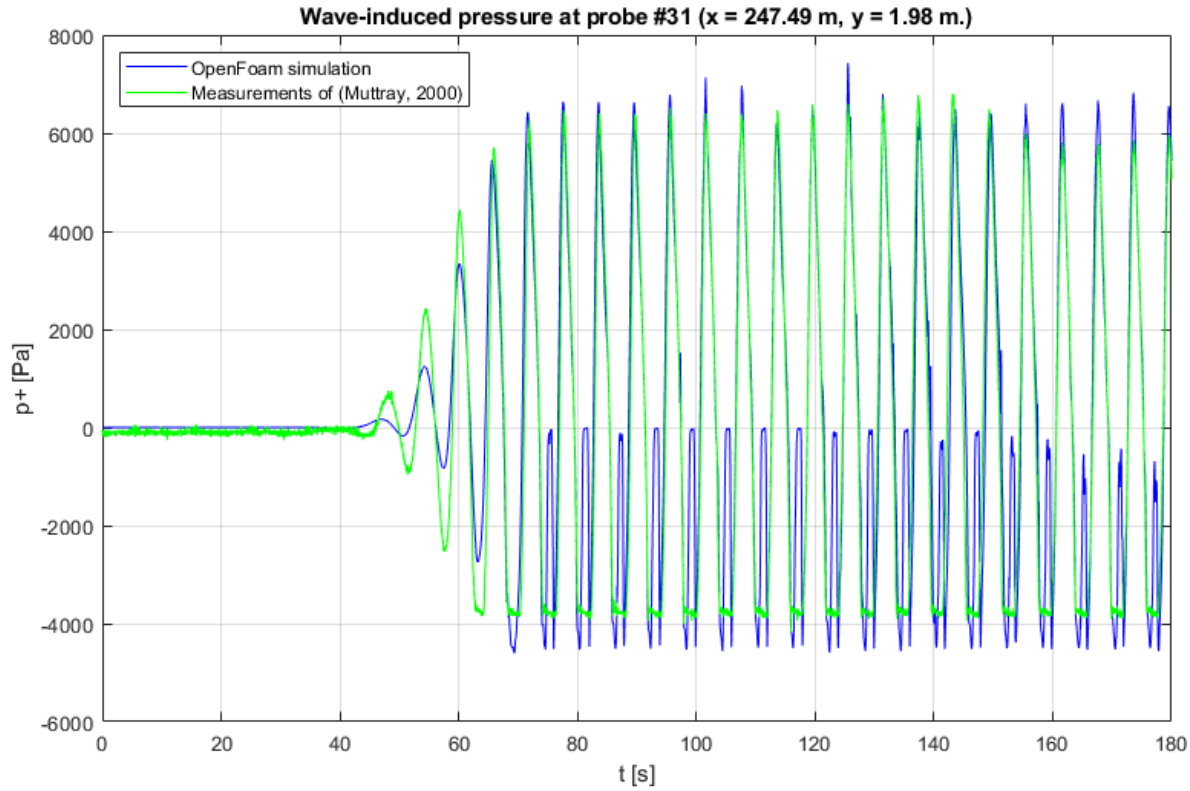

Figure 120 - Measured and simulated pressure in pressure probe #31 ($x = 247.49\ m$, $y = 1.98\ m$)

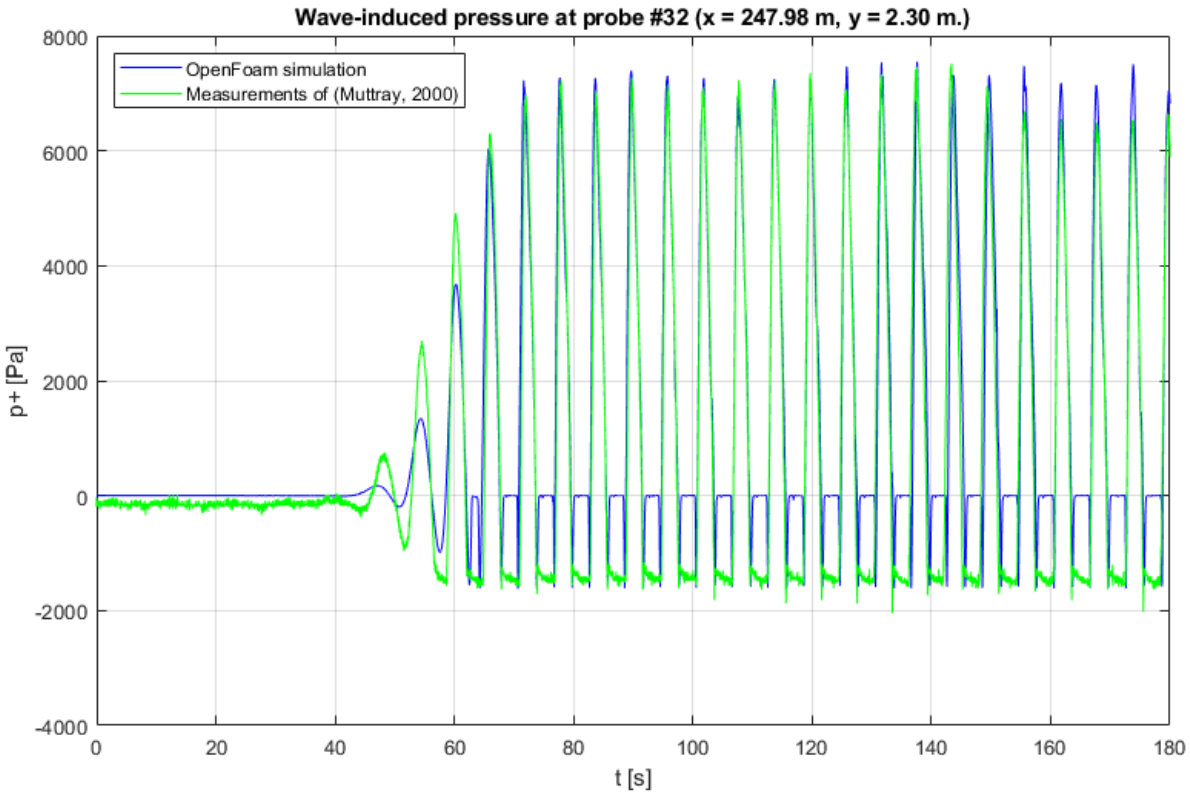

Figure 121 - Measured and simulated pressure in pressure probe #32 ($x = 247.98\ m$, $y = 2.30\ m$)

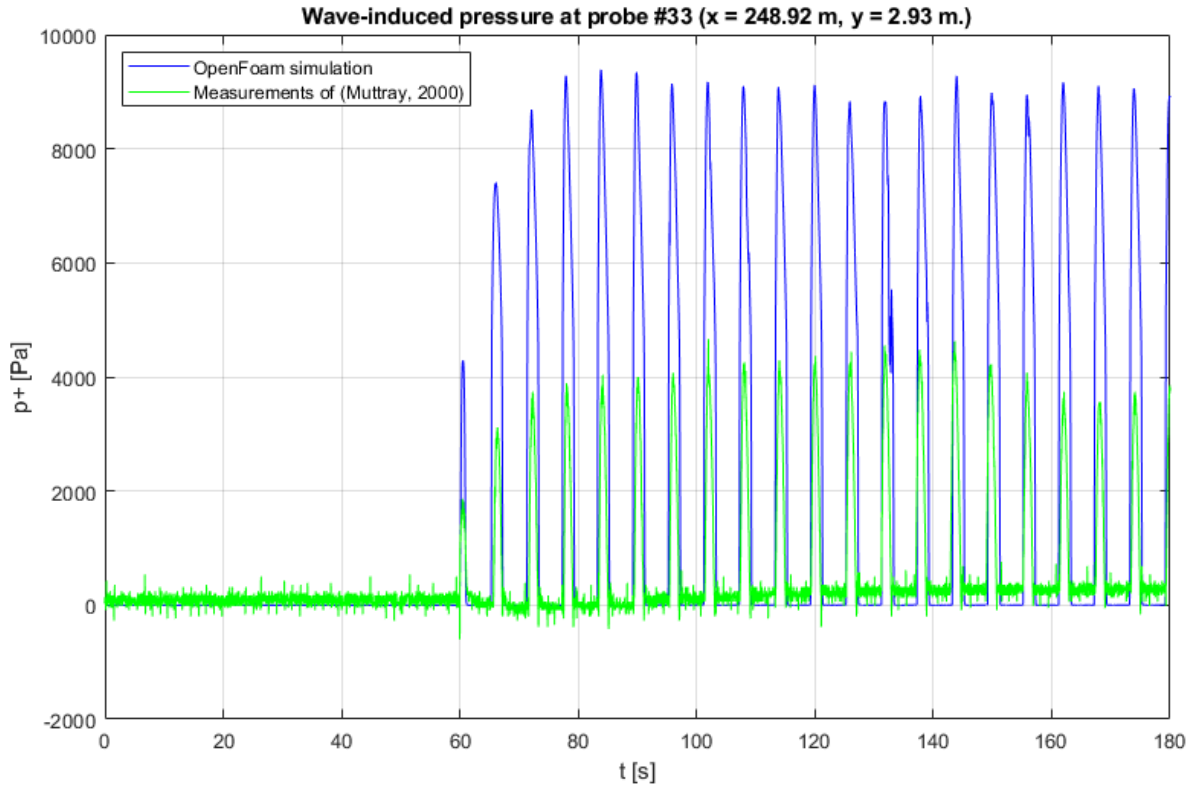

Figure 122 - Measured and simulated pressure in pressure probe #33 ($x = 248.92\ m$, $y = 2.93\ m$)

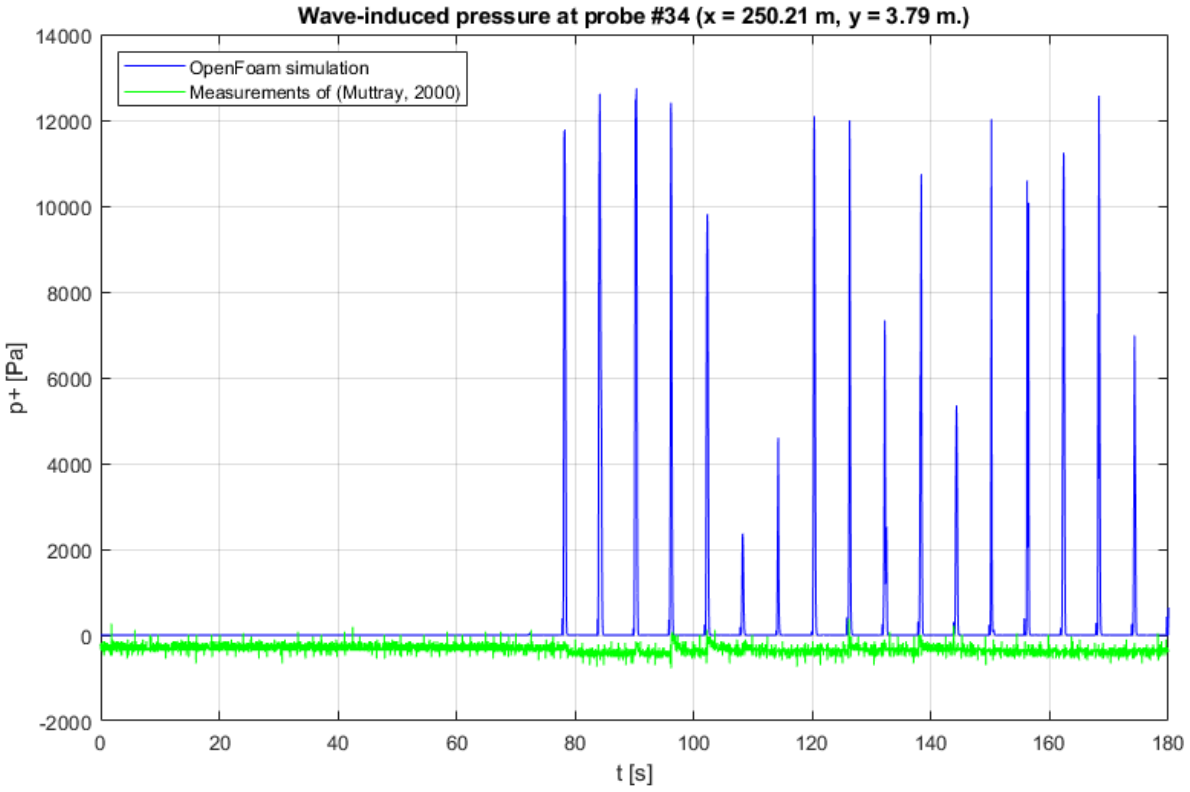

Figure 123 - Measured and simulated pressure in pressure probe #34 ($x = 250.21\ m$, $y = 3.79\ m$)

A.3.6 Pressure lines comparison

In his PhD thesis, (Muttray, 2000) included the pressure lines of test nr. 020694-01 on certain moments in time: $t(R_{u,max})$, $t(R_{u,max}) + 0.13T$, $t(R_{u,max}) + 0.31T$, $t(R_{u,max}) + 0.44T$, $t(R_{u,max}) + 0.75T$ and $t(R_{u,max}) + 0.94T$. These pressure lines were calculated by interpolating the pressures over the six lines described in the previous section and then interpolating the pressures in vertical direction to create the pressure field.

With OpenFoam the same kind of plots can be made. OpenFoam calculates the complete pressure field for every timestep and saves this output for every output moment in time. In theory this gives a more accurate pressure field since the results of the pressure sensors do not have to be interpolated. In the OpenFoam simulation, output was saved every 0.5 seconds of simulation time (for the last 15 seconds of simulation). Unfortunately, these times are not equal to the exact moments in time on which (Muttray, 2000) created the pressure lines plots. Therefore the results of the moments closes in time are compared with the pressure lines included in the PhD thesis of (Muttray, 2000).

The pressure lines of (Muttray, 2000) are compared with the pressure lines simulated with OpenFoam in Figure 124 till Figure 135. Even though the results are not on the exact same time but slightly off, the results look very good. It is clear that the pressure lines from the OpenFoam simulation follow the same pattern as the lines measured by (Muttray, 2000).

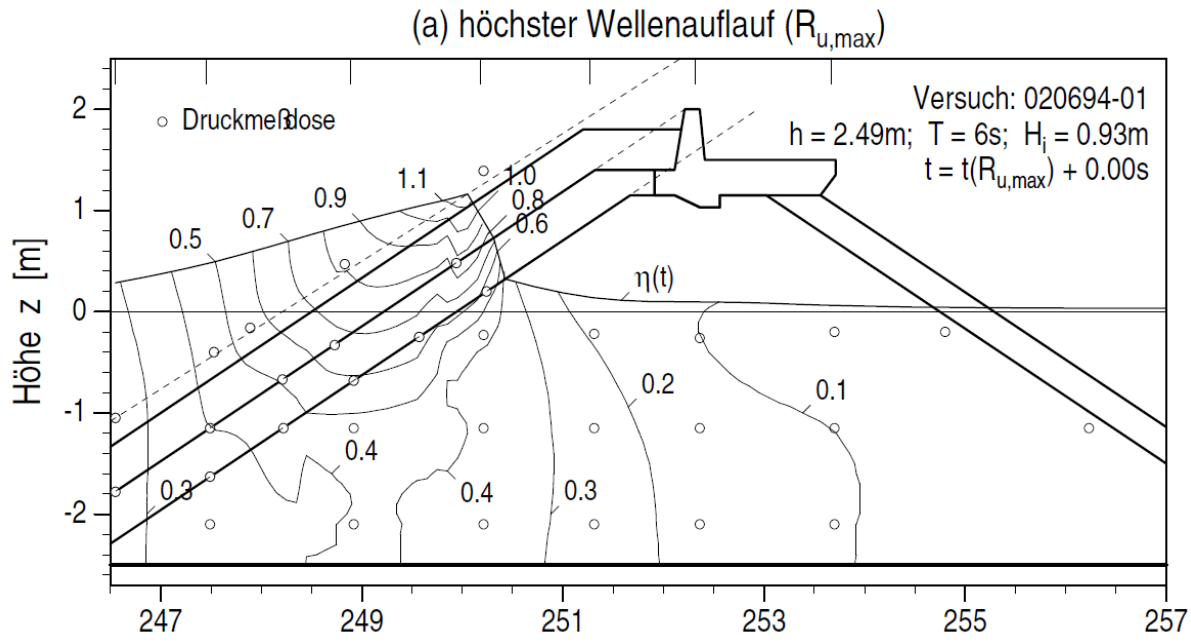

Figure 124 - Pressure lines $\left(\frac{p}{\rho g}\right)$ by (Muttray, 2000) at $t = t(R_{u,max})$

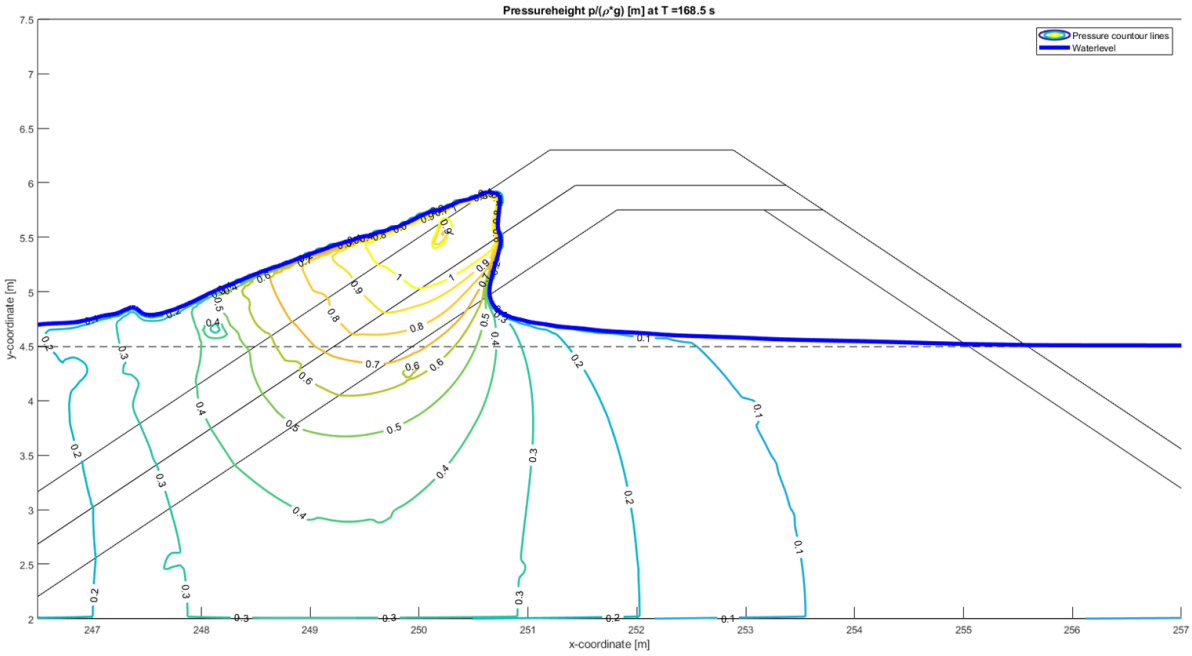

Figure 125 – Simulated pressure lines $\left(\frac{p}{\rho g}\right)$ at $t = 168.5\ s\ (\approx t(R_{u,max}) + 0.03T)$

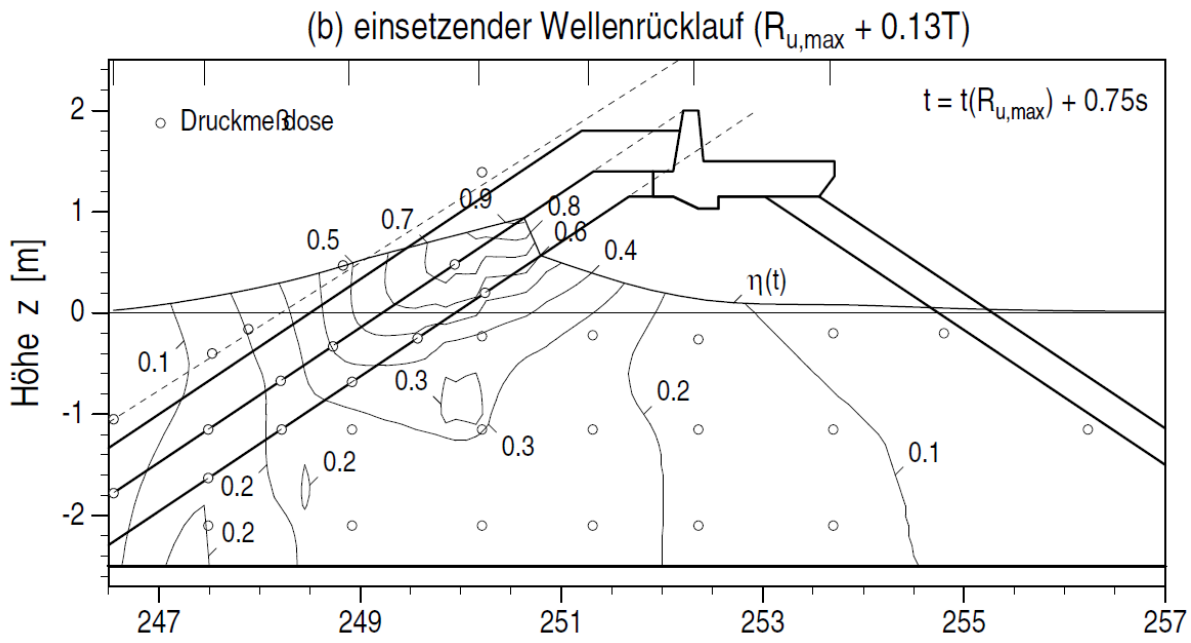

Figure 126 - Pressure lines $\left(\frac{p}{\rho g}\right)$ by (Muttray, 2000) at $t = t(R_{u,max}) + 0.13T$

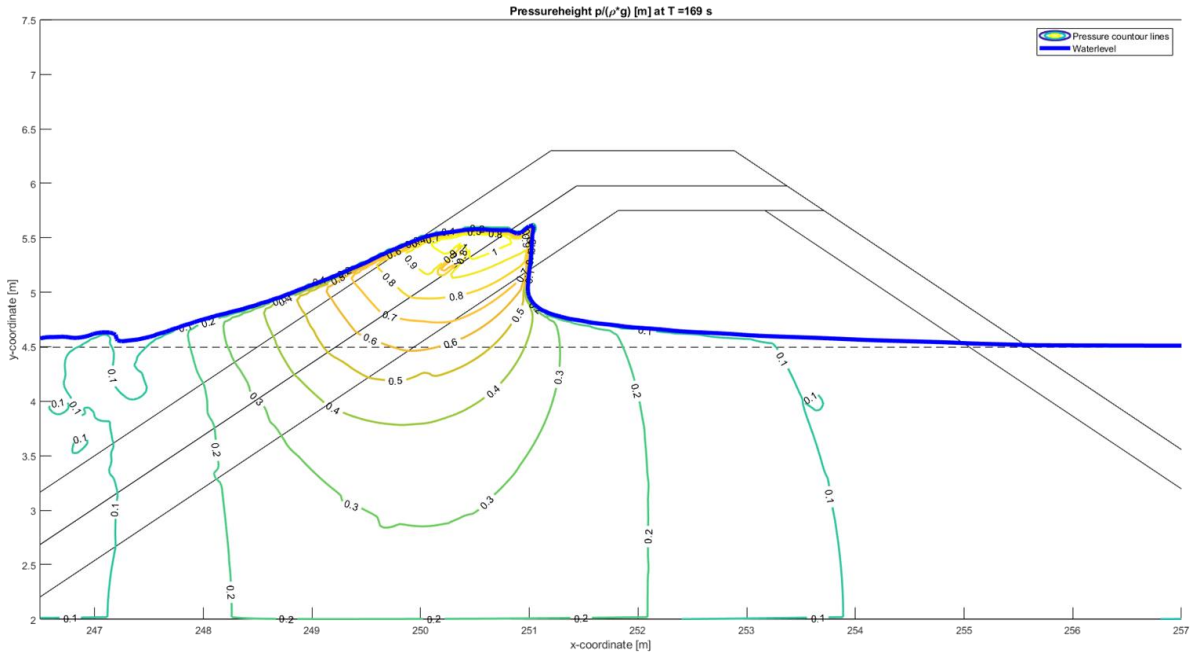

Figure 127 - Simulated pressure lines $\left(\frac{p}{\rho g}\right)$ at $t = 169\ s\ (\approx t(R_{u,max}) + 0.12T)$

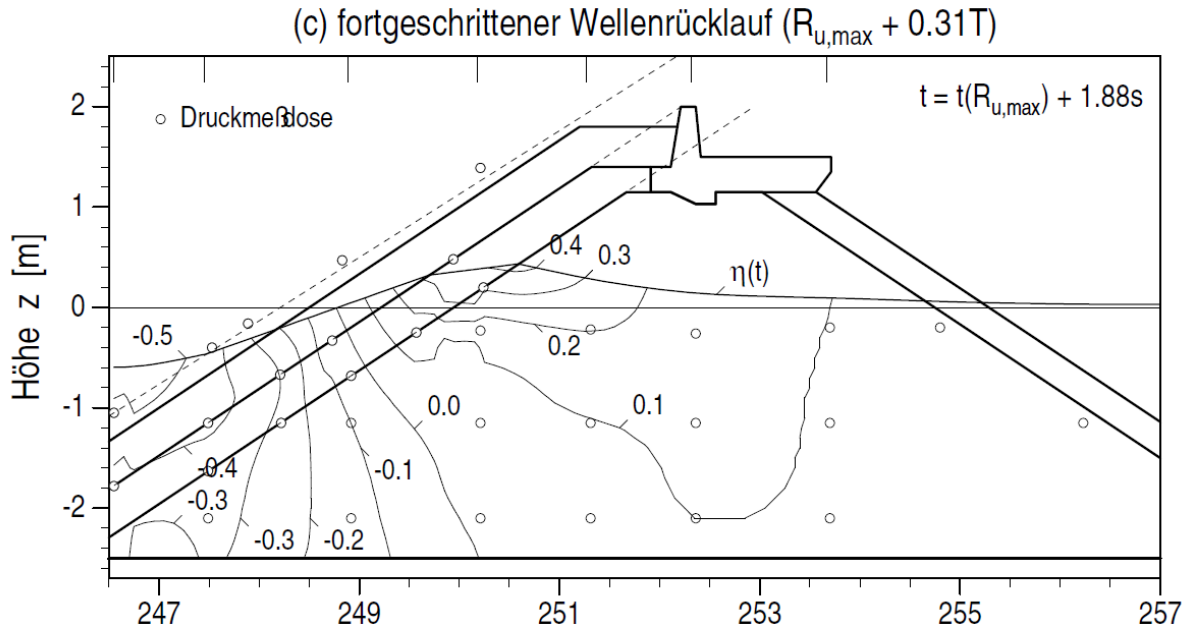

Figure 128 - Pressure lines $\left(\frac{p}{\rho g}\right)$ by (Muttray, 2000) at $t = t(R_{u,max}) + 0.31T$

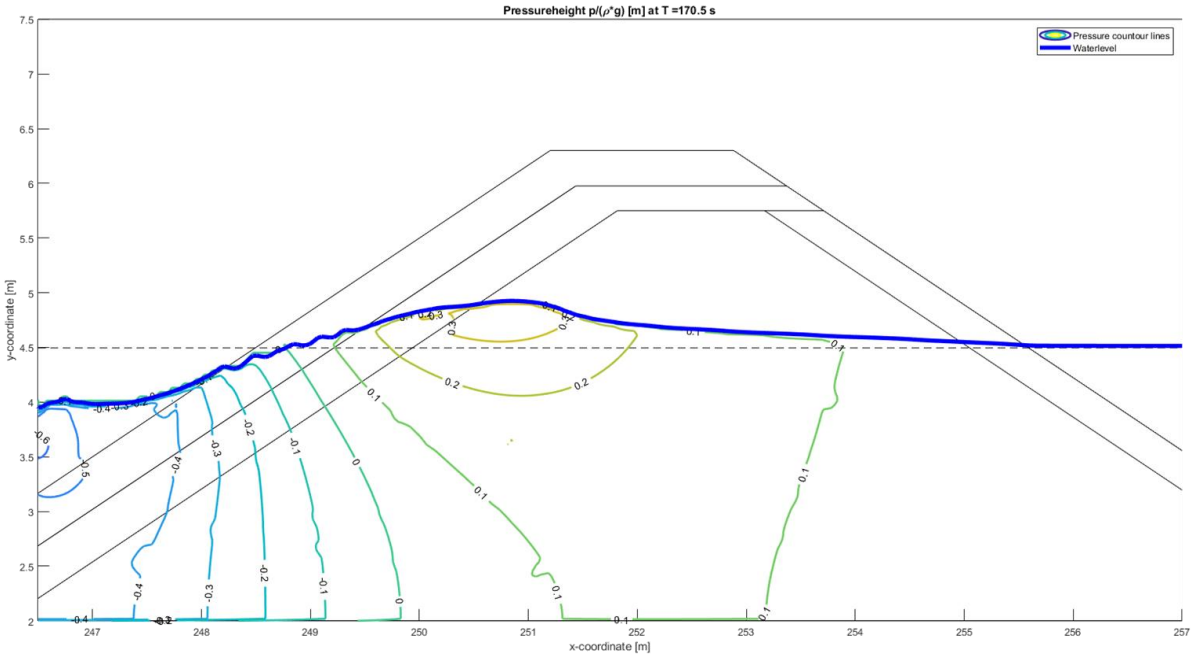

Figure 129 - Simulated pressure lines $\left(\frac{p}{\rho g}\right)$ at $t = 170.5\ s\ (\approx t(R_{u,max}) + 0.37T)$

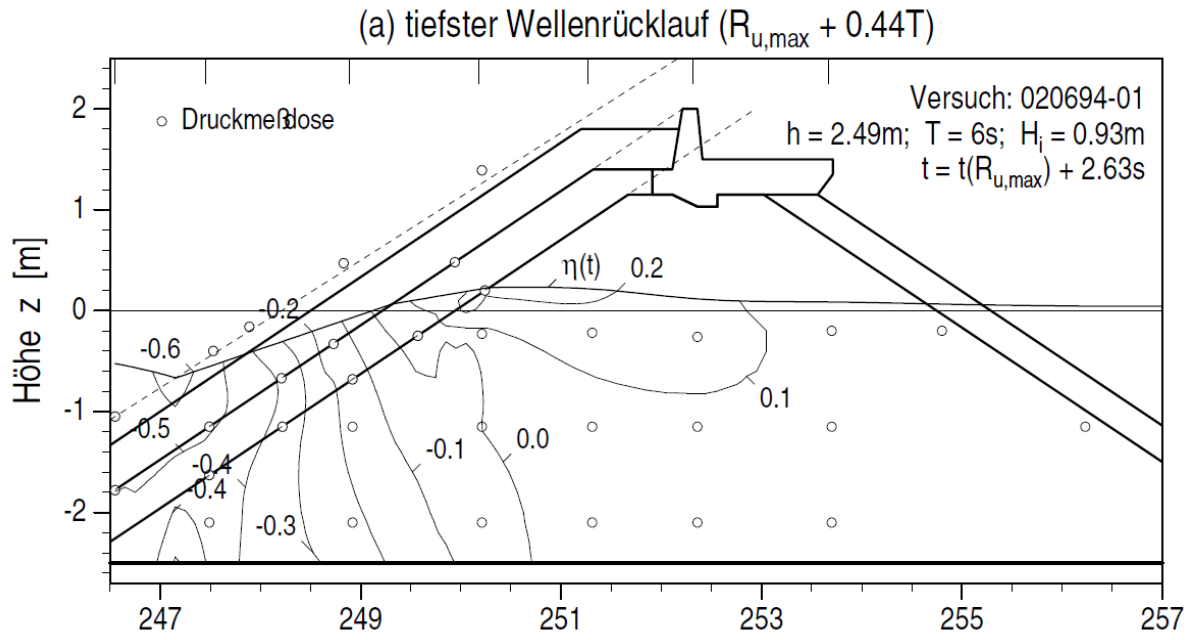

Figure 130 - Pressure lines $\left(\frac{p}{\rho g}\right)$ by (Muttray, 2000) at $t = t(R_{u,max}) + 0.44T$

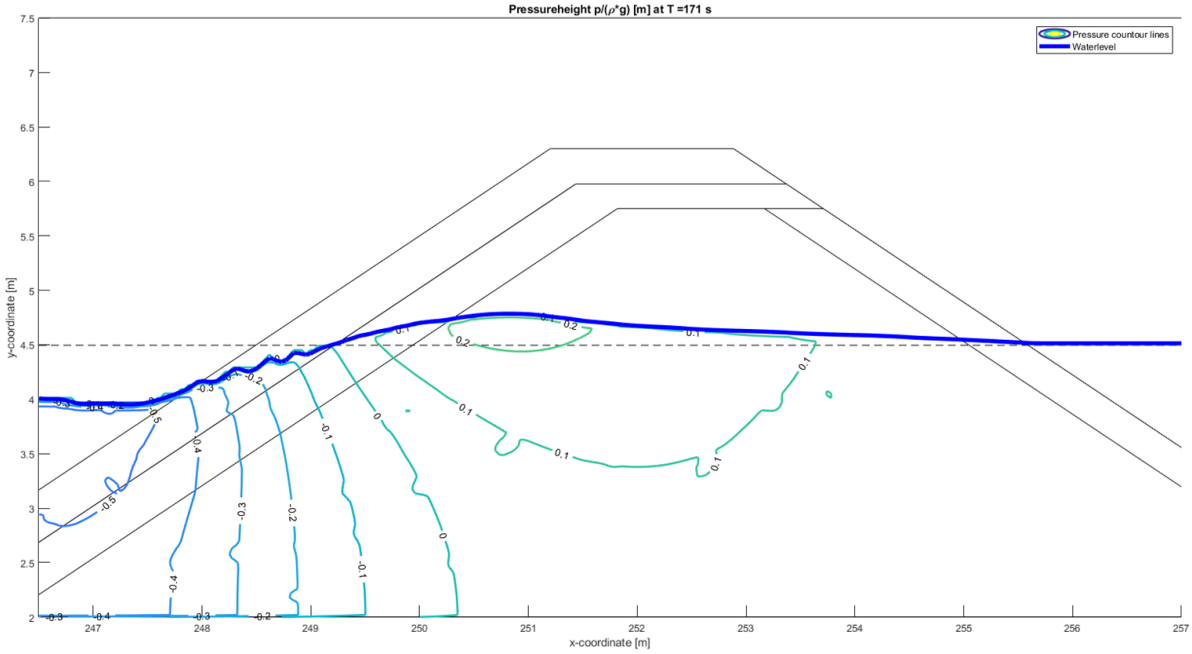

Figure 131 - Simulated pressure lines $\left(\frac{p}{\rho g}\right)$ at $t = 171\ s\ (\approx t(R_{u,max}) + 0.45T)$

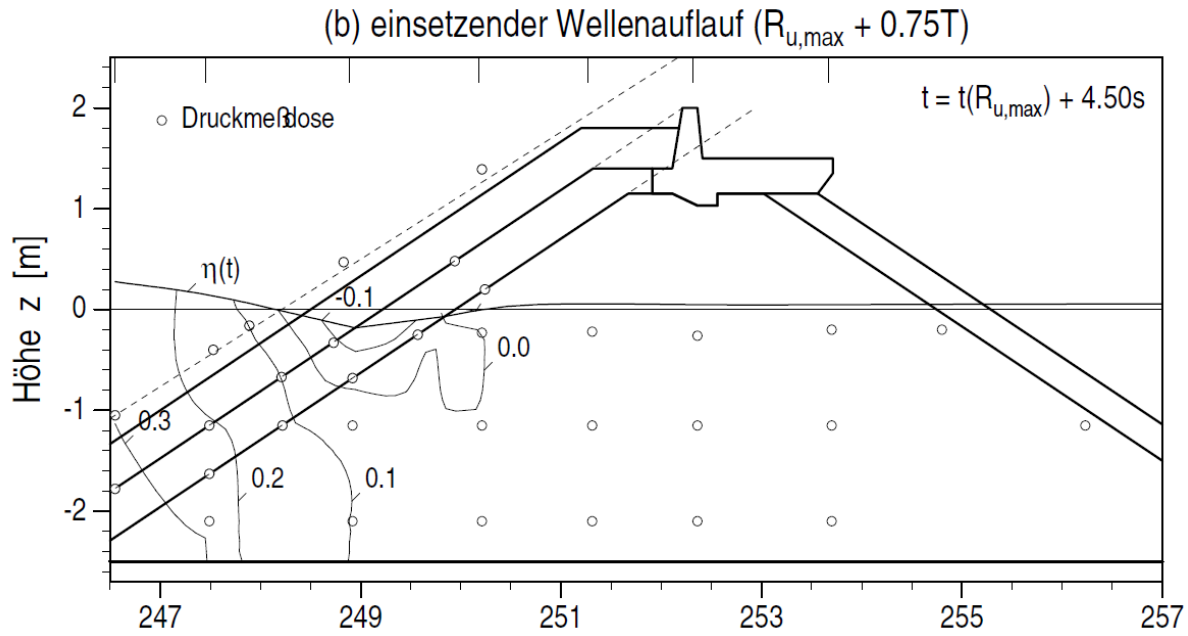

Figure 132 - Pressure lines $\left(\frac{p}{\rho g}\right)$ by (Muttray, 2000) at $t = t(R_{u,max}) + 0.75T$

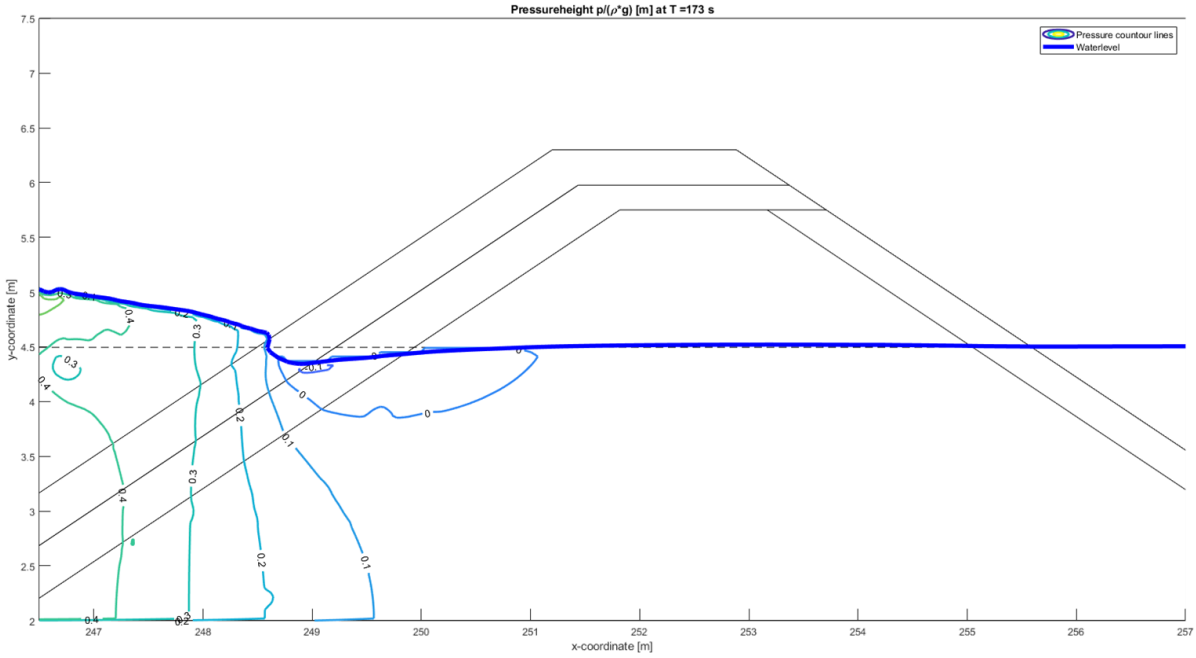

Figure 133 - Simulated pressure lines $\left(\frac{p}{\rho g}\right)$ at $t = 173\ s\ (\approx t(R_{u,max}) + 0.78T)$

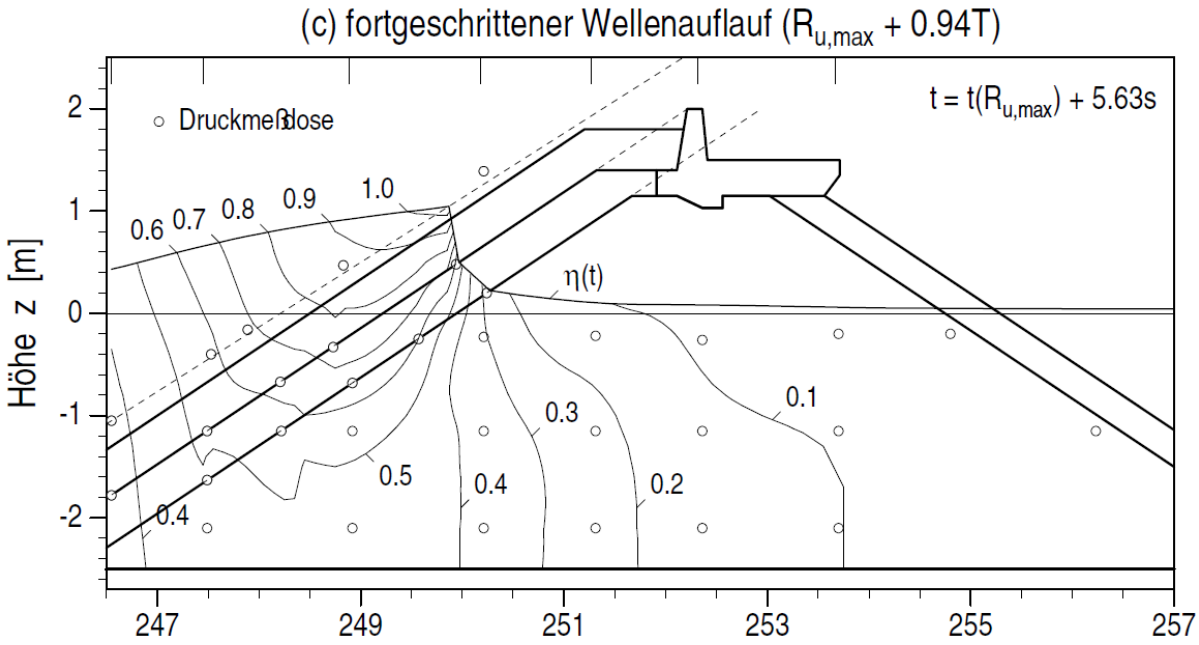

Figure 134 - Pressure lines $\left(\frac{p}{\rho g}\right)$ by (Muttray, 2000) at $t = t(R_{u,max}) + 0.94T$

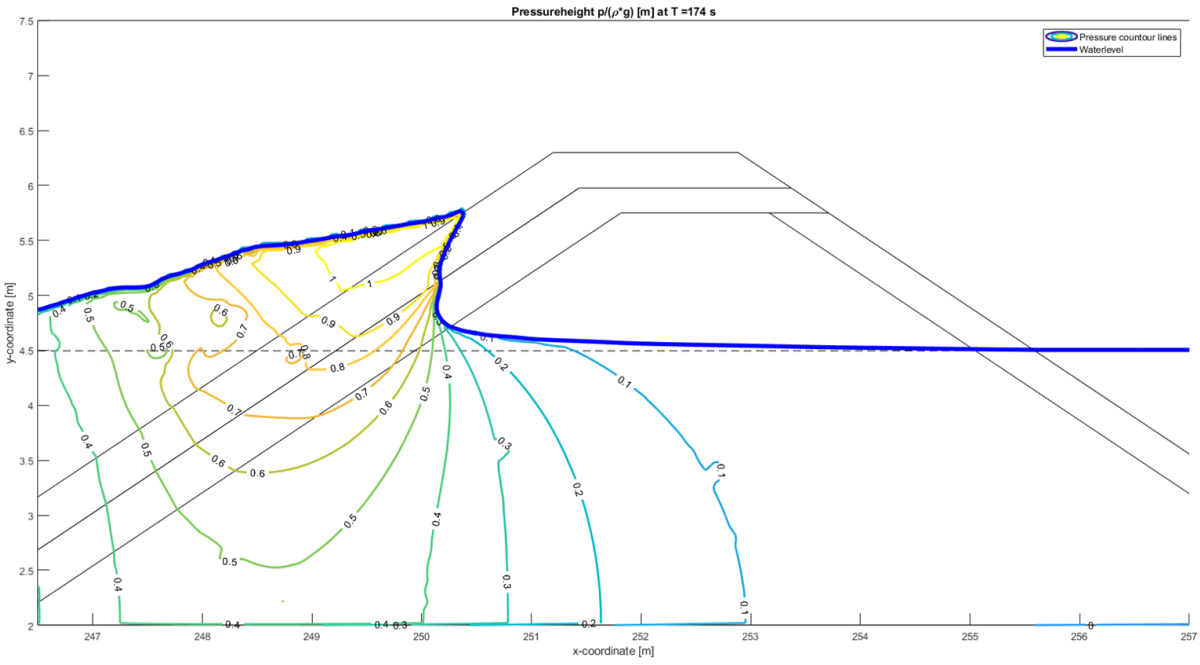

Figure 135 - Simulated pressure lines $\left(\frac{p}{\rho g}\right)$ at $t = 174\ s\ (\approx t(R_{u,max}) + 0.95T)$

Appendix B. Optimization of the model set-up for the model validation simulation

B.1. Physical model of (Muttray, 2000)

The model of (Muttray, 2000) was built in the “Großer Wellenkanal” in Hannover, Germany. A schematic cross-section of the model is shown in Figure 136. A zoomed in schematic cross-section of the breakwater structure is shown in Figure 137. Test nr. 020694-01 of (Muttray, 2000), was done with regular waves with a wave height, H, of $0.85\ m$, a wave period, T, of $6.0\ s$ and a water depth, h, of $4.5\ m$ in front of the foreshore and a water depth, h, of $2.5\ m$ in front of the breakwater structure.

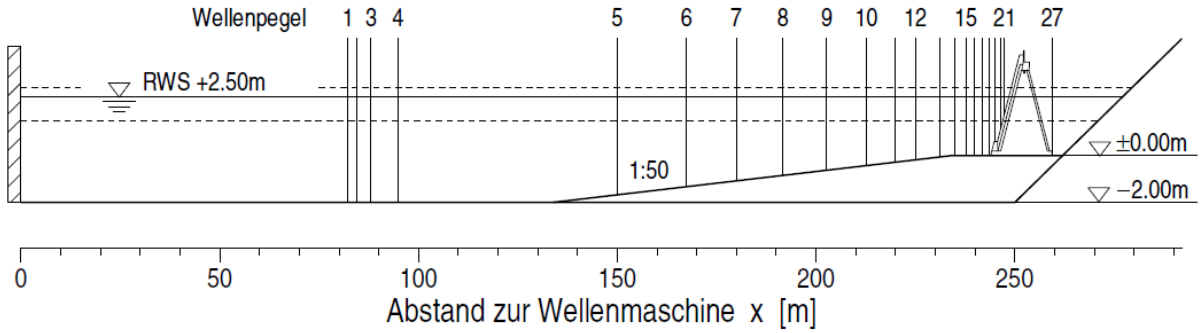

Figure 136 - Schematic cross-section of the model of (Muttray, 2000)

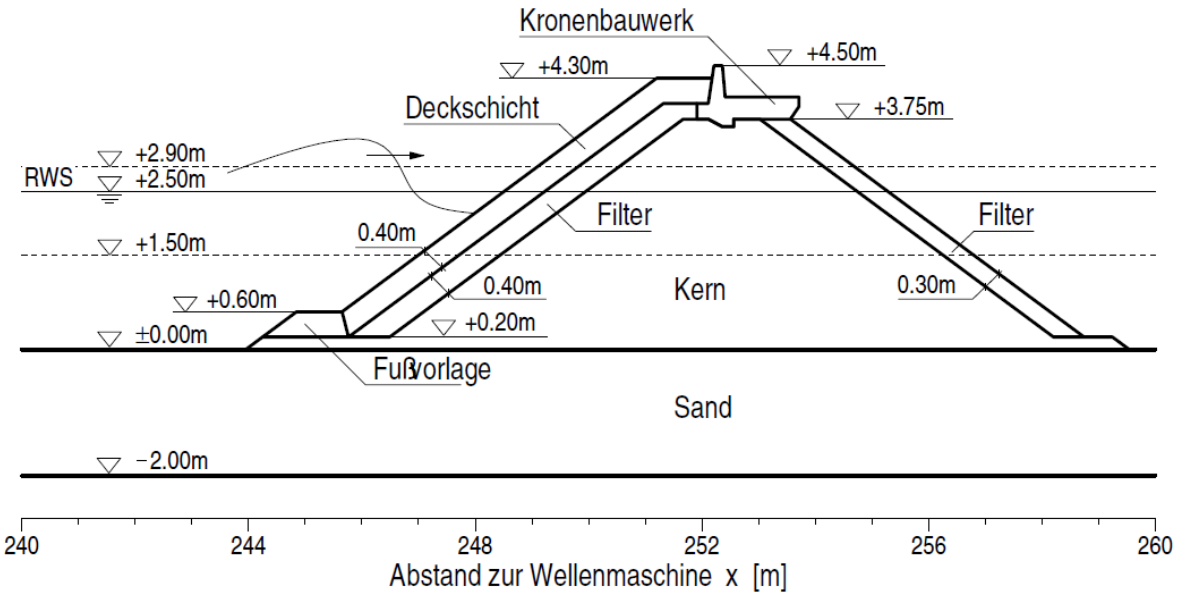

Figure 137 - Schematic cross-section of the breakwater construction of (Muttray, 2000)

B.2. Crest wall element or not?

For a quick first simulation, the structure is modelled in OpenFoam without the sloping foreshore and a much smaller domain to simulate. The domain of this OpenFoam model is shown as a green box in Figure 138, the two yellow boxes are the relaxation zones (the zones where the wave energy is smoothly imposed and dampened to prevent reflection from the boundaries). In the OpenFoam model, the structure is build identical to the structure in the physical model test, so with the same structural parameters (such as D_{n50}, n, α, β, γ, $KC-number$, etc.). For post-process purposes, the coordinates of the structure are kept the same (so the left boundary of the flume in OpenFoam is not at x = 0 but at x = 160).

Changing the flume lay-out can have quite an influence on the results, therefore the height of the incoming regular waves is changed to a value such that the incoming wave energy flux at the left boundary of the OpenFoam domain is the same as the incoming wave energy flux from

the regular waves from test nr. 020694-01 of (Muttray, 2000). This means that the first simulation has an incoming wave height, H, of $0.965\ m$.

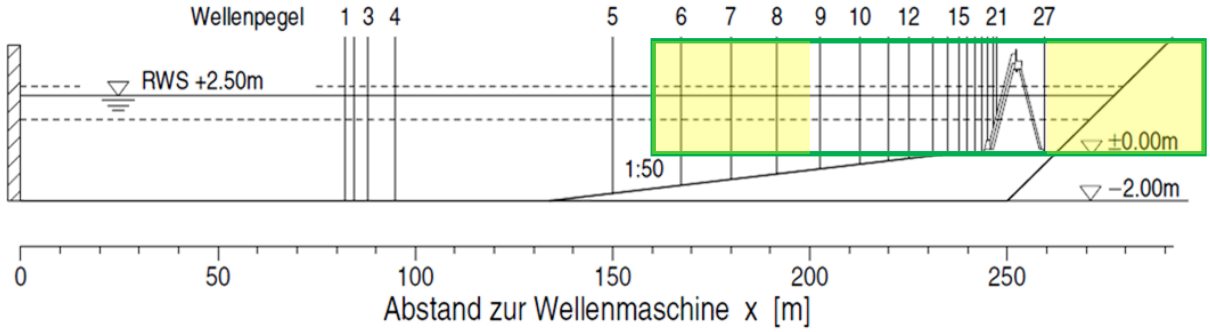

Figure 138 - Schematic cross-section of the model of (Muttray, 2000) with in the green box, the domain of the first OpenFoam simulation.

As can be seen, the breakwater structure (Muttray, 2000) used in his tests has a crown wall element. To implement a crown wall element like this in OpenFoam one has to use the OpenFoam utility SnappyHexMesh. However, using SnappyHexMesh increases the time it takes to set-up a model and furthermore, it sometimes causes instable behavior of the simulation. Besides, one has to be aware of air entrapment, as described in (Jacobsen et al., 2015), when simulating with an crown wall element. Therefore it is preferred to remove the crown wall element if this does not influence the results significantly. In order to see if the crown wall element is required in the simulations, this first simulation is done twice, one time with and one time without the crown wall element (see Figure 139 for the crest of the structure with and without the crown wall element).

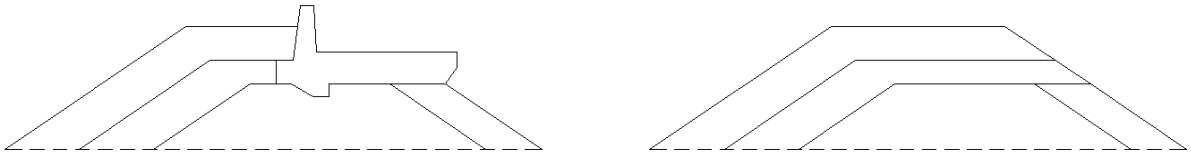

Figure 139 - Crest of structure with crown wall (left) and without crown wall (right)

The results of these first test indicate that the crown wall element can be removed, see section B.5. Therefore all the further models will have a breakwater structure with a crest as shown on the right in Figure 139.

B.3. Coupling OpenFoam with OceanWave3D

To correctly model the physical model test of (Muttray, 2000) including foreshore as efficient as possible, OpenFoam is coupled to OceanWave3D (OCW3D). Five different couplings are tested:

- Case OCW3D_1: Coupling in front of foreshore and cell size varying over foreshore.
- Case OCW3D_2: Coupling on foreshore (relaxation zone parallel to the foreshore) and cell size varying over foreshore.
- Case OCW3D_3: Coupling in front of foreshore and constant cell size (foreshore cut out with SnappyHexMesh)
- Case OCW3D_4: Coupling on foreshore (relaxation zone horizontal) and cell size varying over foreshore.
- Case OCW3D_5: Coupling on foreshore (relaxation zone horizontal) and constant cell size (foreshore cut out with SnappyHexMesh)

See Figure 140 till Figure 144 for the domains of the OpenFoam simulations. The domain of the OpenFoam simulations are shown as a green box again and the yellow boxes are the relaxation zones again. The red areas indicate the areas that are cut out with SnappyHexMesh. For investigating the coupling of OpenFoam with OCW3D only the incoming waves are investigated and compared to the OCW3D simulation, therefore the breakwater structure is not included in the OpenFoam domains in these simulations.

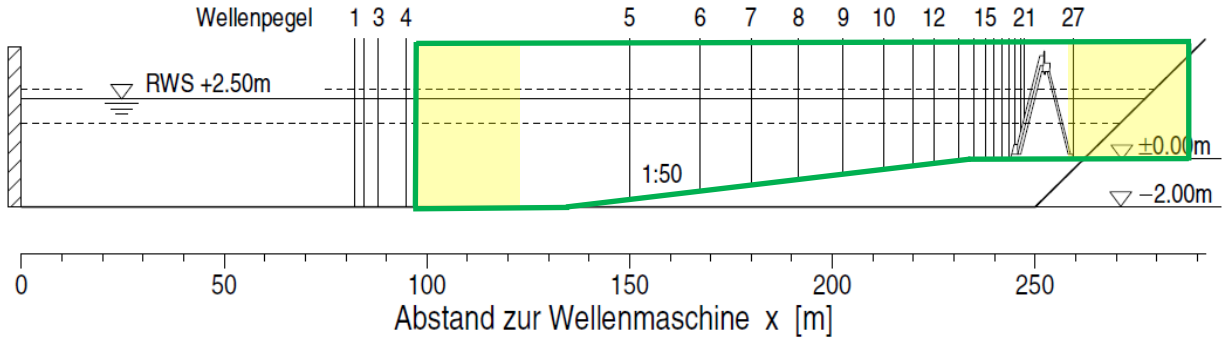

Figure 140 - Case OCW3D_1: Coupling in front of foreshore and cell size varying over foreshore.

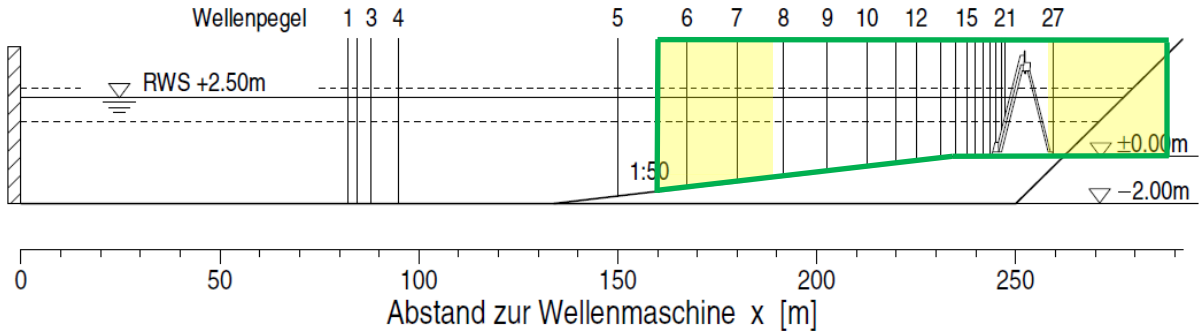

Figure 141 - Case OCW3D_2: Coupling on foreshore (relaxation zone parallel to the foreshore) and cell size varying over foreshore.

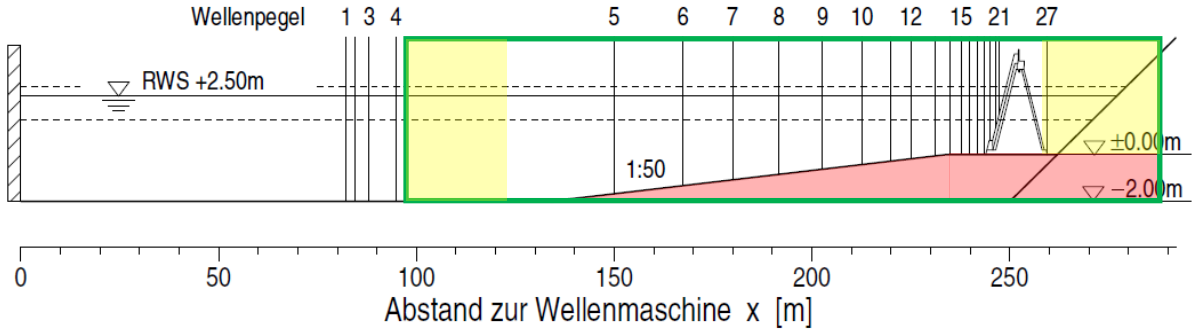

Figure 142 - Case OCW3D_3: Coupling in front of foreshore and constant cell size (foreshore cut out with SnappyHexMesh)

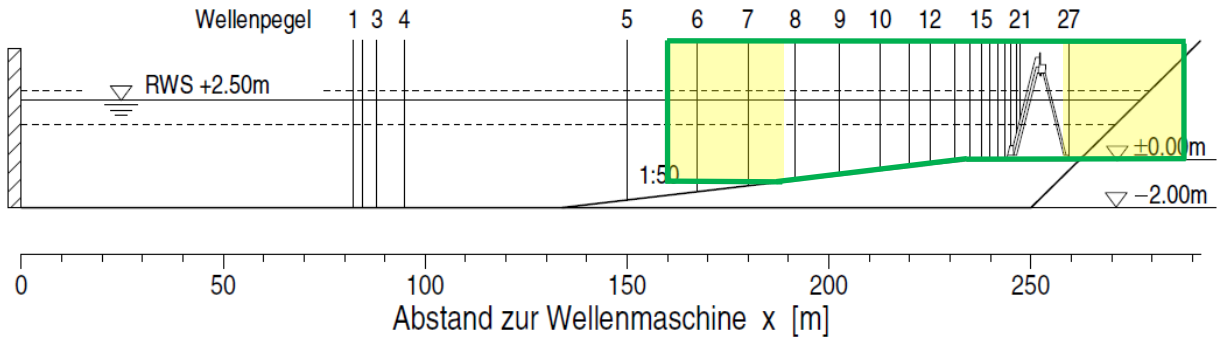

Figure 143 - Case OCW3D_4: Coupling on foreshore (relaxation zone horizontal) and cell size varying over foreshore.

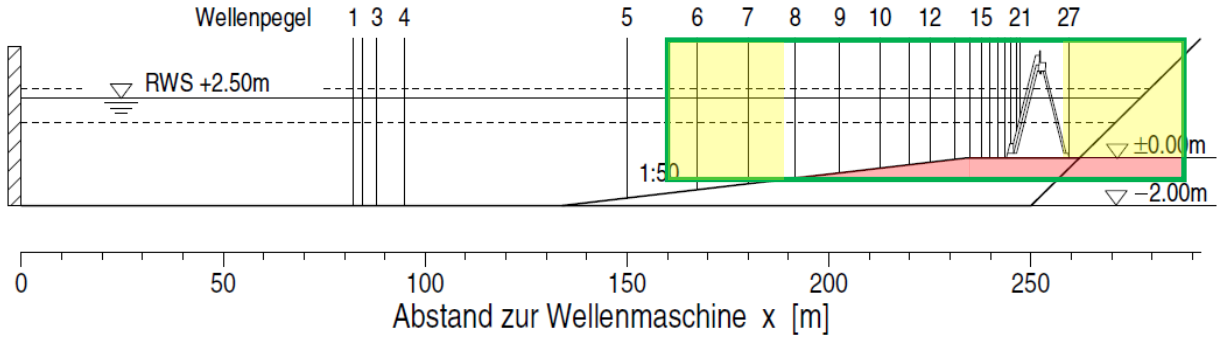

Figure 144 - Case OCW3D_5: Coupling on foreshore (relaxation zone horizontal) and constant cell size (foreshore cut out with SnappyHexMesh)

There are basically two types of cell distribution in the five cases described above: a distribution where the cell size is varying over the foreshore and a cell distribution where the cell size is constant and the foreshore is cut out with SnappyHexMesh. Figure 145 illustrates the cell distribution where the cell size varies over the foreshore. In the vertical direction, the same amount of cells are defined, but since the bottom slopes upward, the total size of the cells in the vertical direction becomes smaller. To keep the aspect ratio of the cells $\left(\frac{\Delta x}{\Delta y}\right)$ as close to 1 as possible, the cell size in the horizontal direction is gradually reduced as well. Figure 146 shows the cell distribution where the cell size is constant. The foreshore is cut out with SnappyHexMesh (the red area).

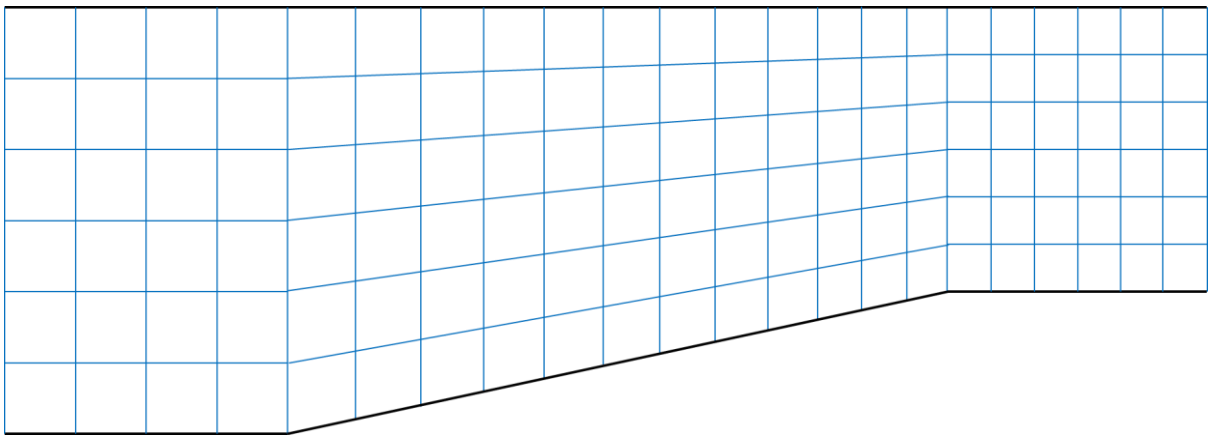

Figure 145 – Cell distribution where the cell size is varying over the foreshore

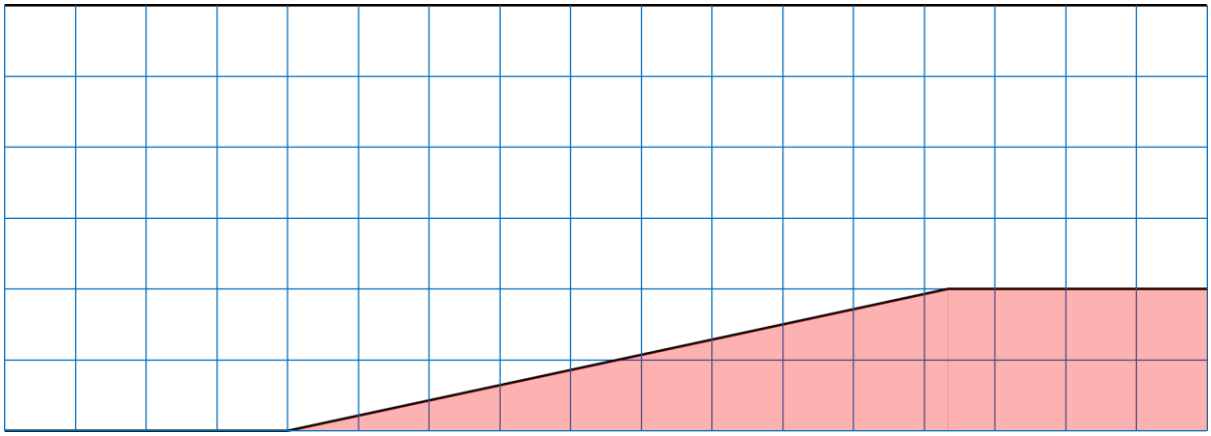

Figure 146 – Cell distribution where the cell size is constant

From the results of these simulations it can be concluded that case OCW3D_4 is the most efficient coupling between OpenFoam and OCW3D, see section B.6 for the results. Therefore, all the further models will have a coupling between OCW3D and OpenFoam as shown in Figure 143.

B.4. Validation model

Taking the tests of sections B.2 and B.3 into account, the model set-up for the validation case is with a breakwater structure without a crown wall element (see Figure 147), with a coupling between OCW3D and OpenFoam on the foreshore as shown in Figure 148 and a varying cell size over the rest of the foreshore (as illustrated in Figure 145).

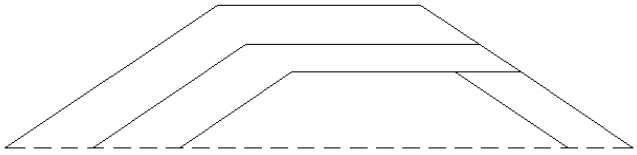

Figure 147 - Crest of the breakwater used in the validation model

Again, the structure is build identical to the structure in the physical model test, so with the same structural parameters (such as D_{n50}, n, α, β, γ, $KC - number$, etc.). The coordinates of the structure are kept the same.

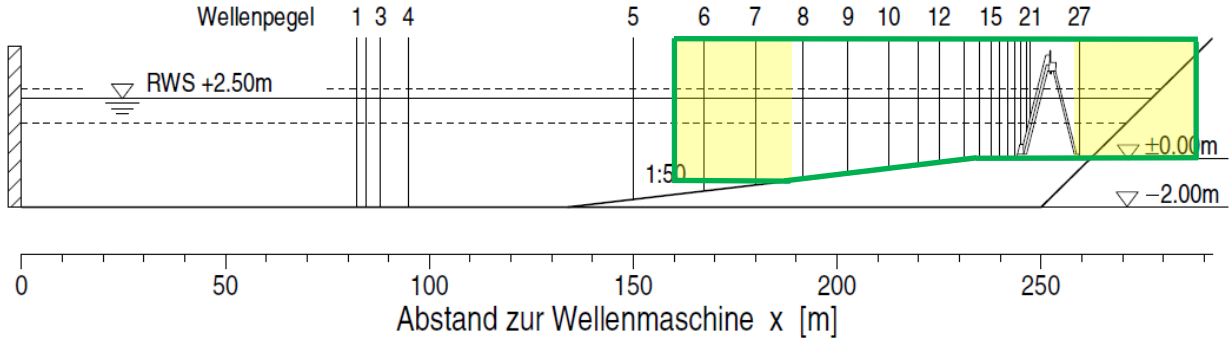

Figure 148 – OpenFoam domain with coupling of OCW3D with OpenFoam on the foreshore

The simulation is done with the same waves as used in test nr. 020694-01 of (Muttray, 2000). So that means that the simulation is done with regular waves with a wave height, H, of $0.85\ m$ and a wave period, T, of $6.0\ s$.

B.5. Crest wall element or not? – Results

Figure 149, Figure 150 and Figure 151 show a comparison between the surface elevation of the two simulations described in section B.2 at the locations $x = 239.97$, $x = 241.83$ and $x = 243.47$ (three locations just in front of the structure). As can be seen, the results of the two simulations match quite good, although they are not 100% the same. It is assumed that the crest wall element can be removed without causing a great loss in accuracy.

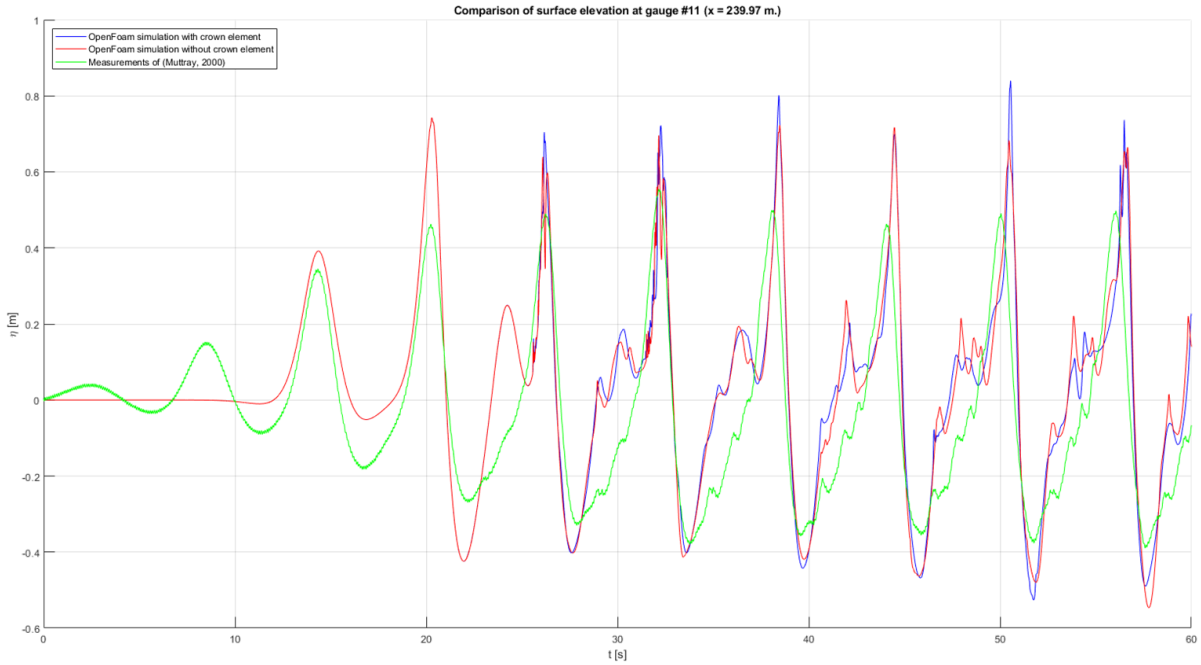

Figure 149 - Surface elevation comparison with and without crown wall element at $x = 239.97$

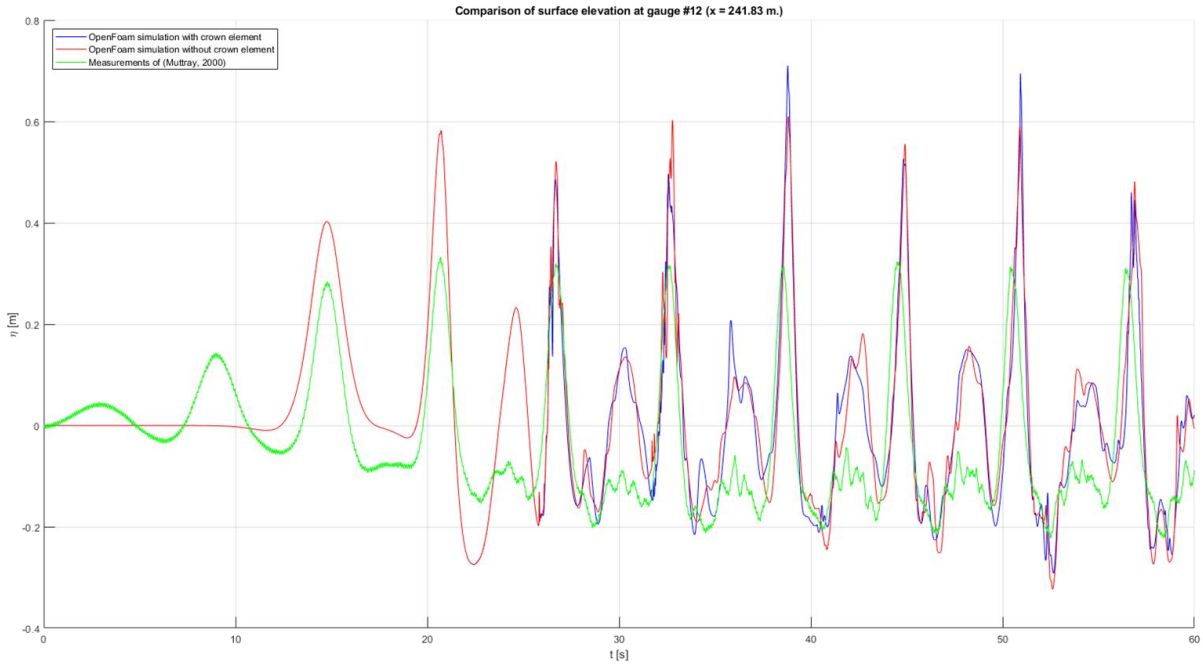

Figure 150 - Surface elevation comparison with and without crown wall element at $x = 241.83$

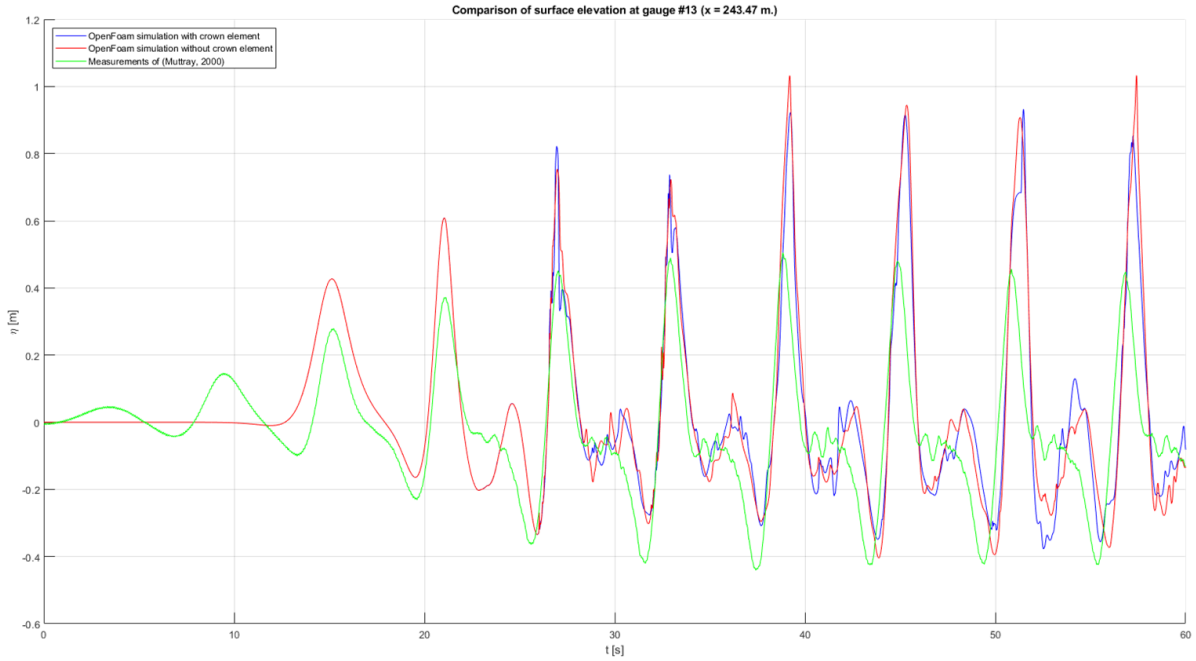

Figure 151 - Surface elevation comparison with and without crown wall element at $x = 243.47$

B.6. Coupling OpenFoam with OceanWave3D - results

Figure 153 till Figure 157 show a comparison between the results of the five cases described in section B.3 at the point $x = 239.97$ (a point just in front of the structure, on the top part of the foreshore). Figure 152 shows a small overview of the five cases used to investigate the connection between OCW3D and OpenFoam. From the results it can be seen that in simulation 1, 3 and 4 OCW3D is correctly coupled with OpenFoam. The coupling in the 2nd simulation is clearly not correct and is therefore not taken into account any further. The coupling in the 5th simulation seems to be quite accurate, however a time lag is introduced and besides, some oscillation occur in one of the throughs of the surface elevation. Therefore case 5 is also not taken into account further.

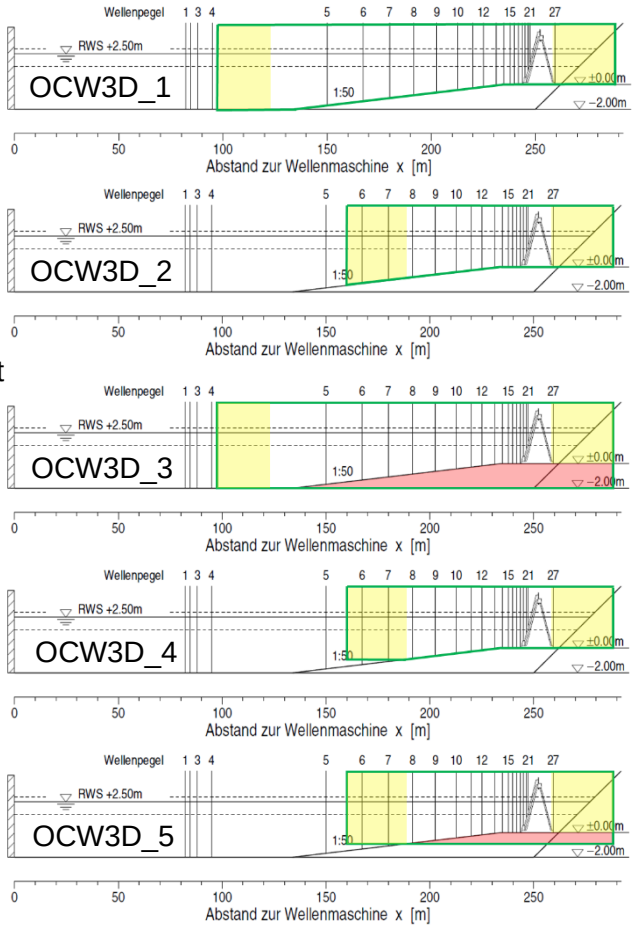

Figure 152 - Small overview of the five cases used to investigate the connection between OCW3D and OpenFoam

The goal is to make the simulation as efficient as possible, which means that the case with the least number of cells in the OpenFoam domain is preferred. Furthermore, SnappyHexMesh increases the time it takes to set-up a model, which is also not desirable. The total number of computation cells in the OpenFoam domain of case 1, 3 and 4 is include in Table 35. From Table 35 it can be seen that case 4 has the least computation cells in the OpenFoam domain and is thus the most efficient from these cases.

Case	# of cells in OpenFoam Domain
OCW3D_1	1.092.092
OCW3D_3	788.826
OCW3D_4	500.960

Table 35 - number of cells in OpenFoam domain

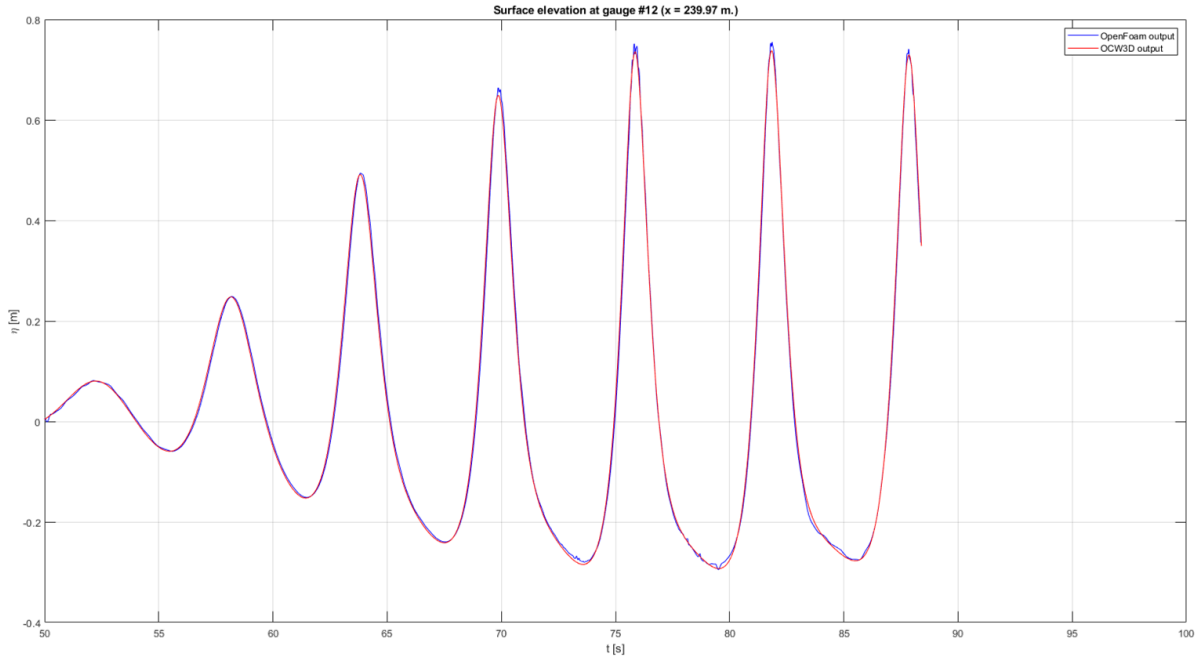

Figure 153 - Surface elevation comparison between OCW3D and OpenFoam for case OCW3D_1 at $x = 239.97$

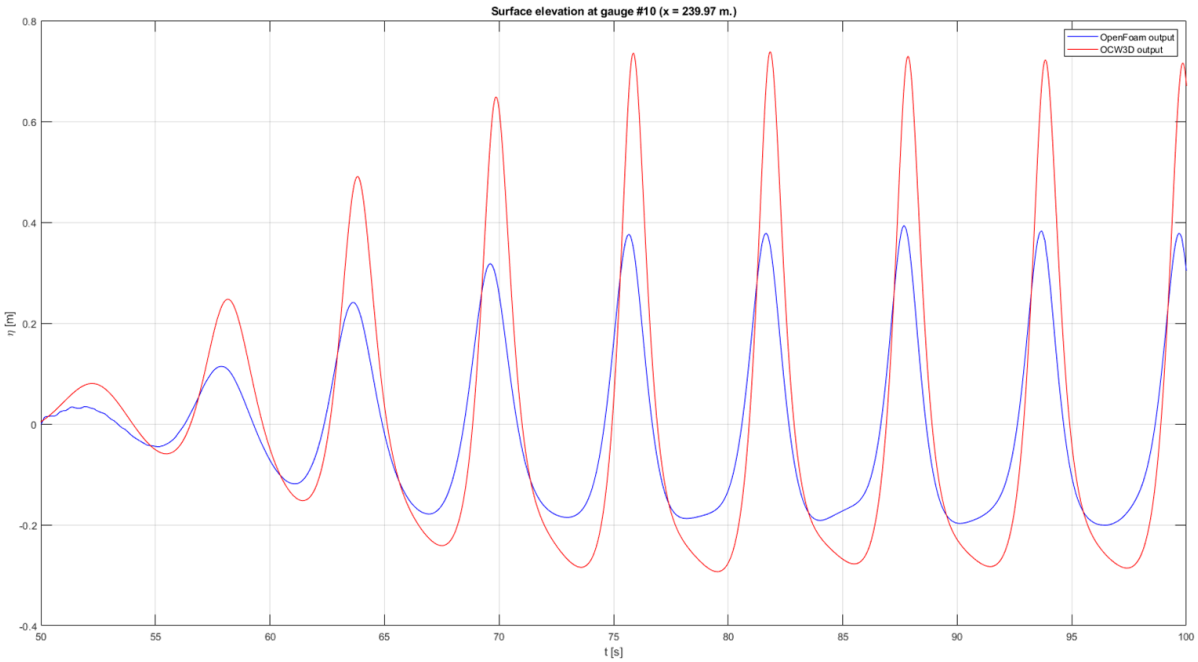

Figure 154 - Surface elevation comparison between OCW3D and OpenFoam for case OCW3D_2 at $x = 239.97$

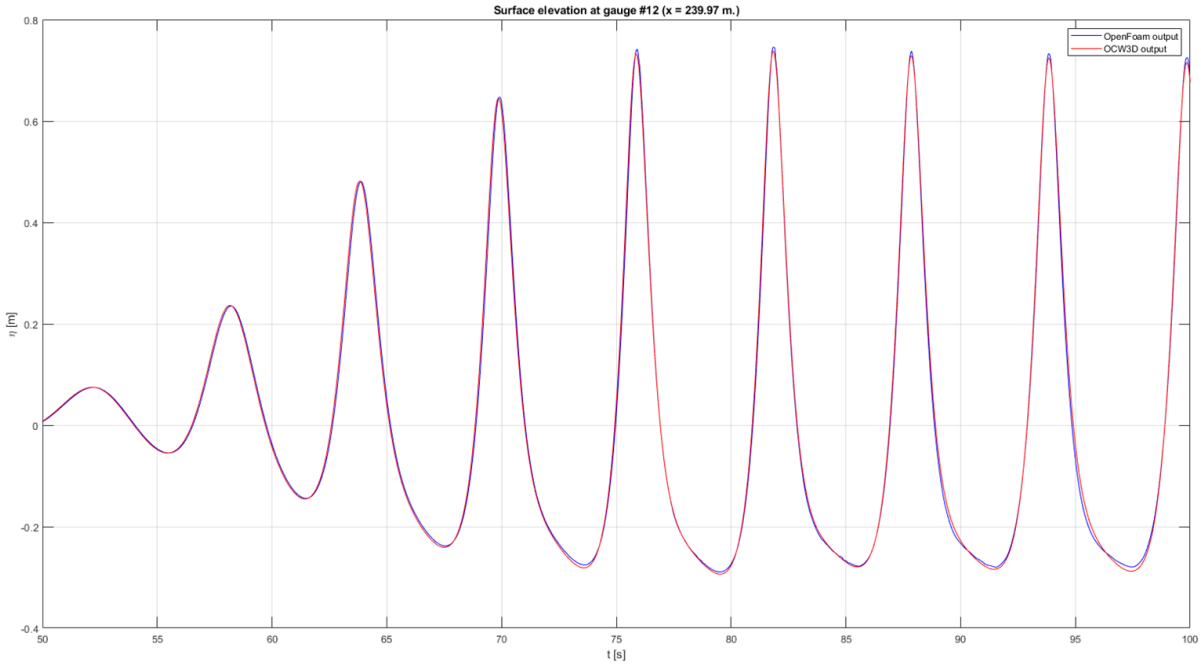

Figure 155 - Surface elevation comparison between OCW3D and OpenFoam for case OCW3D_3 at $x = 239.97$

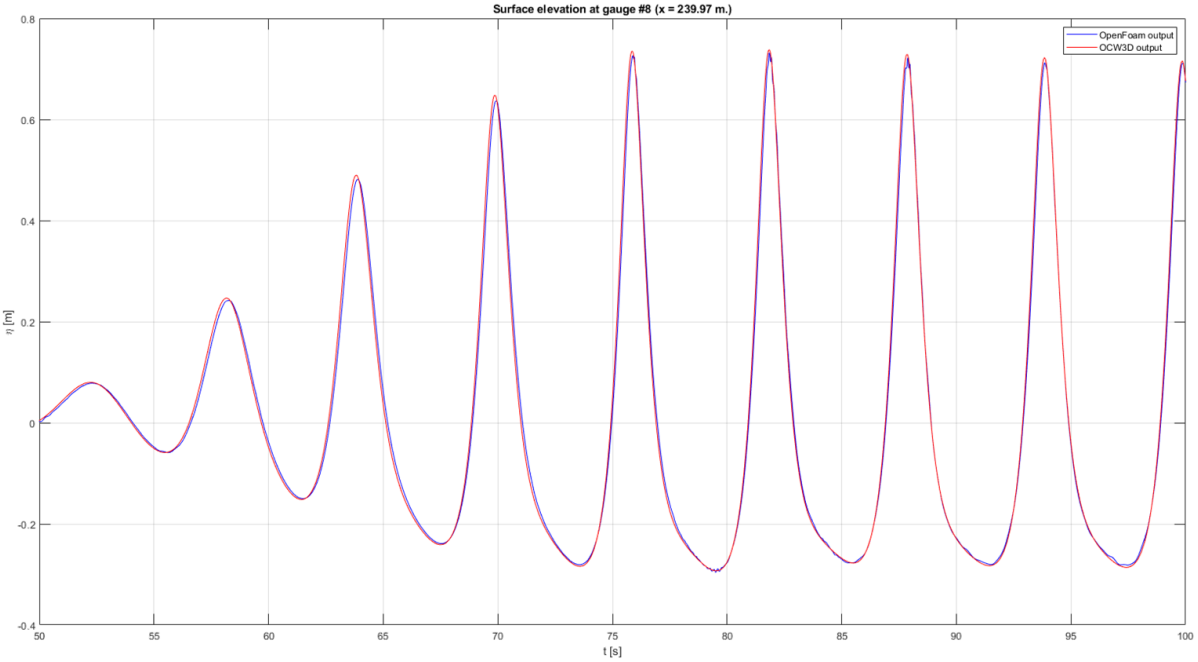

Figure 156 - Surface elevation comparison between OCW3D and OpenFoam for case OCW3D_4 at $x = 239.97$

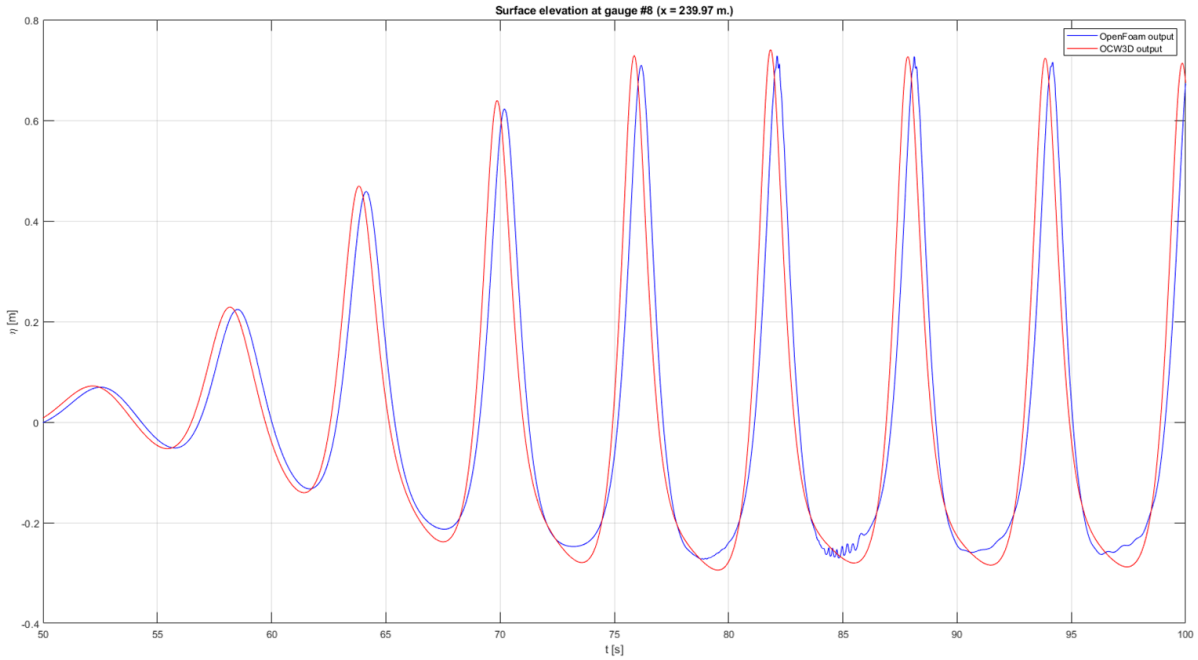

Figure 157 - Surface elevation comparison between OCW3D and OpenFoam for case OCW3D_5 at $x = 239.97$

Appendix C.

Set-up of OpenFoam model for prediction of notional permeability

In this appendix the input files for the OpenFoam simulation of sim 1.0 are shown. Sim 1.0 is the simulation of the structure of Kik for wave spectrum 1, see section 7.2. The input files are sorted per folder in the run-folder.

C.1 Home folder of the run

C.1.1 File: blockMeshDict

```
/*--------------------------------*- C++ -*----------------------------------*\
| =========                 |                                                 |
| \\      /  F ield         | OpenFOAM: The Open Source CFD Toolbox           |
|  \\    /   O peration     | Version:  2.1.0                                 |
|   \\  /    A nd           | Web:      www.OpenFOAM.org                      |
|    \\/     M anipulation  |                                                 |
\*---------------------------------------------------------------------------*/
FoamFile
{
    version     2.0;
    format      ascii;
    class       dictionary;
    object      blockMeshDict;
}
// * * * * * * * * * * * * * * * * * * * * * * * * * * * * * * * * * * * * * //

convertToMeters 1;

vertices
(
    ( 27.00  0.0  -0.03) // vertex number 0
    ( 49.00  0.0  -0.03) // vertex number 1
    ( 49.00  1.5  -0.03) // vertex number 2
    ( 27.00  1.5  -0.03) // vertex number 3

    ( 27.00  0.0  0.03) // vertex number 4
    ( 49.00  0.0  0.03) // vertex number 5
    ( 49.00  1.5  0.03) // vertex number 6
    ( 27.00  1.5  0.03) // vertex number 7

);

blocks
(
    hex (0 1 2 3 4 5 6 7) (2200 150 1) simpleGrading (1 1 1)
);

edges
(
);

```

Figure 158 - File: blockMeshDict (1 of 2)

In the file blockMeshDict the OpenFoam domain can be changed with the vertices. The grid size can be changed in the blocks part. The different boundaries are defined in the patches section. From these parameters, the domain and the grid resolution should be changed such that the domain is long enough and the grid resolution is high enough. So the relaxation zones should have a length of at least 1 wavelength and at least 1 wavelength should be available between the relaxation zone and the structure. The grid should be orthogonal and at least 20 grid cells in y-direction should be present per wave height.

```
41
42  patches
43  (
44      patch inlet
45      (
46          (0 3 7 4)
47      )
48
49      patch outlet
50      (
51          (1 2 6 5)
52      )
53
54      patch atmosphere
55      (
56          (2 3 7 6)
57      )
58
59      patch bottom
60      (
61          (0 1 5 4)
62      )
63
64      empty front
65      (
66          (0 1 2 3)
67      )
68
69      empty back
70      (
71          (4 5 6 7)
72      )
73  );
74
75  mergePatchPairs
76  (
77  );
78
79  // ************************************************************************* //
```

Figure 159 - File: blockMeshDict (2 of 2)

C.1.2 File: OceanWave3D.inp

```
1   Header
2   0 2 1000
3   58.5 1 0.65 585 1 9 0 0 1 1 1 1
4   3 3 3 1 1 1
5   58750 0.02 1 0 0 0
6   9.81 1000
7   1 1 0 23 1e-8 1e-6 1 V 1 1 2
8   1 1 1 1 1 1 1 1 1
9   0 30 30 10
10  370 370 1 1 1 1 1 58750 1
11  390 390 1 1 1 1 1 58750 1
12  410 410 1 1 1 1 1 58750 1
13  430 430 1 1 1 1 1 58750 1
14  440 440 1 1 1 1 1 58750 1
15  450 450 1 1 1 1 1 58750 1
16  460 460 1 1 1 1 1 58750 1
17  470 470 1 1 1 1 1 58750 1
18  480 480 1 1 1 1 1 58750 1
19  490 490 1 1 1 1 1 58750 1
20  1 0
21  1 6 10 0.08 0.08 0.4
22  1 5 1 X 0
23  0 9 0 0 -9 3.5 X 1 X 0
24  1 1
25  49.5 58.5 0 0 1 1 0
26  0 0 0 0 0 0 0
27  0
28  0 3.01 0.13 0.65 5 1 1 0 0 0
```

Figure 160 - File: OceanWave3D.inp

The OceanWave3D.inp file is the input file for the OceanWave3D simulation, for examples of different input files and how other wave types should be implemented, see the OceanWave3D webpage on GitHub: https://github.com/apengsigkarup/OceanWave3D-Fortran90.

It is important that the grid size in x-direction is such that at least 20 grid cells are available per wave length (the average wave length for a spectrum). The grid size is determined by the OceanWave3D domain in x-direction, the first value on line 3, and the number of grid cells in x-direction, the 4th value on line 3.

The selected time step should be such that the courant number is below 1. The time step is the second value in line 5. The total simulation time of the OceanWave3D simulation is defined by this time step and the number of time steps, the first value in line 5.

The wave input values are given in line 28. The first value is for the spectrum type (0 = a P-M spectrum), the second value represents the peak period, the third value the significant wave height, the fourth value the water depth, the fifth value the max kh-value and the sixth and seventh value are the seed values.

In order to use exactly the same wave spectra for simulations with different structures, exactly the same OceanWave3D.inp file should be used in the home folder of the simulation run for every structure.

C.2 Folder: 0.org

C.2.1 File: alpha1

```
/*--------------------------------*- C++ -*----------------------------------*\
| =========                 |                                                 |
| \\      /  F ield         | OpenFOAM: The Open Source CFD Toolbox           |
|  \\    /   O peration     | Version:  1.5-dev                               |
|   \\  /    A nd           | Revision: 1740                                  |
|    \\/     M anipulation  | Web:      http://www.OpenFOAM.org               |
\*---------------------------------------------------------------------------*/
FoamFile
{
    version     2.0;
    format      ascii;
    class       volScalarField;
    location    "0";
    object      alpha1.org;
}
// * * * * * * * * * * * * * * * * * * * * * * * * * * * * * * * * * * * * * //

dimensions      [0 0 0 0 0 0 0];

internalField   uniform 0;

boundaryField
{
    inlet
    {
        type            zeroGradient;
        refValue        uniform 0;
        refGrad         uniform 0;
        valueFraction   uniform 1;
        value           uniform 0;
    }
    bottom
    {
        type            zeroGradient;
    }
    outlet
    {
        type            zeroGradient;
    }
    core.stl
    {
        type            zeroGradient;
    }
    atmosphere
    {
        type            inletOutlet;
        inletValue      uniform 0;
        value           uniform 0;
    }
    front
    {
        type            empty;
    }
    back
    {
        type            empty;
    }
}

// ************************************************************************* //
```

Figure 161 – File: alpha1

The initial and boundary conditions with respect to the value of alpha1. Nothing has to be changes in this file for different structures and/or wave conditions.

C.2.2 File: pd

```
/*--------------------------------*- C++ -*----------------------------------*\
| =========                 |                                                 |
| \\      /  F ield         | OpenFOAM: The Open Source CFD Toolbox           |
|  \\    /   O peration     | Version:  1.5-dev                               |
|   \\  /    A nd           | Revision: 1740                                  |
|    \\/     M anipulation  | Web:      http://www.OpenFOAM.org               |
\*---------------------------------------------------------------------------*/
FoamFile
{
    version     2.0;
    format      ascii;
    class       volScalarField;
    location    "0";
    object      pd;
}
// * * * * * * * * * * * * * * * * * * * * * * * * * * * * * * * * * * * * * //

dimensions      [1 -1 -2 0 0 0 0];

internalField   uniform 0;

boundaryField
{
    inlet
    {
        type            zeroGradient;
    }
    bottom
    {
        type            zeroGradient;
    }
    outlet
    {
        type            zeroGradient;
    }
    core.stl
    {
        type            zeroGradient;
    }
    atmosphere
    {
        type            totalPressure;
        U               U;
        phi             phi;
        rho             none;
        psi             none;
        gamma           1;
        p0              uniform 0;
        value           uniform 0;
    }
    front
    {
        type            empty;
    }
    back
    {
        type            empty;
    }
}

// ************************************************************************* //
```

Figure 162 – File: pd

The initial and boundary conditions with respect to the value of pd. Nothing has to be changes in this file for different structures and/or wave conditions.

C.2.3 File: U

```
/*--------------------------------*- C++ -*----------------------------------*\
| =========                 |                                                 |
| \\      /  F ield         | OpenFOAM: The Open Source CFD Toolbox           |
|  \\    /   O peration     | Version:  2.1.1                                 |
|   \\  /    A nd           | Web:      www.OpenFOAM.org                      |
|    \\/     M anipulation  |                                                 |
\*---------------------------------------------------------------------------*/
FoamFile
{
    version     2.0;
    format      ascii;
    class       volVectorField;
    location    "0";
    object      U;
}
// * * * * * * * * * * * * * * * * * * * * * * * * * * * * * * * * * * * * * //

dimensions      [0 1 -1 0 0 0 0];

internalField   uniform (0 0 0);

boundaryField
{
    inlet
    {
        type            zeroGradient;
        refValue        uniform (0 0 0);
        refGradient     uniform (0 0 0);
        valueFraction   uniform 1;
        value           uniform (0 0 0);
    }
    bottom
    {
        type            slip;
    }
    outlet
    {
        type            slip;
    }
    atmosphere
    {
        type            pressureInletOutletVelocity;
        value           uniform (0 0 0);
    }
    back
    {
        type            empty;
    }
    front
    {
        type            empty;
    }
    core.stl
    {
        type            slip;
    }
}

// ************************************************************************* //
```

Figure 163 - File: U

The initial and boundary conditions with respect to the value of U. Nothing has to be changed in this file for different structures and/or wave conditions.

C.3 Folder: constant/triSurface

C.3.1 File: stlDefinitions

```
/*--------------------------------*- C++ -*----------------------------------*\
| =========                 |                                                 |
| \\      /  F ield         | OpenFOAM: The Open Source CFD Toolbox           |
|  \\    /   O peration     | Version:  1.5                                   |
|   \\  /    A nd           | Web:      http://www.OpenFOAM.org               |
|    \\/     M anipulation  |                                                 |
\*---------------------------------------------------------------------------*/
FoamFile
{
    version     2.0;
    format      ascii;
    class       dictionary;
    object      stlDefinitions;
}
// * * * * * * * * * * * * * * * * * * * * * * * * * * * * * * * * * * * * * //


core
{
    points 3
    (
        (45.9800 -0.0100 -1.0)
        (49.0000 -0.0100 -1.0)
        (49.0000  1.5000 -1.0)
    );
    faces 1(( 0   1   2));

    extrude true;
    extrudeVector (0.0 0.0 2.0);
}

second
{
    points 4
    (
        (45.7676 -0.0100 -1.0)
        (45.9800 -0.0100 -1.0)
        (49.0000  1.5000 -1.0)
        (48.7876  1.5000 -1.0)
    );
    faces 1(( 0  1  2  3));

    extrude true;
    extrudeVector (0.0 0.0 2.0);
}
```

Figure 164 – File: stlDefinitions (1 of 2)

In this file the locations of the porous layers are defined. This file is input to create the STL-files which are used by OpenFoam to define the porous layers. To change a structure, change the coordinates in this file. More layers can simply be added by copying a layer (e.g. core) and re-naming it. Layers can simply be removed just by deleting the part on that layer.

```
46
47  first
48  {
49      points 4
50      (
51          (45.6558 -0.0100 -1.0)
52          (45.7676 -0.0100 -1.0)
53          (48.8076  1.5100 -1.0)
54          (48.6958  1.5100 -1.0)
55      );
56      faces 1(( 0  1  2  3));
57
58      extrude true;
59      extrudeVector (0.0 0.0 2.0);
60  }
61
62  armour
63  {
64      points 4
65      (
66          (45.4433 -0.0100 -1.0)
67          (45.6558 -0.0100 -1.0)
68          (48.6958  1.5100 -1.0)
69          (48.4833  1.5100 -1.0)
70      );
71      faces 1(( 0  1  2  3));
72
73      extrude true;
74      extrudeVector (0.0 0.0 2.0);
75  }
76
77
78  // ************************************************************************* //
```

Figure 165 - stlDefinitions (1 of 2)

C.4 Folder: constant

C.4.1 File: defineWeightedPorosityZones

```
/*--------------------------------*- C++ -*----------------------------------*\
| =========                 |                                                 |
| \\      /  F ield         | foam-extend: Open Source CFD                    |
|  \\    /   O peration     | Version:     3.1                                |
|   \\  /    A nd           | Web:         http://www.extend-project.de       |
|    \\/     M anipulation  |                                                 |
\*---------------------------------------------------------------------------*/
FoamFile
{
    version     2.0;
    format      ascii;
    class       dictionary;
    object      defineWeightedPorosityZones;
}
// * * * * * * * * * * * * * * * * * * * * * * * * * * * * * * * * * * * * * //

armour
{
    geometry
    {
        globalValue 0.0;
        setTrisurfacesEdges
        {
            stlNames ( "armour.stl" );
        }
    }
}

first
{
    geometry
    {
        globalValue 0.0;
        setTrisurfacesEdges
        {
            stlNames ( "first.stl" );
        }
    }
}

second
{
    geometry
    {
        globalValue 0.0;
        setTrisurfacesEdges
        {
            stlNames ( "second.stl" );
        }
    }
}

/*
core
{
    geometry
    {
        globalValue 0.0;
        setTrisurfacesEdges
        {
            stlNames ( "core.stl" );
        }
    }
}
*/
```

Figure 166 - File: defineWeightedPorosityZones

In these files the active porous layers are defined, the name should correspond to the name define in stlDefinitions. If a layer is not included in this file, or is set on non-active, it will not be present in the simulated breakwater structure. A layer is set on non-active by putting /* in front of the layer and */ behind the layer (like is done for the layer core).

C.4.2 File: probeDefinitions

```
/*--------------------------------*- C++ -*----------------------------------*\
| =========                 |                                                 |
| \\      /  F ield         | OpenFOAM: The Open Source CFD Toolbox           |
|  \\    /   O peration     | Version:  1.5                                   |
|   \\  /    A nd           | Web:      http://www.OpenFOAM.org               |
|    \\/     M anipulation  |                                                 |
\*---------------------------------------------------------------------------*/
FoamFile
{
    version     2.0;
    format      ascii;
    class       dictionary;
    object      loggingProperties;
}
// * * * * * * * * * * * * * * * * * * * * * * * * * * * * * * * * * * * * * //


surfaceElevation
{
    type waveGauge;

    pointDistribution userDefinedDistribution;
    N 7;
    xValues nonuniform List<scalar> 7(37.0 39.0 41.0 43.0 44.0 45.0 46.0);
    yValues uniform 0.010;
    zValues uniform 0;
    add         (0 1.480 0);
    axis        y;
    stretch     1.0;
}


waveRunUpOneProbe
{
    type probeGauge;
    outputInterval 1;
    fields (pd U alpha1);
    pointDistribution lineDistribution;

    N 250;
    linestart (45.9127 0.2247 0);
    lineend   (48.4433 1.4900 0);

    stretch   1.0;
}

waveRunUpOneGauge
{
    type waveGauge;

    pointDistribution userDefinedDistribution;
    N 1;
    xValues uniform 45.4833;
    yValues uniform 0.0100;
    zValues uniform 0;
    add         (2.96 1.48 0);
    axis        y;
    stretch   1.0;
}
```

Figure 167 – File: probeDefinitions

In this file, the pressure probes and wave gauges are defined. This are the locations for which output is generated by OpenFoam. One or multiple wave gauges can be defined with the userDefinedDistribution as shown above, N stands for the number of wave gauges and the x and y values of the base of the wave gauge have to be defined. With add, a direction is given to the wave gauges, so waveRunUpOneGauge is a gauge that is located along the front slope of the structure.

C.4.3 File: waveProperties.input

```
1  /*--------------------------------*- C++ -*----------------------------------*\
2  | =========                 |                                                 |
3  | \\      /  F ield         | OpenFOAM: The Open Source CFD Toolbox           |
4  |  \\    /   O peration     | Version:  1.5                                   |
5  |   \\  /    A nd           | Web:      http://www.OpenFOAM.org               |
6  |    \\/     M anipulation  |                                                 |
7  \*---------------------------------------------------------------------------*/
8  FoamFile
9  {
10     version     2.0;
11     format      ascii;
12     class       dictionary;
13     object      environmentalProperties;
14 }
15 // * * * * * * * * * * * * * * * * * * * * * * * * * * * * * * * * * * * * * * * //
16
17 // Specification of the porosity model. This model allows for the 'shared'
18 // resistance inside a single computational cell
19 porosityModel isotropicVelocityAveragingResistanceModel;
20
21 // Specify the location of the sea level
22 seaLevel    0.65;
23
24 // Use the vertical coordinate of the sea level as reference
25 seaLevelAsReference true;
26
27 // Active relaxation zones
28 relaxationNames (inlet);
29 //relaxationNames (inlet outlet);
30
31 // Relaxation zone used for the initialisation of the variables
32 initializationName inlet;
33
34 pName pd;
35
36 // External forcing definition
37 externalForcing oceanWave3D;
38
39 // Coefficients needed for the external forcing
40 externalForcingCoeffs
41 {
42     waveType oceanWave3D;
43     // Define the intervals for the OpenFoam calculations
44     nIntervals 1;
45     startTimes nonuniform List<scalar> 1(0);
46     endTimes nonuniform List<scalar> 1(1175);
47
48     // Should the interval be ramped?
49     rampInterval on;
50     Tsoft 5;
51
52     // Name of the sub-dictionary (without Coeffs), where the externalSource
53     // definition is given. Is needed, when the mapping OceanWave3D to OpenFoam
54     // is performed.
55     mappingZone inlet;
56
57     translateOpenFoamMesh (0 0 0);
58 };
59
```

Figure 168 – File: waveProperties.input (1 of 2)

In the waveProperties.input file, the incoming waves are defined. For irregular waves, this is done by stating externalForcing oceanWave3D in line 40. In this file, the relaxation zones are defined as well. In case of a structure with an impermeable core, there is only a relaxation zone at the inlet (the relaxation zone at the outlet will be cut off by the use of SnappyHexMesh, this cuts out the impermeable part of the structure). In the figure above, there is only a relaxation zone at the inlet, see line 28. In case a relaxation zone at the outlet is needed, comment line 28 and de-comment line 29. Also be aware that in that case the outletCoeffs should be defined by de-commenting the lines 80 till 98. In the inletCoeffs and outletCoeffs, the location and size of the relaxation zones can be changes. Always make sure that the relaxation zones have a length of at least a wave length.

```
60
61  // Specification of the relaxation zone at the inlet
62  inletCoeffs
63  {
64      waveType     externalSource;
65
66      relaxationZone
67      {
68          relaxationScheme SpatialInterpolation;
69          relaxationShape  Line;
70          N 180;
71          relaxType   INLET;
72          startX   (27.0 0.0 -0.03);
73          endX     (36.0 0.0  0.03);
74          orientation (1 0 0);
75      }
76  };
77
78
79  // Specification of the relaxation zone at the outlet
80  /*
81  outletCoeffs
82  {
83      waveType     potentialCurrent;
84      Tsoft        2.50;
85      U            (0 0 0);
86
87      relaxationZone
88      {
89          relaxationScheme Spatial;
90          relaxationShape  Rectangular;
91          beachType        Empty;
92          relaxType   OUTLET;
93          startX   (49.0 0.0 -0.03);
94          endX     (53.5 0.0  0.03);
95          orientation (1 0 0);
96      }
97  };
98  */
99
100
101 // ************************************************************************* //
```

Figure 169 – File: waveProperties.input (2 of 2)

C.4.4 File: wavesPorosityProperties

In the file wavesPorosityProperties, the properties of the porous layers is defined. First make sure that all active porous layers are defined in porosityNames (line 17). The rock diameter and the porosity value of the material can be changed by simply changing the number in the corresponding line (e.g. line 25 or 29 for the armour material). The KC-value can be calculated with formula (19) from section 2.2.4. It is advised to keep the values for alpha and beta constant on respectively 1000.0 and 1.1, see 8.4.

```
/*--------------------------------*- C++ -*----------------------------------*\
| =========                 |                                                 |
| \\      /  F ield         | OpenFOAM Extend Project: Open source CFD        |
|  \\    /   O peration     | Version:  1.6-ext                               |
|   \\  /    A nd           | Web:      www.extend-project.de                 |
|    \\/     M anipulation  |                                                 |
\*---------------------------------------------------------------------------*/
FoamFile
{
    version 2.0;
    format  ascii;
    class   dictionary;
    object  wavesPorosityProperties;
}
// * * * * * * * * * * * * * * * * * * * * * * * * * * * * * * * * * * * * * * * * //

porosityNames (armour first second);

mimickOF true;

armourCoeffs
{
    resistanceFormulation vanGent1995;

    porosity 0.44;
    KC KC [0 0 0 0 0 0 0] 16;
    gammaAddedMass 0.34;

    d50 d50 [0 1 0 0 0 0 0] 0.0476;
    alpha alpha [0 0 0 0 0 0 0] 1000.0;
    beta beta [0 0 0 0 0 0 0] 1.1;
}

firstCoeffs
{
    resistanceFormulation vanGent1995;

    porosity 0.44;
    KC KC [0 0 0 0 0 0 0] 32;
    gammaAddedMass 0.34;

    d50 d50 [0 1 0 0 0 0 0] 0.0238;
    alpha alpha [0 0 0 0 0 0 0] 1000.0;
    beta beta [0 0 0 0 0 0 0] 1.1;
}

secondCoeffs
{
    resistanceFormulation vanGent1995;

    porosity 0.44;
    KC KC [0 0 0 0 0 0 0] 128;
    gammaAddedMass 0.34;

    d50 d50 [0 1 0 0 0 0 0] 0.00595;
    alpha alpha [0 0 0 0 0 0 0] 1000.0;
    beta beta [0 0 0 0 0 0 0] 1.1;
}

/*
coreCoeffs
{
    resistanceFormulation vanGent1995;

    porosity 0.001;
    KC KC [0 0 0 0 0 0 0] 10000;
    gammaAddedMass 0.34;

    d50 d50 [0 1 0 0 0 0 0] 0.0001;
    alpha alpha [0 0 0 0 0 0 0] 1000.0;
    beta beta [0 0 0 0 0 0 0] 1.1;
}
*/

// ************************************************************************* //
```

Figure 170 – File: wavesPorosityProperties.

C.4.5 Other files in this folder

The files dynamicMeshDict, g, RASProperties, transportProperties and turbulenceProperties should be present in the constant-folder as well, but do not require any changes for the simulation of different structures or different wave conditions. Be aware that in the file RASProperties, the RASModel has to be set on linear, otherwise turbulence is taken into account via this RASModel, while it is already included in the Forchheimer coefficients defined in the wavesPorosityProperties file.

C.5 Folder: system

C.5.1 File: controlDict

```
/*--------------------------------*- C++ -*----------------------------------*\
| =========                 |                                                 |
| \\      /  F ield         | OpenFOAM: The Open Source CFD Toolbox           |
|  \\    /   O peration     | Version:  2.1.0                                 |
|   \\  /    A nd           | Web:      www.OpenFOAM.org                      |
|    \\/     M anipulation  |                                                 |
\*---------------------------------------------------------------------------*/
FoamFile
{
    version     2.0;
    format      ascii;
    class       dictionary;
    location    "system";
    object      controlDict;
}
// * * * * * * * * * * * * * * * * * * * * * * * * * * * * * * * * * * * * * //

application     interFoam;

startFrom       startTime;

startTime       0;

stopAt          endTime;

endTime         1175.0;

deltaT          0.004;

writeControl    adjustableRunTime;

writeInterval   47;

purgeWrite      0;

writeFormat     ascii;

writePrecision  7;

writeCompression uncompressed;

timeFormat      general;

timePrecision   7;

runTimeModifiable yes;

adjustTimeStep  yes;

maxCo           0.35;

maxAlphaCo      0.50;

maxDeltaT       1;

libs ("libwaves2FoamAdditionals.so" "libwaves2FoamPorosityAdditionals.so"
"libwaves2FoamSamplingAdditionals.so" );

functions
{
    #includeIfPresent "../waveGaugesNProbes/surfaceElevation_controlDict";

    #includeIfPresent "../waveGaugesNProbes/waveRunUpOneProbe_controlDict";

    #includeIfPresent "../waveGaugesNProbes/waveRunUpOneGauge_controlDict";

}

// ************************************************************************* //
```

Figure 171 – File: controlDict

In the file controlDict, the time setting of the simulation can be changed. Always make sure that deltaT is such that the courant number at the start of the simulation is below 1 (use the wave celerity as flow velocity). Also, be aware that all wave gauges and pressure probes are defined in the functions part of the controlDict (lines 59 till 67). The value of writeInterval represents after how many seconds OpenFoam saves a copy of the files of alpha1, pd and U for the complete OpenFoam domain. These files can be used to restart the OpenFoam simulation in case it crashes, however, these files take up quite some disk-space. An equilibrium between save points and total disk space used has to be found. For the simulations in this thesis a save time of approximately 1/20th of the total simulation time has been used.

C.5.2 Other files in this folder

The files decomposeParDict, fvSchemes, fvSolution and (if applicable) snappyHexMeshDict should be present in the system-folder as well, but do not require any changes for the simulation of different structures or different wave conditions. The file snappyHexMeshDict is only required in case of a structure with an impermeable core, since for these structures, the impermeable core is cut out of the grid with snappyHexMesh, which requires snappyHexMeshDict in the system folder. The number of processor cores which is used to simulate the structure can be changed in the decomposeParDict-file.

C.6 Starting a simulation

A simulation can be started by following two or three scripts (depending on the structure) and executing a command. There are two versions of OpenFoam used in the total simulation process: OpenFoam-v3.0+ and foam-extend-3.1. The meshing tools of OpenFoam-v3.0+ are more robust than those of foam-extend-3.1, therefore OpenFoam-v3.0+ is used for SnappyHexMesh. On the cluster computers which are used for the simulations, only the meshing part of OpenFoam-v3.0+ is installed, for all other parts of the simulation foam-extend-3.1 should be used.

C.6.1 Script 1:

```
#!/bin/bash

# Source run functions
. $WM_PROJECT_DIR/bin/tools/RunFunctions

# Remove log-files and make Paraview-file
rm -f log.* *.foam
touch `basename $PWD`.foam

# remove previous snappyHexMesh data from \0 and constant\polyMesh folders
(cd 0; rm -rf *)
(rm -rf constant/polyMesh/*)
cp blockMeshDict.org constant/polyMesh/blockMeshDict

# Make blockMesh
runApplication blockMesh

# Make the STL-files
runApplication faceSetToSTL
```

Figure 172 – Script 1

This script creates the mesh and creates the STL-files for the porous layers. This script should be executed with foam-extend-3.1

C.6.2 Script 2:

```
#!/bin/bash

# Source run functions
. $WM_PROJECT_DIR/bin/tools/RunFunctions



# Cut out impermeable obstacles from the mesh

runApplication snappyHexMesh -overwrite
#runApplication extrudeMesh
runApplication renumberMesh -overwrite

```

Figure 173 - Script 2

This second script is only necessary for structures with an impermeable core. This script cuts the impermeable core out of the grid with SnappyHexMesh and renumbers the remaining cells with renumberMesh. This script should be executed using OpenFoam-v3.0+.

C.6.3 Script 3:

```
#!/bin/bash

# Source run functions
. $WM_PROJECT_DIR/bin/tools/RunFunctions

# Clean-up log-files and 0-folder
(rm -rf 0/*)
rm -f  log.weightedPorosityFields log.setsToZones \
    log.waveGaugesNProbes log.setWaveParameters log.setWaveField \
    log.relaxationZoneLayout log.decomposePar

# Set the porosity fields
#runApplication faceSetToSTL log.faceSetToSTL
runApplication weightedPorosityFields

# runApplication setSet -batch setSets/cellSetDefinitions.setSet

runApplication setsToZones
rm -rf forces_* OCW3Dhotstart VTK fort.*

# Make a fresh copy of the initial conditions and boundary conditions
(cd 0.org; cp * ../0/.)

# Make wave gauges, set wave parameters and initialize the fields
runApplication waveGaugesNProbes
runApplication setWaveParameters
runApplication setWaveField

# Make a visual output of the relaxation zone for inspection
runApplication relaxationZoneLayout

# Decompose the case
rm -rf processor*
runApplication decomposePar -cellDist
```

Figure 174 - Script 3

The third script prepares the model for the simulation. This script should be executed using foam-extend-3.1

C.6.4 Starting the simulation

When the simulation is set-up, check all the log-files in the home folder of the simulation. When no errors have occurred the simulation is ready to start.

The simulation can be started with the command:

```
nohup -np 8 porousWaveFoam -parallel &
```

This command runs the simulation using porousWaveFoam, it does so split over 8 processors in parallel and the simulation is performed in the background. To see the progress of the simulation, simply type: “tail -100 nohup.out” in the command window to see the last 100 lines of the log-file of the simulation. To continuously see the log-file, type: “tail -f nohup.out”.

Appendix D.
MATLAB scripts

D.1. Calculation of the hydraulic loading parameters

This part of the appendix holds the MATLAB script which is used to calculate the hydraulic loading parameters as described in chapter 6. Before the script with the calculations can be executed, first the results of the OpenFoam simulations have to be translated to a file format which MATLAB can handle. The script used for calculating the hydraulic loading parameters is shown below.

```
function void = CalcHydrLoadPar(sOutFolder, sCase, sProbeFileOnArmourLayer, sProbeFileOnFilterLayer,
percentage, sSaveName, simNumber)

% sOutFolder='\\rbw-nl\applications\scs\HED-MME\Students\OpenFoam\JesperRuns\run1_7_MatlabOutput';
% this is the location of the results of the OpenFoam simulation
% (after processing from raw OpenFoam output to Matlab files)

% sCase='run1_7';
% name of the simulation / case

% sProbeFileOnArmourLayer='run1_7_waveRunUpOneProbe';
% name of the probe file located on the armour layer

% sProbeFileOnFilterLayer='run1_7_waveRunUpTwoProbe';
% name of the probe file located on the filter layer

% percentage = 2;
% the {precentage} exceedance value over time is taken

% sSaveName = '2percent_values';
% the name of the output file

% simNumber = 1;
% parameter used to set the wave conditions, see below

disp(strcat("Startup ",sCase," ..."));

addpath(genpath('..\tudPlotRoutines'));

if ~strcmp(sOutFolder(end),'\')
    sOutFolder = [sOutFolder,'\'];  %add backslash if not provided by user
end

sCaseOutFolder = strcat(sOutFolder, sCase, '\');
load(strcat(sCaseOutFolder, sCase, '.mat'),'Case');  %case files

 % different wave conditions defined, manually overwriting input of the case
% file created in the processing step since these values are not correctly
% read with the processing script due to the irregular waves and coupling
% with OCW3D, in this case, three wave spectra are defined:

if simNumber == 1
    Case.waves.H = 0.13;
    Case.waves.Hm0 = 0.13;
    Case.waves.T = 2.3;
    Case.waves.Tp = 3.01;
    Case.waves.Tm_est = 2.3;
    Case.waves.Nwaves = Case.controls.tEnd/Case.waves.Tm_est;

elseif simNumber == 2
    Case.waves.H = 0.13;
    Case.waves.Hm0 = 0.13;
    Case.waves.T = 1.3;
    Case.waves.Tp = 1.70;
    Case.waves.Tm_est = 1.3;
    Case.waves.Nwaves = Case.controls.tEnd/Case.waves.Tm_est;

elseif simNumber == 3
    Case.waves.H = 0.13;
    Case.waves.Hm0 = 0.13;
    Case.waves.T = 3.6;
    Case.waves.Tp = 4.71;
    Case.waves.Tm_est = 3.6;
    Case.waves.Nwaves = Case.controls.tEnd/Case.waves.Tm_est;

end
```

```
AL = load(strcat(sCaseOutFolder, sProbeFileOnArmourLayer, '.mat'), 't', 'Ux', 'Uy', 'alpha', 'pd', 'xpos',
'ypos');
FL = load(strcat(sCaseOutFolder, sProbeFileOnFilterLayer, '.mat'), 't', 'Ux', 'Uy', 'alpha', 'pd', 'xpos',
'ypos');

%% calculate the value for the local DeltaH (Delta p in the thesis) perpendicular to the front slope

disp('Calculating DeltaH ...');

AL.pdWater = zeros(size(AL.pd));
for rowx = 1:length(AL.pd)
    for colx = 1:length(AL.pd(1,:))
        if AL.alpha(rowx,colx) > 0.5
            AL.pdWater(rowx,colx) = AL.pd(rowx,colx);
        end
    end
end

FL.pdWater = zeros(size(FL.pd));
for rowx = 1:length(FL.pd)
    for colx = 1:length(FL.pd(1,:))
        if FL.alpha(rowx,colx) > 0.5
            FL.pdWater(rowx,colx) = FL.pd(rowx,colx);
        end
    end
end

DeltaH = zeros(size(AL.pdWater));
for i = 1:length(DeltaH(1,:))
    for j = 1:length(DeltaH)
        DeltaH(j,i) = FL.pdWater(j,i)-AL.pdWater(j,i);
    end
end

DeltaHSorted = zeros(size(DeltaH));
indexesH = zeros(size(DeltaHSorted));
PHhelp = linspace(0,1,length(DeltaHSorted(:,1))+2);
PH = PHhelp(2:end-1);
indH = find(PH > ((100-percentage)*0.01),1);
confIntHighH = zeros(size(DeltaHSorted(1,:)));

for i = 1:length(DeltaHSorted(1,:))
    [DeltaHSorted(:,i),indexesH(:,i)] = sort(DeltaH(:,i),'ascend');
    confIntHighH(i) = DeltaHSorted(indH,i);
end

%% calculate the value for the total DeltaH (Delta p in the thesis) perpendicular to the front slope from
level -3Hm0 upwards

disp('Calculating TotPressure ...');

TotPressure = zeros(size(DeltaH(:,1)));
posRel = sqrt((AL.xpos-AL.xpos(1)).^2+(AL.ypos-AL.ypos(1)).^2);
deltaPos = posRel(2)-posRel(1);

for t = 1:length(TotPressure)
    TotPressure(t) = trapz(deltaPos,DeltaH(t,8:end)); % index 8 is at a level of -3 Hm0
end

TotPressureSorted = zeros(size(TotPressure));
% indexesHtot = zeros(size(TotPressureSorted));
PHtothelp = linspace(0,1,length(TotPressureSorted(:,1))+2);
PHtot = PHtothelp(2:end-1);
indHtot = find(PHtot > ((100-percentage)*0.01),1);
% confIntHighHtot = zeros(size(TotPressureSorted(1,:))); % size = 1
[TotPressureSorted, indexesHtot] = sort(TotPressure,'ascend');
confIntHighHtot = TotPressureSorted(indHtot);

%% calculate the value for Q perpendicular to the front slope from level -3Hm0 upwards

disp('Calculating DeltaQ ...');

AL.UxWater = zeros(size(AL.Ux));
for rowx = 1:length(AL.Ux)
    for colx = 1:length(AL.Ux(1,:))
        if AL.alpha(rowx,colx) > 0.5
            AL.UxWater(rowx,colx) = AL.Ux(rowx,colx);
        end
```

```
    end
end

AL.UyWater = zeros(size(AL.Uy));
for rowy = 1:length(AL.Uy)
    for coly = 1:length(AL.Uy(1,:))
        if AL.alpha(rowy,coly) > 0.5
            AL.UyWater(rowy,coly) = AL.Uy(rowy,coly);
        end
    end
end

FL.UxWater = zeros(size(FL.Ux));
for rowx = 1:length(FL.Ux)
    for colx = 1:length(FL.Ux(1,:))
        if FL.alpha(rowx,colx) > 0.5
            FL.UxWater(rowx,colx) = FL.Ux(rowx,colx);
        end
    end
end

FL.UyWater = zeros(size(FL.Uy));
for rowy = 1:length(FL.Uy)
    for coly = 1:length(FL.Uy(1,:))
        if FL.alpha(rowy,coly) > 0.5
            FL.UyWater(rowy,coly) = FL.Uy(rowy,coly);
        end
    end
end

angle = atan(1/2); % the angle of the front slope

AL.Uperpendicularx = (-AL.UxWater)*sin(angle);
AL.Uperpendiculary = AL.UyWater*cos(angle);
AL.Uperp = AL.Uperpendicularx + AL.Uperpendiculary;

FL.Uperpendicularx = (-FL.UxWater)*sin(angle);
FL.Uperpendiculary = FL.UyWater*cos(angle);
FL.Uperp = FL.Uperpendicularx + FL.Uperpendiculary;

DeltaUperp = zeros(size(AL.Uperp));
for i = 1:length(DeltaUperp(1,:))
    for j = 1:length(DeltaUperp)
        DeltaUperp(j,i) = (FL.Uperp(j,i)+AL.Uperp(j,i))/2;
    end
end

DeltaQ = DeltaUperp.*Case.flume.w;
TotDeltaQ = zeros(size(DeltaQ(:,1)));

for t = 1:length(TotDeltaQ)
    TotDeltaQ(t) = trapz(deltaPos,DeltaQ(t,8:end));
end

TotDeltaQSorted = zeros(size(TotDeltaQ));
% indexesQtot = zeros(size(TotDeltaQSorted));
PQtothelp = linspace(0,1,length(TotDeltaQSorted(:,1))+2);
PQtot = PQtothelp(2:end-1);
indQtot = find(PQtot > ((100-percentage)*0.01),1);
% confIntHighQtot = zeros(size(TotDeltaQSorted(1,:))); % size = 1
[TotDeltaQSorted, indexesQtot] = sort(TotDeltaQ,'ascend');
confIntHighQtot = TotDeltaQSorted(indQtot);

disp('Clearing up memory ...');

clear AL.Ux AL.Uy AL.alpha AL.pd AL.pdWater AL.Uperpendicularx AL.Uperpendiculary AL.Uperp
clear FL.Ux FL.Uy FL.alpha FL.pd FL.pdWater FL.Uperpendicularx FL.Uperpendiculary FL.Uperp
clear DeltaUperp PQtothelp PHtothelp PHhelp posRel

%% save results

disp('Saving...');

xArmour = AL.xpos;
xFilter = FL.xpos;
yArmour = AL.ypos;
yFilter = FL.ypos;
t = AL.t;
Upar = AL.Upar;
```

```
sSaveFile = strcat(sCaseOutFolder, sSaveName);
save(sSaveFile, 'confIntHighH', 'confIntHighHtot', 'confIntHighQtot', 'xArmour', 'xFilter', 'yArmour',
'yFilter', 't');


sSaveFile2 = strcat(sCaseOutFolder, sSaveName,'_withExtraOutput');
save(sSaveFile2, 'confIntHighH', 'DeltaH', 'DeltaHSorted', 'indexesH', 'PH', 'confIntHighHtot',
'TotPressure', 'TotPressureSorted', 'indexesHtot', 'PHtot', 'confIntHighQtot', 'DeltaQ', 'TotDeltaQ',
'TotDeltaQSorted', 'indexesQtot', 'PQtot', 'Upar', 'xArmour', 'xFilter', 'yArmour', 'yFilter', 't');


end
```

D.2. Plotting of the prediction method graphs

When the hydraulic loading parameters are calculated for the four different structures, the following code will predict the notional permeability of structure 1 and plot the graphs as shown in chapter 7.3.

```
function void = PredictPvalue(sOutPutFolder, percentage)

% sOutPutFolder = '\\rbw-nl\applications\scs\HED-MME\Students\OpenFoam\JesperRuns';
% location of the maps which include the calculated hydraulic loading parameters

% percentage = 2;


if ~strcmp(sOutPutFolder(end),'\')
    sOutPutFolder = [sOutPutFolder,'\'];  %add backslash if not provided by user
end

structures = ["1" "2" "3" "4"];
runs = ["7"];
runsDisplay = ["0"];
structureNames = ["Kik035" "vdMeer01" "vdMeer05" "vdMeer06"];
Pvalues = [0.1 0.5 0.6];

% Colors for the plots:
Cruns1 = [1,0,0];
Cruns2 = [0.5,0.7,0.3];
Cruns3 = [0.3,0.1,0.6];
Cruns4 = [0.2,1.0,1.0];
Cruns = [Cruns1 Cruns2 Cruns3 Cruns4];
Cpred = Cruns;

for run = 1:length(runs)
    disp(strcat("processing the results of the different structures for simulations of run ",
runsDisplay(run)," ..."));
    for str = 1:length(structures)
        disp(strcat("           structure ", structures(str), " (", structureNames(str), ") ..."));

        if run == 1
            sMatFile =
strcat(sOutPutFolder,"run",structures(str),"_",runs(run),"_MatlabOutput\run",structures(str),"_",runs(run),
"\",num2str(percentage),"percent_values.mat");
        elseif run == 2
            sMatFile =
strcat(sOutPutFolder,"run",structures(str),"_",runs(run),"_MatlabOutput\run",structures(str),"_",runs(run),
"\",num2str(percentage),"percent_values_shortened.mat");
        elseif run == 3
            sMatFile =
strcat(sOutPutFolder,"run",structures(str),"_",runs(run),"_MatlabOutput\run",structures(str),"_",runs(run),
"\",num2str(percentage),"percent_values.mat");
        end

        if str == 1
            Kik035(run) = load(sMatFile, 'confIntHighH', 'confIntHighHtot', 'confIntHighQtot',
'confIntHighUpar', 'confIntLowUpar', 't', 'xArmour', 'xFilter', 'yArmour', 'yFilter');
        elseif str == 2
            vdMeer01(run) = load(sMatFile, 'confIntHighH', 'confIntHighHtot', 'confIntHighQtot',
'confIntHighUpar', 'confIntLowUpar', 't', 'xArmour', 'xFilter', 'yArmour', 'yFilter');
        elseif str == 3
            vdMeer05(run) = load(sMatFile, 'confIntHighH', 'confIntHighHtot', 'confIntHighQtot',
'confIntHighUpar', 'confIntLowUpar', 't', 'xArmour', 'xFilter', 'yArmour', 'yFilter');
        elseif str == 4
            vdMeer06(run) = load(sMatFile, 'confIntHighH', 'confIntHighHtot', 'confIntHighQtot',
'confIntHighUpar', 'confIntLowUpar', 't', 'xArmour', 'xFilter', 'yArmour', 'yFilter');
        end
    end
end
```

```
%% first, prediction based on the local Delta H (Delta p in the thesis)

disp(" ");
figure()
hold on
set(gcf, 'Position',  [500, 200, 900, 600])


Hrel = zeros(1,length(structures)-1);

for run = 1:length(runs)
    plot([0 1.5],[0.37 0.37], 'k:','DisplayName',"Value found by (Kik, 2011)")
    Hmax = max(vdMeer01(run).confIntHighH);
    Hrel(1) = max(vdMeer01(run).confIntHighH)/Hmax;
    Hrel(2) = max(vdMeer05(run).confIntHighH)/Hmax;
    Hrel(3) = max(vdMeer06(run).confIntHighH)/Hmax;
    plot([Hrel(1) Hrel(2) Hrel(3)], [Pvalues(1) Pvalues(2) Pvalues(3)], 'b--
o','DisplayName',strcat("Structures of (Van der Meer, 1988) of run ",runsDisplay(run)))
    Hsearch = max(Kik035(run).confIntHighH)/Hmax;
    Ppredicted = interp1(Hrel,Pvalues,Hsearch);
    disp(strcat("according to run ", runsDisplay(run), " the predicted P-value for comparisson on the local
overpressure is: ",num2str(Ppredicted)));
    plot([Hsearch max(vdMeer06(1).confIntHighH)/max(vdMeer01(1).confIntHighH)], [Ppredicted Ppredicted], '-
.x','Color',Cpred(-2+(run*3):(run*3)),'DisplayName',strcat("Structure of (Kik, 2011) of run
",runsDisplay(run)))
    plot([Hsearch Hsearch], [0.1 Ppredicted], '-.x','Color',Cpred(-
2+(run*3):(run*3)),'HandleVisibility','off')
end

ylim([Pvalues(1) Pvalues(3)]);
xlim([max(vdMeer06(1).confIntHighH)/max(vdMeer01(1).confIntHighH) Hrel(1)]);

legend('Location', 'NorthEast');
ylabel('P-value [-]');
% xlabel({"Relative maximum local overpressure over the armour layer [-]",strcat("(relative exceedance
",num2str(percentage),"%)")});
% title({"Prediction of the notional permeability (P) with the relative ",strcat(num2str(percentage),"%
exceedance maximum  local overpressure over the armour layer")});

xlabel({"Relative \Deltap_{\perp,loc,2%}"});
title({"Prediction of the notional permeability (P) using relative \Deltap_{\perp,loc,2%} "});



%% second,  prediction based on the total Delta H (Delta p in the thesis)

disp(" ");
figure()
hold on
set(gcf, 'Position',  [500, 200, 900, 600])

HtotRel = zeros(1,length(structures)-1);


for run = 1:length(runs)
    plot([0 1.5],[0.37 0.37], 'k:','DisplayName',"Value found by (Kik, 2011)")
    HtotMax = vdMeer01(run).confIntHighHtot;
    HtotRel(1) = max(vdMeer01(run).confIntHighHtot)/HtotMax;
    HtotRel(2) = max(vdMeer05(run).confIntHighHtot)/HtotMax;
    HtotRel(3) = max(vdMeer06(run).confIntHighHtot)/HtotMax;
    plot([HtotRel(1) HtotRel(2) HtotRel(3)], [Pvalues(1) Pvalues(2) Pvalues(3)], 'b--
o','DisplayName',strcat("Structures of (Van der Meer, 1988) of run ",runsDisplay(run)))
    HtotSearch = Kik035(run).confIntHighHtot/HtotMax;
    Ppredicted = interp1(HtotRel,Pvalues,HtotSearch);
    disp(strcat("according to run ", runsDisplay(run), " the predicted P-value for comparisson on the total
overpressure is: ",num2str(Ppredicted)));
    plot([HtotSearch max(vdMeer06(1).confIntHighHtot)/vdMeer01(1).confIntHighHtot], [Ppredicted
Ppredicted], '-.x','Color',Cpred(-2+(run*3):(run*3)),'DisplayName',strcat("Structure of (Kik, 2011) of run
",runsDisplay(run)))
    plot([HtotSearch HtotSearch], [0.1 Ppredicted], '-.x','Color',Cpred(-
2+(run*3):(run*3)),'HandleVisibility','off')
end

ylim([Pvalues(1) Pvalues(3)]);
xlim([max(vdMeer06(1).confIntHighHtot)/vdMeer01(1).confIntHighHtot HtotRel(1)]);

legend('Location', 'NorthEast');
ylabel('P-value [-]');
% xlabel({strcat("Relative total overpressure (exceeded by ", num2str(percentage),"% of the waves)"), "over
the armour layer [-]"});
% title({"Prediction of the notional permeability (P) with the relative ",strcat("total overpressure over
the armour layer (exceeded by ", num2str(percentage),"% of the waves)")});

xlabel({"Relative \Deltap_{\perp,tot,2%}"});
title({"Prediction of the notional permeability (P) using relative \Deltap_{\perp,tot,2%} "});
```

```
%% third, prediction based on the total Q

disp(" ");
figure()
hold on
set(gcf, 'Position',  [500, 200, 900, 600])

Qrel = zeros(1,length(structures)-1);



for run = 1:length(runs)
    plot([0 1.5],[0.37 0.37], 'k:','DisplayName',"Value found by (Kik, 2011)")
    Qmax = vdMeer06(run).confIntHighQtot;
    Qrel(1) = max(vdMeer01(run).confIntHighQtot)/Qmax;
    Qrel(2) = max(vdMeer05(run).confIntHighQtot)/Qmax;
    Qrel(3) = max(vdMeer06(run).confIntHighQtot)/Qmax;

    xHelp = linspace(Qrel(1), Qrel(3));
    yHelp = interp1(Qrel, Pvalues, xHelp, 'cubic');



    plot(xHelp, yHelp, 'b--','HandleVisibility','off')
%     plot(xHelp, yHelp, 'g--')
%     plot([Qrel(1) Qrel(2) Qrel(3)], [Pvalues(1) Pvalues(2) Pvalues(3)], '--o','Color',Cruns(-
2+(run*3):(run*3)),'DisplayName',strcat("Structures of (Van der Meer, 1988) of run ",runsDisplay(run)))
    plot([Qrel(1) Qrel(2) Qrel(3)], [Pvalues(1) Pvalues(2) Pvalues(3)], 'bo','HandleVisibility','off')
    Qsearch = Kik035(run).confIntHighQtot/Qmax;
    Ppredicted = interp1(Qrel,Pvalues,Qsearch,'cubic');
    disp(strcat("according to run ", runsDisplay(run), " the predicted P-value for comparisson on the
discharge through the armour layer is: ",num2str(Ppredicted)));
    plot([0 0.1], [0 0], 'b--o','DisplayName',strcat("Structures of (Van der Meer, 1988) of run
",runsDisplay(run)))
    plot([max(vdMeer01(1).confIntHighQtot)/vdMeer06(1).confIntHighQtot Qsearch], [Ppredicted Ppredicted],
'-.x','Color',Cpred(-2+(run*3):(run*3)),'DisplayName',strcat("Structure of (Kik, 2011) of run
",runsDisplay(run)))
    plot([Qsearch Qsearch], [0.1 Ppredicted], '-.x','Color',Cpred(-
2+(run*3):(run*3)),'HandleVisibility','off')
end


ylim([Pvalues(1) Pvalues(3)]);
xlim([max(vdMeer01(1).confIntHighQtot)/vdMeer06(1).confIntHighQtot Qrel(3)]);

legend('Location', 'SouthEast');
ylabel('P-value [-]');
% xlabel({"Relative total discharge  through the armour layer",strcat("(exceeded by ",
num2str(percentage),"% of the waves)[-]")});
% title({"Prediction of the notional permeability (P) with the relative ",strcat("total discharge through
the armour layer (exceeded by ", num2str(percentage),"% of the waves)")});

xlabel({"Relative Q_{\perp,tot,2%}"});
title({"Prediction of the notional permeability (P) using relative Q_{\perp,tot,2%} "});


end
```